

Clinical and genetic characterisation of hereditary motor neuropathies

Boglarka Bansagi

Institute of Genetic Medicine

January 2017

A Thesis submitted for the degree of Doctor of Philosophy at
Newcastle University



Institute of
Genetic Medicine

*'I dare do all that may become a man;
who dares do more is none.'*

(Shakespeare)

*„Szívet vagy mundért cserélhet az is, ki házat, hazát holtig nem cserél,
de hű maradhat idegenben is, kiben népe mostoha sorsa él.”*

(Tollas Tibor)

Author's declaration

This Thesis is submitted to Newcastle University for the degree of Doctor of Philosophy at Newcastle University. I, Boglarka Bansagi, confirm that the work presented in this Thesis is my own. Where information has been derived from other sources, it has been indicated in the Thesis. I can confirm that none of the material offered in this Thesis has been previously submitted by me for a degree or qualification in this or any other university.

Abstract

Inherited peripheral neuropathies or Charcot-Marie-Tooth disease (CMT) are common neuromuscular conditions, characterised by distal motor atrophy and weakness with variable range of sensory impairment and classified according to demyelinating (CMT1) or axonal (CMT2) pathology. The number of genes causing CMT has rapidly increased due to improved genetic testing technology, even though gene identification has remained challenging in some subgroups of CMT.

Hereditary motor neuropathies (HMN) encompass heterogeneous groups of disorders caused by motor axon and neuron pathology. The distal hereditary motor neuropathies (dHMN) are rare length-dependent conditions, which show significant clinical and genetic overlap with motor neuron diseases. Several (>30) causative genes have been identified for ~20% of dHMN patients, which predicts extreme genetic heterogeneity in this group.

My study was designed to investigate the prevalence, clinical presentation, molecular cause and phenotype-genotype correlations of hereditary motor neuropathies in a large cohort of patients. I aimed to identify novel disease genes and reassessed mutation detection rate in dHMN. Furthermore, I studied common pathomechanisms and targets for therapy approaches in hereditary motor neuropathies.

Detailed neurological and electrophysiological assessments and next generation panel testing or whole exome sequencing were performed in 105 patients with clinical symptoms of distal hereditary motor neuropathy (dHMN, 64 patients), axonal motor neuropathy (motor CMT2, 16 patients) or complex neurological disease predominantly affecting the motor nerves (dHMN plus, 25 patients). I calculated the dHMN prevalence 2.14 affected individuals per 100.000 inhabitants (95% CI: 1.62-2.66) in the North of England.

Causative mutations were identified in overall 47.9% in the motor neuropathy patient cohort. In the dHMN group the diagnostic rate was 42.5%, significantly higher than the previously reported 20%. The significant increase in the mutation detection rate could be attributed to the development of next generation techniques.

Many of the genes were shared between dHMN and motor CMT2, indicating identical disease mechanisms. I examined the phenotypic variability and the correlations with the identified genetic background.

We described the novel phenotype of non-progressive motor neuropathy with fatigable weakness due to presynaptic neuromuscular transmission defect caused by synaptotagmin 2 mutations. I identified further novel genes involved in intracellular signal transduction and

transcriptional regulatory cascades, which might indicate common pathways and highlight further targets in the therapy of motor neuropathies.

We detected a potentially treatable defect of neuromuscular transmission in some genetic forms, which raise the possibility that neuromuscular junction defects can cause or accompany motor neuropathy. The preliminary results suggested the potential treatability of the neuromuscular transmission defect, although long term effects will still need to be evaluated.

In summary, detailed clinical characterisation and segregation analysis improved the detection rate in our cohort and highlighted that clinical expertise are still essential in confirming the diagnosis of inherited motor neuropathies. Increasing knowledge on disease pathways will not only help to identify new genes with shared pathomechanisms but will provide a basis for novel therapy approaches.

Acknowledgements

I would like to specifically thank my supervisor Professor Rita Horvath for her excellent guidance, tuition and motivation throughout my PhD research. I feel extremely fortunate to have had her expertise support and I have thoroughly enjoyed her clinical lead in obtaining my skills in neurogenetics. She has gone above and beyond her role as a supervisor and she provided me with her constant approachability and encouragement.

Special thanks must also go to Professor Hanns Lochmüller, Professor David Elliott, Dr Bobby McFarland and Professor Kate Bushby for their sensible advice and support in my research.

I am grateful to Jennifer Duff, PhD for teaching me the bench work with her huge patience and for always being available to help me in the laboratory investigations.

Thanks also go to Veronika Boczonadi, PhD for helping me with the protein studies and to Juliane Mueller for supporting my work with cell cultures. Thank you also to Michele Giunta for your support in the lab and for your friendship.

Special thanks to Helen Griffin, PhD, Angela Pyle, PhD and to Dr Michael Keogh for their sensible advice in bioinformatics.

I would also like to thank everyone I have worked with in the clinical team; Professor Patrick F Chinnery, Professor Venkateswaran Ramesh, Dr Roger Whittaker, Dr Teresinha Evangelista, Dr Hannah Steele, Gail Eglon and Ingrid Emmerson.

I had the opportunity to have the great company and make friendship with Monica Ensini, Elena Teichmann, Katja Gassner, Beccie Brennan, George Anyfantis, Marina Bartsakoulia, Emily McIlwayne, David Moore, Valeria Chichagova, Carla Mellough, Joseph Collin.

I would like to express my special thanks to the Medical Research Council Centre for Translational Research in Neuromuscular Diseases for funding my PhD research.

Finally, thanks to my family, especially to you mum for your continuous support, encouragement and love that helped me to achieve my goals throughout all my life. Thanks to Bruno for his love, support and help.

Table of Contents

Author's declaration	i
Abstract.....	i
Acknowledgements	iii
Table of Contents	v
List of Figures.....	xiii
List of Tables.....	xv
Abbreviations	xvii
1 Introduction	1
1.1 The inherited neuropathies	1
1.2 Genetics of the inherited neuropathies	4
2 Objectives and Overview.....	8
3 Methodology.....	10
3.1 Clinical data collection	10
3.1.1 Patients	10
3.1.2 Neurophysiology	12
3.2 Laboratory methods.....	13
3.2.1 Next generation sequencing.....	13
3.2.1.1 Inherited Peripheral Neuropathy (IPN) panel gene test.....	13
3.2.1.2 Whole-exome sequencing.....	15
3.2.2 Sanger sequencing	17
3.2.2.1 DNA sequencing	17
3.2.2.2 cDNA sequencing.....	23
3.2.3 Functional protein studies.....	24
3.2.3.1 Fibroblast cell line culture	24
3.2.3.2 Western blot.....	25
4 Identifying the patient cohort and clinical classification of the hereditary motor neuropathies.....	27
4.1 Hereditary motor neuropathies and the revised nosology	27
4.2 Aims	28
4.3 Methods	28
4.3.1 Patient recruitment.....	28
4.3.1.1 Inclusion and classification criteria	30

4.3.1.2	Exclusion criteria	30
4.3.2	Statistic evaluation	30
4.3.3	Neurophysiology studies	31
4.4	Results	31
4.4.1	Distribution and presentation of patients among classified clinical subgroups	31
4.4.2	Epidemiology of hereditary motor neuropathy in the investigated patient cohort	33
4.4.3	Neurophysiology analysis in the clinical subgroups	34
4.5	Discussion	34
4.5.1	Epidemiology of hereditary motor neuropathies in North-East England	34
4.5.2	Phenotype classification of hereditary motor neuropathies	34
5	Identifying genetic frequency and investigating mutational spectrum in hereditary motor neuropathies	42
5.1	Review of hereditary motor neuropathies in the molecular era	42
5.2	Aims	42
5.3	Methods	43
5.3.1	Patient involvement in the genetic study	43
5.3.2	Diagnostic algorithm of applied genetic approaches	43
5.3.3	Genetic methods applied in the study	43
5.3.3.1	Targeted gene testing	43
5.3.3.2	Inherited peripheral neuropathy gene panel testing	44
5.3.3.3	Whole-exome sequencing	44
5.3.4	Statistical analyses of the results	44
5.4	Results	46
5.4.1	Mutation frequency in the HMN cohort and efficacy of applied genetic tools	46
5.4.2	The spectrum of gene mutations and mutation detection rate in dHMN	46
5.4.2.1	Confirmed pathogenic mutations	46
5.4.2.2	Possibly pathogenic mutations	50
5.4.3	The spectrum of gene mutations and mutation detection rate in motor CMT2	50
5.4.4	The spectrum of gene mutations and mutation detection rate in HMN plus	52
5.4.4.1	Confirmed pathogenic mutations	52
5.4.4.2	Possibly causative mutations	54
5.5	Discussion	57
5.5.1	Mutation detection rate in the HMN cohort	57

5.5.2	Advantages and limitations of next generation sequencing in the HMN cohort..	57
5.5.3	Molecular pathways and gene mutations in hereditary motor neuropathies	65
5.5.3.1	Impaired protein translation.....	65
5.5.3.2	Abnormal RNA metabolism.....	65
5.5.3.3	Impaired axonal transport.....	68
5.5.3.4	Channelopathies	70
5.5.3.5	Mitochondrial dysfunction	70
5.5.3.6	Neuromuscular transmission defect.....	77
5.5.3.7	Disturbed intracellular transcription pathways.....	77
5.6	Conclusion.....	79
6	Phenotype-genotype analysis in hereditary motor neuropathies.....	80
6.1	Aminoacyl-tRNA synthetases (ARS)-related motor neuropathies.....	80
6.1.1	Aims	81
6.1.2	Methods	81
6.1.2.1	Patient recruitment.....	81
6.1.2.2	Diagnostic genetic methods.....	81
6.1.2.3	Neurophysiology	81
6.1.2.4	Outcome measure	81
6.1.3	AARS-related neuropathy.....	82
6.1.3.1	Literature review.....	82
6.1.3.2	Clinical and neurology findings in AARS mutant pedigrees	84
6.1.3.3	Neurophysiology findings in pedigrees with AARS-related neuropathy	91
6.1.3.4	Diagnostic genetic methods and identified AARS mutations in the pedigrees .	93
6.1.3.5	Genotype-phenotype correlations in the cohort of AARS-related neuropathy..	95
6.1.3.6	Conclusion.....	97
6.1.4	GARS-related neuropathy	98
6.1.4.1	Literature review.....	98
6.1.4.2	Natural history of GARS-related neuropathy in the identified pedigrees	98
6.1.4.3	Detailed nerve conduction findings in the GARS pedigrees.....	102
6.1.4.4	The identified novel GARS variants in the pedigrees	103
6.1.4.5	Genotype-phenotype correlations in the identified GARS pedigrees	104
6.1.4.6	Conclusion.....	105

6.2	<i>IGHMBP2</i> -related neuropathy	106
6.2.1	Literature review	106
6.2.2	Aims and hypothesis	107
6.2.3	Methods.....	107
6.2.3.1	Patient inclusion.....	107
6.2.3.2	Genetic diagnostic methods	107
6.2.4	Results.....	109
6.2.4.1	Clinical phenotypes of patients diagnosed with <i>IGHMBP2</i> mutations.....	109
6.2.4.2	Experimental genetic studies	112
6.2.5	Discussion	112
6.2.6	Conclusion	115
6.3	<i>TRPV4</i> -related neuropathy	116
6.3.1	Literature review	116
6.3.2	Aims and hypothesis	117
6.3.3	Methods.....	117
6.3.3.1	Patient recruitment	117
6.3.3.2	Muscle histopathology	117
6.3.3.3	Neurophysiology	117
6.3.3.4	Genetic diagnostic methods	117
6.3.4	Results.....	118
6.3.4.1	Clinical phenotypes of patients diagnosed with <i>TRPV4</i> mutations	118
6.3.4.2	Muscle histopathology result in the patients diagnosed with <i>TRPV4</i> neuropathy.....	120
6.3.4.3	Neurophysiology findings in pedigrees with <i>TRPV4</i> -related neuropathy .	120
6.3.4.4	Diagnostic genetic methods and identified <i>TRPV4</i> mutations in the pedigrees	121
6.3.5	Discussion	121
6.3.6	Conclusion	124
6.4	<i>BICD2</i> -related neuropathy	125
6.4.1	Literature review of pedigrees with the common <i>BICD2</i> mutation.....	125
6.4.2	Aims and hypothesis	126
6.4.3	Methods.....	126
6.4.3.1	Patient recruitment and investigations	126
6.4.3.2	Haplotype analysis and experimental genetic studies.....	126
6.4.4	Results.....	128

6.4.4.1	Detailed phenotype characteristics of the investigated <i>BICD2</i> families	128
6.4.4.2	Haplotype analysis in the families carrying the p.Ser107Leu <i>BICD2</i> mutation	130
6.4.5	Discussion.....	132
6.4.6	Conclusion.....	133
6.5	<i>ATP7A</i> -related neuropathy	134
6.5.1	Literature review.....	134
6.5.2	Aims and hypothesis.....	135
6.5.3	Methods	135
6.5.3.1	Patient inclusion	135
6.5.3.2	Next generation sequencing and segregation analysis	136
6.5.3.3	Western blot.....	136
6.5.4	Results	136
6.5.4.1	Detailed clinical phenotype and investigation findings.....	136
6.5.4.2	Identified genetic variants by next generation sequencing.....	138
6.5.4.3	Immunoblot analysis in the patient fibroblasts.....	140
6.5.5	Discussion.....	140
6.5.6	Conclusion.....	142
7	Investigation of novel genes and pathomechanisms in hereditary motor neuropathies .	143
7.1	Presynaptic neuromuscular transmission defect caused by <i>SYT2</i> mutations.....	143
7.1.1	Literature review.....	143
7.1.2	Aims and hypothesis.....	145
7.1.3	Methods	145
7.1.3.1	Patient inclusion	145
7.1.3.2	Electrophysiology studies.....	145
7.1.3.3	Experimental genetic methods	145
7.1.4	Results	145
7.1.4.1	Clinical phenotype of patients diagnosed with <i>SYT2</i> mutation.....	145
7.1.4.2	Detailed electrophysiology findings in the <i>SYT2</i> family.....	149
7.1.4.3	Identified <i>SYT2</i> mutation in the family	149
7.1.5	Discussion.....	151
7.1.6	Conclusion.....	153
7.2	Altered intracellular signal transduction pathways	154
7.2.1	A novel motor neuropathy phenotype caused by mutation in the <i>PTEN</i> gene	154
7.2.1.1	Literature review.....	154

7.2.1.2	Aims and hypothesis	155
7.2.1.3	Methods.....	155
7.2.1.3.1	Patient inclusion.....	155
7.2.1.3.2	Electrophysiology studies	155
7.2.1.3.3	Experimental genetic studies	156
7.2.1.3.4	Western blot	156
7.2.1.3.5	Phosphatase enzyme assay.....	156
7.2.1.4	Results.....	157
7.2.1.4.1	Patient phenotype.....	157
7.2.1.4.2	Electrophysiology findings	159
7.2.1.4.3	Identified <i>PTEN</i> mutation by WES.....	159
7.2.1.4.4	Normal amount of <i>PTEN</i> protein detected by Western blot	159
7.2.1.4.5	Phosphatase activity of the mutant protein	159
7.2.1.5	Discussion	161
7.2.1.6	Conclusion	162
7.2.2	Homozygous <i>STAT5B</i> mutations related to a novel neuromuscular phenotype	163
7.2.2.1	Literature review	163
7.2.2.2	Aims and hypothesis	163
7.2.2.3	Methods.....	163
7.2.2.3.1	Patient inclusion.....	163
7.2.2.3.2	Electrophysiology	163
7.2.2.3.3	Experimental genetic studies	164
7.2.2.4	Results.....	164
7.2.2.4.1	Patient phenotype.....	164
7.2.2.4.2	Electrophysiology findings	164
7.2.2.4.3	Identified <i>STAT5B</i> mutations	164
7.2.2.5	Discussion	166
7.2.2.6	Conclusion	168
7.2.3	Motor neuropathy in Holt-Oram syndrome caused by <i>TBX5</i> mutation	169
7.2.3.1	Literature review	169
7.2.3.2	Aims and hypothesis	169
7.2.3.3	Methods.....	170
7.2.3.3.1	Patient inclusion.....	170
7.2.3.3.2	Electrophysiology	170

7.2.3.3.3	Experimental genetic studies	170
7.2.3.4	Results	170
7.2.3.4.1	Patient phenotype	170
7.2.3.4.2	Electrophysiology findings.....	172
7.2.3.4.3	Identified <i>TBX5</i> mutation	172
7.2.3.5	Discussion.....	174
7.2.3.6	Conclusion.....	175
7.3	A novel mitochondrial metabolic pathway implicated in motor neuropathies.....	176
7.3.1	Literature review.....	176
7.3.2	Aims and hypothesis.....	178
7.3.3	Methods	178
7.3.3.1	Patient inclusion	178
7.3.3.2	Electrophysiology	178
7.3.3.3	Experimental genetic studies	178
7.3.3.4	Metabolomics studies	178
7.3.4	Results	179
7.3.4.1	Patient phenotype	179
7.3.4.2	Electrophysiology findings.....	183
7.3.4.3	Identified gene mutations	183
7.3.4.4	Results of the metabolomics studies.....	184
7.3.5	Discussion.....	184
7.3.6	Conclusion.....	186
8	Investigation of neuromuscular junction as a novel therapeutic target in hereditary motor neuropathies.....	187
8.1	Literature review.....	187
8.1.1	Neurotransmission at the neuromuscular junction	187
8.1.2	Neuromuscular junction defect in motor neuropathy-related gene mutations	188
8.1.2.1	Neurotransmission defect in <i>SYT2</i> mutant neuromuscular junctions	188
8.1.2.2	Neuromuscular junction dysfunction in <i>GARS</i> mutations.....	189
8.2	Aims and hypothesis.....	190
8.3	Methods	190
8.3.1	Patients inclusion.....	190
8.3.2	Therapeutic modification of the neuromuscular junction function	190
8.3.2.1	Treatment with pyridostigmin	190
8.3.2.2	Treatment with 3,4 diamino-pyridin (3,4-DAP).....	191

8.3.3	Neurology and physiotherapy assessments pre- and post-treatment	191
8.3.4	Electrophysiology studies of the neurotransmission pre- and post- treatment	191
8.4	Results.....	193
8.4.1	Pre- and post-treatment investigations in the <i>SYT2</i> mutant patients.....	193
8.4.1.1	Neurology and physiotherapy findings pre- and post-treatment.....	193
8.4.1.2	Electrophysiology findings pre- and post-treatment.....	193
8.4.2	Pre- and post-treatment investigations in the <i>GARS</i> mutant patients.....	195
8.4.2.1	Neurology and physiotherapy findings pre- and post-treatment.....	195
8.4.2.2	Electrophysiology findings pre- and post-treatment.....	195
8.5	Discussion	197
8.5.1	The neurotransmission defect and effects of the therapy in <i>SYT2</i> mutant patients	197
8.5.2	The neurotransmission defect and effects of therapy in <i>GARS</i> mutant patients	198
8.6	Conclusion	198
9	Conclusion and future directions	199
9.1	Overview.....	199
9.2	Summary of the Thesis results	199
9.2.1	Clinical and genetic analysis of the hereditary motor neuropathy cohort.....	199
9.2.2	Phenotype-genotype correlations in the hereditary motor neuropathy cohort	200
9.2.3	Novel disease genes and mechanisms in the hereditary motor neuropathy cohort	202
9.2.4	Novel therapy approaches in hereditary motor neuropathies.....	203
9.3	Concluding remarks	204
Appendix A	205
Appendix B	206
Appendix C	207
Appendix D	208
Appendix E	209
Appendix F	210
Appendix G	211
Appendix H	212
References	213

List of Figures

Figure 1.1 Pathways and genes implicated in inherited neuropathies.....	3
Figure 3.1 TruSeq™ enrichment workflow.....	15
Figure 4.1 Classification of dHMN.....	29
Figure 4.2 Statistic of the hereditary motor neuropathy cohort.....	33
Figure 5.1 Clinical heterogeneity of different forms of HMN.....	58
Figure 5.2 Distribution of mutated genes in the phenotype groups and overlapping phenotypes with key clinical features.....	59
Figure 5.3 Diagnostic flow chart and genes identified in our cohort.....	61
Figure 5.4 Targets of pathomechanisms involved in the motor neuropathy genes.....	66
Figure 6.1 AARS mutant pedigrees.....	85
Figure 6.2 Identified AARS variants, positions and conservation across species.....	94
Figure 6.3 Identified GARS mutant families.....	99
Figure 6.4 Primers designed for IGHMBP2 cDNA sequencing.....	108
Figure 6.5 Photograph illustration of IGHMPBP2-related phenotypes.....	110
Figure 6.6 Segregation of the identified heterozygous IGHMBP2 mutation.....	113
Figure 6.7 Hemizygous IGHMBP2 mutation on cDNA sequencing.....	114
Figure 6.8 TRPV4 mutant patient from Family 10.....	119
Figure 6.9 TRPV4 mutant patient from Family 11.....	119
Figure 6.10 Pedigrees and clinical phenotype of BICD2 mutant families.....	129
Figure 6.11 Haplotype analysis in the BICD2 mutant families.....	131
Figure 6.12 Clinical presentation and neuroimaging of the ATP7A mutant patient.....	137
Figure 6.13 Segregation of SACS variants in the patient's family.....	139
Figure 6.14 The identified novel ATP7A mutation in the patient.....	141
Figure 7.1 Family tree of the SYT2 mutant family with the foot deformities.....	146
Figure 7.2 Identified SYT2 mutation in the family.....	150
Figure 7.3 Drosophila p.Asp362Ala SYT2 disrupts neurotransmitter release.....	152
Figure 7.4 Photo illustration of the clinical symptoms in the PTEN mutant patient.....	158
Figure 7.5 The identified de novo p.Phe90Ser PTEN mutation in the patient.....	160
Figure 7.6 The identified p.Glu315Ala STAT5B mutation in the family.....	165
Figure 7.7 Pathomechanisms of STAT5B.....	167
Figure 7.8 Photo illustration of the phenotype with the identified TBX5 mutation.....	171
Figure 7.9 Sequencing of the identified TBX5 mutation and segregation study.....	173

Figure 7.10 Pathway of lysine, hydroxylysine and tryptophan degradation.....	177
Figure 7.11 The identified <i>DHTKD1</i> mutation in the family	180
Figure 7.12 The identified <i>SLC25A21</i> mutation in the patient	182
Figure 7.13 Increased concentration of the degrading metabolites in the urine	185
Figure 8.1 Marked and sustained post-tetanic potentiation following brief MVC	194
Figure 8.2 Effects of treatment with pyridostigmine and 3,4-DAP	196

List of Tables

Table 1.1 Comparison of the next-generation sequencing based diagnostic methods	6
Table 3.1 CMT Neuropathy Score second version (CMTNSv2)	11
Table 3.2 Inherited peripheral neuropathy gene panel test.....	14
Table 3.3 Standard MyTaq™ PCR protocol	19
Table 4.1 Phenotype statistics, efficacy of genetic methods and mutation detection rate in the classified patient subgroups.....	32
Table 4.2 Nerve conduction parameters in dHMN with confirmed pathogenic mutations.....	35
Table 4.3 Nerve conduction parameters in dHMN with possibly causative mutations	37
Table 4.4 Nerve conduction parameters in motor CMT2.....	38
Table 4.5 Nerve conduction parameters in dHMN plus with confirmed pathogenic mutations	39
Table 4.6 Nerve conduction parameters in dHMN plus patients with possibly causative mutations	40
Table 5.1 Set of genes related to IPN, HSP,SMA and ALS filtered in the WES data of HMN cohort.....	45
Table 5.2 Summary of the clinical presentation of the patients in the dHMN group with confirmed causative mutations	47
Table 5.3 Summary of the clinical presentation of the patients in the dHMN group with possibly causative mutations	51
Table 5.4 Summary of the clinical presentation of the patients with confirmed mutations in the motor CMT2 group.....	53
Table 5.5 Summary of the clinical presentation of the patients in the HMN plus group with confirmed pathogenic mutations	55
Table 5.6 Summary of the clinical presentation of the patients in the HMN plus group with possibly causative mutations	56
Table 5.7 Population frequencies of rare genetic variants from WES	62
Table 5.8 Functional prediction of rare genetic variants from WES.....	63
Table 5.9 Coverage of rare genetic variants from WES.....	64
Table 5.10 Mechanisms of motor neuropathy-related genes identified in the HMN cohort....	67
Table 6.1 Summary of the clinical and electrophysiology findings accompanying the reported AARS variants	83

Table 6.2 Genetic and clinical characteristics of patients with <i>AARS</i> -related neuropathy in the UK/Irish cohort	90
Table 6.3 Summary of neurophysiology results in the <i>AARS</i> mutant UK / Irish families.....	92
Table 6.4 Analysing common SNPs in the affected <i>AARS</i> mutant families	94
Table 6.5 Clinical characteristics of <i>GARS</i> neuropathy patients	101
Table 6.6 Designed primers for the sequencing of SNPs in the <i>BICD2</i> gene.....	127
Table 6.7 Predicted deleterious variants filtered from WES data.....	139
Table 7.1 Clinical and electrophysiological features in the <i>SYT2</i> patients	147
Table 8.1 Baseline CMSS and CMTNSv2 values and beside 3,4 DAP therapy	192
Table 8.2 Pre-treatment electric studies with low-frequency RNS and brief MVC	194

Abbreviations

AARS: alanyl-aminoacyl-tRNA synthetase
ABCB7: ATP-binding cassette subfamily B member 7
ABPM: ambulatory blood pressure monitoring
ACGS: Association for Clinical Genetic Science
AChR: acetylcholine receptor
ADM: abductor digiti minimi
AFO: ankle foot orthosis
AFP: alpha-fetoprotein
A-GVGD: Align Grantham Variation and Grantham Deviation
ALS: amyotrophic lateral sclerosis
ANNOVAR: Annotate Variation
APB: abductor pollicis brevis
ARD: ankyrin repeats
ARHGEF10: Rho guanine nucleotide exchange factor 10
ARS: aminoacyl-tRNA synthetase
ARSACS: autosomal-recessive spastic ataxia of Charlevoix-Saguenay
ASD: autism spectrum disorder
ATP: adenosine triphosphate
ATP7A: ATPase copper transporting alpha
ATP7B: ATPase copper transporting beta
BCYM3: brachyolmia type 3
BICD2: bicaudal D homolog 2
BSA: bovine serum albumin
BSCL2: Berardinelli-Seip Congenital Lipodystrophy 2
BVVL: Brown-Vialetto-Van Laere syndrome
BWA: Burrows-Wheeler Alignment Tool
c12orf65: chromosome 12 open reading frame 65
c20orf54: chromosome 20 open reading frame 54
CADD: combined annotation dependent depletion
cDNA: complementary deoxyribonucleic acid
CDSMA: congenital distal spinal muscular atrophy
CEU: Utah residents with Northern and Western European ancestry
Cg69: 69 complete genomic data
CHN: congenital hypomyelinating neuropathy
CI: confidence interval
CIDP: chronic inflammatory demyelinating neuropathy
CK: creatine kinase
CMAP: compound motor unit action potential / compound muscle action potential
CMS: congenital myasthenic syndromes
CMSS: Congenital Myasthenic Syndromes Scale
CMT: Charcot-Marie-Tooth disease
CMT1: Charcot-Marie-Tooth disease type 1, demyelinating form
CMT2: Charcot-Marie-Tooth disease type 2, axonal form
CMT4: autosomal-recessive Charcot-Marie-Tooth disease
CMTNSv2: Charcot-Marie-Tooth neuropathy score version 2
CMTX: X-linked Charcot-Marie-Tooth disease
CNV: copy number variation
COX: cytochrome c oxidase

COXPD7: combined oxidative phosphorylation deficiency type 7
CSF: cerebrospinal fluid
CSMA: congenital distal spinal muscular atrophy
CT: computed tomography
Cx32: connexin 32
3,4-DAP: 3, 4-diaminopyridine
dbSNP: Single Nucleotide Polymorphism Database
DCTN1: dynactin subunit 1
dHMN: distal hereditary motor neuropathy
DHTKD1: dehydrogenase E1 and transketolase domain containing 1
DI-CMT: dominant intermediate Charcot-Marie-Tooth disease
DMSO: dimethylsulfoxide
DNA: deoxyribonucleic acid
DNM2: dynamin 2
dNTPs: deoxynucleotides
ddNTPs: dideoxynucleotides
dSMA: distal spinal muscular atrophy
DSN: Dejerine-Sottas neuropathy
DYNC1H1: cytoplasmic dynein 1 heavy chain 1
ECG: electrocardiogram
EDTA: ethylenediaminetetraacetic acid
EGR2: early growth response 2
EMG: electromyography
ESI-MR: Electrospray Ionisation-Multiple-Reaction
ESP: Exome Sequencing Project
ExAC: Exome Aggregation Consortium
EXOSC3: exosome component 3
FAD: flavin adenine dinucleotide
fALS: familial amyotrophic lateral sclerosis
FATHMM: functional analysis through hidden Markov models
FDAB: familial digital arthropathy-brachydactyly
FDIO: first dorsal interosseous
FGD4: RhoGEF and PH domain containing 4
FIG4: FIG4 phosphoinositide 5-phosphatase
FLAIR: fluid-attenuated inversion recovery
FMN: flavin mononucleotide
FSHD1: facioscapulohumeral muscular dystrophy-1
FUS: fused in sarcoma
GAN: gigaxonin
GAPDH: glyceraldehyde-3-phosphate dehydrogenase
GARS: glycyl-tRNA synthetase
GATK: Genome Analysis Toolkit
GDAP1: ganglioside-induced differentiation-associated protein 1
GDP: guanosine diphosphate
GEM.app: Genomes Management Application
GERP: Genomic Evolutionary Rate Profiling
GH: growth hormone
GHR: growth hormone receptor
GJB1: gap junction beta-1
GPR144: G-protein coupled receptor 144
GST-PTEN: PTEN fused with glutathione S-transferase tag
GTP: guanosine-5'-triphosphate

HARS: histidyl-tRNA synthetase
HDAC6: histone deacetylase inhibitor
HMN: hereditary motor neuropathy
HMSN: hereditary motor and sensory neuropathy
HNPP: hereditary neuropathy with liability to pressure palsies
hnRNP: heterogeneous nuclear ribonuclear protein
HOS: Holt-Oram syndrome
HRP: horseradish peroxidase
HSP: hereditary spastic paraplegia
HSPB1: heat shock protein family B (small) member 1
HSPB8: heat shock protein family B (small) member 8
IgG: immunoglobulin G
IGF1: insulin-growth factor 1
IGHMBP2: immunoglobulin helicase μ -binding protein 2
IIS: insulin/IGF signalling cascade
IPN: inherited peripheral neuropathy
IRDRC: International Rare Diseases Research Consortium
IVIG: intravenous immunoglobulin
JAK: Janus kinase (JAK) pathway
KARS: lysyl-tRNA synthetase
KIF1B: kinesin family member 1B
LDS: lithium dodecyl sulfate
LITAF: lipopolysaccharide-induced tumour necrosis factor- α factor
LRT: Likelihood Ratio Test
MAF: minor allele frequency
MARS: methionyl-tRNA synthetase
MCD: mean consecutive difference
MDA: multiple displacement amplification
MERRF: myoclonic epilepsy with ragged red fibers
MFN2: mitofusin-2
MLPA: multiplex ligation-dependent probe amplification
MME: Matchmaker Exchange
M/MS: Monitoring Mass Spectrometry
MORC2: microorchidia CW-type zinc finger 2
MPZ: myelin protein zero
MRC: Medical Research Council
MRD13: autosomal-dominant mental retardation-13
MRI: magnetic resonance imaging
mRNA: messenger RNA
MSL: multiple symmetric lipomatosis
MTMR2: myotubularin-related protein 2
MTMR13: myotubularin-related protein 13
mTOR: mechanistic target of rapamycin
MVC: maximum voluntary contraction
MUP: motor unit potential
NCBI: National Center for Biotechnology Information
NCS: nerve conduction studies
NDRG1: N-myc downstream regulated 1
NEFL: neurofilament light chain
NGS: next generation sequencing
NHLBI: National Heart, Lung and Blood Institute
NHS: National Health Service

NIH: National Institute of Health
NK: natural killer
NMJ: neuromuscular junction
Nrp1: neuropilin 1
OHS: occipital horn syndrome
PBS: Phosphate Buffered Saline
PCR: polymerase chain reaction
PEG: percutaneous endoscopic gastrostomy
PHTS: PTEN hamartoma tumour syndrome
PI3-K: phosphoinositide 3-kinase
PI(3,4)P2: phosphatidylinositol 3,4-bisphosphate
PIP2: phosphatidylinositol 4,5-bisphosphate
PIP3: phosphatidylinositol 3,4,5-trisphosphate
PMP22: peripheral myelin protein 22
Polyphen2: Polymorphism phenotyping v2
PRD: proline-rich domain
PRSP: phosphoribosylpyrophosphate synthetase I
PTEN: phosphatase and tensin homolog
PVDF: Polyvinylidene fluoride
R&D: Research and Development
RAB7: Ras-related GTP-binding protein 7
RDCRC: Rare Diseases Clinical Research Centre
RhoGEFs: Rho guanine nucleotide exchange factors (RhoGEFs)
RhoGTPase: Rho family of GTPases
RNA: ribonucleic acid
RNS: repetitive nerve stimulation
SACS: saccin
SBF2: SET-binding factor 2
SCA: spinocerebellar ataxia
SDS: sodium dodecyl sulfate
SEDM: spondyloepimetaphyseal dysplasia, Maroteaux type
SFEMG: single fibre electromyography
SH3TC2: SH3 domain and tetratricopeptide repeats 2
SIFT: Sorting Intolerant From Tolerant
SLC25A21: solute carrier family 25 member 21
SLC25A46: solute carrier family 25 member 46
SLC52A2: solute carrier family 52 member 2
SLC52A3: solute carrier family 52 member 3
SMA: spinal muscular atrophy
SMA-FACM: SMA with focal areas of cortical malformation
SMA-LED: spinal muscular atrophy with lower extremity dominance
SMARD1: spinal muscular atrophy with respiratory distress
SMDK: spondylometaphyseal dysplasia, Kozlowski type
SMN: survival motor neuron
SMN1: survival of motor neuron 1
SNAP: sensory nerve action potential
SNARE: soluble N-ethylmaleimide-sensitive factor attachment protein receptor
SNPs: single nucleotide polymorphisms
SNV: single nucleotide variation
SOX10: SRY-box 10
SPG55: autosomal-recessive spastic paraplegia-55
SPSMA: scapuloperoneal spinal muscular atrophy

SPTLC1: serine palmitoyltransferase long chain base subunit 1
STAT5B: signal transducer and activator of transcription 5B
SYT1: synaptotagmin 1
SYT2: synaptotagmin 2
TA: tibialis anterior
TBX5: T-box 5
TCA: tri-carboxylic acid cycle
tRNA: transfer ribonucleic acid
TRPV4: transient receptor potential vanilloid 4
UCSC: University of California, Santa Cruz
UK: United Kingdom
UPLC: Ultrahigh Performance Liquid Chromatography
USA: United States of America
UV: ultraviolet
VCP: valosin-containing protein
VEGF: vascular endothelial growth factor
VEST3: variant effect scoring tool 3
WES: whole exome sequencing
WGA: whole genome amplification
WGS: whole genome sequencing
YARS: tyrosyl-tRNA synthetase

Chapter 1. Introduction

1.1 The inherited neuropathies

The genetic neuropathies are a heterogeneous group of diseases affecting the peripheral nerves either exclusively or as part of neurological or multisystem disorders (Reilly and Shy, 2009). The inherited neuropathy prototype was reported in 1886 with a familial peroneal type of progressive muscle atrophy and was named Charcot-Marie-Tooth disease (CMT) in honour of the three researchers. Over the years, increasing clinical, diagnostic and genetic data have led to the knowledge that the originally described CMT cannot be considered as a single disease but as a collection of hereditary peripheral neuropathies. Inherited peripheral neuropathies, under the umbrella term of CMT, have been acknowledged among the most common genetic neuromuscular conditions with a population prevalence of 1 in 2500 individuals (Reilly *et al.*, 2011).

The improving field of neurophysiology and neuropathology contributed to the detailed phenotyping of the disease, the term hereditary motor and sensory neuropathy (HMSN) was introduced and the basics of the classification were laid by the pioneering work of Dyck (Dyck and Lambert, 1968a, 1968b), Thomas and Harding (Harding and Thomas, 1980). CMT is separable into autosomal-dominant forms, which are historically divided by the median nerve motor conduction velocity findings of below or above 38 m/s into demyelinating (CMT1) and axonal (CMT2) neuropathies respectively and of 25-45 m/s into the intermediate (DI-CMT) neuropathies. Autosomal-recessive inherited forms are labelled as CMT4, while the term for the X-linked forms is CMTX. Alphabetical referencing indicates the historical order of the discovered genetic causes within each of the subtypes (CMT1A, CMT2A, etc.) (Pareyson *et al.*, 2006; Reilly and Shy, 2009; Reilly *et al.*, 2011).

The classical CMT phenotype is characterised by progressive length-dependent muscle atrophy, weakness, areflexia and sensory loss, and leads to specific foot deformities and walking abnormalities. The severity of the symptoms shows highly variable inter- and intrafamilial differences. Typically the disease starts over the first two decades of life but often is only recognised later. Some patients develop severe early childhood-onset forms, congenital hypomyelinating neuropathy (CHN) and Dejerine-Sottas neuropathy (DSN), while others remain asymptomatic until later adulthood (Saporta *et al.*, 2011; Braathen, 2012).

Spinal motor neurons and dorsal root ganglion sensory neurons extend their axons to form neuromuscular junctions (NMJ) and sensory receptors to transfer information to the muscles and from the skin (Gentil and Cooper, 2012; Li, 2012). The peripheral nervous system consists of a complex network of myelinated and non-myelinated nerves (Juárez and Palau, 2012). The myelinated nerve contains the axon, which is serially enwrapped by the myelin sheath generated by highly specialised Schwann cells and interrupted in the nodes of Ranvier to ensure the rapid propagation of action potentials. The myelination process is dependent on the axonal integrity and axonal signals, while the myelinating Schwann cells tightly regulate the axonal structure and transport. These reciprocal interactions between the two cell types are mediated by signal transduction molecules, including MAG, p75, IGF1, integrins and TGF- β . Neuregulin 1 and the ErbB receptors tyrosine kinases signalling pathway have been implicated in the regulation of cell interactions and Schwann cell migration (Niemann *et al.*, 2006; Juárez and Palau, 2012).

The demyelinating neuropathies show neuropathological changes of primarily aberrant myelination (onion bulb or tomacula formation), while predominant axonal loss and degeneration characterise the axonal neuropathies. Regardless of the primary pathology, the manifestation of CMT is largely determined by the length-dependent axonal degeneration. The majority of the inherited neuropathies belong to the demyelinating group, while the pheno- and genotypically more diverse axonal neuropathies form one third of all CMT cases (Saporta *et al.*, 2011; Juárez and Palau, 2012).

CMT is caused by mutation-induced dysbalance and dysfunction of proteins that are necessary for the normal function of the peripheral nerves. The collaboration of these proteins creates a complex network and forms pathways, including the regulation and maintenance of myelin, protein synthesis and degradation, membrane and vesicle dynamics, cytoskeleton formation, axonal transport and stress response, which are all implicated in the pathomechanisms of CMT (**Figure 1.1**). In demyelinating neuropathies the defect primarily targets proteins involved in the structure and function of the myelin sheath (PMP22, MPZ, Cx32, periaxin), in the transcriptional regulation of the myelination process (EGR2, SOX10) and in the intracellular membrane trafficking (SH3TC2, MTMR2/MTMR13, FIG4, LITAF, NDRG1) (Berger *et al.*, 2006; Niemann *et al.*, 2006; Roberts, 2012). Primary neuronal defects and impairment of the axonal transport lead to axonal degeneration (Niemann *et al.*, 2006). The progress in the knowledge of the molecular mechanisms of CMT enabled the introduction of rational experimental treatment approaches, although a targeted therapy in humans has not yet been identified.

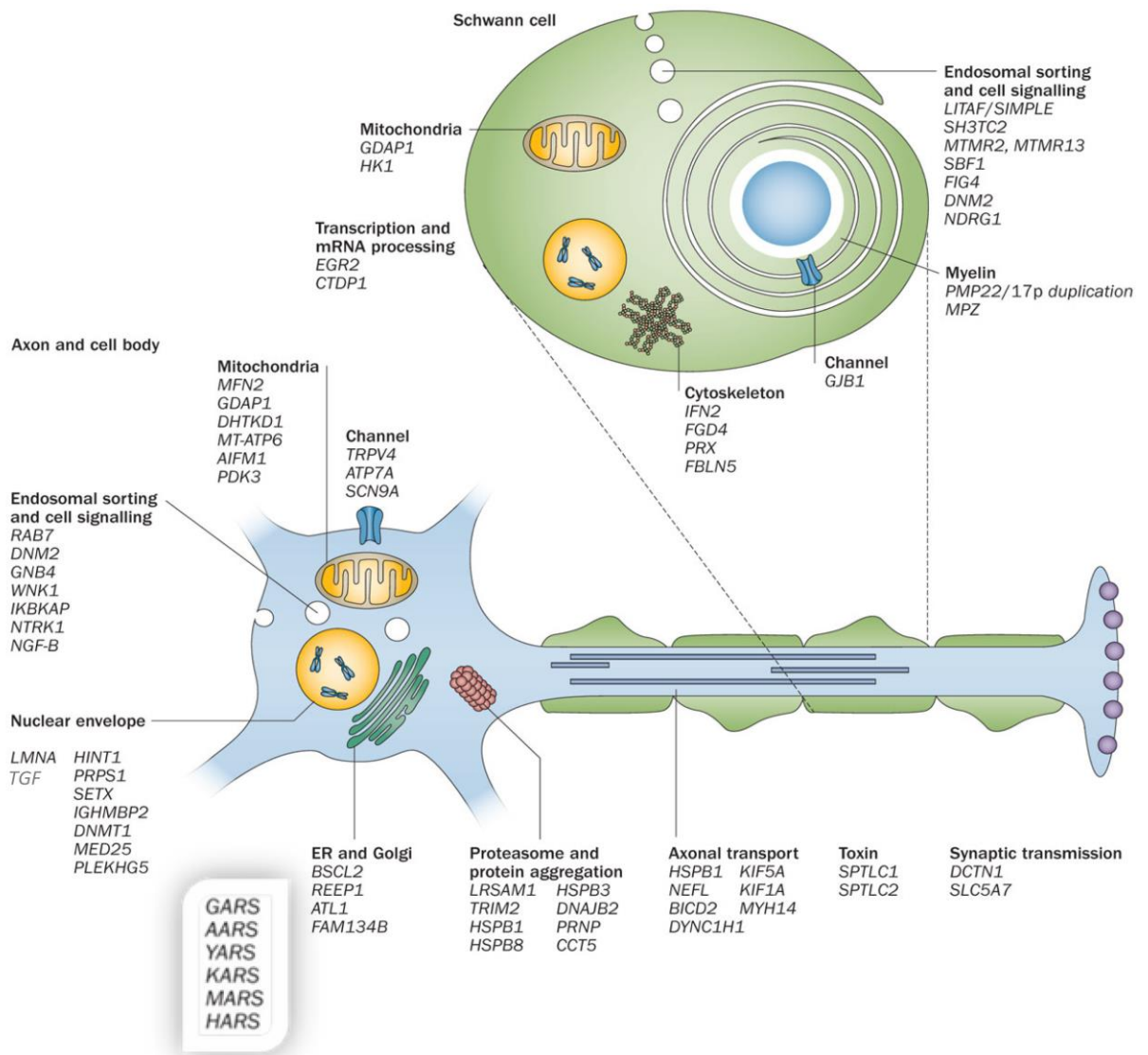


Figure 1.1 Pathways and genes implicated in inherited neuropathies

(taken from Rossor et al., 2013)

The importance of ascorbic acid in the myelination process was underlined by the improved myelination in the demyelinating mouse model treated with vitamin C (Passage *et al.*, 2004). Despite these findings randomised patient trials did not bring a breakthrough in the therapy of CMT1A.

The progesterone antagonist onapristone reduced the toxic overexpression of PMP22 in rodent models and curcumin stimulated autophagy was efficient in mouse models, but the therapies failed in CMT1A patients (Reilly and Shy, 2009; Bouhy and Timmerman, 2013). Recently, the combined application of baclofen, naltrexone and sorbitol has been investigated in a randomised placebo control trial (Attarian *et al.*, 2014). The influence of the neuregulin-1/ErbB system is a promising therapeutic target in CMT1A (Gambarotta *et al.*, 2015; Rossor *et al.*, 2016) and in neuropathies with focal hypermyelination (Bolino *et al.*, 2016).

Furthermore, transcription factors that regulate the PMP22 expression contain TEAD domains and participate in Yap/Taz signalling. Verteporfin, a suppressor of YAP-TEAD complex used in macular degeneration might provide therapeutic potential (Feng *et al.*, 2016; Lopez-Anido *et al.*, 2016). Pharmacological modification of the unfolded protein response and selective inhibition of protein phosphatases are examined in CMT1B animal models (Das *et al.*, 2015; Rossor *et al.*, 2016). Histone deacetylase inhibitor (HDAC6) by reversing the acetylation status of the microtubules and restoring the axonal transport in *HSPB1* and *GARS* mutant mice might serve a targeted therapy of axonal neuropathies (d'Ydewalle *et al.*, 2011 and persona communication Van Den Bosch 2016). The recently described aberrant neuropilin 1 (Nrp1) interaction in *GARS* and other tRNA synthetase-related CMT can also be a future therapy target (He *et al.*, 2015). The gene therapy in CMT faces challenges in the identification of the mutant protein and in developing targeted gene delivery systems (Reilly and Shy, 2009; Bouhy and Timmerman, 2013). Recent gene therapy studies used adeno-associated virus type 9 (AAV9) delivery in *Gars*^{P278KY/+} mice and intrathecal lentiviral delivery in *GJB1* knockout mice (Kagiava *et al.*, 2016 and persona communication Burgess 2016).

1.2 Genetics of the inherited neuropathies

Early linkage studies in 1982 identified the first genetic locus for CMT1 in the Duffy region on chromosome 1 (Bird *et al.*, 1982), which segregated only in some dominant demyelinating families, later grouped as CMT1B. A linkage with chromosome 17 was described in 1989 (Vance *et al.*, 1989) and the locus heterogeneity for CMT1 emerged. The first CMT1 mutation was localised to the chromosomal region 17p11.2-p12 in 1991 (Timmerman *et al.*, 1990) and the duplication of the 17p12 was identified as the cause of CMT1A (Lupski *et al.*,

1991; Raeymaekers *et al.*, 1991). Soon after, the *MPZ* gene was described in CMT1B (Hayasaka *et al.*, 1993) and the *GJB1* gene was associated with CMTX (Bergoffen *et al.*, 1993). This enabled molecular diagnosis in the majority of the demyelinating genetic neuropathies. The most common CMT2 gene, the *MFN2* was reported only 10 years later (Züchner *et al.*, 2004). It has still remained much more difficult to identify a molecular cause in axonal neuropathies. The number of discovered CMT-causing genes has rapidly increased with the introduction of better sequencing technology. More than 1500 mutations in more than 80 genes have been described so far for CMT and related neuropathies (Timmerman *et al.* 2014).

It is critical to establish the genetic diagnosis in CMT to provide patients with a prognosis, genetic counselling and with options for future targeted therapy. The molecular diagnosis is complicated due to the large genetic heterogeneity, the pleiotropic genes causing allelic disorders and due to gene mutations that evoke diseases by both recessive and dominant inheritance (Baets and Timmerman, 2011). The majority of the CMT cases transmitted dominantly or X-linked; while autosomal-recessive inheritance is more frequent in countries with consanguineous marriages. Sporadic cases are more commonly detected not only due to recessive but also due to *de novo* dominant mutations, late-onset disease course and reduced disease penetrance (Reilly and Shy, 2009; Høyer *et al.*, 2014).

Initially, algorithms have been introduced to support the targeted testing of the four common genes (*PMP22*, *GJB1*, *MPZ* and *MFN2*), which were considered to account for a large proportion of genetic CMT (Murphy *et al.*, 2012). Conventional testing methods, based on the clinical and electrophysiology phenotype enabled to identify the molecular cause in 60% of the CMT cases, with higher rates in CMT1.

The next generation technology made it possible to perform parallel sequencing of several genes and to introduce next generation sequencing (NGS) panels that can detect the full spectrum of known CMT mutations (Arnold *et al.*, 2015). The NGS panel testing has a limited capacity in identifying novel genes, but for genes known to be associated with the disease or with overlapping phenotypes it ensures high sequencing coverage. The interpretation is clear by the detection of less variants of unknown significance (Arnold *et al.*, 2015; Lapin *et al.*, 2016).

With the improvement in high-throughput sequencing technologies, the capability of re-sequencing protein-coding gene regions in whole-exome sequencing (WES) enabled the identification of novel disease-associated genes both in research and in clinical settings.

	Targeted gene panels	Whole exome sequencing	Whole genome sequencing
Who	Proband	Proband or Trio	Proband or Trio
Genes sequenced	Genes associated with specific disease Group of disorders with overlapping phenotypes Common clinical features, signaling pathway or protein structure	All ~20,000 genes	All coded genomic DNA No capture required
Analysis focus	Genes specifically in panel	Genes associated with specific disease or clinical feature Genes that are medically actionable (~4600) Genes of unknown significance with suspicious variants (~16,000)	Analysis of both intergenic and intragenic regions Regions known to be associated with disease, include deep intronic variants, rearrangements, copy number variants
Findings	Limited chance for incidental findings Fewer VUS findings	Higher chance of incidental findings Large number of VUS	99 % of genome does not code for genes Much of its functionality is unknown
Phenotype	Specific phenotype or group of disorders	More complex presentation with analysis focused on genes that are specific for symptoms of individual	Complex presentation of an uneasily recognizable disorder where previous panel and WES testing have been unsuccessful
Coverage	Higher coverage than WES Sanger fill-in low cover regions Ancillary tests for pseudogenes, deletions and duplications	Decreased coverage Sanger fill-in focused only on genes associated with proband's features	Decreased coverage of regions difficult to sequence No Sanger fill-in
Yield	Varies by panel	25–28 % (Yang et al. 2013) 50 % (Need et al. 2012)	Unknown 42 % (Gilissen et al. 2014)

Table 1.1 Comparison of the next-generation sequencing based diagnostic methods

(taken from Lapin et al., 2016)

Even though the human exome accounts for only around 1% of the human genome, screening of these protein-coding segments allowed for the detection of mutations responsible for 85% of Mendelian disorders (Montenegro *et al.*, 2011). The diagnostic strategy with the use of WES, which is able to simultaneously screen extensive genetic variations, has changed to primarily focus on the discovery of causal genes in highly heterogeneous diseases such as CMT. The identification of known mutations with atypical clinical phenotypes and the description of novel variants, previously not associated with the disease led to the better understanding of genotype-phenotype correlations (Klein *et al.*, 2014; Drew *et al.*, 2015; Lapin *et al.*, 2016). The possibility of establishing a molecular diagnosis in isolated patients has increased by WES analysis of trios and of unrelated individuals across families throughout the world (Timmerman *et al.*, 2014). Despite the large number of identified novel genes and rare diseases, a molecular diagnostic yield of only 25% was observed by WES analysis in heterogeneous genetic conditions (Yang *et al.*, 2013; Salgado *et al.*, 2016). The main challenge has remained to distinguish disease-causing alleles among the tremendous generated sequence data by cautiously evaluating the pathogenicity of the variants. The limited availability of functional tests, misannotation of variants and non-optimal variant filtering may lead to misinterpretation of mutations and can generate an excess in variants of unknown clinical significance (Bamshad *et al.*, 2011; MacArthur *et al.*, 2014; Timmerman *et al.*, 2014; Arnold *et al.*, 2015; Lapin *et al.*, 2016; Salgado *et al.*, 2016). Further difficulties arise from the technical limitations of insufficient capture, poor uniformity of read depth, incomplete coverage and the inability of WES to detect small tandem repeats, copy number variations and large structural genomic rearrangements (Montenegro *et al.*, 2011; Timmerman *et al.*, 2014; Arnold *et al.*, 2015; Salgado *et al.*, 2016).

Even though whole-genome sequencing (WGS) can mitigate these limitations of the technical performance; the robust data produced by the re-sequencing of the entire genome causes difficulties in the variant classification and in the storage of excessive data (Lelieveld *et al.*, 2015) (**Table 1.1**). Multiple projects developed genome data analysis platforms, such as Genomes Management Application (GEM.app), in order to share large datasets and to discover rare novel genes by screening potentially causative variants across unrelated families (Timmerman *et al.*, 2014; Gonzalez *et al.*, 2015). Currently, the Matchmaker Exchange (MME) project aims to facilitate the identification of cases with similar phenotypic and genotypic profiles (matchmaking) and to enable searches in multiple databases (matchmaker services) (Philippakis *et al.*, 2015). Similarly, the International Rare Diseases Research Consortium (IRDIRC), RD-Connect project provides an integrative platform to link genomic and clinical data in a central research resource for rare diseases (Thompson *et al.*, 2014).

Chapter 2. Objectives and Overview

Among the group of inherited neuropathies, the Thesis focuses on the hereditary motor neuropathies (HMN), where the diverse and overlapping clinical phenotypes arise on a heterogeneous genetic background and the molecular diagnosis is still largely uncovered. The overall aim of the Thesis is to analyse the prevalence and to study the natural history and genetic epidemiology of HMN in a large cohort of patients identified in the North-East of England. A further goal was to discover novel disease-causing genes by implicating next generation sequencing and to identify disease mechanisms, which may provide a target for therapy interventions.

Chapter 3 describes the methods of clinical and electrophysiological data collection and details the series of experimental laboratory techniques that I performed during the study of the Thesis.

In *Chapter 4* the investigated patient cohort is defined with the reviewed HMN classification and epidemiology data is determined for HMN in the North-East of England.

Chapter 5 provides results about the success in the mutation detection rate in the involved patient cohort and analyses the efficacy of the applied genetic methods in HMN. The wide spectrum of the identified genes is discussed based on the framework of common pathways of mechanisms. The findings detailed in these chapters have been recently accepted for publication in *Neurology*. (**Appendix A**)

In *Chapter 6* a series of clinical and experimental studies illustrates the investigation of the natural history of the disease and provides insight into the phenotype-genotype correlations with known HMN-causing genes. Results related to each of the analysed 5 genes of this chapter were all reported in publications in various high impact peer-reviewed journals (Cottenie *et al.*, 2014; Bansagi, Antoniadi, *et al.*, 2015; Bansagi, Griffin, *et al.*, 2015; Evangelista *et al.*, 2015; Bansagi *et al.*, 2016). (**Appendix B, Appendix C, Appendix D, Appendix E, Appendix F**)

Chapter 7 describes a novel presynaptic pathology in a subgroup of distal hereditary motor neuropathy (dHMN) caused by the novel *SYT2* gene, which we have recently published in the *American Journal of Human Genetics* (Herrmann *et al.*, 2014). (**Appendix G**) Furthermore, this chapter discusses novel theoretical pathways, including transcription factor signalling and mitochondrial pathways, in the pathology of HMN, which could be variably supported by performed functional studies.

Finally, in *Chapter 8* the nature of the neuromuscular junction (NMJ) defect is discussed in *SYT2* and *GARS* gene mutations. A potential treatment strategy was investigated in *SYT2* and *GARS* mutant dHMN patients with NMJ defect by the administration of synaptic transmission influencing drugs. Results of the therapy and the unique associated electrophysiological findings have been recently published in *Neurology* (Whittaker *et al.*, 2015).(**Appendix H**)

Chapter 3. Methodology

3.1 Clinical data collection

3.1.1 Patients

Clinical and laboratory data reported in the Thesis have been collected from patients, who attended the specialised Inherited Peripheral Neuropathy service at the Newcastle-upon-Tyne Hospitals NHS Trust. This specialist clinic is one of the main diagnostic centres for inherited neuropathies in the UK, providing medical care and genetic counselling for patients living in North-East England. Patients were referred by primary care physicians or by secondary/tertiary care teams for specialist diagnostic evaluations and for advice regarding the management plan. Patient follow-up was continued in the specialist service once the confirmatory diagnosis was established.

The Medical Research Council (MRC) Centre for Translational Research in Neuromuscular Diseases called for recruitment of clinical research databases to enhance a national cohort for genetic and natural history studies and for experimental trials. In the specialised Inherited Peripheral Neuropathy service at the Newcastle University I was employed as a Clinical Research Associate to identify and recruit patients to the CMT cohort, supervised by Prof Dr Rita Horvath. Patient data from the Newcastle CMT cohort were recorded as part of a natural history study in an internal MRC centre database and were also stored in the database of the National Institutes of Health (NIH) Rare Diseases Clinical Research Centre (RDCRC).

Individual Trust NHS R&D approval was obtained in addition to the MRC ethical approval. The CMT natural history study documentation (MRC 6601) consisted of a Minimal Dataset for Visit Information and for Diagnosis Information and the CMT Neuropathy Score (CMTNSv2) (**Table 3.1**).

I collected data on patients with the hereditary motor neuropathy (HMN), which is presented in the Thesis, from the larger Newcastle CMT cohort. Patient data for the HMN cohort was recorded both retrospectively from medical files and prospectively, when the patient was reviewed in the specialist clinic. Patient information sheets were provided and written informed consent was obtained from all patients. I participated in the deep characterisation of the patient cohort by employing clinical, neurophysiology, genetic and laboratory techniques.

Parameter	0	1	2	3	4	Score	Weighted Score (calculated by DMCC)
Sensory symptoms (1)	None	Symptoms below or at ankle bones	Symptoms up to the distal half of the calf	Symptoms up to the proximal half of the calf, including knee	Symptoms above knee (above the top of the patella)		
Motor symptoms legs	None	Trips, catches toes, slaps feet, shoe inserts	Ankle support or stabilization needed most of the time for ambulation(2)	Walking aids (cane, walker) needed most of the time	Wheelchair most of the time		
Motor symptoms arms	None	Mild difficulty with buttons	Severe difficulty or unable to do buttons	Unable to cut most foods	Proximal weakness (affect movements involving the elbow and above)		
Pinprick sensitivity (3)	Normal	Decreased below or at ankle bones	Decreased up to the distal half of the calf	Decreased up to the proximal half of the calf, including knee	Decreased above knee (above the top of the patella)		
Vibration (4)	Normal	Reduced at great toe	Reduced at ankle	Reduced at knee (tibial tuberosity)	Absent at knee and ankle		
Strengths legs	Normal	4+, 4 or 4- on foot dorsi or plantar flexion	≤ 3 on foot dorsi or plantar flexion	≤ 3 on dorsi or plantar flexion	Proximal weakness		
Strengths arms	Normal	4+, 4 or 4- on intrinsic hand muscles (5)	≤ 3 on intrinsic hand muscles (5)	< 5 on wrist extensors	Weak above elbow		
Ulnar CMAP (Median)	>6mV(>4mV)	4-5.9mV (2.8-3.9)	2-3.9mV (1.2-2.7)	0,1-1.9mV (0.1-1.1)	Absent (Absent)		<input type="checkbox"/> Not Done
Radial SNAP	≥15μV	10 - 14,9 μV	5 - 9,9 μV	1 - 4,9 μV	<1 μV		<input type="checkbox"/> Not Done
CMTSS Subtotal (calculated by DMCC)							
CMTES Subtotal (calculated by DMCC)							
CMTNS Total (calculated by DMCC)							

Notes: (1) Use the picture to discriminate the level of the symptoms; (2) Uses aid most of the time. The patient was prescribed to wear/use or should be wearing/using the aid in the examiner's opinion; (3) Abnormal if patient says it is definitely decreased compared to a normal reference point; (4) Use Rydell Seiffer tuning fork. Definition of Normal: ≥5; (5) Intrinsic hand muscles strength assessment: Test only Abductor Pollicis Brevis (APB) and First Dorsal Interosseus (FDI), then choose the stronger to give the score.

Table 3.1 CMT Neuropathy Score second version (CMTNSv2)

3.1.2 Neurophysiology

Neurophysiology studies have been performed in all patients, who were examined in the specialised neuropathy clinic, apart from the rare clinically uncomplicated cases, when the routine genetic testing for *PMP22* earlier established the diagnosis of the motor and sensory demyelinating neuropathy (CMT1A or HNPP). However, family members of patients with confirmed genetic diagnoses were offered targeted genetic testing before neurophysiology studies were initiated. Some of the clinically affected family members have still undergone neurophysiology testing regardless of the positive genetic diagnosis.

In the majority of the patients the neurophysiology assessment was carried out in the Neurophysiology Department at the Newcastle-upon-Tyne Hospitals NHS Trust by the same expert Neurophysiologist Consultants (Dr Fawcett, Dr Whittaker, Dr Lai and Dr Baker). In other occasions, the referral medical team already arranged electric studies for the patients before they were seen in the specialised clinic or the patients opted for having the test performed at local Neurophysiology services.

I collected the electrophysiology data in the HMN patient cohort presented in the Thesis, by reviewing previous study reports or initial and follow-up electric tests performed mostly by Dr Roger Whittaker. Generally, the neurophysiology investigations consisted of electric motor and sensory nerve conduction studies (NCS) and electromyography (EMG), which provided measurements for the analysis of the parameters discussed in *Chapter 4.3.3*. In some clinically and genetically selected cases additional studies were initiated, including repetitive nerve stimulation (RNS) and single fibre electromyography (SFEMG), in order to investigate the neuromuscular transmission. I accompanied some patients to carry out additional neurological examinations in the electric study setting and I observed the neurophysiology methods of the neuromuscular junction (NMJ) testing, as discussed in *Chapter 8.3.4*.

The studies were performed by the Neurophysiologists on a Dantec Keypoint G4 (UK) EMG machine. Surface electrical stimulation was applied through either CareFusion ring electrodes or a handheld Alpine Biomed bipolar stimulating electrode. Responses were recorded using Natus Neurology disposable disk electrodes (1cm diameter). Amplitudes were measured baseline to peak. SFEMG was performed using Natus Neurology disposable 30G concentric needles with a bandpass of 2 to 10 kHz (Whittaker *et al.*, 2015).

3.2 Laboratory methods

I performed the following computational data analysis and I applied the laboratory methods described in this subchapter on the HMN cohort of the Thesis, unless it is otherwise stated.

3.2.1 Next generation sequencing

3.2.1.1 Inherited Peripheral Neuropathy (IPN) panel gene test

To date, two laboratories (Bristol and Queen Square) offer more comprehensive genetic testing for inherited neuropathies in the UK. The multi-gene panel assay applied in the HMN cohort presented in the Thesis was performed in collaboration with Dr Antoniadi, Dr Greenslade and Dr Forester at the Bristol Genetics Laboratory. Genomic DNA was extracted from the peripheral blood of the patients in the Northern Genetics Service at the Newcastle-upon-Tyne Hospitals NHS Trust and was sent to the Bristol Genetics Laboratory.

When next generation sequencing (NGS) is used to examine specific gene panels and the sample numbers are high, it is more cost-effective and time-efficient to target, capture, and sequence only the genomic regions of interest with developed targeted enrichment methods (Bodi *et al.*, 2013).

Genomic DNA was enzymatically fragmented and enrichment of coding exons and flanking intronic regions was performed using a custom designed 330kbp SureSelect capture (Agilent Technologies), targeting 56 genes associated with inherited peripheral neuropathy (<http://ukgtn.nhs.uk/find-a-test/search-by-disorder-gene/test-service/charcot-marie-tooth-hereditary-neuropathy-54-gene-panel-589/>) (Table 3.2).

Libraries were prepared from genomic DNA according to the manufacturer's protocol (Agilent's SureSelect Target Enrichment System: Product note) and sequenced on an Illumina MiSeq (2x150bp). For data analysis and filtering a bespoke open-source pipeline using Burrows-Wheeler Aligner (BWA) and Genome Analysis Toolkit (GATK) was used to align data to the reference human genome (UCSC hg19). Variant classification was based on Association for Clinical Genetic Science (ACGS) Practice Guidelines (2013). Candidate pathogenic variants were confirmed by Sanger sequencing using an Applied Biosystems 3730 analyser (Bansagi, Antoniadi, *et al.*, 2015).

TABLE 1 Inherited Peripheral Neuropathies - Gene Panel Genetic Testing								
GENE	OMIM	Locus	CMT1	CMT2	HMN	HS(A)N	OMIM	Inheritance
AARS	601065	16q22		CMT 2N			613287	AD
ARHGEF10	608136	8p23	Slowed NCV; hypomyelination				608236	AD
ATL1	606439	14q11-q21				HSN 1D	613708	AD
ATP7A	300011	Xq12-q13			dSMAX3		300489	XL
BAG3	603883	10q26.11	myopathy; myofibrillar, BAG-3 related				612954	AD
BSC12	606158	11q12.3			HMN 5		600794	AD
CCT5	610150	5p15.2				HSN with spastic paraplegia	256840	AR
CTDP1	604927	18q23	CCFDN: Congenital cataracts, facial dysmorphism, neuropathy				604168	AR
DCTN1	601143	2p13.1			HMN 7B		607641	AD
DNM2	602378	19p13.2		CMT DI B/ CMT 2M			606482	AD
DYNC1H1	600112	14q32.31		CMT 2O			614228	AD
EGR2	129010	10q21.1-q22.1	CMT 1D/CMT 4E CHN/ DSS				607678 / 605253	AD / AR
FAM134B	613114	5p15.1				HSAN 2B	613115	AR
FGD4	611104	12p11.21	CMT 4H				609311	AR
FIG4	609390	6q21	CMT 4J				611228	AR
GAN	605379	16q23.2	Giant Axonal Neuropathy 1				256850	AR
GARS	600287	21q22.11		CMT 2D	HMN 5		601472 / 600794	AD
GDAP1	606598	8q21	CMT 4A	CMT 2H/ CMT 2K			608340 / 607706 / 607831	AR/AR/AD
GJB1	304040	Xq13.1	CMT X1				302800	XL
HOXD10	142984	2q31.1	HMSN with Congenital vertical talus				192950	AD
HSPB1	602195	7q11		CMT 2F	HMN 2B		606595/608634	AD
HSPB3	604624	5q11.2			HMN 2C		613376	AD
HSPB8	608014	12q24		CMT 2L	HMN 2A		608673/158590	AD
IGHMBP2	600502	11q13.3			HMN 6		604320	AR
IKBKAP	603722	9q31.3				HSAN 3	223900	AR
KARS	601421	16q23.1	CMT RI B				613641	AR
KIF1B	605995	1p36.22		CMT 2A1			118210	AD
LITAF	603795	16p13.3-p12	CMT 1C				601098	AD
LMNA	150330	1q22		CMT 2B1			605588	AR
LRSAM1	610933	9q33.3		CMT 2P			614436	AD / AR
MED25	610197	19q33.13		CMT 2B2			605589	AR
MFN2	608507	1p35-36		CMT 2A2			609260	AD
MPZ	159440	1q22	CMT 1B/CHN/ CMT DI D	CMT 2I/ CMT 2J			118220 / 605253 / 607791 607677 / 607736	AD
MTMR2	603557	11q21	CMT 4B1				601382	AR
NDRG1	605262	8q24.22	CMT 4D				601455	AR
NEFL	162280	8p21	CMT 1F	CMT 2E			607734/607684	AD
NGFB	162030	1q13.2				HSAN 5, absence of pain	608654	AR
NTRK1	191315	1q23.1				HSAN 4; anhidrosis, insensitivity to pain	256800	AR
PLEKHG5	611101	1p36.31			dSMA 4		611067	AR
PMP22	601097	17p11.2	CMT 1A/ HNPP/ CMT 1E/DSS				118220/162500 118300/145900	AD / AD AD / AR
PRPS1	311850	Xq22.3	CMT X5				311070	XL D/ R
PRX	605725	19q13.1-q13.2	CMT 4F/ DSS				145900	AR
RAB7A	602298	3q21.3		CMT 2B		HSN	600882	AD
REEP1	609139	2p11.2			HMN5B		614751	AD
SBF2	607697	11p15.4	CMT 4B2				604563	AR
SCN9A	603415	2q24.3	Absence of pain/Small fiber neuropathy				243000/133020	AR / AD
SEPT9	604061	17q25.2-q25.3	Hereditary neuralgic amyotrophy, HNS, HNA & symorphic features				162100	AD
SH3TC2	608206	5q32	CMT 4C				601596	AR
SLC12A6	604878	15q14	PN with agenesis of the corpus callosum				218000	AR
SOX10	602229	22q13.1	PCWH syndrome				609136	AD
SPTLC1	605712	9q22.1-q22.3				HSAN 1	162400	AD
SPTLC2	605713	14q24.3				HSAN 1C	162400	AD
TDP1	607198	14q32.11	Spinocerebellar ataxia, with axonal neuropathy				607250	AR
TRPV4	605427	12q24.1		CMT 2C			606071	AD
WNK1	605232	12p13.33				HSAN 2A	201300	AR
YARS	603623	1p13.1	CMT DI C				608323	AD

Table 3.2 Inherited peripheral neuropathy gene panel test

3.2.1.2 Whole-exome sequencing

Exome capture library and whole-exome sequencing

Selected patient DNA samples were subjected to NGS at AROS Applied Biotechnology (Aarhus, Denmark). The enrichment of protein coding exons by DNA hybridisation-capture followed by high-throughput sequencing enables the discovery of disease-causing mutations.

Genomic fragment library was prepared using TruSeq™ DNA Sample Preparation Kit (Illumina Inc., San Diego, USA). The enrichment platform, Illumina TruSeq™ 62 Mbp (Illumina Inc., San Diego, USA) used the denatured single-stranded DNA library hybridised to biotin-labelled probes, which were complementary to the target exome. Enrichment of the targeted region was processed by adding streptavidin beads that bind to the biotinylated probes and the enriched DNA fragments were magnetically eluted for a second enrichment reaction (**Figure 3.1**). The amplified captured fragments (including exonic flanking regions) were sequenced by using the Illumina HiSeq2000 platform (Illumina Inc., San Diego, USA) with paired-end reads of 100 base pair.

The Illumina platform is the cheapest and the required input DNA amount is small for an easy fragment library construction, although the target enrichment efficiency is not the highest. It has a high performance for the coverage of medically interesting rare mutations and with additional sequencing it efficiently detects single nucleotide variations (SNVs) and short insertion/deletions (Bainbridge *et al.*, 2011; Bodi *et al.*, 2013; Shigemizu *et al.*, 2015).

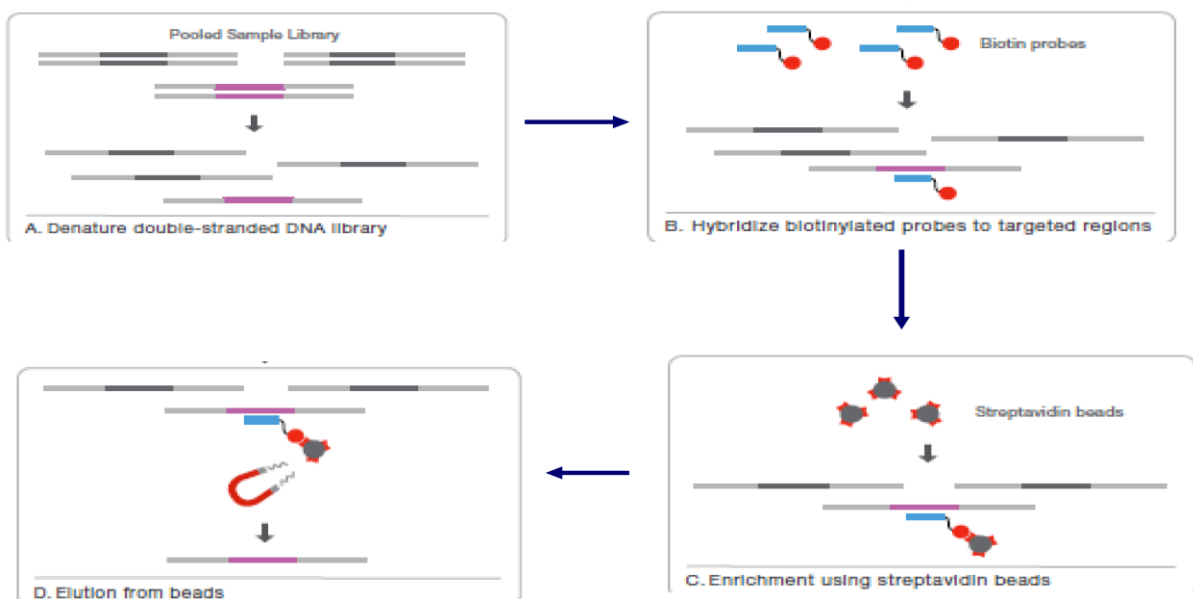


Figure 3.1 TruSeq™ enrichment workflow

(taken from Data sheet: Sequencing, Illumina)

Exome-sequencing data analysis

The sequencing data underwent bioinformatic analysis for sensitivity, specificity, and coverage of the desired regions, which was performed by Dr Helen Griffin in the Institute of Genetic Medicine at the Newcastle University. The NGS data of the HMN cohort was processed by quality control, mapping, variant identification, validation and clinical annotation. The related results will be provided in **Table 5.7** and **Table 5.8** in *Chapter 5.5.2*.

In-house bioinformatic analysis included quality filtering of data and duplicate sequence read removal with FastUniq (H. Xu *et al.*, 2012). Filtered and normalised reads were aligned to the human reference genome (UCSC hg19) with BWA (Li and Durbin, 2009). SNV and small insertion/deletion (indels) calling was performed by Freebayes and variant annotation with ANNOVAR. The small difference in coverage of coding regions directly influences the ability to identify rare variants in the coding regions. Therefore, on-target region coverage, the percentage of targeted bases covered by sequence reads and read-depth, the number of reads that map to the targeted sequence were determined (**Table 5.9**).

I examined the exome data of the HMN patient cohort presented in the Thesis for further on-target variant filtering with the assistance of Dr Helen Griffin. Variants were annotated as exonic/splicing, excluding synonymous variants and rare variants were identified with a minor allele frequency (MAF<0.01) in the context of genotype (heterozygous MAF<0.001; homozygous MAF<0.01). Control data were obtained from several databases downloaded via ANNOVAR (NHLBI_ESP6500, cg69) and also in 281 in-house exomes. By comparison with the Exome Aggregation Consortium (ExAC) database, the rates of rare copy number variations (CNVs) (<0.5% frequency) were investigated in the exome sequencing data (Ruderfer *et al.*, 2016). Protein prediction and evolutionary sequence conservation algorithms downloaded via ANNOVAR were used to define protein altering and/or putative ‘disease-causing’ mutations. Protein prediction algorithms (SIFT, Polyphen2, Mutation Taster, A-GVGD, LRT) were used to analyse the *in silico* effects on protein functioning. Potentially deleterious variants were tested using QIAGEN Ingenuity Variant Analysis. This on-line tool brings multiple biological sources together to help with the filtering challenge in identifying variants. The same interface can be used to construct testable mechanistic hypotheses based on reported biological relationships between genes/variants and the phenotypes (Wendelsdorf and Shah, 2015). We followed the guidelines of the American College of Medical Genetics and Genomics (Rehm *et al.*, 2013).

3.2.2 *Sanger sequencing*

3.2.2.1 DNA sequencing

Selected putative pathogenic variants were confirmed by Sanger sequencing using custom-designed primers and where family members were available segregation analyses were carried out.

Primer designing

Search in Genome browser

The specific gene region of interest was searched by the gene names and exact base pair positions within the chromosomes using the Ensembl Genome Browser website (<http://www.ensembl.org>). Genome browsers provide a graphical interface to extract and summarise information of genomic sequence and annotation data, and promote cross-species comparative analysis. The Ensembl browser contains the most extensive set of gene and transcription-related data and the most extensive presentation of haplotype data (HapMap project) (Furey, 2006; Wang *et al.*, 2013).

Primer selection

The design of primer oligonucleotide sequences specific for the region of interest was assisted by Primer3 (<http://primer3.wi.mit.edu>). Target DNA sequences were uploaded into the online software, which provided primer sequences selected to span the region of interest and specified by the product size, melting temperature and their GC content (%).

Polymerase chain reaction (PCR) amplifying a sequence target requires two primers (forward and reverse) anneal to the 3' ends of the sense and antisense strands. The primers should be long enough to bind complementarily to the target sequence, while needing to be specific to avoid amplifying unwanted regions in the genome. The shorter primers have higher binding efficiency but their specificity is lower. Generally, primers of 18–24 nucleotides in length were selected. A GC content of ~50% of the primers was adjusted to prevent that long stretches of poly(G,C) would increase the chance of mispriming, while high AT content was avoided to prevent unstable pairing (Untergasser *et al.*, 2012; Hung and Weng, 2016).

Primer validating

The generated primer sequences were checked for all possible binding targets using Primer-BLAST (<http://www.ncbi.nlm.nih.gov/tools/primer-blast/>) to exclude chances for mispriming across the genome.

Furthermore, all selected primers were optimised before being applied. A PCR reaction using DNA and negative controls was performed at 3 different temperatures, including the melting temperature advised by Primer3. During a PCR cycle, the primers and the target form a duplex in the annealing step, which requires a lower temperature than the subsequent denaturation step, while the duplex is separated. Therefore appropriate and primer adjusted melting temperatures are required for each PCR reaction (Hung and Weng, 2016).

Polymerase chain reaction (PCR) reaction

The PCR is a powerful method that can amplify a DNA/RNA segment from a small amount of template target sequence. Synthetic oligonucleotides flanking sequences of interest are used in repeated cycles of enzymatic primer extension in opposite and overlapping directions. The introduction of a thermal stable DNA polymerase from the bacterium *Thermus aquaticus* (Taq DNA polymerase) enabled the process to become automatic. Each PCR cycle consists of thermal denaturation of double-stranded target molecules, primer annealing to both strands and enzymatic synthesis of DNA (Vosberg, 1989; Lorenz, 2012).

DNA amplification

The availability of adequate quality and quantity of the genomic DNA is essential for genetic analysis. Although the quantity of DNA in the sample can be determined in ng/ μ l by nanospectrophotometers, the number of molecules (optimal target between 10^4 and 10^7) is more important for a successful PCR.

Whole genome amplification (WGA) has been developed to overcome the limitations of small amounts DNA available from human samples. The multiple displacement amplification (MDA) method does not require high-temperature denaturation to provide a single-stranded template, therefore it reduces DNA degradation and increases the specificity of the amplification (Dean *et al.*, 2002; Wang *et al.*, 2011; Lorenz, 2012).

The REPLI-g ultrafast minikit (Qiagen, Valencia, CA) utilising isothermal MDA with a uniquely processive DNA polymerase was used for the uniform amplification of the whole genomic DNA. The sample DNA was denatured by adding a denaturation buffer and the denaturation was stopped by a neutralisation buffer. A master mix, containing reaction buffer and REPLI-g UltraFast DNA Polymerase was added to the denatured template DNA and an isothermal amplification reaction was processed for 1.5 hours at 30°C.

PCR reaction mixture

The standard PCR reagents that were used included a set of primers designed to the target sequence to be amplified, DNA polymerase (Immolase™ DNA Polymerase, Bioline or MyTaq™ DNA Polymerase, Bioline), a buffer for the specific DNA polymerase, DNA template and sterile water. The advanced formulation of MyTaq Reaction Buffer system already contained the deoxynucleotides (dNTPs) and MgCl₂, which otherwise needed to be added to other DNA polymerase systems (**Table 3.3**).

In each PCR reaction negative control and normal DNA positive control was introduced. When multiple PCR experiments were planned, a mixture of reagents common to all reactions (Master Mix) was initially prepared. All reagents were kept and the set up of the reaction mixture was performed on fresh ice.

Standard MyTaq Protocol			
The following protocol is for a standard 50µl reaction and can be used as a starting point for reaction optimization.			
PCR reaction set-up: All reactions must be set-up on ice.			
5x MyTaq Reaction Buffer		10µl	
Template		as required	
Primers 20µM each		1µl	
MyTaq DNA Polymerase		0.25 - 1µl	
Water (ddH ₂ O)		up to 50µl	
PCR cycling conditions We suggest these conditions in the first instance:			
Step	Temperature	Time	Cycles
Initial denaturation	95°C	1min	1
Denaturation	95°C	15s	25-35
Annealing*	User determined	15s	
Extension*	72°C	10s	
* These parameters may require optimization, please refer to the Important Considerations and PCR Optimization section if needed.			

Table 3.3 Standard MyTaq™ PCR protocol

(taken from Product note, Bioline)

PCR cycling conditions

The cycling times and temperatures varied, dependent on the DNA polymerase and the template characteristics used in the experiment (**Table 3.3**). The reaction started with an initial activation/denaturation at a high temperature, generally for 1 minute. Longer initial denaturation times were required to facilitate complete melting of the DNA. Generally, 25 to 35 rounds of a three-step temperature cycle was the next step, including a short (15-30 seconds) high temperature denaturation, followed by the annealing step at a lower temperature set ideally between 52 °C to 58 °C and an extension step at 72 °C. The final phase of thermal cycling contained an extended elongation period of 10 minutes, which allowed the addition of an adenine residue to the 3' ends of all PCR products. Termination of the reaction was achieved by cooling the mixture down to 4 °C.

Electrophoresis on Agarose gel

PCR products can be detected by loading aliquots of each reaction into wells of an Agarose gel. Orange G loading dye (dH₂O, 15% glycerol, 1% orange dye) was used at a 1:1 ratio to stain the PCR product and usually 6µl was mixed with 6µl PCR product. The stained DNA product was uploaded into a 2% Agarose gel (2g agarose gel in 1xTAE, Tris base Acetic acid and EDTA (Ethylenediaminetetraacetic acid) buffer pH8.0) mixed with 40 µl/100ml of ethidium bromide. The stained PCR product migrated into the gel following electrophoresis for a minimum of 30 minutes at 75V. Gel images were captured on a GelDoc-It 310 Imaging system (UVP). Ethidium bromide intercalated between the bases of the DNA strands and allowed the PCR bands to be visualized under UV light.

Analysis of the PCR bands

Parallel to the PCR products a ready to use molecular weight marker (HyperLadder™ 100 bp, Bionline) was loaded to the gel in order to determine the detected band sizes. If there was a discrete band detected at the expected molecular weight, the PCR product was further processed for sequencing. Occasionally dimer formation of the primers (small bands <100 bp near the bottom) were visible on the gel, indicating self anneal or anneal to the other primer in the reaction. At other times, non-specific PCR bands were detected indicating that the primers were designed to highly repetitive sequences or there was a lack of PCR product. The PCR reaction was then repeated adding dimethylsulfoxide (DMSO) or betaine (N,N,N-trimethylglycine) or both to enhance the PCR amplification of G-C rich targets. Modifications were also applied in the cycling conditions and ultimately designing a new primers pair was required (Lorenz, 2012).

Sequencing

PCR sample clean-up

Amplified samples were subsequently treated with a mixture of two hydrolytic enzymes, exonuclease I (20U/ μ L, Thermo Fisher) and thermosensitive alkaline phosphatase, FastAP (1U/ μ L, Thermo Fisher) for rapid and efficient removal of unincorporated primers and degradation of unwanted deoxynucleotides left from the PCR reaction (Mardis and McCombie, 2016).

The reaction mix of 0.5 μ l ExoI and 1 μ l FastAP with 3 μ l PCR product was loaded to each well of the 96-well plate and incubated at 37°C for 15 minutes, while the reaction was stopped by heating the mixture at 85°C for 15 minutes.

Alternatively purified DNA was recovered from the PCR products on the 2% Agarose gel utilising spin-column (nucleic acid purification column) technology by a commercially available kit (QIAquick Gel Extraction Kit, QIAGEN®) using salt reagents (TAE buffer, Tris acetate/EDTA or TBE buffer, Tris borate/EDTA).

After electrophoresis separated DNA bands were visualised on a UV transilluminator and the desired bands were excised from the gel with sharp scalpel, cautiously removing extra agarose gel. DNA fragments were extracted from the gel by dissolving the gel-slice in 3 volumes (300 μ l to 100mg gel) of chaotropic salt buffer reagent (Buffer QG) at 50°C for 10 minutes. To increase the yield of the DNA fragment one volume of isopropanol was added to the sample. The sample solution was then applied to the QIAquick spin-column to bind the DNA fragments after spinning at 13.000rpm for 1 minute. To remove all traces of agarose, an additional 0.5ml BufferQG was applied with spinning at 13.000rpm for 1 minute. The spin column was washed by using an ethanol containing BufferPE with a two-step spinning at 13.000rpm. Finally, the DNA was eluted in a small volume (30 μ L) of BufferEB and was centrifuged to collect. The received sample was kept immediately on ice and the DNA content was measured by nanospectrophotometer.

Dye-terminator cycle sequencing

Automated large-template DNA sequencing uses fluorescent dyes for the detection of the electrophoretically resolved DNA fragments (Rosenblum *et al.*, 1997). The dyes attach to the terminating ddNTP. The implication of DNA polymerases, which do not discriminate between dNTP and ddNTP, is that false terminations will not be detected and the spectral resolution will be higher with increased brightness (Sanger *et al.*, 1977; Rosenblum *et al.*, 1997; Heiner *et al.*, 1998). Fluorescent cycle sequencing of the PCR products was performed by utilising the dye-terminator cycle sequencing approach (ABI BigDye® v3.1 3130xl

Genetic Analyzer, Life Technologies). A 15µl mixture consisted of 1µl BigDye® Terminator v3.1 (Applied Biosystems), 2µl BigDye® Terminator v1.1/v3.1 5X Sequencing Buffer, 1µl primer (forward or reverse) and 11µl sterile water was added to the ExoFAP reaction already in the 96-well plate, reaching the 20µl final volume for cycle sequencing. An initial denaturation at 96°C for 1 minute was followed by 25 cycles of 96°C for 10 seconds, 50°C for 5 seconds and 60°C for 4 minutes, then the reaction was stopped with cooling down to 4°C.

Ethanol precipitation

Excess dye terminators in sequencing reactions obscure data and can interfere with base calling. Unincorporated dye terminators should be removed prior to electrophoresis by purification methods. Ethanol/EDTA precipitation was carried out in two wash-out steps. Initially 2µl 125mM EDTA, 2µl 3M Sodium acetate and 70µl 100% Ethanol were added to each well of the plate and was incubated for 15 minutes at room temperature. Subsequently, the plate was centrifuged for 30 minutes at 2000g, which was followed by spinning the inverted plate up to 100g. In the second step an additional 70µl 70% Ethanol was added to the wells and the plate was centrifuged at 1650g for 15 minutes, followed by a repeated inverted spin up to 100g. The plate was air dried in dark for 10 minutes and was ready for sequencing or could be stored sealed at -20°C.

Capillary sequencing

Capillary electrophoresis uses a denaturing flowable polymer to separate the fluorescently labelled DNA fragments according to their molecular weight. An optical detection device of Applied Biosystems genetic analysers detects the fluorescence. A minimum of 10µl sample volume was required in the 96-well plate, so that the ends of the capillaries remain submerged in liquid to inject each sample multiple times. Hi-Di™ Formamide (Applied Biosystems) was used to re-suspend the sample to reach 10µl volume. The sample re-suspended in Hi-Di™ was heated for 2 minutes at 97°C and then sequenced with the 3130xl Genetic Analyser.

Data analysis

Raw data were analysed with Seqscape® v2.6 (ThermoFisher) or more preferably with Mutation Surveyor® v4.0.5 (Softgenetics). Reference sequence was created for the region of interest by using the RefSeq database, which was accessible in NCBI resources including Entrez Gene, Map Viewer and BLAST. The sequenced raw files were uploaded to the software and were compared to reference and control negative sequences.

3.2.2.2 cDNA sequencing

RNA isolation

To purify RNA from small amounts of blood or fibroblast cells a commercial kit (RNeasy[®] mini kit, QIAGEN) was used, which utilises a specialised high-salt buffer system to prepare up to 100µg total RNA per sample.

Blood samples collected in specialised RNA tubes were defrosted and 4 ml blood was centrifuged at 3500g for 10 minutes, while the supernatant was discarded by cautious pipetting. The pellets were re-suspended in 5ml RNase free water and centrifuged at 3500g for 10 minutes and the overflow was discarded. The sample was first lysed and homogenised in the presence of a highly denaturing guanidine-thiocyanate-containing buffer (600µl RLT Buffer), which immediately inactivated RNases. When RNA was purified from fibroblast cell lines, which are rich in RNases, then 10µl β-mercaptoethanol was added to the Buffer RLT before use. Subsequently, 70% Ethanol was added to provide appropriate binding conditions and a 700µl sample was then applied to an RNeasy Mini spin column. Total RNA was bound to the membrane and optionally treated with DNase I. Membrane contaminants were washed away in multiple steps using 700µl RW1 Buffer and 500µl ethanol containing RPE Buffer with centrifugation at 11.000rpm for 15 seconds. The high-quality RNA was eluted by adding 30µl RNase-free water and the RNA content was measured by nanospectrophotometer.

Reverse-transcription (RT) PCR

The total RNA extracted from the cells was converted to a single-stranded cDNA by applying the High Capacity cDNA Reverse Transcription Kit (Applied Biosystems). For each reaction a 10µl reaction mix consisted of 2µl 10X RT Buffer, 0.8µl 25X dNTP Mix (100mM), 2µl 10X RT Random Primers, 1µl MultiScribe[™] Reverse Transcriptase and 4.2µl nuclease-free water was prepared and added to the 10µl RNA sample in a 96-well reaction plate. A reverse transcription was performed in a thermal cycler at 25°C for 10 minutes, 37°C for 2 hours, 85°C for 5 minutes and then cooled down to 4°C. The produced cDNA content was measured by nanospectrophotometer, considering that it also measured the primers in the sample. Subsequently, the converted cDNA was validated in a PCR reaction performed with optimised working cDNA primer pairs and by using negative control and genomic DNA as a positive control.

RT-PCR amplification required designing primers, complimentary with the cDNA sequence of the genomic region of interest. The PCR and sequencing processes were carried out according to the same protocol described earlier in *Chapter 3.2.2.1*.

3.2.3 *Functional protein studies*

3.2.3.1 **Fibroblast cell line culture**

Punch skin biopsies were taken after ethical approval and informed consent from controls and patients using standard techniques. The tissue was stored in culture medium and fibroblasts were obtained for further studies and stored at -80°C in the Biobank at the Institute of Genetic Medicine, Newcastle University.

The human primary fibroblasts were grown in plastic flasks (CELLSTAR[®], Greiner Bio-One International, T25, 25 cm² Item No: 690175 and T75, 75 cm², Item No:658175) in 1x Dulbecco Modified Eagle Medium (DMEM) (Gibco[®]), which was additionally supplied with 50ml 10% FBS (F7524, Sigma), 5ml 1% Pen/Strep (10,000U/mL, Gibco[®]), 5ml DMEM Vitamin Solution 100x (11120-037, GIBCO), 5ml Sodium Pyruvate (S8636, SIGMA), 5ml Non-essential Amino Acids 100x (11140-035, GIBCO), 5ml L-Glutamine 200mM 100x (25030-024, GIBCO) and 1ml Uridine 25mg/ml (U3003, SIGMA).

Frozen aliquots of fibroblasts were thawed and diluted in 5 ml culture media in a T25 flask, mixed gently and cells were checked under light microscope for viability. The fibroblast containing flasks were incubated under standard sterile culture conditions in a 5% CO₂ incubator at 37°C. Soon, when the cells attached, the medium containing DMSO was removed and replaced with 5 ml of fresh DMEM media. Once a confluent cell monolayer was seen under the light microscope, fibroblasts were dissociated with 0.05M Trypsin-EDTA 10x (15400-054, GIBCO) and were diluted in 10 ml culture DMEM medium in a new T75 flask. During the incubation of the cells intermittently the culture DMEM medium was changed, using autoclaved water dissolved PBS (Oxoid Ltd., BR0014G). In order to grow a larger amount of cells, once a confluent monolayer was achieved in the T75 flask, fibroblasts were dissociated using Trypsin-EDTA and were split into new T75 flasks containing fresh DMEM media.

The fibroblast cells grown for further protein immunoblotting were detached by Trypsin-EDTA and were transferred into a 15 ml falcon tube to spin at 1300rpm for 5 minutes. The supernatant was cautiously removed and the pellet was stored at -20°C until further manipulation.

Alternatively, the grown fibroblast cells were frozen down for future growth by using a freezing media (90% Fetal Bovine Serum and 10% DMSO), which was added to the pellets and stored in cryovials at -80°C.

3.2.3.2 Western blot

Protein extraction

Total protein was isolated from cell lysate supernatants by solubilising fibroblast cells dependent on pellet size in a 30µl / 80µl RIPA buffer (Radio Immuno Precipitation Assay buffer) containing 50mM Tris HCl pH8, 1mM EDTA, 150mM NaCl, 0.5% sodium deoxycholate, 0.1% SDS (sodium dodecyl sulphate) and 1% NP-40. After incubation for 10 minutes at 4°C cells were frozen-thawed twice and the insoluble pellet was removed by centrifugation at 4°C 13.000 rpm for 10 minutes.

Determination of protein concentration

The protein concentration of the supernatant was determined by Bradford Protein Assay utilising the Coomassie blue G-250 dyeing system, which indicates protein binding with colour change. This can be measured at 595 nm with the Infinite® F50 (Tecan) plate reader spectrometer. Standard serial dilutions were prepared using control bovine serum albumin (BSA, 1µg/µl) at concentrations of 0µg/ml; 0.1µg/ml; 1µg/ml; 3µg/ml; 5µg/ml; 10µg/ml; 15µg/ml by adding 200µl Bradford reagent (BioRad Protein Assay Solution) and sterile water up to 1 ml. From the sample protein 1µl was added to 200µl Bradford reagent and 799µl deionised water. The concentrations were measured and absorbance readings of the standards determined a standard curve, where the actual absorbance value of the sample protein could be plotted and the protein concentration in µg/µl could be determined.

Preparation of protein sample

Antibodies recognise only small epitopes of the protein. In order to enable access to this protein region of interest, the complex protein structure needs to be unfolded by denaturation using a loading buffer and an anionic denaturing agent. A total of 20µg and 25µg sample/control protein was planned to upload for electrophoresis and the necessary protein volumes were calculated based on the Bradford assay. A total volume of 10µl mixture was prepared by adding 2.5µl NuPAGE® LDS Sample Buffer (4x; Life technologies), 1µl NuPAGE® Reducing Agent (10x) to the necessary volumes of the proteins made up with deionised water. The samples were then boiled at 70°C for 10 minutes.

Electrophoresis

The electrophoresis is a standard method to separate proteins according to their molecular weight. Both sample and control proteins were loaded at a 20µg and 25µg amount into a 4-12% SDS polyacrylamide gel (NuPAGE® Bis-Tris Mini Gel, Novex®) along with protein

molecular weight ladders, Biotynilated Protein Ladder (#7727, CellSignal) and SeeBlue[®] Plus2 Pre-stained Protein Standard (Novex[®]). The electrophoresis tank was filled with a 20 times diluted NuPAGE[®] MES SDS Running Buffer (20X) (Novex[®]) as running buffer and 500µl of NuPAGE[®] Antioxidant (Novex[®]) was added to the internal chamber of the tank. Samples, accompanied by the markers, were run on the gel for 40-50 minutes dependent on the molecular weight under 150V.

Protein transfer

Proteins were transferred to a PVDF membrane with an iBlot[®]2 PVDF Mini transfer stack (ThermoFisher) according to the manual protocol. For proteins with smaller molecular weight the transfer time was reduced to 5 minutes from the generally used 7 minutes. The success of the protein transfer was visualised by detecting the protein bands with Ponceau Red staining (2% Ponceau S in 30% trichloroacetic acid and 30% sulfosalicylic acid).

Antibodies incubation

The membrane was thoroughly washed with the blotting buffer, TTBS (20 ml 1M Tris HCl pH 7.5, 29.2g NaCl, 1ml Tween[®] (Sigma) made up to 1L dH₂O). To avoid non-specific binding of the antibodies, the membrane was blocked with 5% non-fat dry milk (5g non-fat milk powder per 100ml of Tris HCl Buffer Saline Tween20 (TBST) buffer) for 1 hour at room temperature. Antibody solutions were prepared by appropriate dilution of the relevant primary/secondary antibodies in 5% milk in blotting buffer (TTBS). The membrane was incubated in the antibody solution containing the primary antibody at 4°C overnight. Subsequently, the membrane was washed with 3 or more changes of blotting buffer for 30 minutes at room temperature. Then the membrane was incubated in the antibody solution containing HRP-conjugated secondary antibody for 1 hour at room temperature.

Blot development

Following a thorough wash with 5 or more changes of blotting buffer for 30 minutes, the membrane was developed with a chemiluminescent detection method. The membrane was incubated for 5 minutes in the dark with a Clarity[™] Western ECL Blotting Substrate peroxide solution and luminol/enhancer solution (Bio-rad). The chemiluminescence signal was detected and transformed into a digital image by the Amersham Imager 600 (GE Healthcare Life Science). To analyse the blot, GAPDH was used as a loading control for normalisation. The membrane was incubated with anti-GAPDH antibody at 4°C overnight and the membrane was developed and detected as described above.

Chapter 4. Identifying the patient cohort and clinical classification of the hereditary motor neuropathies

4.1 Hereditary motor neuropathies and the revised nosology

The hereditary motor neuropathies (HMN) encompass clinically and genetically heterogeneous groups of disorders characterised by lower motor neuron weakness due to the involvement of spinal motor neurons and motor axons in the peripheral nervous system (Irobi *et al.*, 2006; Dierick *et al.*, 2008; Rossor *et al.*, 2012). The last population survey from North-East England in 1979 estimated the prevalence of hereditary motor neuropathies around 10% among spinal muscular atrophy cases (Pearn and Hudgson, 1979). Later in the same region the cumulative incidence of CMT was identified as 11.8 per 100.000 inhabitants (Norwood *et al.*, 2009; Foley *et al.*, 2012).

The classical phenotype of the distal hereditary motor neuropathy (dHMN) is a length-dependent motor weakness and atrophy, initially affecting the intrinsic feet muscles and the peroneal compartment of the leg (Jonghe *et al.*, 1998). Foot deformities, such as pes cavus and clawing of the toes are frequently seen in conjunction with dHMN. The majority of the cases show a slowly progressive disease course gradually involving the more proximal leg muscles and/or affecting the intrinsic hand muscles. Congenital non-progressive conditions have been described as congenital distal spinal muscular atrophy (CDSMA) (Fiorillo *et al.*, 2012). Other congenital- or infantile-onset forms with lower limb involvement and static or very slow disease progression were grouped in the entity of spinal muscular atrophy with lower extremity dominance (SMA-LED) (Harms *et al.*, 2012). Various ages of onset, varying clinical course and accompanying neurological features complicate the phenotypes further and serve as a basis for disease classification. Primary or predominant upper limb manifestation, upper motor neuron and bulbar symptoms, isolated cranial nerve involvement, respiratory impairment, skeletal and hip dysplasia may be essential clues to establish a phenotype led molecular diagnosis (Bansagi *et al.*, 2017).

In respect of the concept that CMT and related disorders present a clinical continuum from pure sensory along sensorimotor toward pure motor neuropathies, dHMN could be acknowledged as the pure motor endpoint of the CMT spectrum. However, there is still a debate to what extent the involvement is always exclusively motor, as many forms of dHMN clinically show minor sensory changes (Irobi *et al.*, 2006; Rossor *et al.*, 2012). A considerable clinical and genetic overlap exists between axonal CMT (CMT2) and dHMN. Different

mutations in the same gene can cause both allelic phenotypes (Dierick *et al.*, 2008). It has still remained difficult to distinguish clinically between the two entities and the differentiation continues to rely on the presence or absence of sensory electric nerve changes, regardless of the presence of clinical sensory deficits (Jonghe *et al.*, 1998). In addition, detailed neurophysiology studies revealed somatosensory abnormalities in patients complaining about sensory symptoms, suggesting proximal sensory pathway changes alongside normal peripheral sensory nerve tests (Devic *et al.*, 2012).

Furthermore, dHMN is also referred to as distal spinal muscular atrophy (dSMA) emphasizing the hypothesis that the primarily pathology resides in the lower motor neurons and classifying it as a separate disease entity within the group of hereditary motor neuropathies (Irobi *et al.*, 2006; Rossor *et al.*, 2012). This presumption might be supported by the combined upper and lower motor neuron involvement in some dHMN patients. An increasing number of identified dHMN-related genes is also causative for overlapping motor neuron diseases, including amyotrophic lateral sclerosis (ALS), hereditary spastic paraplegia (HSP), spinal muscular atrophy (SMA) and Kennedy's disease (Irobi *et al.*, 2006; Van Den Bosch and Timmerman, 2006; Rossor *et al.*, 2012) (**Figure 4.1**).

4.2 Aims

I designed a longitudinal population based study to investigate the epidemiology, clinical and electrophysiology features of hereditary motor neuropathies and to review the classification.

4.3 Methods

4.3.1 Patient recruitment

Patients suffering from motor and sensory neuropathy symptoms were referred either directly or after general neurology investigations to the specialised clinic for inherited peripheral neuropathies at the Institute of Genetic Medicine, Newcastle University. Referrals were accepted from the catchment area of Newcastle-upon-Tyne Hospitals NHS Trust (Northumberland, Durham, Cumbria, parts of Yorkshire and Lancashire) and were analysed over a period between 2010 and 2015. Jointly with the clinical service, a specialist research laboratory, as part of the Medical Research Council for Neuromuscular Research UK, is run for research based investigations of CMT. Therefore this service is well placed to provide representative epidemiologic data about CMT and related disorders in the North-East of England.

DISEASE	TRAIT	CLINICAL PHENOTYPE	GENE
dHMN type I	AD	Juvenile onset, lower limb + sensory deficit → CMT2F/CMT2L	HSPB1, HSPB8 DYNC1H1
dHMN type II	AD	Adult onset, lower limb + sensory deficit → CMT2F/CMT2L	HSPB1, HSPB8 BSCL2, HSPB3, FBXO38
dHMN type III	AR	Chronic form	Unknown
dHMN type IV	AR	Chronic form + <i>diaphragm palsy</i>	Unknown
dHMN type V	AD	Upper limb onset/predominance + sensory deficit → CMT2D	GARS BSCL2
dHMN type VI	AR	Infancy, SMA, respiratory distress, <i>SMARD1</i>	IGHMBP2
dHMN type VII	AD	Adult onset, lower limb + <i>vocal cord palsy</i>	DCTN1, TRPV4 Unknown
X linked dHMN	X	Distal onset	ATP7A
dHMN +pyramidal	AD AR	Jerash ethnicity	SETX, BSCL2, HSPB1, DCTN1
Congenital dSMA/SMA-LED	AD	At birth, distal onset, arthrogryphosis	TRPV4, BICD2, DYNC1H1

Rossor AM *et al*,
JNNP 2012

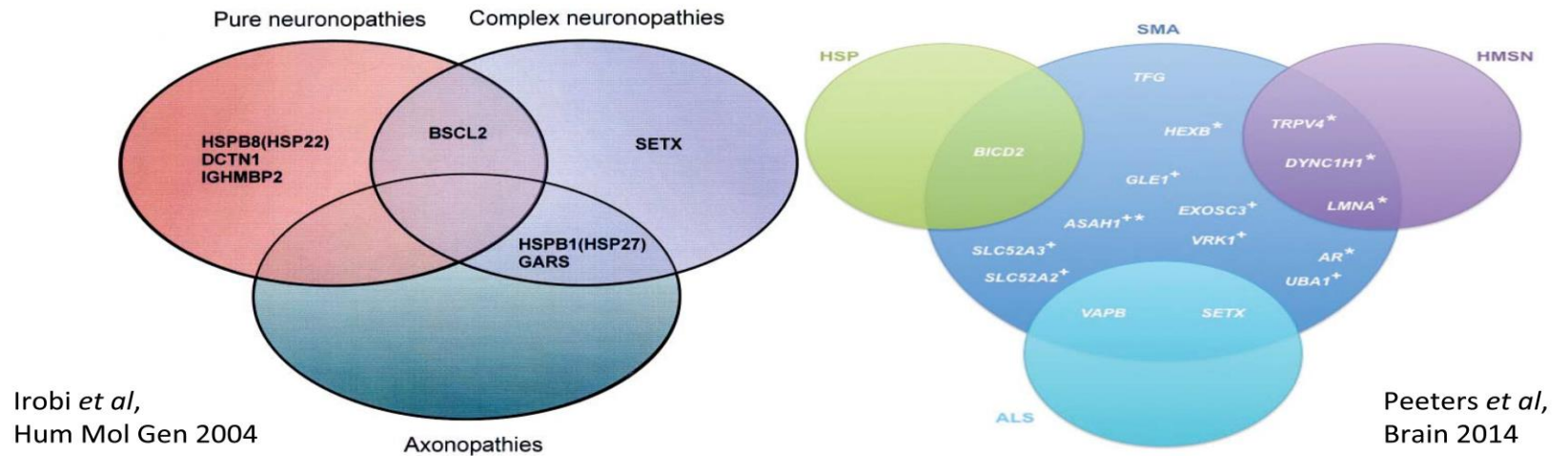


Figure 4.1 Classification of dHMN

4.3.1.1 Inclusion and classification criteria

Patients presenting hereditary motor neuropathies were exclusively included in the study. They were selected from the individuals we diagnosed with genetic neuropathies among the total referrals. All selected patients were further classified based on detailed family and clinical history, physical examination, neurology and electrophysiology findings into one of the overlapping groups of pure dHMN (*dHMN*), motor predominant CMT2 (*motor CMT2*) and complex motor neuron- or neuropathies (*HMN plus*).

Diagnosis of the *dHMN* group relied on the predefined set of clinical criteria, suggested by the 2nd European CMT Consortium, with preserved sensory nerve studies and normal or reduced compound motor unit action potentials (CMAP) and/or neurogenic changes on needle EMG examination (Jonghe *et al.*, 1998).

Patients with dHMN phenotype but presenting decreased sensory action potentials (SNAP) indicative of an accompanying sensory axonopathy were grouped as *motor CMT2*.

We considered *HMN plus* when the hereditary motor neuropathy was accompanied by other neurological complications, e.g. upper motor neuron and/or cranial nerve involvement, extrapyramidal disorder or cerebellar symptomatology.

All participants provided written informed consent to be involved in the clinical and genetic studies, which were performed according to standard protocols approved by local research ethics committees.

4.3.1.2 Exclusion criteria

Acquired neuropathy causes were excluded in all study patients applying a wide range of investigations. According to the clinical features, we performed specific laboratory tests for antibodies and immunological abnormalities, metabolic studies for acyl-carnitines, very long chain fatty acids, serum and urinary amino acids and organic acids, alpha-fetoprotein, neuroimaging, nerve and/or muscle biopsies.

4.3.2 Statistic evaluation

The distribution of patients among the proposed clinical subgroups was determined in percentage (%) of patients diagnosed with hereditary motor neuropathies.

The epidemiology of distal hereditary motor neuropathy (dHMN) was further analysed by determining the frequency as a percentage (%) of patients seen with inherited neuropathy in the referral centre between 2010 and 2015. The prevalence of dHMN was determined as the number of affected individuals per 100.000 inhabitants in the population of North-East England estimated by the 2011 UK census. The amount of uncertainty associated with our

sample estimate of the population parameter was described by confidence interval. The confidence interval (CI) was calculated based on the sample size (population size by 2011 UK census) and based on the number of positive results (number of patients diagnosed with dHMN) when the desired level of confidence was adjusted at 0.95.

4.3.3 Neurophysiology studies

Electrophysiology studies were analysed in patients, where previous results were available and/or new tests were initiated in order to evaluate actual concomitant electric findings. Conduction velocities and action potential amplitudes were determined on motor and sensory nerve testing while qualitative and quantitative analysis of motor unit potentials (MUP) and features of spontaneous activity were assessed on electromyography. Interpretation of the measured parameters provided basis for patient classification into the established study groups.

The electrophysiology tests were performed according to standard techniques as described in *Chapter 3.1.2* and they were reported by the same expert Neurophysiologist Consultants (Dr Whittaker, Dr Lai and Dr Baker) at the Neurophysiology Department, Newcastle-upon-Tyne Hospitals NHS Trust. Patients unavailable for testing at Newcastle-upon-Tyne Hospitals NHS Trust were referred and tested in local Neurophysiology services. Electrophysiology studies were not carried out in genetically identified family members, if they were unwilling or uncomfortable to undertake study testing.

4.4 Results

4.4.1 Distribution and presentation of patients among classified clinical subgroups

All together 461 patients were diagnosed with genetic neuropathy from the total referrals between 2010 and 2015 to the specialist inherited neuropathy clinic at the Institute of Genetic Medicine, Newcastle University. According to the study criteria, we included 105 patients from 73 families presenting either with length-dependent distal, predominantly motor symptoms or with distal motor neuropathy as part of a more complex clinical syndrome. A total of 64 patients from 40 families were compatible with the defined criteria of the *dHMN* diagnosis. Clinical manifestation of motor neuropathy with accompanied sensory changes on electric nerve testing enrolled 16 patients from 10 families in the *motor CMT2* group. A further 25 patients from 23 families were classified into the *HMN plus* group showing complex neuropathology and overlapping symptoms between the previous entities.

	Patients	Family	Patient distribution			Positive diagnostic genetic test			Genetic diagnosis in families			Mutation detection rate		Summary detection rate
	Number	Number	Phenotype	M/F	Age onset	Target test (total 296)	Panel test (total 46)	WES (total 40)	Confirmed genes	Possible genes	Unknown	Confirmed	Possible	Confirmed + Possible
dHMN	64	40	60.9%	39/25	16y	3/169	5/25	9/22	13	4	23	32.5%	10%	42.5%
motor CMT2	16	10	15.2%	11/5	23.8y	0/40	6/10	1/3	7	-	3	70%	-	70%
dHMN plus	25	23	23.8%	20/5	17.6y	2/87	1/11	8/15	6	5	12	26%	21.7%	47.7%
Summary	105	73	100%	70/35	17.6y	5/296	12/46	18/40	26	9	38	35.6%	12.3%	47.9%

Abbreviations: M, male; F, female; y, years

Table 4.1 Phenotype statistics, efficacy of genetic methods and mutation detection rate in the classified patient subgroups

(Bansagi *et al.*, 2017)

There was a male predominance in all phenotype groups. Clinical symptoms started at a significantly younger age in the *dHMN* (mean age onset: 16 years) and *HMN plus* groups (mean age onset: 17.6 years) compared to the *motor CMT2* (mean age onset: 23.8 years) (**Table 4.1**). The main inheritance pattern was autosomal-dominant in *motor CMT2* families while autosomal-recessive and X-linked inheritance were more frequent in the group of *HMN plus*. The *dHMN* group consisted of an almost equal large number of dominant families (n=16) and ‘isolated’ patients with negative or unavailable family history (n=20), while clearly recessive cases were in minority.

4.4.2 Epidemiology of hereditary motor neuropathy in the investigated patient cohort

The frequency distribution of patients belonging to the groups of *motor CMT2* (16/105) and *HMN plus* (25/105) was 15.2% and 23.8% of the cohort, respectively. According to our preset inclusion criteria 64 out of 105 patients (60.9%) received the diagnosis of distal hereditary motor neuropathy (*dHMN*), which accounted for 13.8% (64/461) of all patients diagnosed with inherited neuropathy in the specialist clinic between 2010 and 2015 (**Table 4.1**).

Considering that the population of North-East England (Northumberland, Durham, Cumbria, parts of Yorkshire and Lancashire) is estimated at 2.99 million people (2011 UK census), which is the catchment area of the referral centre, the prevalence of *dHMN* was calculated as 2.14 affected individuals per 100.000 inhabitants (95% CI: 1.62-2.66) (**Figure 4.2**).

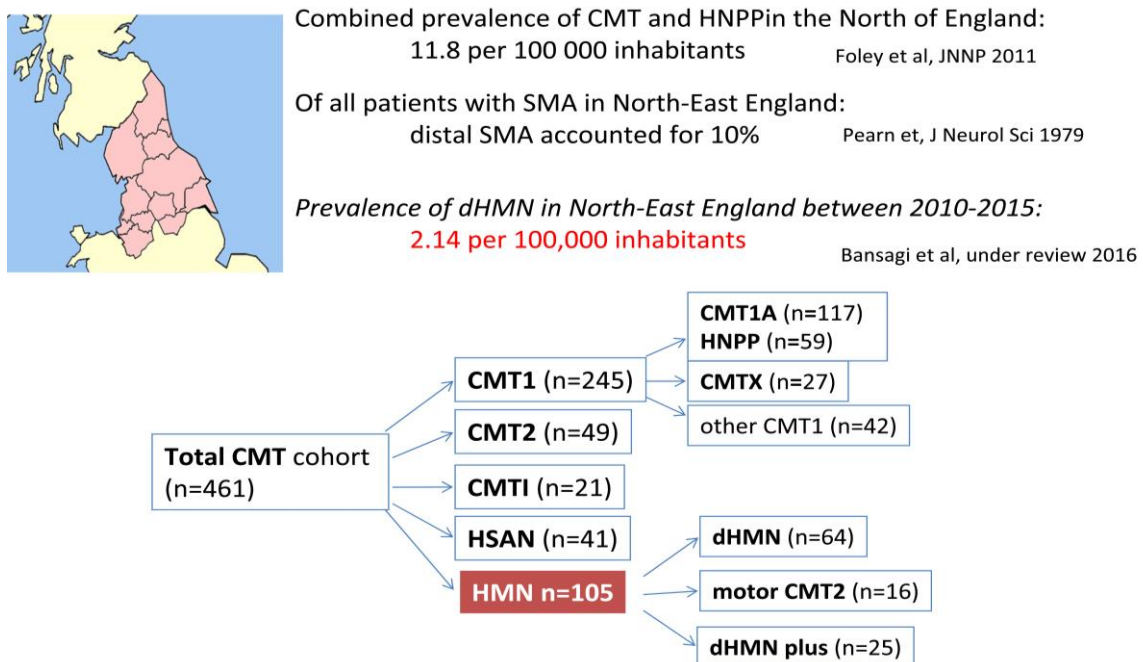


Figure 4.2 Statistic of the hereditary motor neuropathy cohort

4.4.3 Neurophysiology analysis in the clinical subgroups

Electrophysiology data were available for evaluation in 96 patients. Ninety-two patients were examined at the Newcastle-upon-Tyne Hospitals NHS Trust, while 4 patients had the test performed at different hospitals and detailed parameter values could not be gathered.

Genetically diagnosed 9 patients from 7 families did not undergo electric nerve studies.

Motor and sensory nerve conduction parameters are highlighted in selected 60 patients (36 dHMN, 12 motor CMT2, 12 HMN plus), where we could identify pathogenic or likely causative genetic mutations (**Table 4.2; Table 4.3; Table 4.4; Table 4.5; Table 4.6**).

4.5 Discussion

4.5.1 Epidemiology of hereditary motor neuropathies in North-East England

Although hereditary motor neuropathies are suggested to be rare, we diagnosed HMN in 105 patients from 73 families of North-East England origin. We determined the minimum prevalence of dHMN in the same population, which was calculated as 2.14 affected individuals per 100.000 inhabitants (95% CI: 1.62-2.66). There has been no recent data reported on the prevalence of dHMN. In comparison to earlier findings that the point prevalence of spinal muscular atrophy was 1.87/100.000 in the same region in 2009 (Norwood *et al.*, 2009) and a previous study estimated the occurrence of dHMN around 10% among spinal muscular atrophy cases, the minimum prevalence of dHMN in our cohort was significantly higher (**Figure 4.2**).

4.5.2 Phenotype classification of hereditary motor neuropathies

The motor predominant manifestation in *dHMN* and *motor CMT2* patients caused diagnostic difficulties solely on clinical findings and required precise neurophysiology assessments for the differentiation. However, *dHMN* is strictly considered as the pure motor end of the CMT spectrum, many patients show minor sensory abnormalities (Irobi *et al.*, 2006; Rossor *et al.*, 2012). Furthermore, the identification of pathogenic mutations in the same genes in dHMN and motor CMT2, which will be discussed in *Chapter 5*, support that dHMN should not be classified as a different disease group. We suggested that dHMN should be considered clinically as a subcategory of CMT.

The phenotype and inheritance based classification of dHMN delineated by Harding has remained the prevalent framework we followed. However, it has become apparent that it is warranted to complete these previous categories with new clinical and molecular knowledge (**Figure 4.1**) (Harding, 1992; Rossor *et al.*, 2012).

Family / Patient / Age / Sex	Gene	Nucleotide / Amino acid change	n.med CMAP (mV)	n.med MNCV (m/s)	n.uln CMAP (mV)	n.uln MNCV (m/s)	n.peron CMAP (mV)	n.peron MNCV (m/s)	n.tib CMAP (mV)	n.tib MNCV (m/s)	n.med SNAP (uV)	n.med SNCV (m/s)	n.uln SNAP (uV)	n.uln SNCV (m/s)	n.rad SNAP (uV)	n.rad SNCV (m/s)	n.sur SNAP (uV)	n.sur SNCV (m/s)
F1 / P1 26y / f	HSPB8	c.421A>G p.Lys141Glu	n/a	n/a	n/a	n/a	n/a	n/a	n/a	n/a	n/a	n/a	n/a	n/a	n/a	n/a	n/a	n/a
F2 / P2 36y / m	GARS	c.647A>G p.His216Arg	0.6	46	11	54.2	0.4	NR	0.4	NR	8.4	47.1	5.1	54	6.7	48.3	14	36
F2 / P3 66y / f	GARS	c.647A>G p.His216Arg	0.2	39.7	11.5	50	NR	NR	NR	NR	3.5	48.4	6.5	48.1	6.1	41.7	0.1	32.3
F3 / P4 51y / f	GARS	c.1528A>C p.Lys510Gln	15.1	55.9	10.5	59.3	2.4	47.9	n/a	n/a	13	63	11	54.8	n/a	n/a	36	58.1
F3 / P5 28y / f	GARS	c.1528A>C p.Lys510Gln	n/a	n/a	n/a	n/a	n/a	n/a	n/a	n/a	n/a	n/a	n/a	n/a	n/a	n/a	n/a	n/a
F3 / P6 9y / f	GARS	c.1528A>C p.Lys510Gln	11.5	59.3	n/a	n/a	4.3	55.8	n/a	n/a	n/a	n/a	n/a	n/a	n/a	n/a	38	43.9
F4 / P7 46y / f	SYT2	c.923C>T p.Pro308Leu	9.4	60	11.2	62	2.1	46	8.2	49	15	50	12	54	16	54	16	50
F4 / P8 29y / f	SYT2	c.923C>T p.Pro308Leu	3.8	64	4.6	n/a	0.5	42	3.5	41	29	51	19	51	n/a	n/a	19	40
F4 / P9 8y / m	SYT2	c.923C>T p.Pro308Leu	6.8	n/a	n/a	n/a	n/a	n/a	n/a	n/a	n/a	n/a	n/a	n/a	n/a	n/a	n/a	n/a
F4 / P10 17y / m	SYT2	c.923C>T p.Pro308Leu	8.2	n/a	10.6	n/a	2	n/a	n/a	n/a	n/a	n/a	n/a	n/a	n/a	n/a	n/a	n/a
F4 / P11 43y / m	SYT2	c.923C>T p.Pro308Leu	n/a	n/a	n/a	n/a	n/a	n/a	n/a	n/a	n/a	n/a	n/a	n/a	n/a	n/a	n/a	n/a
F4 / P12 14y / f	SYT2	c.923C>T p.Pro308Leu	15.9	57.6	11.4	64	12	42.9	n/a	n/a	21	63.6	11	60.1	n/a	n/a	31	43.9
F5 / P13 19y / m	BICD2	c.320C>T p.Ser107Leu	10.5	64.3	14.6	56.5	4.9	55.6	8	54.8	36	68	11	80	n/a	n/a	38	59.1
F6 / P14 42y / f	BICD2	c.320C>T p.Ser107Leu	11	62.5	16.2	68.2	5.8	49.4	2	50	43.8	52.7	19.5	49.2	25.8	48.8	28.1	47.8
F6 / P15 7y / f	BICD2	c.320C>T p.Ser107Leu	n/a	n/a	n/a	n/a	n/a	n/a	n/a	n/a	n/a	n/a	n/a	n/a	n/a	n/a	n/a	n/a

Abbreviations: F, family; P, patient; y, year; m, male; f, female; n, nervous; med, median; uln, ulnar; peron, peroneal; tib, tibial; rad, radial; sur, sural; CMAP, compound muscle action potential; MNCV, motor nerve conduction velocity; SNAP, sensory nerve action potential; SNCV, sensory nerve conduction velocity; NR, not recordable; n/a, not available

Table 4.2 Nerve conduction parameters in dHMN with confirmed pathogenic mutations

<i>Family / Patient / Age / Sex</i>	<i>Gene</i>	<i>Nucleotide / Amino acid change</i>	<i>median CMAP (mV)</i>	<i>median MNCV (m/s)</i>	<i>ulnar CMAP (mV)</i>	<i>ulnar MNCV (m/s)</i>	<i>peroneal CMAP (mV)</i>	<i>peroneal MNCV (m/s)</i>	<i>tibial CMAP (mV)</i>	<i>tibial MNCV (m/s)</i>	<i>median SNAP (uV)</i>	<i>median SNCV (m/s)</i>	<i>ulnar SNAP (uV)</i>	<i>ulnar SNCV (m/s)</i>	<i>radial SNAP (uV)</i>	<i>radial SNCV (m/s)</i>	<i>sural SNAP (uV)</i>	<i>sural SNCV (m/s)</i>
F6 / P16 6y / m	BICD2	c.320C>T p.Ser107Leu	n/a	n/a	n/a	n/a	n/a	n/a	n/a	n/a	n/a	n/a	n/a	n/a	n/a	n/a	n/a	n/a
F6 / P17 6y / m	BICD2	c.320C>T p.Ser107Leu	n/a	n/a	n/a	n/a	n/a	n/a	n/a	n/a	n/a	n/a	n/a	n/a	n/a	n/a	n/a	n/a
F7 / P18 28y / m	DYNC1H1	c.1834G>A p.Val612Met	n/a	n/a	n/a	n/a	2.5	54	4.3	49	n/a	n/a	n/a	n/a	n/a	n/a	18	54
F8 / P19 3y† / m	IGHMBP2	c.292_303 delinsATGCT p.Gly98fs	NR	NR	2	24.3	NR	NR	n/a	n/a	NR	NR	n/a	n/a	NR	NR	NR	NR
F8 / P20 6mo† / m	IGHMBP2	c.292_303 delinsATGCT p.Gly98fs	n/a	n/a	n/a	n/a	n/a	n/a	n/a	n/a	n/a	n/a	n/a	n/a	n/a	n/a	n/a	n/a
F9 / P21 21y / m	IGHMBP2	c.1813C>T p.Arg605*	21	60.8	2.7	50	NR	NR	n/a	n/a	26	65.9	5.9	68.3	n/a	n/a	24	45.9
F9 / P22 19y / f	IGHMBP2	c.1813C>T p.Arg605*	13.9	55.6	6.7	54.1	2.1	46.4	2.6	NR	25	51.8	19	50	n/a	n/a	38	41.2
F10 / P23 9y / m	TRPV4	c.805C>T p.Arg269Cys	12.1	60	n/a	n/a	1.4	57	7.1	48	26	63	n/a	n/a	n/a	n/a	n/a	n/a
F11 / P24 49y / f	TRPV4	c.184G>A p.Asp62Asn	18.1	56.8	18.5	63	1.7	44.4	5	n/a	12	56.5	18	52.1	n/a	n/a	4	29
F11 / P25 43y / m	TRPV4	c.184G>A p.Asp62Asn	n/a	n/a	n/a	n/a	N	N	N	N	n/a	n/a	n/a	n/a	n/a	n/a	N	N
F12 / P26 16y / m	MFN2	c.1126 A>G p.Met376Val	12.5	47.5	9.3	54.9	1.4	55.6	NR	NR	15	48.2	6.9	46	4.7	44.2	5.7	40.5
F13 / P27 70y / m	MFN2	c.2119C>T p.Arg707Trp	8.1	53	8.9	67	NR	NR	3.8	n/a	2	37	9	57	5	59	n/a	n/a

Abbreviations: F, family; P, patient; y, year; m, male; f, female; mo, month; †, deceased; CMAP, compound muscle action potential; MNCV, motor nerve conduction velocity; SNAP, sensory nerve action potential; SNCV, sensory nerve conduction velocity; N, normal; NR, not recordable; n/a, not available

Table 4.2 continued Nerve conduction parameters in dHMN with confirmed pathogenic mutations

<i>Family / Patient / Age / Sex</i>	<i>Gene</i>	<i>Nucleotide / Amino acid change</i>	<i>median CMAP (mV)</i>	<i>median MNCV (m/s)</i>	<i>ulnar CMAP (mV)</i>	<i>ulnar MNCV (m/s)</i>	<i>peroneal CMAP (mV)</i>	<i>peroneal MNCV (m/s)</i>	<i>tibial CMAP (mV)</i>	<i>tibial MNCV (m/s)</i>	<i>median SNAP (uV)</i>	<i>median SNCV (m/s)</i>	<i>ulnar SNAP (uV)</i>	<i>ulnar SNCV (m/s)</i>	<i>radial SNAP (uV)</i>	<i>radial SNCV (m/s)</i>	<i>sural SNAP (uV)</i>	<i>sural SNCV (m/s)</i>
F14 / P28 32y / f	IGHMBP2	c.2752 C>T p.Arg918Cys	3	42.9	2.5	43.8	NR	NR	NR	NR	NR	NR	NR	NR	n/a	n/a	NR	NR
F14 / P29 13y / m	IGHMBP2	c.2752 C>T p.Arg918Cys	11.3	43	9	53	NR	NR	1.4	NR	8	52	5	53	8	47	7	47
F14 / P30 30y / m	IGHMBP2	c.2752 C>T p.Arg918Cys	9.7	53	n/a	n/a	n/a	n/a	NR	NR	8	43	8	51	n/a	n/a	2	32
F14 / P31 48y / m	IGHMBP2	c.2752 C>T p.Arg918Cys	3.7	50	4.9	47	n/a	n/a	n/a	n/a	NR	NR	NR	NR	NR	NR	n/a	n/a
F15 / P32 3,5y / m	IGHMBP2	c.767C>G p.Ala256Gly	n/a	n/a	n/a	n/a	5.6	40.3	6.2	n/a	n/a	n/a	n/a	n/a	n/a	n/a	9.6	44.7
F16 / P33 72y / f	DHTKD1	c.628G>T p.Ala210Ser	20	54	14.6	53	6.7	44	9.3	45	12	46	13	58	10	65	18	42
F16 / P34 48y / m	DHTKD1	c.628G>T p.Ala210Ser	11.6	56	12.3	56	4.7	41	23.4	49	14	60	9	62	11	58	14	50
F16 / P35 45y / m	DHTKD1	c.628G>T p.Ala210Ser	16.8	63	9.7	64	7.6	43	3.5	44	29	62	24	62	14	58	8	42
F17 / P36 33y / f	ARHGEF10	c.1949G>A p.Cys650Tyr	n/a	n/a	12.9	66	n/a	n/a	n/a	n/a	12	54.3	10	54.1	n/a	n/a	NR	NR

Abbreviations: F, family; P, patient; y, year; m, male; f, female; CMAP, compound muscle action potential; MNCV, motor nerve conduction velocity; SNAP, sensory nerve action potential; SNCV, sensory nerve conduction velocity; NR, not recordable; n/a, not available

Table 4.3 Nerve conduction parameters in dHMN with possibly causative mutations

<i>Family / Patient / Age / Sex</i>	<i>Gene</i>	<i>Nucleotide / Amino acid change</i>	<i>median CMAP (mV)</i>	<i>median MNCV (m/s)</i>	<i>ulnar CMAP (mV)</i>	<i>ulnar MNCV (m/s)</i>	<i>peroneal CMAP (mV)</i>	<i>peroneal NCV (m/s)</i>	<i>tibial CMAP (mV)</i>	<i>tibial MNCV (m/s)</i>	<i>median SNAP (uV)</i>	<i>median SNCV (m/s)</i>	<i>ulnar SNAP (uV)</i>	<i>ulnar SNCV (m/s)</i>	<i>radial SNAP (uV)</i>	<i>radial SNCV (m/s)</i>	<i>sural SNAP (uV)</i>	<i>sural SNCV (m/s)</i>
F18 / P37 56y / m	AARS	c.986G>A, p.Arg329His	6.1	54	11.4	44.3	0.4	21.9	NR	NR	1.9	53.7	0.8	38.2	n/a	n/a	NR	NR
F18 / P38 32y / m	AARS	c.986G>A, p.Arg329His	20	43	18	47	NR	NR	0.4	34	1	48	NR	45	8	45	NR	NR
F19 / P39 77y † / m	AARS	c.986G>A, p.Arg329His	n/a	n/a	n/a	n/a	n/a	n/a	n/a	n/a	n/a	n/a	n/a	n/a	n/a	n/a	n/a	n/a
F19 / P40 50y / m	AARS	c.986G>A, p.Arg329His	2	27	9.3	46	NR	NR	NR	NR	NR	NR	NR	NR	NR	NR	NR	NR
F20 / P41 20y / m	AARS	c.986G>A, p.Arg329His	14.4	40	11	44	3	24	3.6	31	3	31	1	30	3	35	NR	NR
F21 / P42 54y / f	AARS	c.986G>A, p.Arg329His	17.8	39.8	9.8	47.4	NR	NR	0.1	33.6	2.5	44.7	4.9	42.5	1.5	40	NR	NR
F22 / P43 59y / m	DNM2	c.1739T>C p.Met580Thr	n/a	n/a	2.6	41.4	n/a	n/a	0.1	15.9	1.1	36	0.8	32	NR	NR	NR	NR
F22 / P44 36y / f	DNM2	c.1739T>C p.Met580Thr	n/a	n/a	n/a	n/a	n/a	n/a	n/a	n/a	n/a	n/a	n/a	n/a	n/a	n/a	n/a	n/a
F22 / P45 30y / f	DNM2	c.1739T>C p.Met580Thr	11.7	48.9	n/a	n/a	n/a	n/a	0.7	40.6	2.1	57.4	3.4	54.2	2.9	52.6	0.2	20
F23 / P46 35y / f	MFN2	c.1403G>A, p.Arg468His	n/a	n/a	n/a	n/a	n/a	n/a	n/a	n/a	n/a	n/a	n/a	n/a	n/a	n/a	n/a	n/a
F24 / P47 59y / m	MORC2	c.C754T, p.Arg252Trp	NR	NR	11.9	34	n/a	n/a	7	45	NR	NR	NR	NR	NR	NR	NR	NR
F24 / P48 59y / m	MORC2	c.C754T, p.Arg252Trp	n/a	n/a	n/a	n/a	n/a	n/a	n/a	n/a	n/a	n/a	n/a	n/a	n/a	n/a	n/a	n/a

Abbreviations: F, family; P, patient; y, year; m, male; f, female; CMAP, compound motor action potential; MNCV, motor nerve conduction velocity; SNAP, sensory nerve action potential; SNCV, sensory nerve conduction velocity; NR, not recordable; n/a, not available

Table 4.4 Nerve conduction parameters in motor CMT2

<i>Family / Patient / Age / Sex</i>	<i>Gene</i>	<i>Nucleotide / Amino acid change</i>	<i>median CMAP (mV)</i>	<i>median MNCV (m/s)</i>	<i>ulnar CMAP (mV)</i>	<i>ulnar MNCV (m/s)</i>	<i>peroneal CMAP (mV)</i>	<i>peroneal MNCV (m/s)</i>	<i>tibial CMAP (mV)</i>	<i>tibial MNCV (m/s)</i>	<i>median SNAP (uV)</i>	<i>median SNCV (m/s)</i>	<i>ulnar SNAP (uV)</i>	<i>ulnar SNCV (m/s)</i>	<i>radial SNAP (uV)</i>	<i>radial SNCV (m/s)</i>	<i>sural SNAP (uV)</i>	<i>sural SNCV (m/s)</i>
F25 / P49 14y / f	SLC52A2	c.916G>A, p.Gly306Arg c.1016T>C, p.Leu339Pro	n/a	n/a	n/a	n/a	3.5	50	6.9	NR	NR	NR	n/a	n/a	n/a	n/a	NR	NR
F26 / P50 25y / m	C12orf65	c.96_99dup ATCC, p.Pro341Ilefs*25	2	n/a	5	50	n/a	n/a	n/a	n/a	28	50	n/a	n/a	n/a	n/a	12	24
F27 / P51 52y / m	FUS	c.1529A>G p.Lys510Arg	n/a	n/a	n/a	n/a	n/a	n/a	n/a	n/a	n/a	n/a	n/a	n/a	n/a	n/a	n/a	n/a
F28 / P52 74y / m	DCTN1	c.3406C>T p.Arg1136Cys	1	41.8	7.2	53.6	1.2	40.4	6.2	57.1	6	54.5	6	50	1	55.8	15	47.8
F29 / P53 29y / m	ATP7A	c.A2279G: p.Tyr760Cys	4.3	57	n/a	n/a	6.6	46	n/a	n/a	3.6	60	n/a	n/a	n/a	n/a	9	42
F30 / P54 71y / m	SACS	c.1580C>G, p.Ser527* c.6781C>A, p.Leu2261Ile	4.2	47	11.1	46	NR	NR	NR	NR	NR	NR	NR	NR	3	36	NR	NR

Abbreviations: F, family; P, patient; y, year; m, male; f, female; CMAP, compound muscle action potential; MNCV, motor nerve conduction velocity; SNAP, sensory nerve action potential; SNCV, sensory nerve conduction velocity; NR, not recordable; n/a, not available

Table 4.5 Nerve conduction parameters in dHMN plus with confirmed pathogenic mutations

<i>Family / Patient / Age / Sex</i>	<i>Gene</i>	<i>Nucleotide / Amino acid change</i>	<i>median CMAP (mV)</i>	<i>median MNCV (m/s)</i>	<i>ulnar CMAP (mV)</i>	<i>ulnar MNCV (m/s)</i>	<i>peroneal CMAP (mV)</i>	<i>peroneal MNCV (m/s)</i>	<i>tibial CMAP (mV)</i>	<i>tibial MNCV (m/s)</i>	<i>median SNAP (uV)</i>	<i>median SNCV (m/s)</i>	<i>ulnar SNAP (uV)</i>	<i>ulnar SNCV (m/s)</i>	<i>radial SNAP (uV)</i>	<i>radial SNCV (m/s)</i>	<i>sural SNAP (uV)</i>	<i>sural SNCV (m/s)</i>
F31 / P55 25y / m	FIG4	c.2386C>T p.Gln796*	n/a	n/a	n/a	n/a	n/a	n/a	n/a	n/a	n/a	n/a	n/a	n/a	n/a	n/a	n/a	n/a
F32 / P56 24y / m	SLC52A3 SLC52A2	c.1371C>G, p.Phe457Leu c.819C>T p.Met273Ile	2.5	45.7	13.4	54.7	2.7	39.2	3	39.2	4.2	63	3	59.1	n/a	n/a	3.8	37
F33 / P57 19y / m	TBX5	c.331G>T, p.Asp111Tyr	11.8	47.9	10.6	37.5	1.4	30.8	NR	NR	2.3	41.2	NR	NR	NR	NR	4.3	28.3
F34 / P58 16y / m	STAT5B	c.944A>C, p.Glu315Ala	D	N	n/a	n/a	n/a	n/a	D	N	N	N	n/a	n/a	n/a	n/a	N	N
F34 / P59 17y / f	STAT5B	c.944A>C, p.Glu315Ala	N	N	D	N	n/a	n/a	D	N	N	N	n/a	n/a	n/a	n/a	N	N
F35 / P60 29y / m	PTEN	c.269T>C p.Phe90Ser	2.9	37.5	7	57.1	0.6	46.2	0.4	36.6	12	61.5	13	59.3	13	68.9	14	52.4

Abbreviations: F, family; P, patient; y, year; m, male; f, female; CMAP, compound muscle action potential; MNCV, motor nerve conduction velocity; SNAP, sensory nerve action potential; SNCV, sensory nerve conduction velocity; N, normal; D, decreased; NR, not recordable; n/a, not available

Table 4.6 Nerve conduction parameters in dHMN plus patients with possibly causative mutations

The distinct entity of SMA-LED has been introduced to characterise the congenital or early childhood-onset non-progressive form of dHMN, caused by autosomal-dominant disorders of motor neuron development (Rossor *et al.*, 2015). The clinical phenotype of 17 patients was compatible with SMA-LED in the examined cohort. By definition these are non-length-dependent conditions, predominantly affecting the lower limb distal muscles with prominent additional proximal leg muscle involvement. Foot deformities and arthrogryposis-like lower limb contractures are frequently seen. At a later disease stage mild upper limb involvement may be present but sensory changes are absent. Motor nerve studies are often normal with only rare presence of axonal motor neuropathy, but electromyography indicates chronic neurogenic denervation. Correction of early-onset deformities is important, since these patients do not develop significant deterioration in the later disease course.

The dHMN in some patients was complicated with other neurological signs overlapping with familial amyotrophic lateral sclerosis (ALS), hereditary spastic paraplegia (HSP), spinal muscular atrophy (SMA) or Kennedy's disease (Irobi *et al.*, 2006; Van Den Bosch and Timmerman, 2006; Rossor *et al.*, 2012). Accompanying complex neurological and/or other organ impairments observed in some cohort patients with distal predominant motor neuropathy urged us to introduce the *HMN plus* group. Patients with motor neuropathy enrolled in this phenotype group well illustrated the significant overlap with other genetic motor neuron disorders.

Chapter 5. Identifying genetic frequency and investigating mutational spectrum in hereditary motor neuropathies

5.1 Review of hereditary motor neuropathies in the molecular era

Gene identification in hereditary motor neuropathies used to rely on linkage studies performed in rare extended families. Recent development of next generation techniques has shifted the focus on small nuclear families and isolated patients and enabled new genes to be discovered in these previously genetically undefined groups of patients (Timmerman *et al.*, 2014). Furthermore, next generation sequencing (NGS) helped to identify numerous novel mutations in known disease genes providing further knowledge on genetic heterogeneity. The dHMN phenotype can arise with mutations in numerous genes at different chromosomal loci (locus heterogeneity) while different mutations in the same gene can lead to variable allelic phenotypes (allelic heterogeneity) (Berciano *et al.*, 2012; Timmerman *et al.*, 2014).

Compared to the previously reported 7 genes and 13 chromosomal loci 10 years ago (Irobi, De Jonghe, *et al.*, 2004; Irobi *et al.*, 2006; Dierick *et al.*, 2008), to date we acknowledge around 30 genes responsible for autosomal-dominant, recessive and X-linked forms of dHMN. Despite the increasing number of novel genes, a large proportion of patients with motor neuropathies, estimated around 75-80%, have still remained without genetic diagnosis (Rossor *et al.*, 2012; Rossor *et al.*, 2015).

The so far identified genes encode ubiquitously expressed proteins involved in diverse cellular functions, most of which may be responsible for motor neuron vulnerability and/or may provide insights into underlying complex mechanisms. Affected pathways linked to HMN pathology include DNA/RNA metabolism, protein translation and synthesis, stress response and apoptosis, axonal guidance, intracellular trafficking and synaptic activity. Detailed analysis of gene- and phenotype specific data of patients' cohorts and natural history studies along with unravelling gene and protein functions will facilitate the better understanding of common pathomechanisms. This will also trigger the introduction of new therapy approaches (Peeters *et al.*, 2014; Timmerman *et al.*, 2014).

5.2 Aims

I aimed to determine the mutation frequency in the North-East England cohort of patients with hereditary motor neuropathies by performing diagnostic and research based genetic

studies. The main goal of the study was to reassess the mutation detection rate in distal hereditary motor neuropathy (dHMN) with the use of next generation techniques and compare the result to previously studied cohorts. I also aimed to examine the efficacy and limitations of next generation sequencing as a tool in gene and mutation discovery in these highly heterogeneous diseases. Furthermore, I studied the spectrum of mutated genes and affected molecular pathways among the classified overlapping phenotypes.

5.3 Methods

5.3.1 Patient involvement in the genetic study

We included the same 105 patients from the North-East of England in the genetic study, who were clinically diagnosed with hereditary motor neuropathies in *Chapter 4*. We applied diagnostic and/or research based genetic testing methods in all patients, who were previously classified into one of the phenotype subgroups of *dHMN*, *motor CMT2* or *HMN plus*. All participants provided written informed consent to be involved in genetic studies.

5.3.2 Diagnostic algorithm of applied genetic approaches

Initially, targeted gene testing was carried out in patients from each phenotype group. Routinely, *PMP22* gene mutation was excluded in all participants. Testing for candidate CMT2 and dHMN-related genes was led by clinical and inheritance features based on algorithms suggested by previous groups (Saporta *et al.*, 2011; Murphy *et al.*, 2012; Rossor *et al.*, 2012). We proceeded with inherited peripheral neuropathy (IPN) gene panel testing in undiagnosed patients, in order to screen for the batch of known motor and sensory neuropathy-related genes. Where diagnosis could not be achieved by available diagnostic genetic methods, we applied whole-exome sequencing (WES) in the specialist research laboratory at Newcastle University (*Chapter 3.2.1*).

Family members of participants, who demonstrated similar phenotype and nerve conduction findings, assumed to have the same genetic mutation or they were genetically tested.

5.3.3 Genetic methods applied in the study

5.3.3.1 Targeted gene testing

DNA was obtained by standard methods from peripheral white blood cells. Candidate gene sequencing after PCR amplification of coding exons and flanking intronic regions was performed by automatic DNA sequencing on an Applied Biosystems 3730xl DNA Analyser in the Institute of Genetic Medicine at Newcastle University.

5.3.3.2 Inherited peripheral neuropathy gene panel testing

The multi-gene panel assay utilising next generation sequencing (NGS), as described in *Chapter 3*, was performed by Dr Antoniadis, Dr Greenslade and Dr Forester in the Bristol Genetics Laboratory, using the UK Genetic Testing Network approved approach (*Chapter 3.2.1.1*).

5.3.3.3 Whole-exome sequencing

Whole-exome sequencing (WES) was performed in the index patients or occasionally in more family members of selected pedigrees. Blood genomic DNA was fragmented, exome enriched and sequenced (Illumina TruSeq™ 62 Mb and HiSeq 2000, 100 bp paired-end reads) and bioinformatics analysis was carried out as described in (*Chapter 3.2.1.2*). Putative pathogenic variants were confirmed by Sanger sequencing according to the description in (*Chapter 3.2.2*). Where family members were available, variants were tested for segregation.

I aimed to discover novel gene mutations by intersecting patients' WES data with datasets from members of same family or from independent patients, who shared a similar fully penetrating phenotype. Furthermore, I filtered the annotated WES data of index patients against a set of 132 known or likely causative IPN-related genes, as well as against a batch of 69 known motor neuron disease-related genes (9 SMA, 41 ALS and 19 HSP) (**Table 5.1**). Novel sequence variants of known disease genes and novel gene mutations were assessed for the likelihood of their pathogenicity. Variants were defined as '*confirmed pathogenic*', if the variant was previously shown to be pathogenic or if the novel sequence variant of a known motor neuropathy associated gene or a novel gene was predicted to affect protein structure or function and segregated with the disease in at least one additional affected family member. Highly conserved *in silico* deleterious novel sequence variants of known or novel genes were determined as '*possibly pathogenic*' in case segregation studies could not be carried out (Pyle *et al.*, 2015).

5.3.4 Statistical analyses of the results

Many patients came from the same pedigree and therefore the mutation frequency in each phenotype group was determined at the pedigree level to avoid risk of bias. The mutation detection rate in the cohort of hereditary motor neuropathy was provided in percentage (%) and was calculated from the number of genetically diagnosed families out of the total number of involved pedigrees. The cumulative mutation detection rate consisted of '*confirmed*' and '*possibly*' subcomponents based on the confirmed or possibly causative nature of the identified gene mutations.

IPN						HSP	SMA	ALS	
AARS	DYNC1H1	HSJ1	NEFL	SBF2	TRIM1	CYP7B1	ASAH1	ALS2	PRPH
ABCA1	EGR2	HSPB1	NGF	SCN9A	TRPV4	FA2H	EXOSC3	ANG	SETX
ABCD1	FAM126A	HSPB3	NGFB	SCN11A	TTR	GJC2	GLE1	ATXN2	SIGMAR1
AIFM1	FAM134B	HSPB8	NMNAT2	SEPT	TTMP	HSPD1	HEXB	CHCHD10	SMN1
ALS2	FBLN5	IGHMBP2	NTRK1	SETDB2	TUBB3	KIAA0196	SLC52A2	CHMP2B	SOD1
ANG	FBXO38	IKBKAP	OPTN	SETX	TYMP	KIAA0415	SLC52A3	c9orf72	SPG11
ARHGEF10	FGD4	IARS	PBGD	SGPL1	UBA1	L1CAM	SMN1	DAO	SS18L1
ARSA	FIG4	INF2	PDHA1	SH3TC2	VAPB	NIPA1	UBA1	DCTN1	SQSTM1
ATL1	FUS	KARS	PDK3	SIL1	VCP	NIPA1	VRK1	DPP6	TAF15
ATM	FXN	KIF1A	PEX12	SLC5A7	WNK1	PLP1		ELP3	TARDBP
ATP7A	GAN	KIF1B	PHYH	SLC12A6	XPC	RTN2		ERBB4	TBK1
BAG3	GARS	KIF5A	PLEKHG5	SLC25A21	YARS	SLC33A1		ERLIN2	TUBA4A
BICD2	GALC	LARS	PMP22	SLC25A46		SPG3A		EWSR1	UBQLN2
BSCL2	GDAP1	LITAF	POLG	SOD1		SPG7		FUS	UNC13A
C12ORF65	GFAP	LMNA	PRPS1	SOX10		SPG8		GRN	VAPB
CCT5	GJB1	LRSAM1	PRX	SPAST		SPG20		HNRNPA1	VCP
CTDP1	GLA	MARS	PTEN	SPG11		SPG21		HNRNPA2B1	
CYP27A1	HADHA	MED25	RAB7	SPTLC1		SPG39		MATR3	
DCTN1	HADHB	MFN2	RAB7A	SPTLC2		ZFYVE26		NEFH	
DHTKD1	HARS	MORC2	REEP1	SYT2				NEK1	
DNAJB2	HINT1	MPZ	RFVT2	TARDBP				OPTN	
DNM2	HINT2	MTMR2	SACS	TDP1				PFN1	
DNMT1	HK1	NDRG1	SARM1	TFG				PON1	
DST	HOXD10	NDUFAF5	SBF1	TNNT2				PON3	

Table 5.1 Set of genes related to IPN, HSP, SMA and ALS filtered in the WES data of HMN cohort

The efficacy of each applied genetic method was characterised by the test detection rate in percentage (%), which was calculated from the number of positive test results out of the total number of performed tests.

5.4 Results

5.4.1 Mutation frequency in the HMN cohort and efficacy of applied genetic tools

We managed to identify causative mutations in 35 families (60 patients) out of 73 families (105 patients), which provided a 47.9% cumulative mutation detection rate in the cohort. Molecular diagnosis could not be reached in 45 patients from 38 families (**Table 4.1**). The mutation detection rate and spectrum of affected genes determined in the phenotype subgroups will be discussed in the following paragraphs.

Targeted gene testing led to the molecular diagnosis in 5 out of 105 patients only (4.7%), while 12 index patients were diagnosed by the IPN gene panel testing out of the 46 performed tests (26%) and a further 18 index patients by WES from a total of 40 analyses (45%) (**Table 4.1**). There were no novel shared genes and/or mutations in the exome negative cases.

5.4.2 The spectrum of gene mutations and mutation detection rate in dHMN

We diagnosed causative gene mutations in 17 index patients from 40 dHMN families. The cumulative mutation detection rate was 42.5%, which proved to be significantly higher compared to previous studies (**Table 4.1**).

The implication of combined genetic methods was required to achieve molecular results in most of the cases. The spectrum of the genes identified among dHMN families was highly variable. Interestingly, we did not detect mutations in some otherwise frequent dHMN-related genes, such as *HSPB1* and *BSCL2*, in the cohort.

5.4.2.1 Confirmed pathogenic mutations

Mutations were considered ‘*confirmed pathogenic*’ in 13 index patients and the ‘*confirmed*’ mutation detection rate was calculated as 32.5% (**Table 4.1**). Among them, 7 index patients carried known pathogenic dHMN mutations. In 5 families novel sequence variants of known dHMN-related genes were detected. These were predicted deleterious by various bioinformatics tools and segregated appropriately in the families. Furthermore, a novel dHMN-causing gene was identified with distinct pathomechanism in a large autosomal-dominant pedigree (**Table 5.2**).

A young female patient with dominant family history (*Family I*) carried the previously reported heterozygous missense c.421A>G, p.Lys141Glu pathogenic mutation in the

Family / Patient / Age / Sex	Gene	Nucleotide / Amino acid change	Phenotype	Inherit	Age onset	Lower limb				Upper limb				Deformity / Contracture	Walking / Orthotics	Additional features
						Weakness	Wasting	Reflexes ankle /knee	Sensory	Weakness	Wasting	Reflexes	Sensory			
F1 / P1 26y / f	HSPB8	c.421A>G p.Lys141Glu	dHMN-II	AD	10y	d ++	d +	a / ↑	pain	d +	-	n	-	pes cavus	HW / AFO	-
F2 / P2 36y / m	GARS	c.647A>G p.His216Arg	dHMN-V upper limb	AD	14y	d +	d +	↓/n	+	d +++	d+++	a	+	split hand pes cavus	-	swollen tongue
F2 / P3 66y / f	GARS	c.647A>G p.His216Arg	dHMN-V upper limb	AD	12y	d +	d +	↓/↓	+	d +++	d +++	a	+	split hand	-	swollen tongue immune arthritis
F3 / P4 51y / f	GARS	c.1528A>C p.Lys510Gln	dHMN-V lower limb	AD	5y	d ++	d ++	a / ↑	pain	d ++	d ++	↑	pain	pes cavus / tight Achilles	tiptoeing, HW	hearing deficit
F3 / P5 9y / f	GARS	c.1528A>C p.Lys510Gln	dHMN-V lower limb	AD	5y	d +	d +	↓/ ↑	-	-	-	n	-	tight Achilles	tiptoeing, falls	-
F3 / P6 28y / f	GARS	c.1528A>C p.Lys510Gln	dHMN-V lower limb	AD	6y	d ++	d ++	a / n	+	d +	d +	n	+	pes cavus / tight Achilles	tiptoeing, HW	-
F4/ P7 46y / f	SYT2	c.923C>T p.Pro308Leu	SMA-LED	AD	birth	R d +++ p ++ L d +++	R d +++ p ++ L d +++	a / a	+	d +	-	a	+	pes cavus splayed toes / hip dysplasia	HW,TW / knee splint	-
F4/ P8 29y / f	SYT2	c.923C>T p.Pro308Leu	SMA-LED	AD	birth	d +++	d +++	a / a	+	d +	-	a	+	pes cavus hammer toes / hip dysplasia	waddling / AFO	-
F4/ P9 8y / m	SYT2	c.923C>T p.Pro308Leu	SMA-LED	AD	birth	-	-	a / a	+	-	-	a	-	pes planus	HW / insoles	motor delay ADHD
F4/ P10 17y / m	SYT2	c.923C>T p.Pro308Leu	SMA-LED	AD	birth	-	-	a / a	-	-	-	a	-	pes cavus hammer toes	-	-
F4/ P11 43y / m	SYT2	c.923C>T p.Pro308Leu	SMA-LED	AD	birth	d +++	d +++	a / a	-	-	-	a	-	hammer toes	HW, TW	reflex facilitation on exercise
F4/ P12 14y / f	SYT2	c.923C>T p.Pro308Leu	SMA-LED	AD	birth	R d ++ L d +	-	a / a	-	-	-	a	-	pes cavus splayed toes / hip dysplasia	HW	-
F5/ P13 19y / m	BICD2	c.320C>T p.Ser107Leu	SMA-LED	isolated de novo	birth	d +++	d ++	a / ↓	-	-	d +	↓	-	club feet scapular winging	steppage	motor delay
F6/ P14 42y / f	BICD2	c.320C>T p.Ser107Leu	SMA-LED	AD	birth	d + p +	d ++	↑/ ↑	-	-	-	n	-	crowded toes scapular winging	difficulties	motor delay
F6/ P15 7y / f	BICD2	c.320C>T p.Ser107Leu	SMA-LED	AD	birth	d + p +	d ++	↑/ ↑	-	-	-	↑	-	pes equinovarus, scapular winging	difficulties	motor delay

Abbreviations: F, family; P, patient; y, year; m, male; f, female; †, deceased; AD, autosomal dominant; AR, autosomal recessive; d, distal; p, proximal; R, right; L, left; +, mild; ++, moderate; +++, severe; a, absent; n, normal; ↑, increased; ↓, decreased; -, none; HW, impaired heel walking; TW, impaired toe walking; AFO, ankle foot orthosis; SGA, small for gestational age, SMA-LED, spinal muscular atrophy with lower extremity dominance

Table 5.2 Summary of the clinical presentation of the patients in the dHMN group with confirmed causative mutations

(Bansagi *et al.*, 2017)

Family / Patient / Age/ Sex	Gene	Nucleotide / Amino acid change	Phenotype	Inherit	Age onset	Lower limb				Upper limb				Deformity / Contracture	Walking / Orthotics	Additional features
						Weakness	Wasting	Reflexes ankle /knee	Sensory	Weakness	Wasting	Reflexes	Sensory			
F6 / P16 6y / m	BICD2	c.320C>T p.Ser107Leu	SMA-LED	AD	birth	d + p +	d ++	↑ / ↑	-	-	-	↑	-	scapular winging	difficulties	motor delay
F6 / P17 6y / m	BICD2	c.320C>T p.Ser107Leu	SMA-LED	AD	birth	d + p +	d ++	↑ / ↑	-	-	-	↑	-	scapular winging	difficulties	motor delay
F7 / P18 28y / m	DYNC1H1	c.1834G>A p.Val612Met	SMA-LED	AD	6y	d +++	d +++	a / ↓	-	-	-	n	-	pes cavus, crawled toes	HW, TW / splints	pyramidal signs
F8 / P19 3y† / m	IGHMBP2	c.292_303 delinsATGCT p.Gly98fs	SMARD1	AR	birth	d +++ p ++	d ++	a / a	-	d +++ p ++	d ++	a	-	pes cavus / flexed fingers tight Achilles	not developed	preterm, SGA, respiratory failure
F8 / P20 6mo† / m	IGHMBP2	c.292_303 delinsATGCT p.Gly98fs	SMARD1	AR	birth	d +++	d +	a / a	-	d +++	d +	a	-	pes cavus	not developed	preterm, SGA, respiratory failure
F9 / P21 21y / m	IGHMBP2	c.1813C>T p.Arg605*	dHMN	AR	7y	d +++ p +++	d +++ p ++	a / ↓	-	d ++	d +	n	-	pes cavus	ambulant with crutch, wheelchair	-
F9 / P22 19y / f	IGHMBP2	c.1813C>T p.Arg605*	dHMN	AR	10y	d ++	d ++	a / a	-	d +	d +	a	-	pes cavus	HW, TW / AFO	-
F10 / P23 9y / m	TRPV4	c.805C>T p.Arg269Cys	congenital dHMN	de novo	birth	d +++ p ++	d ++	a / a	-	-	-	↓	-	pes cavus, scapular winging / tight Achilles	HW, TW / splints, wheelchair	intermittent horse voice
F11 / P24 49y / f	TRPV4	c.184G>A p.Asp62Asn	congenital dHMN	AD	41y	d +++	d ++	a / a	-	-	-	n	-	pes cavus, crawled toes	HW, TW / splints, crutches	livid skin
F11 / P25 43y / m	TRPV4	c.184G>A p.Asp62Asn	congenital dHMN	AD	birth	-	-	n	-	-	-	n	-	talipes	-	-
F12 / P26 16y / m	MFN2	c.1126 A>G p.Met376Val	dHMN	isolated de novo	14y	d +++	d ++	↑ / ↑	pain	-	-	↑	-	pes cavus, hammer toes / tight Achilles	HW tiptoeing	-
F13 / P27 70y / m	MFN2	c.2119C>T p.Arg707Trp	dHMN	isolated de novo	55y	R d +++ p +++	d ++	a / a	-	R d ++ p +++	R d +	a	-	-	non-ambulant / wheelchair	Alzheimer disease

Abbreviations: F, family; P, patient; y, year; m, male; f, female; AR, autosomal recessive; AD, autosomal dominant; d, distal; p, proximal; R, right; +, mild; ++, moderate; +++, severe; a, absent; ↑ increased; ↓, decreased; n, normal; -, none; HW, impaired heel walking; TW, impaired toe walking, SMA-LED, spinal muscular atrophy with lower extremity dominance; SMARD1, spinal muscular atrophy with respiratory distress

Table 5.2 continued Summary of the clinical presentation of the patients in the dHMN group with confirmed causative mutations

(Bansagi *et al.*, 2017)

HSPB8 gene (Irobi, Van Impe, *et al.*, 2004). She presented with a juvenile-onset, rapidly progressive lower limb predominant phenotype.

Two novel **GARS** mutations were found in two independent families. The novel heterozygous c.647A>G, p.His216Arg missense variant was detected in a two-generation family (*Family 2*) with predominant upper limb involvement (dHMN-V). Another novel heterozygous c.1528A>C, p.Lys510Gln missense mutation co-segregated in a three-generation dominant family (*Family 3*) with prominent lower limb weakness, foot deformities and less severe hand involvement.

Six patients from a three-generation dominant pedigree (*Family 4*) were identified to carry the heterozygous missense c.923C>T, p.Pro308Leu mutation in the **SYT2** gene (Herrmann *et al.*, 2014).

The common c.320C>T, p.Ser107Leu **BICD2** mutation was diagnosed in 5 patients from two independent families (*Families 5-6*) presenting with distal congenital non-progressive SMA-LED (Bansagi, Griffin, *et al.*, 2015).

One male patient carried the heterozygous c.1834G>A, p.Val612Met missense mutation in the **DYNC1H1** gene. His phenotype was compatible with SMA-LED (*Family 7*). This variant has been previously reported in 4 SMA-LED families worldwide, even though a common founder could not be identified (Scoto *et al.*, 2015).

The homozygous frameshift c.292_303delinsATGCT, p.Gly98fs mutation in the **IGHMBP2** gene led to the spinal muscular atrophy with respiratory distress (SMARD1) phenotype in 2 male siblings of consanguineous Pakistani origin (*Family 8*).

A brother and sister from another family presented with childhood-onset slowly progressive distal spinal muscular atrophy and lack of respiratory involvement (*Family 9*). They carried the heterozygous c.1813C>T, p.Arg605* nonsense **IGHMBP2** mutation, which was hemizygous in the cDNA suggesting the loss of the second allele (Cottenie *et al.*, 2014).

The *de novo* c.805C>T, p.Arg269Cys **TRPV4** mutation (Auer-Grumbach *et al.*, 2010) was reported in a young boy with clinical and electrophysiological signs of scapuloperoneal SMA combined with metatropic dysplasia (*Family 10*) and the c.184G>A, p.Asp62Asn variant in a 48-year-old woman (*Family 11*) with a predominant motor neuropathy affecting the lower limbs (Evangelista *et al.*, 2015).

An adolescent-onset, rapidly progressive dHMN was diagnosed in a young male patient (*Family 12*) with the *de novo* heterozygous c.1126A>G, p.Met376Val mutation in the **MFN2** gene, which has been previously reported in a Spanish CMT2 family (Casasnovas *et al.*, 2010). The heterozygous c.2119C>T, p.Arg707Trp **MFN2** mutation (Nicholson *et al.*, 2008;

Carr *et al.*, 2015) was identified in a late adult-onset, unilaterally distributed dHMN phenotype in a 70-year-old man (*Family 13*).

5.4.2.2 Possibly pathogenic mutations

‘Possibly pathogenic’ mutations were considered in 4 additional families carrying possibly causative variants in known dHMN/CMT-related genes, where segregation studies were not available or not sufficient to confirm the diagnosis (**Table 5.3**).

A single heterozygous c.2752 C>T, p.Arg918Cys *IGHMBP2* variant co-segregated in a large Pakistani family with motor neuropathy and no signs of respiratory dysfunction (*Family 14*). A second mutation could not yet been identified in the family.

Another heterozygous c.767C>G, p.Ala256Gly *IGHMBP2* variant was detected in a 3,5-year-old boy with juvenile-onset phenotype, where the pathogenicity could not yet been confirmed due to the lack of a second mutation (*Family 15*).

In a dominant dHMN pedigree we found the co-segregating novel heterozygous c.628G>T, p.Ala210Ser missense *DHTKDI* variant (*Family 16*).

In a young female patient (*Family 17*) a heterozygous, not yet reported c.1949G>A, p.Tyr650Cys sequence change was identified in the *ARHGEF10* gene, causing the substitution of the highly conserved amino acid downstream to the catalytic Dbl homology domain, that is required to activate RhoGTPases (Verhoeven *et al.*, 2003).

5.4.3 The spectrum of gene mutations and mutation detection rate in motor CMT2

The diagnosis of motor CMT2 was established in 16 patients from 10 families. We recorded 70% ‘confirmed’ mutation detection rate in this group as a result of a ‘confirmed pathogenic’ molecular diagnosis in 7 CMT2 families (**Table 4.1**).

IPN gene panel testing determined the genetic cause in 6 families. All identified variants were previously described as pathogenic mutations linked to axonal neuropathies. Interestingly, the incidence of CMT2A (*MFN2* mutations) was lower in the cohort than it was expected from previous studies. However, alanyl-aminoacyl-tRNA synthetase gene mutations (*AARS*) were commonly found in this overlapping phenotype group (**Table 5.4**).

The recurrent heterozygous c.986G>A, p.Arg329His *AARS* mutation was identified in 6 patients from 4 independent families (*Families 18-21*) (Bansagi, Antoniadi, *et al.*, 2015). A dominant pedigree presented with early-onset intermediate motor neuropathy (*Family 22*) linked to the previously reported missense c.1739T>C, p.Met580Thr *DNM2* mutation (Haberlová *et al.*, 2011). The 59-year-old index patient had hearing impairment, split hand

Family / Patient / Age / Sex	Gene	Nucleotide / Amino acid change	Phenotype	Inherit	Age onset	Lower limb				Upper limb				Deformity / Contracture	Walking / Orthotics	Additional features
						Weakness	Wasting	Reflexes ankle /knee	Sensory	Weakness	Wasting	Reflexes	Sensory			
F14 / P28 32y / f	IGHMBP2	c.2752 C>T p.Arg918Cys	dHMN	AR	6y	d ++	d ++	a / a	+	d ++	d ++	n	-	hammer toes	HW,TW / splints	-
F14 / P29 13y / m	IGHMBP2	c.2752 C>T p.Arg918Cys	dHMN	AR	4y	d ++	d ++	a / a	-	-	-	n	-	pes cavus	HW,TW / splints	-
F14 / P30 30y / m	IGHMBP2	c.2752 C>T p.Arg918Cys	dHMN	AR	10y	d ++	d ++	a / a	-	-	-	n	-	pes cavus	HW,TW / splints	-
F14 / P31 48y / m	IGHMBP2	c.2752 C>T p.Arg918Cys	dHMN	AR	7y	d +++	d +++	a / a	+++	d ++	d +	n	-	pes cavus	HW,TW / splints	-
F15 / P32 3,5y / m	IGHMBP2	c.767C>G p.Ala256Gly	dHMN	isolated	birth	d +++	d ++	a / ↓	-	-	-	↓	-	pes cavus scapular winging	falls	motor delay
F16 / P33 72y / f	DHTKD1	c.628G>T p.Ala210Ser	dHMN	AD	10y	d ++	d +++	a / a	-	d ++	d ++	a	-	pes cavus, clawed toes	HW	'crane leg' ulnar split hand
F16 / P34 48y / m	DHTKD1	c.628G>T p.Ala210Ser	dHMN	AD	39y	d ++ p ++	d +++	a / a	+	d ++	d ++	a	+	pes cavus clawed toes	HW, TW / insoles	'crane leg' ulnar split hand
F16 / P35 45y / m	DHTKD1	c.628G>T p.Ala210Ser	dHMN	AD	21y	d ++	d +++	a / a	-	d +	d ++	a	-	pes cavus clawed toes	HW	'crane leg' ulnar split hand
F17 / P36 33y / f	ARHGEF10	c.1949G>A p.Cys650Tyr	dHMN	isolated	birth	d ++	d +	a / a	-	d ++	d +	a	-	arthrogryposis talipes / hip dyslocation	HW,TW	keratosis swallowing difficulties

Abbreviations: F, family; P, patient; y, year; m, male; f, female; AD, autosomal dominant; AR, autosomal recessive; R, right; L, left; d, distal ; p, proximal; +, mild; ++, moderate; +++, severe; a, absent; n, normal; ↑, increased; ↓, decreased; -, none; HW, impaired heel walking; TW, impaired toe walking; AFO, ankle foot orthosis; ADHD, attention deficit hyperactivity disorder; SMA-LED, spinal muscular atrophy with lower extremity dominance

Table 5.3 Summary of the clinical presentation of the patients in the dHMN group with possibly causative mutations

(Bansagi *et al.*, 2017)

deformity and respiratory muscle involvement. Despite the lack of sensory symptoms, the deficit was clearly present on sensory nerve testing.

A female patient with the unusual manifestation of severe upper limb motor weakness (*Family 23*) carried the pathogenic heterozygous c.1403G>A, p.Arg468His *MFN2* mutation, which has been previously reported in lower limb predominant neuropathy (Casasnovas *et al.*, 2010).

The recently reported heterozygous c.754C>T, p.Arg252Trp mutation in the microorchidia CW-type zinc finger 2 *MORC2* gene was identified by whole-exome sequencing in a de novo form in identical twin male patients (*Family 24*). They presented with an early-onset motor predominant neuropathy, progressively affecting the distal and proximal limb muscles and leading to a severe disability in adulthood (Albulym *et al.*, 2016; Sevilla *et al.*, 2016).

5.4.4 The spectrum of gene mutations and mutation detection rate in HMN plus

Overlapping symptoms of hereditary motor neuropathy, motor neuron degeneration and/or other neurology features were observed in the 25 patients from 23 families, who belonged to the HMN plus group. The genetic diagnosis was 'confirmed pathogenic' in 6 patients, while 'possibly pathogenic' mutations were identified in an additional 5 index patients. The cumulative mutation detection rate was 47.7 % in this phenotype group (**Table 4.1**).

WES proved to be a highly efficient diagnostic tool by providing molecular diagnosis in 9 out of 11 index patients in this group.

5.4.4.1 Confirmed pathogenic mutations

Previously described pathogenic mutations were found in 3 out of 6 patients (**Table 5.5**).

The compound heterozygous c.916G>A, p.Gly306Arg and c.1016T>C, p.Leu339Pro mutations were detected in the *SLC52A2* gene (*Family 25*) (Foley *et al.*, 2014) and the homozygous truncating c.96_99dupATCC, p.Pro34Ilefs*25 mutation in the *c12orf65* gene (*Family 26*) (Pyle *et al.*, 2014). The heterozygous previously reported c.1529A>G, p.Lys510Arg *FUS* mutation (Waibel *et al.*, 2010, 2013) was identified in a 52-year-old male patient with dominant family history (*Family 27*). Initially, he demonstrated asymmetric lower limb motor weakness with electric nerve studies indicative of dHMN. His progression was rapid with evolving frontal dementia and loss of ambulation within half a year.

Gradually evolving combined upper and lower motor neuron involvement, dystonia and ataxia characterized the male patient, who carried the heterozygous c.3823C>T, p.Arg1275Cys missense *DCTN1* mutation (*Family 28*) (Daud *et al.*, 2015).

A 29-year-old male patient was examined with upper and lower motor neuron pathology and cerebellar dysfunction (*Family 29*). WES identified the hemizygous missense c.2279A>G,

Family / Patient / Age/ Sex	Gene	Nucleotide / Amino acid change	Inherit	Age onset	Lower limb				Upper limb				Deformity / Contracture	Walking/ Orthotics	Additional features
					Weakness	Wasting	Reflexes ankle /knee	Sensory	Weakness	Wasting	Reflexes	Sensory			
F18 / P37 56y / m	AARS	c.986G>A, p.Arg329His	AD	50y	d +++	d ++	a / a	+	-	-	n	-	pes cavus / tight Achilles	HW,TW / AFO	Dupuytren's contracture
F18 / P38 32y / m	AARS	c.986G>A, p.Arg329His	AD	28y	d ++	d ++	a / a	++	d ++	d ++	a	++	pes cavus	HW,TW / AFO	JRA , bilateral hip replacement
F19 / P39 77y †/ m	AARS	c.986G>A, p.Arg329His	AD	60y	d +++	d +++	a / a	++	d ++	d ++	a	++	pes cavus toe drop	HW, TW / AFO crutches	-
F19 / P40 50y / m	AARS	c.986G>A, p.Arg329His	AD	30y	d ++	d ++	a / a	++	d ++	d ++	a	++	pes cavus split hand	stepping / stick hand splint	TIA
F20 / P41 20y / m	AARS	c.986G>A, p.Arg329His	AD	12y	d +++	d ++	a / a	+	-	-	n	-	pes cavo- equinus / tight Achilles	stepping / insoles	-
F21 / P42 54y / f	AARS	c.986G>A, p.Arg329His	AD	20y	d +++	d +++	a / a	++	d ++	d +	↓	-	pes cavus	HW,TW stepping / AFO	hearing deficit
F22 / P43 59y / m	DNM2	c.1739T>C p.Met580Thr	AD	5y	d +++	d +++	a / a	+	d +++	d +++	a	+	clawed toes curled fingers split hand	HW,TW / AFO	hearing deficit respiratory muscle weakness
F22 / P44 36y / f	DNM2	c.1739T>C p.Met580Thr	AD	11y	d +++	d +++	a / a	+	d +++	d +++	a	+	clawed toes curled fingers	HW,TW / AFO	-
F22 / P45 30y / f	DNM2	c.1739T>C p.Met580Thr	AD	13y	d ++	d ++	a / a	+	d ++	d ++	a	+	clawed toes	HW, TW / AFO	-
F23 / P46 35y / f	MFN2	c.1403G>A, p.Arg468His	AD	20y	d+	d+	a/a	+	d+++	d+++	a	+	clawed fingers	hand splint	-
F24 / P47 59 / m	MORC2	c.C754T, p.Arg252Trp	AD	13y	d+++	d+++	a/a	+++	d+++	d+++	a	++	pes cavus arthrodesis	non- ambulant	mild deafness
F24 / P48 59 / m	MORC2	c.C754T, p.Arg252Trp	AD	10y	d+++	d+++	a/a	+++	d+++	d+++	a	++	pes cavus arthrodesis	non- ambulant	mild deafness

Abbreviations: F, family; P, patient; y, year; m, male; f, female; AD, autosomal dominant; d, distal ; +, mild; ++, moderate; +++, severe; a, absent; n, normal; ↓, decreased; -, none; HW, impaired heel walking; TW, impaired toe walking; AFO, ankle foot orthosis; JRA, juvenile rheumatoid arthritis; TIA, transient ischaemic attack

Table 5.4 Summary of the clinical presentation of the patients with confirmed mutations in the motor CMT2 group

(Bansagi *et al.*, 2017)

p.Tyr760Cys novel *ATP7A* variant, which was carried by the patient and his healthy mother and *in silico* prediction tools suggested deleterious effects (Bansagi *et al.*, 2016).

The novel compound heterozygous c.1580C>G, p.Ser527* and c.6781C>A, p.Leu2261Ile *SACS* mutations were identified in a 71-year-old man with late teen-onset gait difficulties, evolving leg spasticity and lower limb predominant motor neuropathy (*Family 30*) (Yu-Wai-Man *et al.*, 2014).

5.4.4.2 Possibly causative mutations

'Possibly pathogenic' novel sequence changes were identified in 5 index patients (**Table 5.6**). Despite that all mutations affected known disease-causing genes and had deleterious predictions, the molecular diagnosis remained possibly causative due to either a lack of segregation or insufficient supportive functional studies.

A 17-year-old man presented with distal motor neuropathy and optic atrophy compatible with CMT type 6 (*Family 31*), who carried the single, previously reported heterozygous c.2386C>T, p.Gln796* nonsense mutation in the *FIG4* gene (DiVincenzo *et al.*, 2014).

The pathogenic c.1371C>G, p.Phe457Leu *SLC52A3* mutation (Green *et al.*, 2010) was found in heterozygous form by WES in a 19-year-old man (*Family 32*), who presented with characteristic symptoms of Brown-Vialetto-Van Laere syndrome (BVVL) and responded to riboflavin therapy. However, a second mutation could not yet been identified, even after re-analysing WES data for copy number variations in the gene.

The pathogenic heterozygous c.331G>T, p.Asp111Tyr *TBX5* mutation, which was previously linked to Holt-Oram syndrome (Granados-Riveron *et al.*, 2012) was detected in a 19-year-old male patient with a multifocal motor neuropathy (*Family 33*).

A sibling pair presented with postnatal growth retardation, limb girdle and facial muscle weakness jointly with peripheral motor neuropathy carried the novel homozygous c.944T>G, p.Glu315Ala missense mutation in the *STAT5B* gene (*Family 34*).

A *de novo* c.269T>C, p.Phe90Ser *PTEN* mutation was identified in a 29-year-old male patient with asymmetric motor weakness, cranial nerve involvement, pyramidal signs and multifocal motor neuropathy with conduction blocks (*Family 35*).

Family / Patient / Age / Sex	Gene	Nucleotide / Amino acid change	Inherit	Age onset	Lower limb				Upper limb				Deformity / Contracture	Walking / Orthotics	Additional features
					Weakness	Wasting	Reflexes ankle /knee	Sensory	Weakness	Wasting	Reflexes	Sensory			
F25 / P49 14y / f	SLC52A2	c.916G>A, p.Gly306Arg c.1016T>C, p.Leu339Pro	AR	18mo	d +	d +	a / a	-	d +++ p +++	d +++	a	-	curled fingers	ataxic	optic atrophy sensorineural hearing loss bulbar palsy axial weakness ataxia
F26 / P50 25y / m	C12orf65	c.96_99dupATCC, p.Pro341Ilefs*25	AR	2y	d +++	d ++	↑ / ↑	-	d ++	d ++	↑	-	pes cavus / tight Achilles	tiptoeing, HW, TW	optic atrophy spasticity pyramidal signs autistic
F27 / P51 52y / m	FUS	c.1529A>G p.Lys510Arg	AD	48y	d +++ p +++	d +++ p +++	↑ / ↑	-	-	-	↑	-	-	HW, TW / wheelchair	mild frontal dementia
F28 / P52 74y / m	DCTN1	c.3406C>T p.Arg1136Cys	AD de novo	63y	d +++ p ++	d +++	a / a	-	d +++ p +++	d +++ p +++	↑	-	pes cavus	HW, TW / AFO	cranial nerves ataxia dystonia
F29 / P53 29y / m	ATP7A	c.A2279G: p.Tyr760Cys	X	10y	d ++	d ++	↑ / ↓	-	-	-	↑	-	-	HW, TW spastic – ataxic / wheelchair	cranial nerves tetraspasticity pyramidal signs extrapyramidal ataxia
F30 / P54 71y / m	SACS	c.1580C>G, p.Ser527* c.6781C>A, p.Leu2261Ile	AR	19y	d +++	d +++	a / ↑	+	d ++	d +++	↑	+	pes cavus curled fingers	HW, TW spastic - paraparetic	dysarthria spasticity ataxia learning difficulties

Abbreviations: F, family; P, patient; y, year; mo, month; m, male; f, female; AD, autosomal dominant; AR, autosomal recessive; X, X-linked; R, right; L, left; d, distal ; p, proximal; +, mild; ++, moderate; +++, severe; a, absent; ↑, increased; ↓, decreased; -, none; HW, impaired heel walking; TW, impaired toe walking; AFO, ankle foot orthosis

Table 5.5 Summary of the clinical presentation of the patients in the HMN plus group with confirmed pathogenic mutations

(Bansagi *et al.*, 2017)

Family / Patient / Age / Sex	Gene	Nucleotide / Amino acid change	Inherit	Age onset	Lower limb				Upper limb				Deformity / Contracture	Walking / Orthotics	Additional features
					Weakness	Wasting	Reflexes ankle /knee	Sensory	Weakness	Wasting	Reflexes	Sensory			
F31 / P55 25y / m	FIG4	c.2386C>T p.Gln796*	AD	17y	d ++	d +++	a / ↑	++	-	-	↑	++	pes cavus clawed toes	HW, TW	optic atrophy pyramidal signs
F32 / P56 24y / m	SLC52A3 SLC52A2	c.1371C>G, p.Phe457Leu c.819C>T p.Met273Ile	AR	19y	d ++	d ++	a / a	+	d +++ p +++	d +++ p +	a	+	curled fingers	ataxic HW, TW / wheelchair	ophthalmoplegia sensorineural hearing loss bulbar palsy ataxia respiratory failure
F33 / P57 19y / m	TBX5	c.331G>T, p.Asp111Tyr	AD	2y	d ++	d ++	↑ / ↑	+	d ++	d +	↑	+	pes cavus clawed toes	clumsy	shoulder deformity thoracic kyphosis scapular winging
F34 / P58 16y / m	STAT5B	c.944A>C, p.Glu315Ala	AR	10y	d ++	d ++	↓ / ↓	-	-	-	↓	-	-	HW, TW	postnatal growth retardation face dysmorphia ptosis facial weakness
F34 / P59 17y / f	STAT5B	c.944A>C, p.Glu315Ala	AR	10y	d ++	d +	↓ / ↓	-	-	-	↓	-	-	HW, TW	postnatal growth retardation face dysmorphia ptosis facial weakness
F35 / P60 29y / m	PTEN	c.269T>C p.Phe90Ser	isolated	3y	R d +++	R d ++	↑ / ↑	-	L d +++ p +++ R d ++	L d +++ p +++ R p ++	a	-	pes cavus clawed toes	falls, HW, TW	cranial nerve III., IV., VII., X., XII. macrocephaly development delay

Abbreviations: F, family; P, patient; y, year; m, male; f, female; AD, autosomal dominant; AR, autosomal recessive; X, X-linked; R, right; L, left; d, distal; p, proximal; +, mild; ++, moderate; +++, severe; a, absent; ↑, increased; ↓, decreased; -, none; HW, impaired heel walking; TW, impaired toe walking; AFO, ankle foot orthosis

Table 5.6 Summary of the clinical presentation of the patients in the HMN plus group with possibly causative mutations

(Bansagi *et al.*, 2017)

5.5 Discussion

5.5.1 Mutation detection rate in the HMN cohort

While the demyelinating forms of CMT can receive diagnoses in the majority of cases, the causative mutations remain often uncovered in axonal predominant motor neuropathies and in distal hereditary motor neuropathies. The mutation detection rate has been reported ~20% in axonal forms, including dHMN and motor CMT2 (Rossor *et al.*, 2015).

In this study mutational screen was performed by implicating next generation techniques in hereditary motor neuropathies and the mutation detection rate was reviewed in the group of dHMN. Detailed neurological and electrophysiology assessments were carried out (*Chapter 4*) in order to determine phenotype-genotype correlations and to distinguish between overlapping allelic phenotypes (**Figure 5.1**).

Potentially pathogenic mutations were identified in 47.9% of the patients with hereditary motor neuropathies, including confirmed mutations in 35.6% and possibly causative variants in an additional 12.3%. In the dHMN group the genetic diagnosis was achieved in 32.5% of the patients and a possibly causative mutation was identified in an additional 10% (**Table 4.1**). This result is significantly higher than the 15-20% detection rate reported in previous studies (Dierick *et al.*, 2008; Rossor *et al.*, 2015)

There was a large genotype heterogeneity observed with each HMN phenotype (**Figure 5.2**). Furthermore, different mutations in the same gene led to various disease phenotypes. As an illustrative sample, 17 patients were diagnosed with the SMA-LED phenotype. The causative mutations were identified in the *SYT2*, *BICD2*, *DYNC1H1* and *ARHGEF10* genes, while the genetic cause could not be detected in 4 patients. Mutations in the *DYNC1H1* gene have been reported to cause not only SMA-LED but more complex clinical phenotypes (Scoto *et al.*, 2015; Strickland *et al.*, 2015). There was no major common pathway found to explain the mechanism of the various gene mutations, which resulted in the SMA-LED phenotype.

5.5.2 Advantages and limitations of next generation sequencing in the HMN cohort

Improving genetic testing technology led to a rapid increase in discovering CMT-causing gene mutations. More and more patients can be genetically diagnosed not only with common, but also with rare CMT forms.

Targeted candidate gene sequencing proved to have less benefit in the HMN cohort, where the clinical presentation may be atypical and varied within the families, the inheritance pattern is often uncertain and wide range of genes contribute to the phenotype (Klein *et al.*, 2014).



Figure 5.1 Clinical heterogeneity of different forms of HMN

dHMN (top 2 rows), motor CMT2 (third row) and dHMN plus (bottom row)

A) Patient 2 and 3: *GARS* **B)** Patient 19: *IGHMBP2* **C)** Patient 23: *TRPV4* **D)** Patient 32: *IGHMBP2* **E)** not yet diagnosed dHMN **F)** Patient 18: *DYNC1H1* **G)** Patient 10: *SYT2* **H)** Patient 16: *BICD2* **I-J)** not yet diagnosed SMA-LED **K)** Patient 42: *AARS* **L)** Patient 39: *AARS* **M)** Family 22: *DNM2* **N)** Patient 51: *FUS* **O)** Patient 53: *ATP7A* **P)** Patient 57: *TBX5* **Q)** Patient 58: *STAT5B* **R)** not yet diagnosed dHMN plus.

(Bansagi *et al.*, 2017)

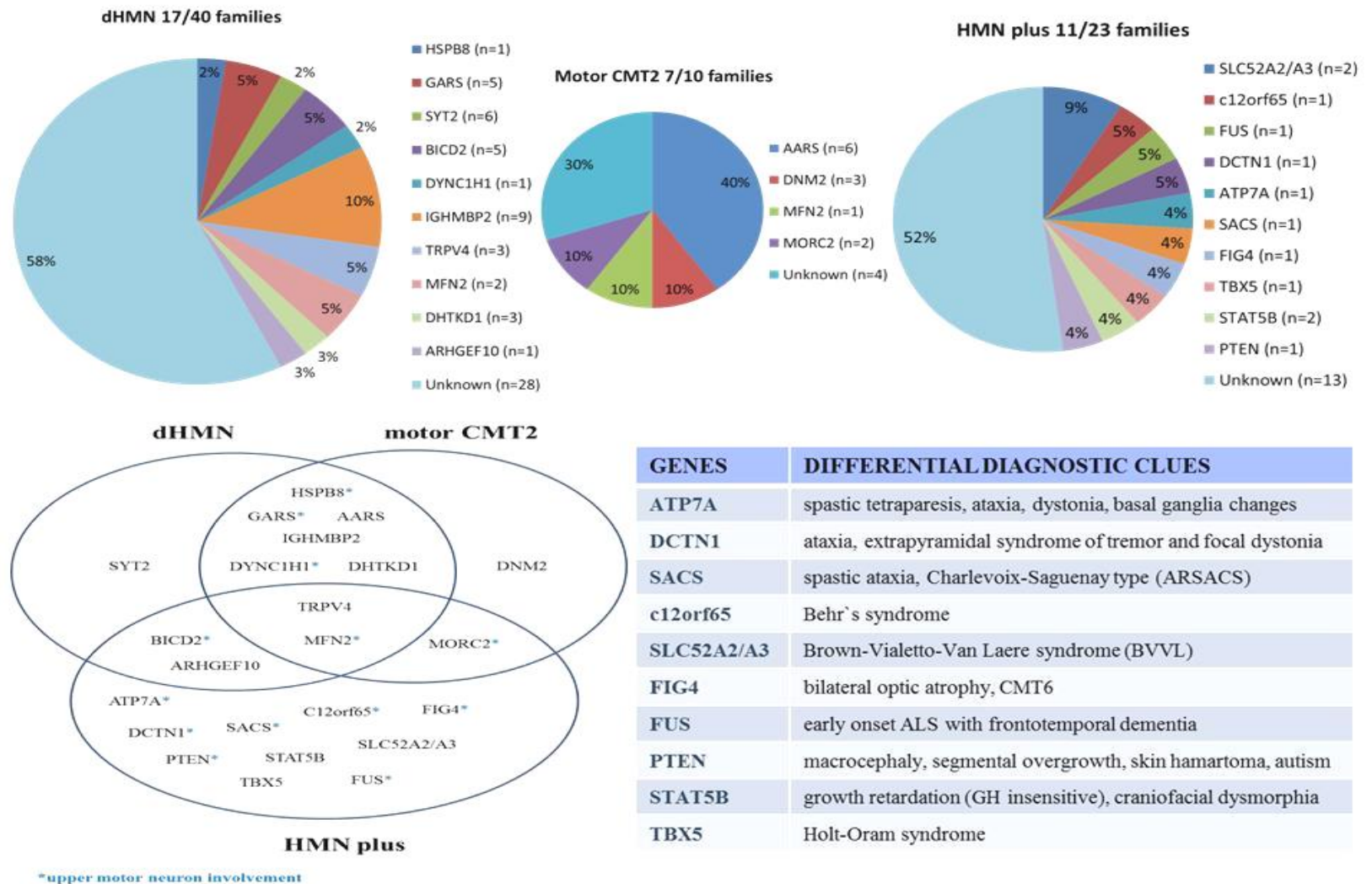


Figure 5.2 Distribution of mutated genes in the phenotype groups and overlapping phenotypes with key clinical features

(Bansagi *et al.*, 2017)

The multi-gene IPN panel testing has been assessed to be a powerful tool, by its 26% (12 index patients/46 pedigrees) diagnostic efficacy in the cohort. The power of gene panel testing was to reveal novel variants in known and rare axonal CMT2/dHMN-related genes. This is an unbiased approach overcoming the limitation of deciding testing based on the limited information available for very rare genes.

WES has the capacity to simultaneously screen large number of genetic heterogeneities and to discover novel genes and extend phenotype–genotype associations (Klein *et al.*, 2014). The diagnostic efficacy of WES was 45% in the cohort by detecting the causative gene mutations in 18 index patients out of 40 pedigrees (**Figure 5.3**).

The high throughput sequencing approaches generate tremendous DNA sequence data. Therefore it is critical to assess the candidate variants further to the likelihood of their pathogenicity. Validation by using segregation, normal controls and analyses of conservation and bioinformatics tools or where it was available, perform functional studies could help us to provide evidence (MacArthur *et al.*, 2014; Timmerman *et al.*, 2014; Drew *et al.*, 2015) (**Table 5.7, Table 5.8**).

On the other hand, the advantage of large data sets, that they can be stored and re-analysed for future *in silico* identification of mutations in newly-discovered genes (Montenegro *et al.*, 2011). This was the diagnostic process in the identification of *MORC2* mutation in a cohort family.

Another limitation of WES is the incomplete coverage of the genes, which lead to significant differences between areas of highest and lowest read depth (Montenegro *et al.*, 2011). The coverage of the identified cohort genes is shown on (**Table 5.9**).

Furthermore, WES is unable to detect intronic mutations, gene rearrangements and copy number variations (Montenegro *et al.*, 2011; Timmerman *et al.*, 2014; Drew *et al.*, 2015). These might serve an explanation for some genetically not clarified cohort patients with meticulously analysed WES data and for the single heterozygous mutations identified in some pedigrees (e.g. *IGHMBP2*). Isolated patients with probable *de novo* autosomal-dominant mutations cause further diagnostic challenges. Analysing whole-exome sequences in trios and/or detecting variations in the same gene among other affected families throughout the world can strongly support the diagnosis (Klein *et al.*, 2014; Timmerman *et al.*, 2014). The international collaboration by sharing phenotype and genotype datasets was utmost important, as the genetic matchmaking highly supported us in the novel gene discovery (*SYT2*).

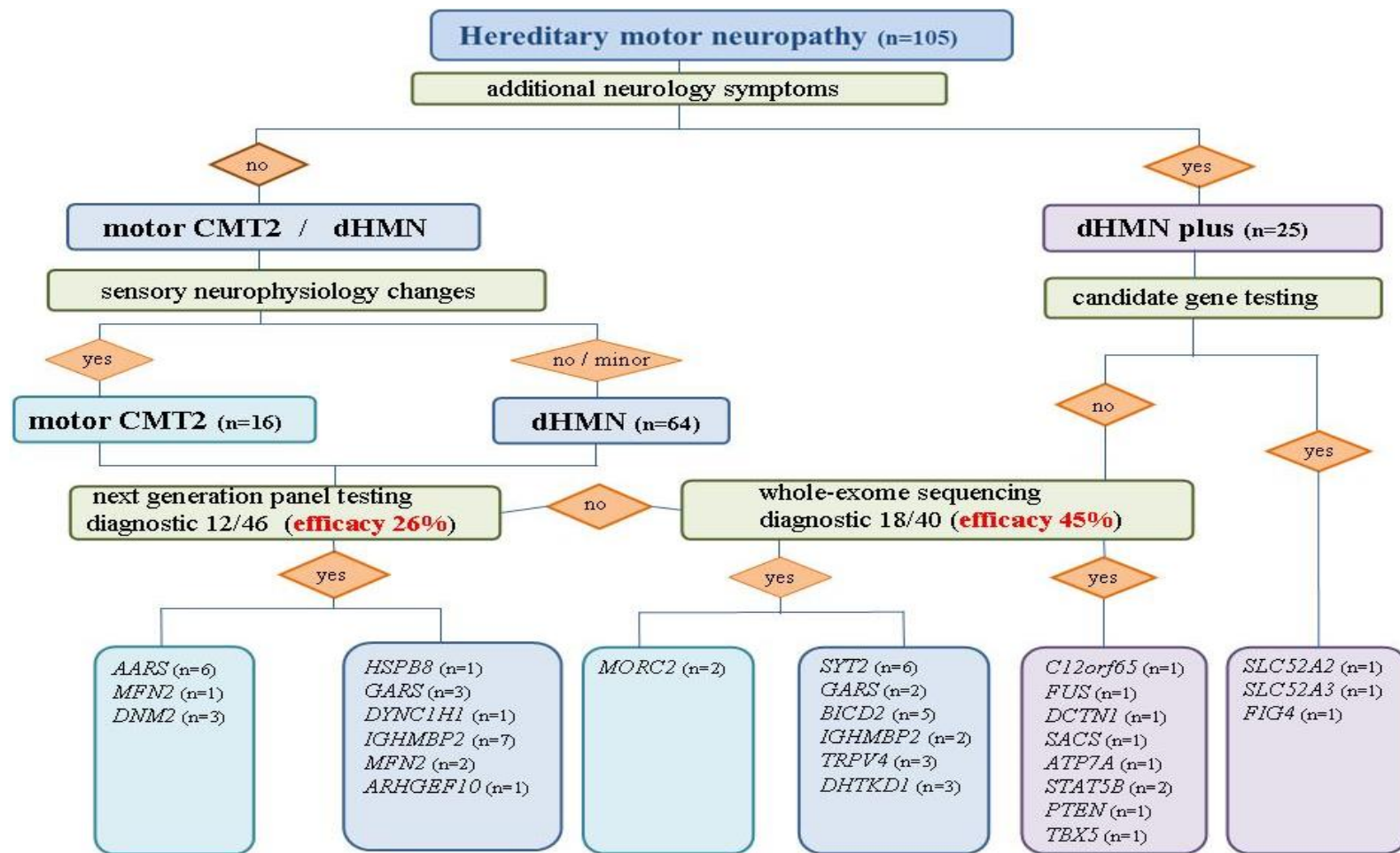


Figure 5.3 Diagnostic flow chart and genes identified in our cohort

(Bansagi *et al.*, 2017)

SAMPLE INFO	DETAILS OF VARIATION		POPULATION ALLELE FREQUENCIES / IDS				
			Sample ID(s)	Gene Name	protein	ExAC	NHLBI_ESP6500
F2/P2	GARS	p.H216R	8.28E-06	.	.	0.00178	.
F3/P4-5	GARS	p.K510Q	.	.	.	0.00356	.
F4/P8-P9	SYT2	p.P308L	.	.	.	0.00356	.
F5/P13,F6/P14-15	BICD2	p.S107L	.	.	.	0.00534	rs398123028
F9/P21-22	IGHMBP2	p.R605X	.	.	.	0.00356	.
F10/P23	TRPV4	p.R269C	.	.	.	0.00178	rs267607146
F11/P24-25	TRPV4	p.D62N	8.44E-06	.	.	0.00178	.
F16/P34-35-36	DHTKD1	p.A210S	0.0029	0.0028	.	0.00890	rs146741810
F24/ P47	MORC2	p.R190W	.	.	.	0.00178	.
F26/P50	C12orf65	p.L32fs	4.13E-05	.	.	0.01068	rs765675424
F27/P51	FUS	p.K511R	.	.	.	0.00178	.
F28/P52	DCTN1	p.R1275C	8.29E-06	.	.	0.00178	.
F29/P53	ATP7A	p.Y760C	4.56E-05	.	.	0.00356	.
F30/P54	SACS	p.L2261I	0.0048	0.0037	.	0.00356	rs146722795
F30/P54	SACS	p.S527X	.	.	.	0.00178	.
F31/P55	FIG4	p.Q796X	.	.	.	0.00178	.
F32/P56	SLC52A3	p.F457L	0.0005	0.0005	.	0.00178	rs145431028
F33/P57	TBX5	p.D111Y	0.0034	0.0034	.	0.00534	rs77357563
F34/P58-59	STAT5B	p.E315A	0.0027	.	.	0.00712	rs572536541
F35/P60	PTEN	p.F90S	.	.	.	0.00178	.

Table 5.7 Population frequencies of rare genetic variants from WES

(Bansagi *et al.*, 2017)

SAMPLE INFO	DETAILS OF VARIATION		FUNCTIONAL PREDICTIONS / SCORES								
			SIFT	Polyphen2	LRT	MutationTaster	MutationAssessor	FATHMM	VEST3 score	CADD (phred)	SiPhy 29way (log Odds)
F2/P2	GARS	p.H216R	D	D	D	D	M	T	0.908	22.4	10.631
F3/P4-5	GARS	p.K510Q	T	B	D	D	L	D	0.507	18.38	13.659
F4/P8-P9	SYT2	p.P308L	D	D	N	D	H	T	0.953	25.6	17.948
F5/P13,F6/P14-15	BICD2	p.S107L	T	D	D	D	M	T	0.787	28.7	16.783
F9/P21-22	IGHMBP2	p.R605X	T	.	D	D	.	.	.	25	12.81
F10/P23	TRPV4	p.R269C	T	D	D	D	N	D	0.957	13.58	12.232
F11/P24-25	TRPV4	p.D62N	D	D	U	D	L	D	0.201	18.86	14.004
F16/P34-35-36	DHTKD1	p.A210S	D	B	D	D	N	T	0.287	11.18	14.921
F24/ P47	MORC2	p.R190W	D	D	D	D	L	T	0.936	19.12	14.304
F26/P50	C12orf65	p.L32fs
F27/P51	FUS	p.K511R	D	D	D	D	M	D	0.844	15.36	10.436
F28/P52	DCTN1	p.R1275C	D	D	D	D	N	T	0.654	31	18.468
F29/P53	ATP7A	p.Y760C	D	D	D	D	H	D	0.97	21.4	14.894
F30/P54	SACS	p.L2261I	D	P	D	D	M	D	0.688	18.64	19.949
F30/P54	SACS	p.S527X	T	.	D	A	.	.	.	40	20.024
F31/P55	FIG4	p.Q796X	T	.	D	A	.	.	.	40	18.787
F32/P56	SLC52A3	p.F457L	D	D	D	D	M	T	0.978	17.17	10.944
F33/P57	TBX5	p.D111Y	D	D	D	D	M	D	0.936	22.9	18.282
F34/P58-59	STAT5B	p.E315A	T	B	D	D	L	T	0.354	13.9	9.432
F35/P60	PTEN	p.F90S	.	D	D	D	H	D	0.968	23.8	14.841

Table 5.8 Functional prediction of rare genetic variants from WES

Abbreviations: A, disease causing automatic; B, benign; D, deleterious; H, high; L, low; M, medium; N, neutral; P, possibly damaging; T, tolerated; U, unknown (Bansagi *et al.*, 2017)

Sample ID(s)	Average Read Depth(s)	Gene Name	Ensembl Gene ID	Ensembl Transcript ID	Exon	chromosome	genomic (hg19)	cDNA	protein	Genotype
F2/P2	51.2	GARS	ENSG00000106105	ENST00000389266	5	7	g.30642727A>G	c.A647G	p.H216R	Heterozygous
F3/P4-5	55.4, 57.5	GARS	ENSG00000106105	ENST00000389266	12	7	g.30661993A>C	c.A1528C	p.K510Q	Heterozygous
F4/P8-P9	77.1, 75.9	SYT2	ENSG00000143858	ENST00000367268	8	1	g.202568476G>A	c.C923T	p.P308L	Heterozygous
F5/P13,F6/P14-15	76.9, 70.5, 68.2	BICD2	ENSG00000185963	ENST00000375512	2	9	g.95491439G>A	c.C320T	p.S107L	Heterozygous
F9/P21-22	78.6, 72.8	IGHMBP2	ENSG00000132740	ENST00000255078	13	11	g.68703761C>T	c.C1813T	p.R605X	Heterozygous
F10/P23	73.3	TRPV4	ENSG00000111199	ENST00000538125	5	12	g.110238471G>A	c.C805T	p.R269C	Heterozygous
F11/P24-25	43.4	TRPV4	ENSG00000111199	ENST00000538125	2	12	g.110252418C>T	c.G184A	p.D62N	Heterozygous
F16/P34-35-36	80.9, 82.0, 48.1	DHTKD1	ENSG00000181192	ENST00000263035	4	10	g.12129639G>T	c.G628T	p.A210S	Heterozygous
F24/P47	85.1	MORC2	ENSG00000133422	ENST00000215862	10	22	g.31337490G>A	c.C568T	p.R190W	Heterozygous
F26/P50	114.8	C12orf65	ENSG00000130921	ENST00000546132	3	12	g.123738316_123738317insATCC	c.95_96insATCC	p.L32fs	Homozygous
F27/P51	63.5	FUS	ENSG00000089280	ENST00000568685	14	16	g.31202419A>G	c.A1532G	p.K511R	Heterozygous
F28/P52	74.7	DCTN1	ENSG00000204843	ENST00000361874	32	2	g.74588640G>A	c.C3823T	p.R1275C	Heterozygous
F29/P53	72.1	ATP7A	ENSG00000165240	ENST00000341514	10	X	g.77268482A>G	c.A2279G	p.Y760C	Homozygous
F30/P54	75.1	SACS	ENSG00000151835	ENST00000382298	10	13	g.23911234G>T	c.C6781A	p.L2261I	Heterozygous
F30/P54	75.1	SACS	ENSG00000151835	ENST00000382298	8	13	g.23929171G>C	c.C1580G	p.S527X	Heterozygous
F31/P55	55.0	FIG4	ENSG00000112367	ENST00000230124	21	6	g.110113794C>T	c.C2386T	p.Q796X	Heterozygous
F32/P56	51.8	SLC52A3	ENSG00000101276	ENST00000217254	5	20	g.741709G>C	c.C1371G	p.F457L	Heterozygous
F33/P57	46.2	TBX5	ENSG00000089225	ENST00000405440	4	12	g.114837349C>A	c.G331T	p.D111Y	Heterozygous
F34/P58-59	70.3, 84.0	STAT5B	ENSG00000173757	ENST00000293328	8	17	g.40370786T>G	c.A944C	p.E315A	Homozygous
F35/P60	67.1	PTEN	ENSG00000171862	ENST00000371953	5	10	g.89692785T>C	c.T269C	p.F90S	Heterozygous

Table 5.9 Coverage of rare genetic variants from WES

(Bansagi *et al.*, 2017)

5.5.3 Molecular pathways and gene mutations in hereditary motor neuropathies

It is of utmost importance to analyse the molecular pathways implicated in hereditary motor neuropathies in order to determine common disease mechanisms for potential biomarkers and for novel therapy targets. The identification of causative gene mutations in patients with hereditary motor neuropathies enabled us to explore numerous potential disease mechanisms. Some of the gene defects affect the proximal part of motor neurons (SMA/dHMN), while others involve the axons or nerve endings. Some further gene mutations may result in a non-length-dependent, selective impairment of certain neuron groups (e.g. upper limb, brainstem neurons) (**Figure 5.4**).

The various neuropathy-causing pathways will be highlighted and discussed through the genes identified in the hereditary motor neuropathy cohort (**Table 5.10**).

5.5.3.1 Impaired protein translation

Aminoacyl-tRNA synthetases (ARS) conjugate amino acids with their cognate tRNA molecules during protein translation. Mutations in many *aminoacyl-tRNA synthetase* genes (*GARS*, *AARS*, *HARS*, *KARS*, *MARS* and *YARS*) have been associated with CMT, indicating the importance of intact protein translation for normal motor neuron functioning (Griffin *et al.*, 2014).

Mutations in aminoacyl-tRNA synthetases were frequently diagnosed (10.47 %) in the cohort patients. Four dominant families carried the recurrent c.986G>A, p.Arg329His *alanyl-tRNA synthetase* (*AARS*) mutation with a heterogeneous phenotype spectrum, described in detail in *Chapter 6.1.3*.

Phenotype-genotype correlations in 2 families identified with the novel *glycyl-tRNA synthetase* (*GARS*) mutations discussed in *Chapter 6.1.4*.

5.5.3.2 Abnormal RNA metabolism

Abnormal RNA metabolism has been implicated both in motor neuron diseases and in hereditary motor neuropathies.

Mutations in the *immunoglobulin μ -binding protein 2* (*IGHMBP2*) gene cause distal spinal motor neuron loss and dysfunction leading to neurogenic muscle atrophy (Grohmann *et al.*, 2001; de Planell-Saguer *et al.*, 2009). Single heterozygous *IGHMBP2* mutations have already been linked to the recessive phenotype and this was studied in the cohort patients together with the related phenotype heterogeneity in *Chapter 6.2*.

A further gene involved in RNA metabolism, the *fused in sarcoma* (*FUS*), was defected in a 52-year-old man (*Family 27*) with an atypical motor neuropathy phenotype.

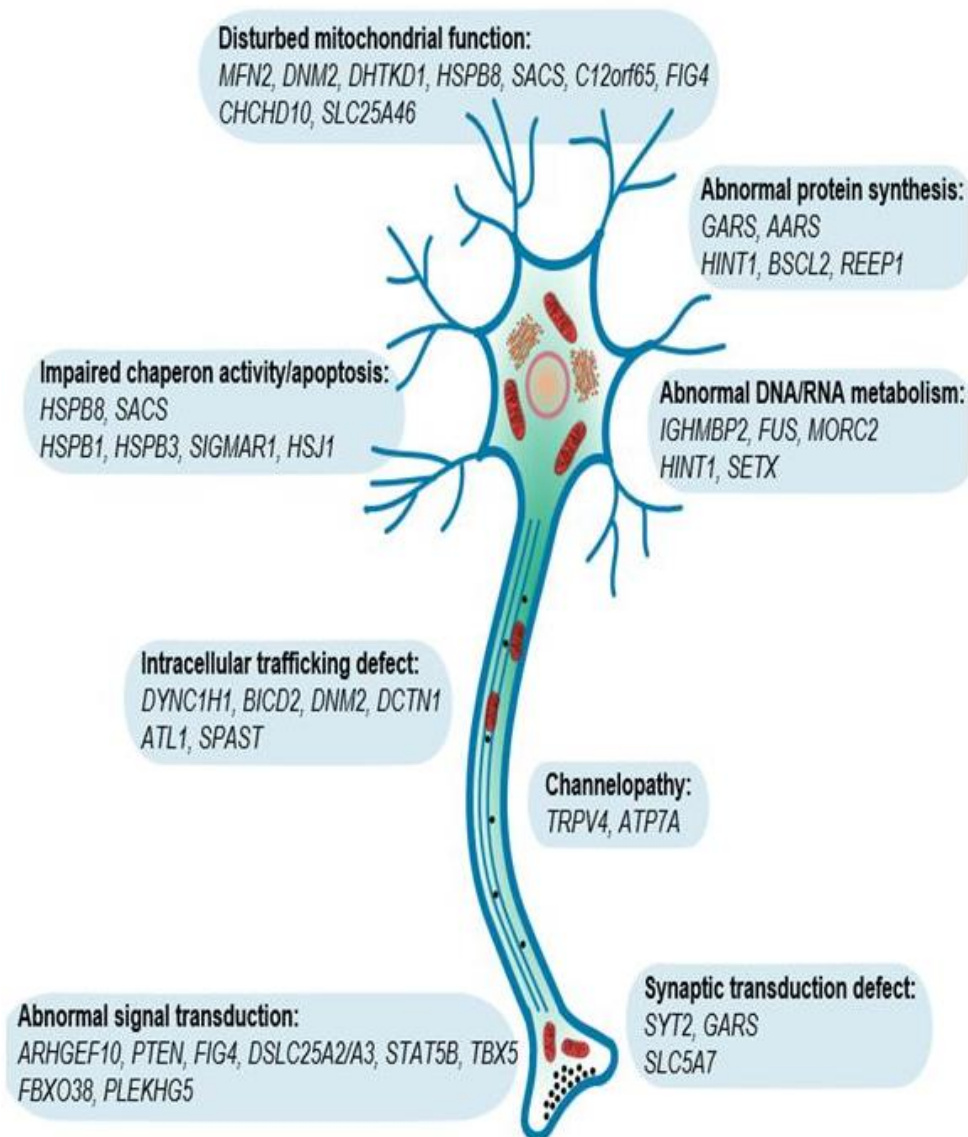


Figure 5.4 Targets of pathomechanisms involved in the motor neuropathy genes

(Bansagi *et al.*, 2017)

GENE	PHENOTYPE	ABNORMAL PROTEIN SYNTHESIS	ABNORMAL DNA/ RNA METABOLISM	MITOCHONDRIAL DYSFUNCTION	ABNORMAL INTRACELLULAR TRAFFICKING	SIGNAL TRANSDUCTION DEFECT	PRESYNAPTIC DEFECT	CHANNELOPATHY
HSPB8	dHMN-II */ CMT2L			X				
GARS	dHMN-V*/ CMT2D	X						
SYT2	SMA-LED*						X	
BICD2	SMA-LED*				X			
DYNC1H1	SMA-LED* / CMT2O				X			
IGHMBP2	SMARD1*/ dHMN-VI */CMT2		X					
TRPV4	congenital dSMA */ CMT2C							X
MFN2	CMT2A*/ ARCMT2 / dHMN*			X				
DHTKD1	CMT2Q / dHMN*			X				
ARHGEF10	CMT1/ dHMN*					X		
AARS	CMT2N* / CMT-I / dHMN	X						
DNM2	CMT2M* / CMTDIB			X				
MORC2	CMT2 +/- pyramidal signs*					X		
SLC52A2/A3	BVVL*			X		X		
c12orf65	AR CMT6, Behr sy*, Leigh sy			X				
FUS	ALS / dHMN plus*		X					
FIG4	CMT4J / ALS / dHMN plus*				X	X		
SACS	ARSAC*			X				
DCTN1	dHMN7B* / ALS / Perry sy				X			
ATP7A	Menkes / OCH / dHMN-X*							X
PTEN	dHMN plus*					X		
STAT5B	GH insensitivity / + dHMN plus*					X		
TBX5	Holt- Oram sy / + dHMN plus*					X		

*phenotype in this study

Table 5.10 Mechanisms of motor neuropathy-related genes identified in the HMN cohort

He presented with unilateral lower limb weakness, predominantly affecting the distal leg muscles, while electrophysiology studies indicated motor neuropathy. Mutations in the *FUS* gene have been associated with the familial amyotrophic lateral sclerosis fALS6. The encoded FUS functions as a heterogeneous nuclear ribonuclear protein (hnRNP) with DNA/RNA-binding properties via a glycine-rich C-terminal motif. FUS has been implicated in DNA transcription and repair, and also in mRNA process and transport. Formation of FUS containing protein aggregates is a common cytopathology feature of the disease. It predominantly accumulates in the spinal motor neurons but it can also be found in the cortex and in the motor nuclei of the brainstem. Several affected pathways have been suggested, such as impaired intracellular trafficking, mRNA processing defect, redistribution of SMN protein causing axonal defect, altered DNA repair machinery and defective presynaptic function. However, the precise disease mechanism still needs to be clarified. (Armstrong and Drapeau, 2013; Groen *et al.*, 2013; Qiu *et al.*, 2014; Tibshirani *et al.*, 2015)

The heterozygous missense c.1529A>G, p.Lys510Arg *FUS* mutation carried by the patient has been earlier reported causing a mild ALS phenotype with a longer survival time (Waibel *et al.*, 2010, 2013). On the contrary, the progression observed in the patient was rather rapid, developing motor loss and frontal dementia 6 months after the onset of the disease. We suggested that the identified *FUS* mutation presented with overlapping symptoms between ALS and dHMN.

5.5.3.3 Impaired axonal transport

The unusual size of the motor neurons and their large metabolic activity require appropriate communication between the cell and its periphery. Mutations affecting different members of the complex trafficking system have been associated with overlapping degenerative neurological conditions of upper and/or lower motor neuron pathology. Impairment of the kinesin family (*KIF1B*) directed anterograde and the dynein-dynactin mediated (*DYNC1H1*, *BICD2*, *DCTN1*) retrograde trafficking have been both implicated in motor neuron degeneration.

Mutations in the *cytoplasmic dynein 1 heavy chain 1 (DYNC1H1)* gene have been described in a range of central and peripheral nervous system disorders, providing a continuum from developmental neuron migration defect to impaired axonal trafficking. The cytoplasmic DYNC1H1 is a large protein (>530 kDa) and is the most important component of the dynein motor complex by binding dynein subunits. DYNC1H1 is implicated in recruiting subcellular cargos via its N-terminal tail domain and in generating force to move along the

microtubules through its C-terminal microtubule-binding and through ATP hydrolysing units. Reported phenotypes include axonal motor and sensory neuropathy type O (CMT2O) OMIM# 614228, autosomal-dominant lower extremity predominant spinal muscular atrophy-1 (SMALED1) OMIM#158600, hereditary spastic paraplegia (HSP), congenital lower motor neuron disease associated with focal areas of cortical malformation (SMA-FACM) and autosomal-dominant mental retardation-13 (MRD13) OMIM#614563 with or without cortical malformation defect (Weedon *et al.*, 2011; Harms *et al.*, 2012; Tsurusaki *et al.*, 2012; Peeters *et al.*, 2015; Scoto *et al.*, 2015; Strickland *et al.*, 2015).

The heterozygous missense c.1834G>A, p.Val612Met *DYNC1H1* mutation was identified in a cohort patient (*Family 7*) with the presentation of SMA-LED. Neurology examination found distal motor leg weakness and pes cavus foot deformities accompanied by EMG evidence of chronic neurogenic denervation. There was an incomplete disease penetrance in his family with variably severe foot deformities. The p.Val612Met amino acid change is located on the dimerization domain of the DYNC1H1 N-terminal tail, where all other SMA-LED-related mutations seem to cluster. The same p.Val612Met *DYNC1H1* mutation has been previously reported worldwide on different haplotype backgrounds. The *DYNC1H1*-related SMA-LED is typically accompanied by various degrees of joint contractures, including Achilles tightness, hip dislocation or congenital arthrogyriposis. Learning difficulties, attention and behaviour problems and epilepsy have occasionally been described.

There were numerous polymorphisms found in the large *DYNC1H1* gene in further cohort patients. In addition to that, no clear genotype-phenotype correlations exist with *DYNC1H1* mutations. Therefore, cautious analysis of all novel variants is warranted before considering them to be pathogenic.

The *bicaudal D homolog 2 (BICD2)* mutation identified in the cohort families (*Family 5-6*) will be discussed in detail in *Chapter 6.4*. We supported that the common p.Ser107Leu is a mutational ‘hot spot’ and that mutations in the *BICD2* gene should be considered even in sporadic SMA-LED cases (Bansagi, Griffin, *et al.*, 2015; Rossor, Oates, *et al.*, 2015b).

The *dynactin-1 (DCTN1)* gene encodes the p150 subunit of the transporter protein dynactin. *DCTN1* mutations contribute to various forms of neurodegenerative conditions, including Perry syndrome OMIM#168605, ALS, frontotemporal dementia and different types of parkinsonism. A distinct pattern of motor neuron involvement can be seen in distal hereditary motor neuronopathy type VIIB (dHMN7B) OMIM#607641, which presents with

combined spinal and bulbar muscular atrophy. The distal predominant upper limb amyotrophy is accompanied by vocal cord paralysis (Puls *et al.*, 2003, 2005; Araki *et al.*, 2014; Caroppo *et al.*, 2014).

The heterozygous missense c.3823C>T, p.Arg1275Cys *DCTN1* mutation was identified in the cohort patient (*Family 28*), who presented with distal motor neuropathy and extrapyramidal dystonia (Daud *et al.*, 2015).

5.5.3.4 Channelopathies

Channelopathies have been implicated in the pathology of motor neuropathies by disrupting metabolic homeostasis and impairing intracellular trafficking.

Disturbed calcium homeostasis by mutations in the *transient receptor potential vanilloid 4 channel (TRPV4)* gene cause widely diverse phenotypes. Phenotype-genotype correlations and cohort patients (*Family 10-11*) identified with *TRPV4* mutations will be analysed in *Chapter 6.3*.

X-linked length-dependent metabolic axonopathy has been reported with mutations in the *APTase copper transporting alpha (ATP7A)* gene inducing aberrant intracellular trafficking (Kennerson *et al.*, 2010). The complex motor neurodegeneration observed in the cohort patient (*Family 29*) related to the novel c.2279A>G, p.Tyr760Cys *ATP7A* mutation (Bansagi *et al.*, 2016) will be detailed in *Chapter 6.5*.

5.5.3.5 Mitochondrial dysfunction

Impairment in the oxidative metabolism and in the energy maintenance of neurons has been implicated in degenerative motor neuron diseases. The importance of undisturbed mitochondrial function in motor neurons has been highlighted by the numerous gene defects affecting mitochondrial fusion/fission and mitochondrial metabolism.

Mitochondrial abnormalities were commonly found in the cohort patients with all forms of motor neuropathies. Gene mutations contributed to the symptoms by altering mitochondrial fusion/fission (*MFN2*, *DNM2*, *SLC25A46*), axonal transport of mitochondria (*HSPB1*, *HSPB8*), mitochondrial protein synthesis (*C12orf65*, *SACS*), or transport of mitochondrial cofactors (*SLC52A2/3*).

Mitochondrial fusion/fission

Mitochondria are highly dynamic structures going through repetitive fission and fusion processes, called mitochondrial dynamics, which is required for mitochondrial function maintenance. Efficient mitochondrial dynamics is essential to provide energy supply for the

complex machinery of axonal transport and to maintain the formation of axons by regulating apoptotic pathways (Westermann, 2010; Pareyson *et al.*, 2015).

Mitofusin 2 (MFN2) is the commonest gene mutated in CMT2 leading to axonal motor and sensory neuropathy (CMT2A) with large inter- and intrafamilial variability. MFN2 is an outer mitochondrial membrane protein that is responsible for mitochondrial fusion, aided by special structural features of a GTPase domain for GTP hydrolysis and two coiled coil regions (HR1 and HR2) for tethering opposing mitochondria. *MFN2*-related phenotypes have been differentiated according to the age of onset and disease severity. Additional symptoms of optic atrophy, pyramidal signs, vocal cord palsy and central nervous system involvement often complicate the clinical presentation (Züchner *et al.*, 2004, 2006, Chung *et al.*, 2006, 2010; Verhoeven *et al.*, 2006; Klein *et al.*, 2011; Choi *et al.*, 2015). Among the around 100 *MFN2* variants some have been linked to sensory autonomic axonal neuropathy (Martikainen *et al.*, 2014) but no association with demyelinating CMT (CMT1) or with dHMN has been reported.

The phenotype heterogeneity related to *MFN2* mutations was well illustrated in the cohort pedigrees presenting adolescent-onset dHMN (*Family 12*), late adult-onset dHMN (*Family 13*) and asymmetric upper limb motor CMT2 (*Family 23*). The 2 patients presenting with the dHMN phenotype were diagnosed with previously reported *MFN2* mutations.

A young male patient from the cohort (*Family 12*) carried the heterozygous missense c.1126A>G, p.Met376Val *MFN2* mutation, which caused an amino acid change in the protein region linking the GTPase domain with the first coiled coil domain. The mutation detected *de novo* in the patient caused an adolescent-onset rapidly progressive dHMN phenotype. He developed bilateral pes cavus and hammer toes deformities and his gait was impaired by unsteady tiptoeing due to severe ankle contractures. Absent distal CMAP responses with preserved sensory amplitudes in the lower limbs indicated distal spinal motor neuron pathology. The same p.Met376Val *MFN2* mutation has been reported in one CMT2 family of Spanish origin (Casasnovas *et al.*, 2010). The same methionine 376 residue was exchanged for an isoleucine in a German patient (Engelfried *et al.*, 2006) and for a threonine in a Korean pedigree (Chung *et al.*, 2006) with a late-onset mild CMT2 phenotype.

The heterozygous missense c.2119C>T, p.Arg707Trp *MFN2* mutation was found *de novo* in a 70-year-old patient from the cohort (*Family 13*). The p.Arg707Trp change locates in the *MFN2* C-terminal coiled coil region (HR2) and presumably disrupts the coiled coil bond tethering and fusion of apposed mitochondria. He presented with a late adult-onset slowly deteriorating motor weakness affecting both proximal and distal muscle groups in his

unilateral extremities. Deep tendon reflexes were absent with no jointed upper motor neuron symptoms. He developed Alzheimer disease and became wheelchair bound. The EMG studies revealed a chronic neurogenic process in the upper and lower limb muscles on the right body side suggesting anterior horn cell pathology. The p.Arg707Trp *MFN2* mutation has been reported to cause CMT2 with a semidominant inheritance pattern. Homozygous or compound heterozygous mutations involving the p.Arg707Trp change resulted in an early-onset severe axonal CMT2A phenotype while heterozygous transitions led to a milder form of axonal neuropathy with incomplete penetrance (Nicholson *et al.*, 2008; Carr *et al.*, 2015). Interestingly, the homozygous p.Arg707Trp *MFN2* mutation has been recently linked to the clinical entity of multiple symmetric lipomatosis (MSL) and neuropathy, where MSL causing MERRF mutations could not be identified (Sawyer *et al.*, 2015).

Dynamin-2 (DNM2) belongs to the large GTPase family, similarly to *MFN2*, and mediates intracellular membrane trafficking, endo- and exocytosis through the membrane fission process (Sidiropoulos *et al.*, 2012; Tinelli *et al.*, 2013). Deletion and missense mutations in the *DNM2* gene have been reported with dominant intermediate CMT type B (CMTDIB) and axonal CMT2 (CMT2M) accompanied by mutation specific additional features of neutropenia and cataract (Claeys *et al.*, 2009). Different set of *DNM2* mutations cause autosomal-dominant centronuclear myopathy (Tinelli *et al.*, 2013). The majority of the neuropathy-related mutations affect the pleckstrin homolog domain of the *DNM2* protein. Proposed pathological pathways include abnormal axonal transport, disturbed protein trafficking and a clathrin-mediated endocytosis defect (Claeys *et al.*, 2009; Sidiropoulos *et al.*, 2012).

The heterozygous c.1739T>C, p.Met580Thr missense *DNM2* mutation was detected in a dominant two-generation family from the cohort (*Family 22*) with a heterogeneous intermediate motor neuropathy phenotype. The affected methionine 580 residue is located in the highly conserved hydrophobic dipeptide, which is required for membrane association. The replacement of methionine with a polar threonine presumably impairs the membrane fission process (Haberlová *et al.*, 2011). All family members presented with first decade-onset lower limb distal motor weakness with clawed toes and pes cavus foot deformities. The disease progression was slow with the involvement of intrinsic hand muscles at later ages, leading to decreased strength of the handgrip and fixed contractures of the fingers. The 59-year-old index patient had accompanying hearing impairment, split hand deformity and respiratory muscle involvement. Nerve conduction velocities were reduced but not in the range typically

seen in demyelinating neuropathy, while motor and sensory amplitude responses were significantly diminished. EMG revealed a chronic neurogenic pattern or remained normal. The same p.Met580Thr *DNM2* mutation was reported with striking intrafamilial variability in a large pedigree of Czech origin, including CMT2, intermediate motor CMT and dHMN disease phenotypes (Haberlová *et al.*, 2011). A similar motor predominant neuropathy characterised the family in the cohort with sensory deficits on electric nerve testing. In contrast to the Czech patients, upper limb involvement was more prominent in the cohort family. The possibility that patients with motor neuropathy may develop concomitant myopathy can be supported with the overlapping symptom observed in the p.Glu368Gln *DNM2* mutation (Echaniz-Laguna *et al.*, 2007). This may provide an explanation, why the index patient of the cohort family developed respiratory muscle weakness.

Axonal transport of mitochondria

Mutations in the *small heat-shock protein 22-kDa protein 8 (HSPB8)* have been associated with dHMN type II (HMN2A) (Irobi, Van Impe, *et al.*, 2004), CMT2 (CMT2L) (Tang *et al.*, 2005) and most recently with combined distal myopathy and motor neuropathy (Ghaoui *et al.*, 2016). The disease mechanism of heat-shock proteins is complex and not yet fully clarified. Intracellular aggregate formation due to impaired chaperone activity (Irobi, Van Impe, *et al.*, 2004; Carra *et al.*, 2005), selective degeneration of motor neurites with subsequent axonal transport damage (Ackerley *et al.*, 2006; Irobi *et al.*, 2010; Pareyson *et al.*, 2015) and defected chaperone-associated selective autophagy (Kwok *et al.*, 2011) have been all implicated in the pathology.

The heterozygous c.421A>G, p.Lys141Glu *HSPB8* mutation in the cohort patient (*Family 1*) presented with an early-onset rapidly progressive dHMN. The missense *HSPB8* mutations, which were reported so far all affect the Lys141 residue, suggesting that this is a mutational `hot spot` within the conserved alpha-crystallin domain of the small heat shock protein 22 kDa (Hsp22) (Irobi, Van Impe, *et al.*, 2004; Nakhro *et al.*, 2013).

Defected mitochondrial protein synthesis

The autosomal-recessive spastic ataxia of Charlevoix-Saguenay (ARSACS) is a complex disorder with progressive cerebellar and corticospinal tract degeneration caused by mutations in the *sacsin (SACS)* gene (Blumkin *et al.*, 2015). The diagnosis can be prompted by the classical triad of early childhood-onset ataxia, spasticity and peripheral neuropathy, which is accompanied by specific neuroimaging features of superior vermis atrophy and signal changes in the pons (Gregianin *et al.*, 2013; Synofzik *et al.*, 2013).

However, atypical and incomplete symptom presentations complicate the phenotype spectrum of the sacinopathies (Takiyama, 2006; Synofzik *et al.*, 2013). Patients predominantly presenting with peripheral neuropathy (Pyle *et al.*, 2012), spastic paraplegia (Gregianin *et al.*, 2013), autonomic disturbances (Synofzik *et al.*, 2013) or retinal changes (Yu-Wai-Man *et al.*, 2014; Blumkin *et al.*, 2015) cause challenges in the differential diagnosis.

The novel compound heterozygous c.1580C>G, p.Ser527* nonsense and c.6781C>A, p.Leu2261Ile missense *SACS* mutations were identified by WES in a male patient from the cohort (*Family 30*). His phenotype was dominated by a motor predominant neuropathy-causing gait difficulties from his late 10's and the diagnosis could be achieved later with the evolving lower limb spasticity.

More than 170 mutations have been reported in the *SACS* gene so far, providing a highly heterogeneous genotype background. Homozygous or compound heterozygous *SACS* mutations have loss-of-function consequences. The encoded highly conserved sacin protein seems to have an essential role in the regulation of mitochondrial physiology. Mitochondrial dynamics and localisation have been implicated in the disease pathology. Sacin localises to the mitochondria and interacts with dynamin-related protein 1, which is a large GTPase required for mitochondrial fission (Girard *et al.*, 2012; Blumkin *et al.*, 2015; Pilliod *et al.*, 2015). The domains of the sacin protein contain analogous regions with heat-shock and ubiquitin proteins, which suggests common pathways involving chaperon mediated protein folding (Takiyama, 2006; Anesi *et al.*, 2011; Gregianin *et al.*, 2013).

Homozygous mutations in the ***chromosome 12 open reading frame 65 (c12orf65)*** gene impair the mitochondrial protein translation. The encoded c12orf65 has a common glycine-glycine-glutamine (GGQ) motif with the mitochondrial class I release factors, which have an essential role in the termination of the mitochondrial protein translation. It is suggested that c12orf65 recycles the peptidyl-tRNAs, which were prematurely released and ensures an intact mitochondrial protein translation (Antonicka *et al.*, 2010; Shimazaki *et al.*, 2012; Buchert *et al.*, 2013). *C12orf65* mutations induce multiple mitochondrial defects. Mitochondrial copy number and membrane potential changes, such as impairments in the oxidative phosphorylation have been reported (Tucci *et al.*, 2014). There is a well-defined genotype correlation with the severity spectrum of the allelic phenotypes. The triad of optic nerve atrophy, spastic paraparesis and axonal neuropathy defines all phenotypes (Spiegel *et al.*, 2014).

The combined oxidative phosphorylation deficiency type 7 (COXPD7) is induced by the mutational disruption of the c12orf65 GGQ motif. Severe Leigh-syndrome like symptoms

present with a slow but unfavourable progress (Antonicka *et al.*, 2010; Heidary *et al.*, 2014). Behr's syndrome can be considered as the intermediate *c12orf65* phenotype, supported by the fact that *c12orf65* mutations have been the most frequently identified genetic changes in this condition. Behr's syndrome is a complex childhood-onset neurological disorder with psychomotor retardation, optic atrophy, ataxia and pyramidal signs. The male patient from the cohort (*Family 26*), who presented with Behr's syndrome and axonal motor neuropathy carried the homozygous truncating c.96_99dupATCC, p.Pro34Ilefs*25 *c12orf65* mutation (Pyle *et al.*, 2014).

C12orf65 mutations leading to shorter protein length have been reported with milder allelic phenotypes, such as autosomal-recessive spastic paraplegia-55 (SPG55) and autosomal-recessive CMT type 6 (CMT6) (Shimazaki *et al.*, 2012; Tucci *et al.*, 2014). CMT6 is a group of variably inherited conditions with a combined presentation of motor and sensory neuropathy and optic atrophy. Axonal neuropathy-related *MFN2* mutations occasionally cause optic nerve involvement and autosomal-dominant CMT6 phenotype. Mutations in the X-linked phosphoribosylpyrophosphate synthetase I (*PRSP*) gene have been also linked to CMT6 (Tucci *et al.*, 2014). A most recent report on recessive mutations in the solute carrier family 25 member 46 (*SLC25A46*) described a recessive CMT6 phenotype by disrupting mitochondrial dynamics (Abrams *et al.*, 2015).

A young male patient from the cohort (*Family 31*) developed distal motor weakness and atrophy in his legs with pes cavus and clawed toes deformities and mild sensory loss. His visual acuity deteriorated soon after the disease-onset and he was diagnosed with bilateral optic nerve atrophy. The muscle biopsy analysis indicated combined respiratory chain defects with decreased mitochondrial complex I, III and IV activity, although mitochondrial mutations could not be identified. A heterozygous c.2386C>T, p.Gln796* nonsense mutation in the *FIG4* gene was detected by next generation sequencing, which was earlier reported as a pathogenic variant (DiVincenzo *et al.*, 2014). *FIG4* mutations cause autosomal-recessive motor and sensory neuropathy (CMT4J) with demyelinating features and highly variable phenotype (Chow *et al.*, 2007; Nicholson *et al.*, 2008). Compound heterozygous *FIG4* mutations were described but in the cohort patient no second mutation could be found. Heterozygous *FIG4* mutations have been reported with adult-onset ALS with no evidence of optic nerve involvement (Chow *et al.*, 2009).

Transport of mitochondrial cofactors

Riboflavin (vitamin B2) and its bioactive intracellular forms, flavin adenine dinucleotide (FAD) and flavin mononucleotide (FMN), are essential cofactors for mitochondrial oxidation-

reduction pathways and mitochondrial protein translation. They play key roles in the metabolism, signal transduction, apoptosis and DNA repair (Johnson *et al.*, 2012; Ciccolella *et al.*, 2013; Timmerman and De Jonghe, 2014). Three transporters are responsible for the riboflavin homeostasis in humans by providing carrier mediated riboflavin absorption from the intestine and by distributing riboflavin to the central nervous system. Mutations in the riboflavin transporter encoding *solute carrier family 52 members (SLC52A2 and SLC52A3)* have been reported to cause Brown-Vialetto-Van Laere syndrome (BVVL) (Bennett, 2012; Bosch *et al.*, 2012; Johnson *et al.*, 2012; Ciccolella *et al.*, 2013; Yonezawa and Inui, 2013). The classical BVVL consists of progressive bulbar palsy, preceded by sensorineuronal hearing loss and generalised muscle weakness, with less commonly recognised sensory changes. Mutations in *SLC52A3* have been identified and riboflavin introduction proved to have beneficial therapeutic effects. However, the majority of the childhood-onset BVVL was associated with mutations in *SLC52A2* and showed a progressive axonal motor and sensory neuropathy phenotype. The initial sensory ataxia is followed by progressive motor weakness in the neck and in the distal upper limb muscles. Sensorineuronal hearing loss and progressive bulbar palsy leading to respiratory impairment are shared features in both phenotypes, such as the therapy response to riboflavin supplementation (Foley *et al.*, 2014; Srour *et al.*, 2014; Timmerman and De Jonghe, 2014).

The 5-year-old girl from the cohort (*Family 25*) diagnosed with upper limb predominant axonal motor and sensory neuropathy and with hearing loss carried the compound heterozygous c.916G>A, p.Gly306Arg and c.1016T>C, p.Leu339Pro missense mutations in the *SLC52A2* gene.

The single heterozygous missense c.1371C>G, p.Phe457Leu *SLC52A3* mutation was identified in a 19-year-old man (*Family 32*) with BVVL phenotype and with a dramatic response on riboflavin administration. This same *SLC52A3* variant was earlier reported as pathogenic (Green *et al.*, 2010). The presence of a second *SLC52A3* mutation could not yet be identified. Interestingly, the heterozygous c.819C>T, p.Met273Ile missense change in *SLC52A2* was also found by WES, affecting the weakly conserved Met273 residue with ambiguous pathological *in silico* consequences.

His disease started with bilateral hand weakness, gait ataxia and hearing impairment. Later, his motor weakness became prominent, primarily affecting the axial and upper limb muscles and his intrinsic hand muscles were strikingly wasted. Deep tendon reflexes were lost but there were no pyramidal tract signs. Progressive bulbar palsy evolved with facial weakness, ophthalmoplegia, tongue fasciculations and bilateral vocal cord palsy requiring an intermittent ventilation therapy. Laboratory tests indicated a normal serum riboflavin level and an intact

acyl-carnitine profile. Neurophysiology suggested a rapidly progressive motor and sensory axonal neuropathy with neurogenic muscle changes. Neuroimaging showed extensive signal abnormalities bilaterally in the posterior columns of the spinal cord, extending from the cervical level down to the conus.

We speculated that either deep intronic mutations / intragenic rearrangements in *SLC52A3* might have remained undetected or the combination of the heterozygous missense mutations in *SLC52A3* and *SLC52A2* might have led to the disruption in the riboflavin homeostasis.

5.5.3.6 Neuromuscular transmission defect

Non-progressive motor neuropathy and fatigable weakness due to a presynaptic neuromuscular transmission defect was caused by *synaptotagmin 2 (SYT2)* mutations in the cohort patients (*Family 4*) (Herrmann *et al.*, 2014).

The related distal motor neuropathy phenotype and the novel disease mechanism will be discussed in *Chapter 7.1* and in *Chapter 8*, respectively.

5.5.3.7 Disturbed intracellular transcription pathways

Altered intracellular signal transduction and disturbed transcriptional regulatory cascades form common pathways and highlight further targets in the therapy of motor neuropathies.

A missense mutation affecting the *Rho guanine nucleotide exchange factor 10 (ARHGEF10)* gene co-segregated in a large dominant Belgian pedigree with intermediate nerve conduction velocities and thinly myelinated axons (Verhoeven *et al.*, 2003).

ARHGEF10, as part of the larger RhoGEFs family, participates in a signal transduction pathway unique for vertebrates. They share a common catalytic Dbl homology domain, which is required for the activation of RhoGTPases by catalysing the replacement of GDP with GTP. RhoGTPases have been implicated in numerous cellular processes, involving cytoskeleton dynamics, neuronal morphogenesis and plasticity. The non-progressive, very mild neuropathy phenotype linked to the described *ARGHEF10* mutation was suggested to cause a constitutively active RhoGTPase mutant, which led to Schwann cell dysfunction and migration defect (Verhoeven *et al.*, 2003; Mohl *et al.*, 2006; Chaya *et al.*, 2011).

The heterozygous missense c.1949G>A, p.Tyr650Cys *ARHGEF10* mutation was found in a young female patient from the cohort. At birth she had bilateral congenital talipes and hip dislocation and her motor development was also delayed by patella femoral instability.

Intrinsic hand muscle weakness, swallowing difficulty and keloid formation complicated the course of her disease. Upper limb conduction studies were intact, while no responses could be recorded in the lower extremities. EMG showed evidence of longstanding neurogenic changes

suggesting slowly progressive anterior horn cell pathology. SFEMG showed complex potentials with a significantly increased jitter. The identified c.1949G>A *ARHGEF10* sequence change caused the substitution of a highly conserved cysteine for a tyrosine at the 650 codon downstream to the catalytic Dbl homology domain. Detrimental effects were predicted by *in silico* tools.

A 10 base pair deleted c.1955_58+6delCACGGTGAGC *ARHGEF10* splice variant has been recently described to induce loss of function effects in Leonberger dogs. These large bodied dogs presented with juvenile-onset pelvic motor weakness and with degeneration of the recurrent laryngeal nerve. Histopathology indicated axonal degeneration with subsequent neurogenic muscle changes. Homozygous deletions were strongly correlated with a juvenile-onset rapidly progressive phenotype, while variable clinical courses were seen with heterozygous deletions (Ekenstedt *et al.*, 2014). The human and canine *ARHGEF10* sequences are largely homolog and the mutation of the patient was located close to the Leonberger deletion. Earlier studies proved that the C-terminal truncated *ARHGEF10* mutant was hardly able to activate RhoGTPases (Mohl *et al.*, 2006). Further investigations are necessary to decide on the pathogenicity of the identified *ARHGEF10* variant.

In an additional 3 cohort families possibly pathogenic variants were found in not neuropathy-related genes, where affected intracellular signal pathways and previous experimental studies suggested that the deficiency of these genes might cause peripheral nerve involvement.

Mutations in the *T-box 5 (TBX5)* gene are located within the DNA-binding T-box domain, such as the pathogenic c.331G>T, p.Asp111Tyr variant in the cohort patient (*Family 33*) and they influence transcriptional regulatory cascades (Heinritz *et al.*, 2005). Segregation studies and phenotype characteristics will be discussed in *Chapter 7.2.3*.

Signal transducer and activator of transcription 5B (STAT5B) mutations have been implicated in insulin-growth factor 1 (IGF1) signal pathways and cause postnatal growth retardation (Kofoed *et al.*, 2003). The clinical phenotype related to the homozygous c.944T>G, p.Glu315Ala *STAT5B* mutation identified in the consanguineous family (*Family 34*) and the theoretical disease mechanisms will be detailed in *Chapter 7.2.2*.

Mutations in the ***phosphatase and tensin homolog located on chromosome 10 (PTEN)*** inhibit the phosphoinositide 3-kinase (PI3-K) signalling pathway, which has been implicated in peripheral neuron plasticity, axonal outgrowth and hypermyelination (Christie *et al.*, 2010) (Christie *et al.*, 2010). The multifocal motor neuropathy phenotype with the *de novo* c.269T>C, p.Phe90Ser *PTEN* mutation (*Family 35*) and experimental functional studies will be discussed in *Chapter 7.2.1*.

5.6 Conclusion

In summary, this study extensively investigated the phenotypic variability and the genetic spectrum of motor neuron- neuronopathies. Considering all HMN subgroups, a significant 47.9% mutation detection rate was achieved by identifying potentially causative gene mutations in the large representative patient cohort. More importantly, the genetic cause was diagnosed in 32.5% of dHMN and in a further 10% possibly causative gene mutations were identified. The mutation detection rate achieved in the study was significantly higher compared to the 20% reported in previous cohorts. The significant increase in the diagnostic detection rate might be attributable for the development of next generation techniques and international genetic databases. The genetic spectrum was widely heterogeneous, although it showed some geographical distribution specificities. It is highly likely, that the genetically not yet clarified motor neuropathy pedigrees possess mutations in novel genes and unravelling these genes will remain in the focus of further investigations. Many of the undiagnosed patients have been included in the 100.000 genome project. The increasing data and knowledge about the implicated disease pathways will not only help to identify new genes with shared pathomechanisms but it will also provide a basis for novel therapy approaches. An illustrative example can be the *SYT2* mutation, where therapeutic modification of the neurotransmission proved to have beneficial effects (Whittaker *et al.*, 2015). Genotype-phenotype correlations in large patient cohorts and natural history studies along with unravelling the function of responsible genes and proteins facilitate the development of novel approaches for therapy (Peeters *et al.*, 2014; Timmerman *et al.*, 2014).

Chapter 6. Phenotype-genotype analysis in hereditary motor neuropathies

6.1 Aminoacyl-tRNA synthetases (ARS)-related motor neuropathies

Mutations in six genes encoding aminoacyl-tRNA synthetases (ARS) have been implicated in axonal pathology. The majority of the mutations were reported to affect glycyl-tRNA synthetase (GARS, OMIM#600287) causing CMT2 type D (CMT2D) or distal spinal muscular atrophy type V (dSMA-V), both are autosomal-dominant upper limb predominant motor axonal neuropathies. Mutations in alanyl-aminoacyl-tRNA synthetase (AARS, OMIM#601065) were described in autosomal-dominant axonal CMT type 2N (CMT2N) and distal hereditary motor neuropathy. Mutations in tyrosyl-tRNA synthetase (YARS, OMIM#603623) cause dominant intermediate CMT type C (CMTDIC). Histidyl-tRNA synthetase (HARS, OMIM#142810) and methionyl-tRNA synthetase (MARS, OMIM#156560) mutant variants were identified in autosomal-dominant CMT2 patients. Compound heterozygous lysyl-tRNA synthetase (KARS, OMIM#601421) mutations were present in one patient with recessive intermediate CMT type B (CMTIRB) manifesting as part of a more complex neurological condition (Jordanova *et al.*, 2006; McLaughlin *et al.*, 2010, 2012; Zhao *et al.*, 2012; Gonzalez *et al.*, 2013; Vester *et al.*, 2013; Griffin *et al.*, 2014; Safka Brozkova *et al.*, 2015).

Aminoacyl-tRNA synthetases (ARS) are ubiquitously expressed and highly conserved enzymes. They maintain the fidelity of the genetic code during protein translation by binding and activating amino acids and conjugate them with their cognate tRNA molecules (Latour *et al.*, 2010; Griffin *et al.*, 2014). There have been 37 nuclear genes identified encoding ARSs for cytoplasmic or mitochondrial protein synthesis. Mutations in the so far described neuropathy-related ARS genes are mostly missense amino acid substitutions leading to dominant CMT phenotypes. Several hypotheses have been proposed in the mechanisms of ARS-related CMT pathology. In vitro aminoacylation assays were suitable for detecting impaired enzyme activity or qualitative defects from non-cognate bindings. Yeast viability assays investigated in vivo functional consequences of the ARS mutations and loss of function characteristics. These studies suggested that impaired tRNA charging is a component of the pathogenesis. However, reduced aminoacylation activity is not general for all mutant ARS variants and gain of toxic function was also considered. Protein localisation studies revealed altered distribution of some of the ARS proteins in cultured neurons suggesting

spatially inappropriate protein synthesis (Motley *et al.*, 2010; McLaughlin *et al.*, 2012; Griffin *et al.*, 2014).

6.1.1 Aims

My interest was focused on dominant *AARS* and *GARS* mutant pedigrees, where abnormal protein translation resulted in the manifestation of motor neuropathy. I aimed to characterise the natural history of patients diagnosed with these gene mutations. I was looking for gene specific and overlapping symptoms and I aimed to analyse phenotype-genotype correlations in each genetic subgroups.

6.1.2 Methods

6.1.2.1 Patient recruitment

Patients diagnosed with *AARS*-related neuropathy between 2010 and 2015 were involved from England and Ireland. Three pedigrees of North-East England origin (*Families 18-20*) were recruited from the motor neuropathy cohort (*Chapter 5.4.3*), while 1 family from the South of England was followed up by Dr Hilton-Jones and 2 families from Ireland by Dr Murphy. Two pedigrees with novel *GARS* variants (*Families 2-3*) were selected from the motor neuropathy cohort (*Chapter 5.4.2.1*) for comparison with the so far reported *GARS*-related phenotypes. From all included patients detailed medical and family history was collected and clinical assessments were carried out by me or by the above named neurologists. All participants provided written informed consent to be involved in the study, which was approved by local research ethics committees.

6.1.2.2 Diagnostic genetic methods

All included *AARS* and *GARS* mutant pedigrees were diagnosed by IPN gene panel assay utilising next generation sequencing (NGS) in the Bristol Genetics Laboratory (*Chapter 3.2.1.1*).

6.1.2.3 Neurophysiology

Nerve conduction studies and needle electromyography were performed in the index patients and in additional affected relatives from all families by local neurophysiologists.

6.1.2.4 Outcome measure

Validated CMT Neuropathy Score (CMTNSv2) was applied for monitoring disease progression in the patients (Murphy *et al.*, 2011) (**Table 3.1**).

6.1.3 AARS-related neuropathy

6.1.3.1 Literature review

Mutations in the *AARS* (OMIM#601065) gene, which encodes alanyl-aminoacyl-tRNA synthetase, have been associated with autosomal-dominant axonal CMT type 2N (OMIM#613287) and distal hereditary motor neuropathy. Only a few dominant families with *AARS* mutations have been reported so far, presenting clinically with heterogeneous phenotypes. The recurrent c.986G>A, p.Arg329His mutation was reported in two unrelated French pedigrees, where distal motor and sensory degeneration secondary to predominant axonal neuropathy manifested at various ages of onset (Latour *et al.*, 2010). The same p.Arg329His variant caused sensorineural deafness and early-onset axonal neuropathy with intermediate nerve conduction velocities in a large Australian family (McLaughlin *et al.*, 2012). Another c.2333A>C, p.Glu778Ala mutation with motor and sensory axonal neuropathy and rippling muscles and cramps was identified in an Australian patient, while only rippling muscles were present in three affected relatives (McLaughlin *et al.*, 2012). Pure axonal neuropathy in a Taiwanese pedigree associated with the c.211A>T, p.Asn71Tyr variant (Lin *et al.*, 2011). A distal hereditary motor neuropathy (dHMN) phenotype with neurogenic electromyography changes was related to the c.2677G>A, p.Asp893Asn mutation in a three generation dominant Chinese family (Zhao *et al.*, 2012). Recently, a novel heterozygous missense c.304G>C, p.Gly102Arg *AARS* mutation was described presenting with a novel myeloneuropathy phenotype in a large family (Motley *et al.*, 2015). Autosomal-recessive loss of function *AARS* mutations (compound heterozygous p.Lys81Thr and p.Arg751Gly and homozygous p.Arg751Gly) were reported in two unrelated families causing severe infantile epileptic encephalopathy with a central myelin defect and peripheral neuropathy (Simons *et al.*, 2015) (**Table 6.1**).

The alanyl-aminoacyl-tRNA synthetase (*AARS*) protein has a 968 amino acids structure organised from the N-terminal into an aminoacylation or catalytic domain (AD), a helical or tRNA-binding domain (HD) and an editing domain (ED). Uniquely, a single base pair in the acceptor arm of tRNA^{Ala} is provided for specific alanine binding. The evolutionary integrated editing domain is responsible for eliminating mischarged tRNA^{Ala}. *AARS* domains possess highly conserved amino acid sequences throughout species from *E.coli* to *H. sapiens* (Latour *et al.*, 2010; Zhao *et al.*, 2012).

Origin	Family/ Patient Number	Nucleotide change	Amino acid Change	Age onset	Phenotype	Clinical symptoms			Nerve conduction study		Reference
						Lower limb	Upper limb	Symmetry	Motor NCV (m/s)	Motor / Sensory	
Taiwanese	F1 / P5	c.211A>T	p.Asn71Tyr	varied (11-30y)	CMT2	distal weakness, wasting mild sensory loss	mild weakness, wasting mild sensory loss	symmetric	m 38.1 p absent	MS	Lin KP <i>et al</i>
	F1 / P2				CMT2	mild weakness and wasting	none	symmetric			
French	F1 / P16	c.986G>A	p.Arg329His	varied (6-54y)	CMT2	bilateral distal weakness distal sensory loss	distal weakness distal sensory loss	symmetric	m 32.4-50	MS	Latour P <i>et al</i>
	F1 / P1				CMT2	severe distal wasting sensory loss	none	asymmetric			
French	F2 / P1	c.986G>A	p.Arg329His	14y	CMT2	mild distal weakness	none	symmetric	m 35-39	MS	Latour P <i>et al</i>
Australian	F1 / P9	c.986G>A	p.Arg329His	early	CMT2 + sensorineural deafness	distal weakness feet deformities sensorineural deafness	none	symmetric	intermediate	MS	McLaughlin HM <i>et al</i>
Australian	F1 / P4	c.2333A>C	p.Glu778Ala	n/a	CMT2 + rippling muscle	rippling muscles and cramps distal wasting mild distal sensory loss	none	symmetric	n/a	MS	McLaughlin HM <i>et al</i>
Chinese	F1 / P4	c.2677G>A	p.Asp893Asn	varied (11-55y)	dHMN	distal weakness and wasting, feet deformities	none	symmetric	normal	M	Zhao Z <i>et al</i>
Mixed European	F1 / P2	c.242A>C c.2251A>G	p.Lys81Yhr p.Arg751Gly	birth / months	CMT2 + CNS demyelination + epileptic encephalopathy	congenital vertical tali loss of reflexes dystonia	dystonia	symmetric	-	-	Simons C <i>et al</i>
	F2 / P1	c.2251A>G	p.Arg751Gly		CMT2 + CNS demyelination + epileptic encephalopathy						
American	F1 / P5	c.304G>C	p.Gly102Arg	varied (22-48y)	CMT2 + myelopathy	mild axonal neuropathy hyperreflexia	-	-	-	-	Motley WW <i>et al</i>

Abbreviations: F, family; P, patient; y, year; LL, lower limb; n/a, not available; m/s, meter per second; m, median nerve; p, peroneal nerve; M, pure motor; MS, motor and sensory; -, no data

Table 6.1 Summary of the clinical and electrophysiology findings accompanying the reported AARS variants

(Bansagi, Antoniadi, *et al.*, 2015)

6.1.3.2 Clinical and neurology findings in AARS mutant pedigrees

UK Family 1 (Family 19)

The 50-year-old male proband (III.1) (**Figure 6.1, A; B**) of a three generation North-British family developed symmetric distal muscle weakness, decreased grip strength and numbness in his upper limbs with a relatively sudden-onset at age 30. His fluctuating upper limb symptoms were later complicated by distal motor weakness and painful dysaesthesia in his legs, which led to gait deterioration and frequent falls. Aged 33 he developed an episode resembling an acute ischaemic cerebral attack, which involved the right side of his body with paralysis and paraesthesia and caused speech difficulties. He was unresponsive to therapy trials of steroids and IVIG, which was initiated with the suggestion of chronic inflammatory demyelinating neuropathy (CIDP) on electric nerve testing. The aetiology of the acute neurological symptoms has remained uncertain despite extensive investigations, including neuroimaging. After recovering, he continued to present with a lower limb predominant motor and sensory neuropathy. Pursuant to neurology follow-ups he demonstrated right sided predominant fingers and grip weakness (MRC grade 4-/5). He required bilateral hand splint support for manipulation. He had pes cavus deformities and dropped foot. His ankle plantar- and dorsiflexion was equally weak (MRC grade 3/5). Pinprick and vibration sensation was lost bilaterally below his mid calves and wrists. His poorly balanced steppage gait was aided by a unilateral walking stick. No cranial nerve involvement, pyramidal signs and cerebellar symptoms were observed. The CMTNSv2 was assessed 19/36.

The 77-year-old father of the proband (II.4) (**Figure 6.1, A; B**) presented with a childhood-onset, slowly progressive neuropathy, which resulted in gait difficulties only in his late adulthood. He underwent several foot surgeries during his childhood. In his late 60's he experienced pain in his lower limbs in a distribution characteristic for lumboischialgia, even though spinal images did not show related changes. He developed an exercise-induced limping with no underlying peripheral vascular pathology. After the age of 70 he deteriorated, rapidly losing his balance. The neurology examination of his lower limbs found distal muscle wasting and weakness with pes cavus deformities and severe foot drop. His ankle plantar- and dorsiflexion was markedly weak (MRC grade 1/5) and he was unable to move his toes. There was a mild atrophy and weakness affecting his intrinsic hand muscles (MRC grade 4+/5). His reflexes were globally absent. Pinprick sensation was lost below his wrists and ankles, while the level of the vibration loss was more proximal at his elbows and knees.

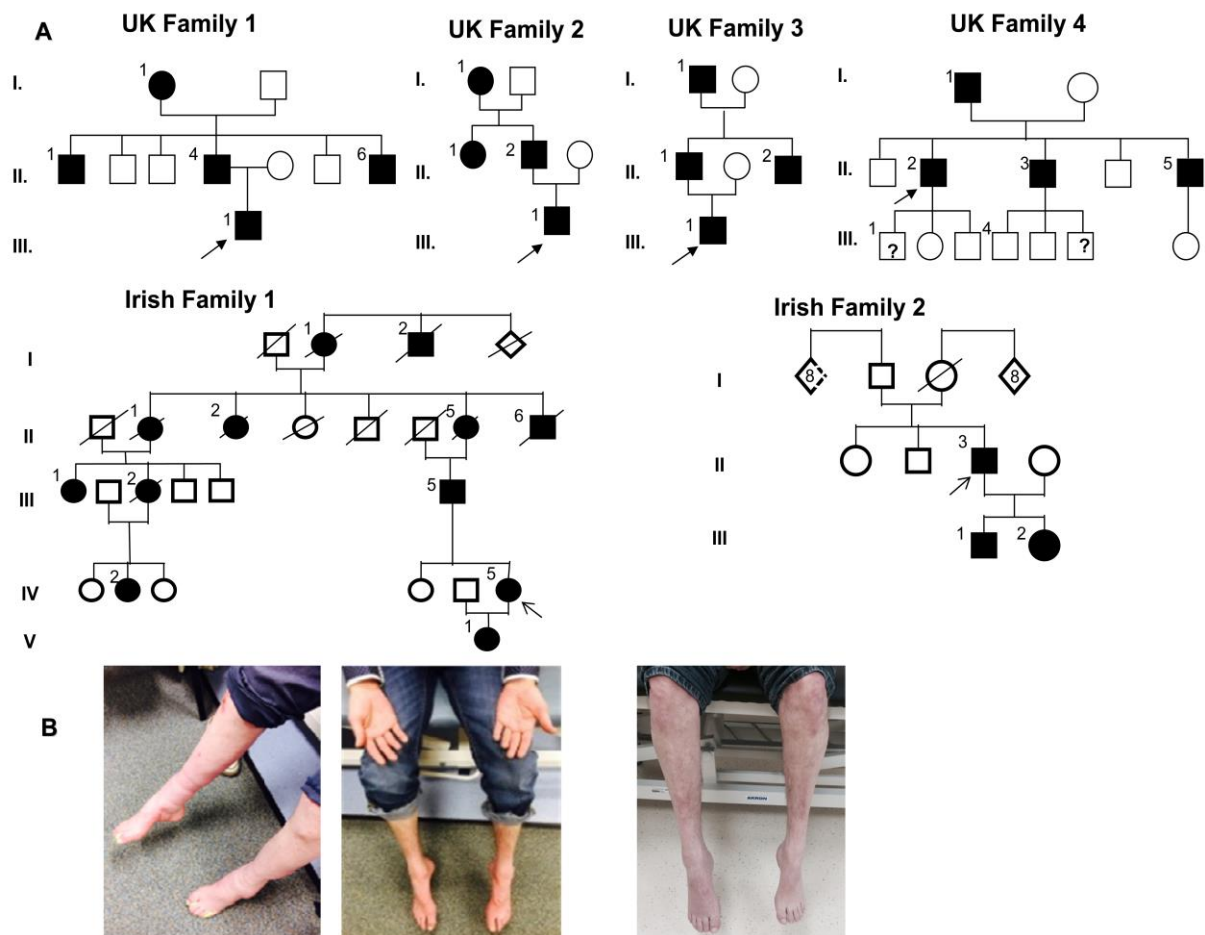


Figure 6.1 AARS mutant pedigrees

(A) Pedigrees of UK and Irish families. The arrows indicate the index patients of each family.

(B) Image of patient II/4 in UK family 1 showing predominantly lower limb symptoms presenting with bilateral pes cavus and severe foot drop. Index patient of the same UK1 family (III/1) representing moderate intrinsic hand muscles wasting accompanied by lower limb distal wasting and weakness. Image of patient (II.1) from UK family 3 showing severe bilateral foot drop and distal muscle wasting.

(Bansagi, Antoniadi, *et al.*, 2015)

His gait was supported by bilateral rigid splints and two crutches. The CMTNSv2 score was assessed 11/28, just before he passed away due to unrelated health issues.

Two of his 6 brothers (II.1 and II.6) and his mother (I.1) (**Figure 6.1, A**) were also diagnosed with peripheral neuropathy. Aged 53 his brother (II.6) developed distal motor and sensory loss with bilateral foot drop, but he remained ambulant with the aid of orthotic splints (**Table 6.2**).

UK Family 2 (Family 20)

The 20-year-old index patient (III.1) (**Figure 6.1, A**) of North-East England origin presented with a childhood-onset, slowly progressive distal motor neuropathy involving his lower extremities. At the age of 12 he developed Achilles tendons tightness with subsequent tiptoe walk and clumsiness. He deteriorated with painful distal muscle weakness and atrophy in his legs. He underwent orthopaedic surgical interventions and his foot deformities were corrected by combined osteotomy and tendon transfer.

Neurology examination found symmetrical wasting and pronounced weakness in his distal leg muscles. He had weak ankle dorsiflexion (MRC grade 3/5) and cavo-equinus foot deformities. There were no signs of upper limb involvement, although his deep tendon reflexes were globally absent. Mildly impaired pinprick sensation was detected below the level of his ankles. He remained physically active and ambulant with a steppage gait requiring insoles. CMTNSv2 was 8/36.

His father (II.2) (**Figure 6.1, A**) had a similar, but milder disease course suggesting a dominant inheritance pattern in the family. He remained fully active and ambulant with no need of orthotic aid support. His paternal aunt (II.1) and paternal grandmother (I.1) (**Figure 6.1, A**) were also affected by the disease. Although they required walking aids at the later stages of their life, they all remained ambulant (**Table 6.2**).

UK Family 3 (Family 18)

The 32-year-old patient (III.1) (**Figure 6.1, A**) from a North-East England family was clumsy over his childhood ages. He had a longstanding history of autoimmune ankylosing spondylitis. He underwent bilateral hip replacement and required combined anti-inflammatory and immunotherapy. Aged 28 he additionally developed asymmetric motor weakness and intermittent numbness in his left sided extremities. His decreased grip strength and finger weakness caused difficulties in typing and handwriting. He complained of general tiredness and fatigability. Inflammatory and autoimmune causes of neuropathy were excluded by thorough investigations, including CSF analysis and neuroimaging.

His neurology assessment proved distal muscle atrophy and weakness in his extremities more on the left body side. His fingers and intrinsic hand muscles were mildly weak (MRC grade 4/5), while he had more pronounced distal leg weakness (MRC grade 3/5). Wasted feet muscles caused pes cavus foot deformities. Deep tendon reflexes were overall absent. Disturbed sensation for light touch and pinprick modalities was noted in his left hand. His gait was supported by bilateral ankle foot orthosis (AFO). The CMTNSv2 measured 11/36.

Upon conclusion of the neuropathy diagnosis in patient (III.1), his father (II.1) (**Figure 6.1, A; B**) was referred in his late 50's with rapid deterioration of his walking abilities. He reported congenital foot deformities, which were surgically corrected in the first year of his life. Despite his tiptoe gait difficulties, he trained to be a football coach and remained fully active until he presented to the clinic. His symptoms progressed quickly, over a year and resulted in severe distal motor neuropathy affecting exclusively his lower extremities. He suffered from severe pain caused by the damaged ankle joints.

Neurology investigation revealed markedly decreased distal muscle strength and severe bilateral foot drop. His ankle plantarflexion was better preserved (MRC grade 3/5) compared to the prominently weak dorsiflexion (MRC grade 1/5). His lower limb reflexes were absent with no long tract signs. Very mild hyperaesthesia for pinprick was indicated above his feet. There was no upper limb involvement and he had preserved upper limb muscle power and deep tendon reflexes. He had Dupuytren's contracture on his right hand. The CMTNSv2 was assessed 5/28.

In terms of the family history, the 82-year-old paternal grandfather (I.1) had bilateral foot drop but remained ambulant by wearing splints. The paternal uncle (II.2) had surgery due to ankle problems in the past and his two sons needed evaluations for orthopaedic issues. (**Figure 6.1, A**) (**Table 6.2**)

UK Family 4

The 55-year-old proband (II.2) of a Southern UK family (**Figure 6.1, A**) presented with asymmetric right lower limb wasting in his 30's and developed walking difficulties due to foot drop. Earlier in his 20's he was diagnosed with right sided sciatica and lower back pain caused by a prolapsed disc. He deteriorated progressively and developed motor weakness and wasting from the lower thighs distally in both legs, the right leg remaining more severely affected. He experienced numbness from ankles downwards and he could not appreciate vibration sensation below his knees. Upper limb involvement accompanied at later stages with intrinsic hand muscles wasting and weakness, predominantly affecting finger abduction. Superficial sensation was impaired in the distal parts of his fingers.

Aged 40 he was assessed having striking clinical features of bilateral dropped foot and hallux. Ankle plantar- and dorsiflexion were both markedly weak (MRC grade 1/5). He suffered from unbalanced gait and frequent falls. He required AFO support and aid of a unilateral walking stick to remain ambulant. He displayed substantial difficulties in his upper limb strength and dexterity and he underwent tendon transfer surgery to achieve better thumb and grip function. CMTNSv2 was assessed 11/36.

His father (I.1) (**Figure 6.1, A**) developed progressive gait difficulties from his 40's onwards and was eventually diagnosed with chronic demyelinating neuropathy at the age of 60 years. Two of his four brothers (II.3 and II.5) received intermediate CMT diagnosis for a similar disease course. They suffered from frequent ankle sprains and they developed progressive ankle instability with a late teen-onset. They presented with progressive distal amyotrophy, areflexia, bilateral pes cavus and mild sensation loss from their 20's. They ended up with prominent walking difficulties in their middle ages due to the slowly progressive condition. The younger of them (II.5) also developed bilateral wasting of the first dorsal interossei muscles with no accompanying hand function impairment. Their offspring has not yet presented functional difficulties, albeit that the oldest son of patient II.2 had dropped toes while the youngest son of patient II.3 had overriding toes (**Table 6.2**).

Irish Family 1

The 46-year-old proband (IV.5) (**Figure 6.1, A**) struggled with recurrent patellar dislocations in her school age years and had poor performance in sports. Until her mid-30's she deteriorated further with gait balance difficulties and experienced reduced sensation in her feet. In her 40's she complained of some difficulties in writing and typing. Her examination revealed mild ptosis and a high arched palate. Her muscle strength was decreased in the intrinsic hand muscles (MRC grade 4/5), in hip flexion (MRC grade 4/5), in ankle dorsiflexion (MRC grade 2/5) and in plantarflexion (MRC grade 4/5). Her deep tendon reflexes were globally absent. Her gait was slightly waddling and she had bilateral foot drop. Pinprick sensation was reduced at ankles and vibration was impaired at costal margins. CMTNSv2 score was 15/36 indicating moderate CMT severity.

Her daughter (V.1) (**Figure 6.1, A**) was clumsy and walked on her toes in the first decade of her life. Aged 7 she had mild proximal and more distal weakness in her lower limbs, absent ankle reflexes and diminished fine touch distally in her feet. The proband's father (III.5) (**Figure 6.1, A**) suffered from schizophrenia but a stamping gait difficulty had been reported for many years previously. He progressed slowly developing muscle wasting and weakness in the hands and distal legs. He required PEG tube insertion due to swallowing

difficulties aged 70. He lost ambulatory skills when he was 76 years old. Several other family members were reported to become wheelchair bound in later life (I.2, II.1, II.2, II.5) (**Table 6.2**).

Irish Family 2

The 37-year-old proband (II.3) (**Figure 6.1, A**) was clumsy, turned easily on his ankles while walking and fell frequently in his childhood. He presented with upper limb fine motor difficulties in his teens. His symptoms progressed gradually involving both distal upper and lower extremities.

He had muscle wasting from the mid forearm and from the knees distally. There was a motor weakness of intrinsic hand muscles; abductor pollicis brevis (APB) (MRC grade 1/5), first dorsal interosseous (FDIO) (MRC grade 4-/5) and abductor digiti minimi (ADM) (MRC grade 4/5). He demonstrated hand tremor induced by weakness and difficulties in dexterity. Ankle dorsi- and plantarflexion were equally weak (MRC grade 1/5). He had an unsteady gait with frequent falls, caused by Achilles tendon contractures and bilateral foot drop. His deep tendon reflexes were overall absent. Sensation to pin was reduced to above the wrists and proximal shin, vibration was decreased to costal margin bilaterally but proprioception was normal. His CMTNSv2 score was 17/28.

Both his children were affected indicating dominant family history. His 6-year-old son (III.1) (**Figure 6.1, A**) developed toe walk and fell frequently. He wore AFO from the age of 5. He had a poor pencil grip. He had mild intrinsic hand muscles weakness, APB weaker than FDIO. His ankle dorsiflexion was markedly weak with concomitant bilateral foot drop. He was areflexic throughout. The proband's 5-year-old daughter (III.2) (**Figure 6.1, A**) had delayed motor and developmental milestones and attended special needs school. She fell frequently due to toe walk and required boots for ankle support. She had mild motor hand and APB weakness. Her impaired ankle dorsiflexion led to bilaterally dropped foot. Reflexes were absent apart from available triceps and knee jerks. Sensory testing was unreliable in the children (**Table 6.2**).

Family / Patient / Age / Sex	Origin	Nucleotide / Amino acid change	Age onset	Clinical course	First sign	Clinical signs						Mobility/ Orthotics	CMT score	Nerve conduction study	
						Distal Lower limb			Distal Upper limb					Motor NCV (m/s)	Motor / Sensory
						Motor	Sensory	Deformity	Motor	Sensory	Deformity				
F1/PIII.1 50y M	UK	c.986G>A / p.Arg329His	30y	rapid fluctuant symmetric LL asymmetric UL	UL	++	++	bilateral <i>pes cavus</i> bilateral foot drop	++	++	R>L mild split hand	walking difficulties/ walking stick bilateral hand splint	19 / 36	m 38-50 p absent	MS
F1/PII.4 77y M	UK	c.986G>A / p.Arg329His	<10	slow progress symmetric	LL	+++	++	bilateral <i>pes cavus</i> bilateral foot drop bilateral toe drop	+	++	none	walking difficulties/ bilateral AFOs crutches	11 / 28	intermed.	MS
F1/PII.6 70y M	UK	c.986G>A / p.Arg329His	53y	slow progress symmetric	LL	++	++	bilateral foot drop	none	none	none	walking difficulties/ bilateral AFOs	n / a	intermed.	MS
F2/PIII.1 20y M	UK	c.986G>A / p.Arg329His	12y	slow progress symmetric	LL	+++	+	bilateral tight Achilles <i>pes cavo-equinus</i>	none	none	none	tiptoe walking / insoles	8 / 36	m 40 p 24	MS
F3/PIII.1 32y M	UK	c.986G>A / p.Arg329His	28y	rapid progress asymmetric	UL LL	++	++	bilateral <i>pes cavus</i>	++	++	none	walking difficulties/ AFO	11 / 36	m 43 p 34	MS
F3/PII.1 59y M	UK	c.986G>A / p.Arg329His	birth	slow progress symmetric	LL	+++	+	bilateral tight Achilles bilateral foot drop	none	none	none	walking difficulties/ feet surgeries	5 / 28	n/a	n/a
F4/PII.2 55y M	UK	c.986G>A / p.Arg329His	30y	slow progress asymmetric	LL	+++	++	bilateral foot drop bilateral toe drop	+++	++	split hand	walking difficulties/ bilateral AFO hand surgery	11 / 36	m 26 u 34	MS
F4/PII.5 49y M	UK	c.986G>A / p.Arg329His	18y	slow progress symmetric	LL	+++	+	bilateral <i>pes cavus</i> bilateral foot drop	+	none	mild split hand	walking difficulties	n / a	intermed.	MS
F1/PIV.5 46y F	Ireland	c.986G>A / p.Arg329His	<10y	slow progress symmetric	LL	++	++	bilateral foot drop	+	none	none	walking difficulties	15/36	m 39 u 44.9	MS
F1/PV.1 10y F	Ireland	c.986G>A / p.Arg329His	<10y	slow progress symmetric	LL	+	+	bilateral tight Achilles	none	none	none	tiptoe walking	n / a	m 47.6 p 31.6	MS
F2/PII.3 37y M	Ireland	c.2063A>G / p.Glu688Gly	<10y	slow progress symmetric	LL	+++	++	bilateral tight Achilles bilateral foot drop	++	++	split hand	tiptoe walking	17/28	u 28.7	MS
F2/PIII.1 6y M	Ireland	c.2063A>G / p.Glu688Gly	<1y	slow progress symmetric	LL	++	n/a	bilateral tight Achilles bilateral foot drop	+	n/a	mild split hand	tiptoe walking bilateral AFOs	n / a	m 36.8 p 27.6	MS
F2/PIII.2 5y F	Ireland	c.2063A>G / p.Glu688Gly	<1y	slow progress symmetric	LL	+	n/a	bilateral tight Achilles bilateral foot drop	+	n/a	mild split hand	tiptoe walking bilateral AFOs	n / a	m 29.3	MS

Abbreviations: F, family; P, patient; y, year; M, male; F, female; UL, upper limb; LL, lower limb; +, mild; ++, moderate; +++, severe; AFO, ankle foot orthosis; n/a, not available; m/s, meter per second; m, median nerve; p, peroneal nerve; u, ulnar nerve; intermed., intermediate; MS, motor and sensory.

Table 6.2 Genetic and clinical characteristics of patients with AARS-related neuropathy in the UK/Irish cohort

(Bansagi, Antoniadi, *et al.*, 2015)

6.1.3.3 Neurophysiology findings in pedigrees with AARS-related neuropathy

In the proband (III.1) of **UK Family 1** (*Family 19*) repeated nerve conduction studies were carried out due to differential diagnostic difficulties. Initially, multifocal patchy demyelinating changes with conduction blocks were recorded, suggestive of CIDP but the patient did not improve on immunosuppressive therapy. Follow-up recordings indicated intermediate, combined axonal and demyelinating motor neuropathy with patchy dispersion of the motor neuronal conduction velocities and severe sensory polyneuropathy. Family members (II.4 and II.6) also showed intermediate nerve conduction velocities indicating both demyelinating and axonal features.

The proband (III.1) of **UK family 2** (*Family 20*) showed both demyelinating and axonal motor and sensory neuropathy with nerve conduction velocities in the intermediate range.

The index patient (III.1) of **UK family 3** (*Family 18*) with progressive asymmetric distal motor and sensory neuropathy had intermediate nerve conduction parameters.

The proband (II.2) of **UK family 4** had motor conduction velocities in the demyelinating range compatible with demyelinating CMT. In his father (I.1) nerve conduction studies also showed profound demyelination with significant axonal loss. Both his affected brothers (II.3 and II.5) had severe, predominantly axonal sensorimotor neuropathy with reduced conduction velocities.

Electric testing in the **Irish families** revealed length-dependent motor and sensory neuropathy with intermediate conduction velocities.

Needle EMG recordings did not show changes in spontaneous activity and in motor unit potentials in either of the families (**Table 6.3**).

Patient	Age/ Sex	Median SAP (μ V)	Median SNCV (m/s)	Ulnar SAP (μ V)	Ulnar SNCV (m/s)	Radial SAP (μ V)	Radial SNCV (m/s)	Sural SAP (μ V)	Sural SNCV (m/s)	Median CMAP (mV)	Median MNCV (m/s)	Ulnar CMAP FDIO (mV)	Ulnar MNCV FDIO (m/s)	Ulnar CMAP ADM (mV)	Ulnar MNCV ADM (m/s)	Peroneal CMAP (mV)	Peroneal MNCV (m/s)	Tibial CMAP (mV)	Tibial MNCV (m/s)
UK families																			
F1/PIII.1	50y M	NR	NR	NR	NR	NR	NR	NR	NR	2	27	n/a	n/a	9.3	46	NR	NR	NR	NR
F2/PIII.1	20y M	3	31	1	30	3	35	NR	NR	14.4	40	n/a	n/a	11	44	3	24	3.6	31
F3/PIII.1	32y M	1	50	NR	NR	8	45	NR	NR	18	43	n/a	n/a	18	47	NR	NR	0.4	34
F4/PII.2	55y M	NR	NR	n/a	n/a	n/a	n/a	n/a	n/a	2.5	26	n/a	n/a	3.3	34	n/a	n/a	n/a	n/a
Irish families																			
F1/IV.5	46 F	0.4	33.3	n/a	n/a	1.2	53.8	NR	NR	4.5	39	7.1	44.9	n/a	n/a	NR	NR	2.6	n/a
F1/V.1	7 F	5.8	34.8	4.7	36	11.6	n/a	n/a	n/a	9.7	47.6	17.75	46.3	n/a	n/a	2.44	31.6	5.81	39.7
F2/II.3	37 M	NR	NR	NR	NR	NR	NR	NR	NR	NR	NR	0.11	28.7	3.4	28.5	NR	NR	NR	NR
F2/III.1	6 M	NR	NR	n/a	n/a	NR	NR	NR	NR	3.2	36.8	n/a	n/a	7.6	44	1.35	27.6	10.2	38.1
F2/III.2	5 F	NR	NR	n/a	n/a	n/a	n/a	n/a	n/a	3.6	29.3	n/a	n/a	n/a	n/a	n/a	n/a	n/a	n/a

Abbreviations: F, family; P, patient; y, year; M, male; F, female; SAP, sensory action potential; SNCV, sensory nerve conduction velocity; CMAP, compound motor action potential; MNCV, motor nerve conduction velocity; FDIO, first dorsal interosseous; ADM, abductor digiti minimi; NR, not recordable; n/a, not available

Table 6.3 Summary of neurophysiology results in the AARS mutant UK / Irish families

(Bansagi, Antoniadi, *et al.*, 2015)

6.1.3.4 Diagnostic genetic methods and identified AARS mutations in the pedigrees

Initially, targeted candidate gene tests were performed taking into consideration leading clinical features, inheritance patterns and changes on nerve conduction studies. Mutations in genes involved in axonal pathology (*MFN2*, *NEFL*, *GDAP1*) and common demyelinating neuropathy-related genes (*PMP22*, *MPZ*) were excluded in all patients. Upper limb symptoms at disease-onset and/or predominant involvement of first dorsal interossei muscles prompted testing for mutations in the *GARS* gene. *BICD2* mutations were excluded in patients with early-onset lower extremity predominant motor symptoms and Achilles contractures. Prominent sensory symptoms in some patients indicated a need for screening for *SPTLC1* mutations.

IPN gene panel assay was initiated next in all included families. The previously reported pathogenic heterozygous c.986G>A, p.Arg329His variant in exon 8 of the *AARS* gene was identified in all of the 4 UK families and in the first Irish family. Another, so far not yet described c.2063A>G, p.Glu688Gly *AARS* variant was found to segregate with the dominant motor and sensory neuropathy in the second Irish family. This variant has not been recorded in dbSNP, 1000 genomes, Exome Variant Server or Exome Aggregation Consortium www.exac.broadinstitute.org. Alignment of protein sequences from multiple species supported that the affected glutamic acid residue is highly conserved among all species from *E.coli* to *H.sapiens*. *In silico* prediction tools indicated the missense change to be likely deleterious (SIFT: deleterious; Polyphen2: probably pathogenic; Mutation Taster disease-causing) (**Figure 6.2**).

Furthermore, detailed bioinformatics analysis was carried out on the IPN gene panel results, with the help of Dr Thalia Antoniadis at Bristol Genetic Laboratory and Dr Helen Griffin at Institute of Genetic Medicine, Newcastle University. We were looking at single nucleotide polymorphisms (SNPs) occurring in the *AARS* and closely located other genes (*KARS*, *GAN*) on chromosome 16q. We examined the SNP database (dbSNP) / NHLBI Exome Sequencing Project (ESP) frequency. We identified common SNPs carried by the patients among the different UK and Irish families (**Table 6.4**).

AARS gene (NM_001605.2) chr 16q21.1

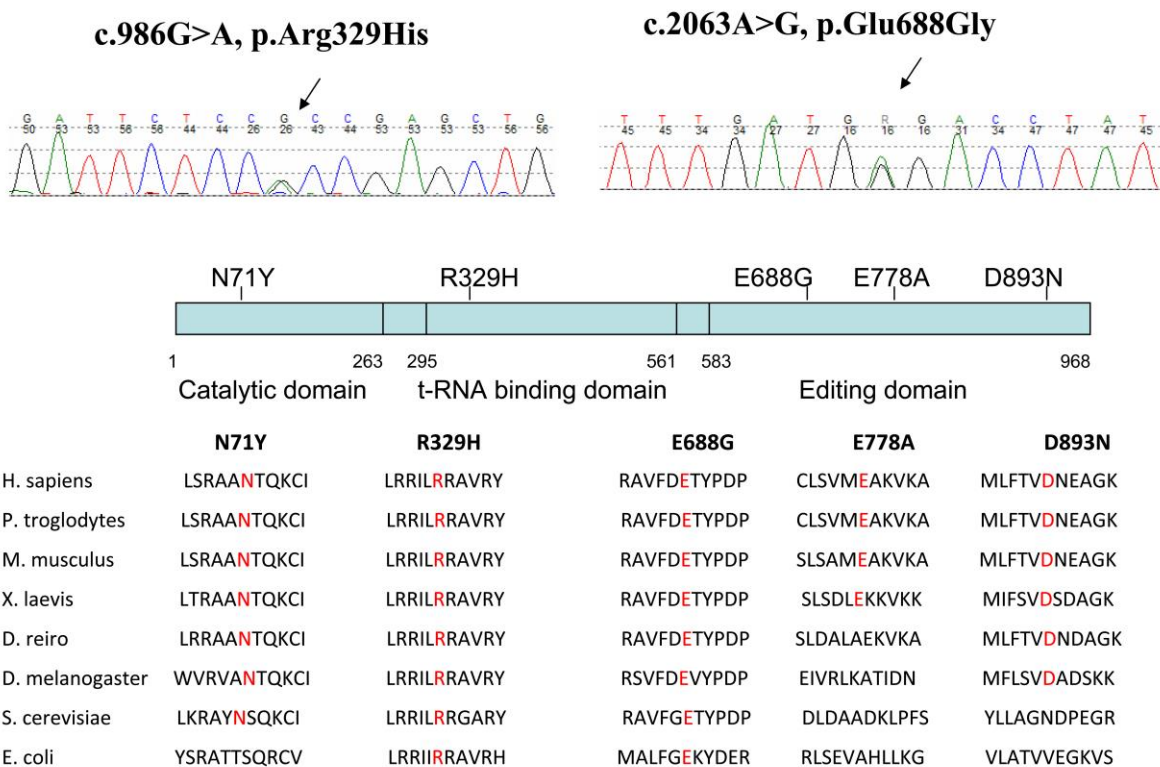


Figure 6.2 Identified AARS variants, positions and conservation across species

(Bansagi, Antoniadis, *et al.*, 2015)

Chr:ChrPos	Type	Exon Number	HGVSCoding	Protein	Rs	UK Family 1	UK Family 2	UK family 3	UK Family 4	Irish Family 1	Irish Family 2	dbSNP	ESP
16:70302259	missense	8	c.986G>A	p.Arg329His	N/A	AARS	AARS	AARS	AARS	AARS		N/A	N/A
16:70287177	synonymous	20	c.2715T>C	p.Val905Val	rs4081753	AARS	AARS	AARS	AARS	AARS	AARS	12%	15.08%
16:75675609	synonymous	3	c.159A>G	p.Arg53Arg	rs5030748	KARS	KARS	KARS	KARS			4.17%	8.12%
16:70303580	synonymous	7	c.903C>T	p.His301His	rs2070203	AARS	AARS	AARS	AARS		AARS	46.20%	49.07%
16:75661803	missense	15	c.1868C>G	p.Thr623Ser	rs6834		KARS			KARS		10.76%	13.65%

Table 6.4 Analysing common SNPs in the affected AARS mutant families

6.1.3.5 Genotype-phenotype correlations in the cohort of AARS-related neuropathy

We identified a remarkable cohort of UK and Irish families diagnosed with AARS-related neuropathy by using a multi-gene panel approach. I have thoroughly investigated phenotype manifestations in the group of neuropathies caused by dominant AARS mutations, in order to delineate genotype-phenotype correlations by comparing our families to the previously worldwide reported cases.

Clinically variable neuropathy phenotypes, including motor and sensory axonal CMT2 (CMT2N), intermediate CMT and dHMN, have been reported with mutations affecting all 3 AARS domains.

Phenotypes associated with AARS mutations in the aminoacylation domain

In a Taiwanese pedigree axonal CMT2 was described related to the p.Asn71Tyr missense variant located in the AARS aminoacylation domain (**Table 6.1**). Impaired aminoacylation activity was proved by *in vitro* and *in vivo* assays, which resulted in reduced charging capacity (Lin *et al.*, 2011; McLaughlin *et al.*, 2012).

A novel heterozygous missense c.304G>C, p.Gly102Arg AARS variant segregated in a large dominant American pedigree (**Table 6.1**). The mutated region of the activation domain and the affected residue was highly conserved from a range of divergent species and *in silico* predictions indicated that the mutation was probably damaging. Yeast complementation assay proved loss-of-function characteristics. The affected family members presented with mild axonal neuropathy and hyperreflexia indicating superimposed myelopathy (Motley *et al.*, 2015).

Phenotypes related to common p.Arg329His AARS mutation in tRNA-binding domain

The p.Arg329His AARS variant was considered a recurrent mutation worldwide, previously reported in 2 French, 1 Australian pedigrees (**Table 6.1**). We additionally diagnosed 4 families from the UK and 1 Irish family with the same p.Arg329His AARS mutation (**Table 6.2**). Functional studies revealed that the variant is associated with impaired enzyme activity. Furthermore, the affected arginine residue is located in the middle helical/tRNA-binding domain of the AARS protein, in a highly methylated CpG site, where a methylation-mediated process might give rise to a mutational hot spot. Haplotype analysis in the 2 French and Australian pedigrees with p.Arg329His AARS mutation demonstrated a different founder among the three families (Latour *et al.*, 2010; McLaughlin *et al.*, 2012).

A limited haplotype analysis of 4 polymorphic variants in the proximity of the causative *AARS* mutation showed identical haplotype background for our 4 families of UK origin, while a close haplotype similarity was suggested (3/4 identical variants) with the Irish family. We concluded that the p.Arg329His might be potentially a founder mutation in our families (Bansagi, Antoniadi, *et al.*, 2015) (**Table 6.4**).

Despite the common genetic background, the disease presentation in our families was largely heterogeneous. Lower limb predominant motor and sensory neuropathy with various degree of upper limb involvement was observed in **UK Family 1**. Slowly progressive motor weakness and mild or absent sensory changes affected exclusively the lower extremities in **UK Family 2**. Interfamilial phenotype heterogeneity was characteristic in **UK Family 3**, where the proband presented with young adult-onset asymmetric motor and sensory symptoms, while his father had late-onset distal motor neuropathy in his legs. Slow progression, predominant lower limb motor loss with mild to moderate sensory changes and variable upper limb weakness with split hand formation presented in **UK Family 4**. Lower limb motor and sensory symptoms progressed slowly with later accompanying hand weakness in **Irish Family 1**. Motor predominant lower limb weakness with contractures and early split hand deformities were seen in **Irish Family 2** (**Table 6.2**).

In general, lower extremity involvement was predominant in all our families, variably impairing motor and sensory functions. Some patients showed exclusively or predominantly distal motor symptoms consistent with the dHMN phenotype. Pes cavus foot deformities and severe foot drop due to ankle dorsiflexion weakness were strikingly common features throughout the affected families. Walking abilities were impaired in all cases leading to ambulatory loss in some of the patients. Split hand malformation was frequently observed among the families, manifesting as an overlapping feature with *GARS*-related pathology. Acute episodes of worsening, mimicking acquired neuropathies caused diagnostic difficulties in some cases. Similarly to the French pedigree, asymmetric distribution of symptoms was seen in our families, but in contrast to the Australian cohort, sensorineural deafness was not present. Variable age of onset, disease progression and severity of symptoms gave rise to further phenotype heterogeneity.

Compared to the previously reported pedigrees, intermediate motor nerve conduction velocities were detected at a larger extent in all families, which indicated a greater demyelination process in addition to the accompanying axonal dysfunction. Sensory nerve responses were frequently severely impaired jointly with the occasional prominent sensory loss. We did not detect neuromuscular junction dysfunction in *AARS*-related neuropathy,

illustrating the variable mechanisms of different AARS-related conditions (Bansagi, Antoniadi, *et al.*, 2015) (**Table 6.3**).

Phenotypes observed with AARS mutations in the editing domain

There were two different phenotypes reported in relation to AARS editing domain mutations. In a dominant Australian family with rippling muscle disease the p.Glu778Ala AARS variant segregated. However, the missense change did not affect an evolutionarily conserved amino acid and diminished editing capacity also could not be proven (McLaughlin *et al.*, 2012). The p.Asp893Asn AARS variant was identified in a dominant Chinese pedigree with pure motor pathology resulting in a dHMN phenotype. The amino acid change affected a highly conserved residue in the C-terminal editing domain and prediction programs indicated deleterious pathogenicity (Zhao *et al.*, 2012) (**Table 6.1**).

We found the novel p.Glu688Gly AARS variant segregating in the second Irish family. Alignment of protein sequences from multiple species supported that the affected glutamate in the editing domain is a highly conserved residue among all species from E.coli to H.sapiens (**Figure 6.2**). Further functional studies would be necessary to investigate its impact on the editing capacity and to determine the pathogenicity. Early-onset slowly progressive and predominant motor impairment of both upper and lower extremities was characteristic for the associated phenotype. Split hand deformity and milder sensory changes manifested at later ages. Nerve conduction findings were compatible with an intermediate CMT (**Table 6.2; Table 6.3**) (Bansagi, Antoniadi, *et al.*, 2015).

6.1.3.6 Conclusion

We investigated a cohort of patients with AARS-related neuropathy among pedigrees of UK and Irish origin. In view of previously worldwide reported pedigrees, I evaluated the natural history of AARS-related neuropathies and I examined phenotype correlations with the underlying genetic background.

Our patient cohort supported that the p.Arg329His AARS variant is a recurrent mutation, which occurs worldwide. The AARS phenotype spectrum is largely heterogeneous, which may cause difficulties in achieving diagnosis based only on neurology examination, underlying the importance of next generation sequencing. Genetic screening for AARS and other aminoacyl-tRNA synthetase mutations should be considered in axonal neuropathology.

6.1.4 *GARS*-related neuropathy

6.1.4.1 Literature review

The CMT associated ARS mutations have predominantly been reported in the *GARS* gene. At least 13 neuropathy-causing *GARS* mutations have been identified so far (Griffin *et al.*, 2014). Dominant *GARS* mutations manifest either as axonal motor and sensory neuropathy (CMT2D, OMIM# 601472) or as the allelic form, distal hereditary motor neuropathy or distal spinal muscular atrophy (dHMNV/HMN5A or DSMAV, OMIM# 600794). Upper limb predominant symptoms are characteristic but not exclusive and the clinical manifestation may rely on the localisation of the mutation. dHMN-V is typically caused by catalytic domain mutations (Nangle *et al.*, 2007; Xie *et al.*, 2007; Griffin *et al.*, 2014), while CMT2D is caused by anticodon-binding domain mutations (Del Bo *et al.*, 2006; James *et al.*, 2006; Xie *et al.*, 2007; Eskuri *et al.*, 2012). Reduced aminoacylation activity, altered axonal localisation (Antonellis *et al.*, 2003; Griffin *et al.*, 2014) and impaired catalytic function (Jordanova *et al.*, 2006) was attributed to variable disease mechanisms. Abnormal neuromuscular transmission has been described in *Drosophila* and in mouse models of *GARS* mutations (Ermanoska *et al.*, 2014; Sleight *et al.*, 2014).

6.1.4.2 Natural history of *GARS*-related neuropathy in the identified pedigrees

Family 2

The proband (III/1) (**Figure 6.3, A; B**) developed asymmetric weakness and atrophy in his hand muscles aged 14. His condition progressed slowly with deteriorating grip strength and dexterity. Milder lower limb motor symptoms were accompanied with no functional impact.

His neurology examination found prominent motor wasting and weakness (MRC grade 2/5) in the bilateral first dorsal interosseous muscles, causing weak pincer grip and split hand malformation. The muscle power of the proximal upper limb and shoulder muscles was preserved. His ankle dorsi- and plantarflexion were equally weak (MRC grade 4/5) with mild bilateral foot drop. He was unable to toe walk. He had no sensory impairment in his upper limbs but there was a decreased sensation of pinprick and vibration below his ankles. The CMTNSv2 score was 11/36 (**Table 6.5**).

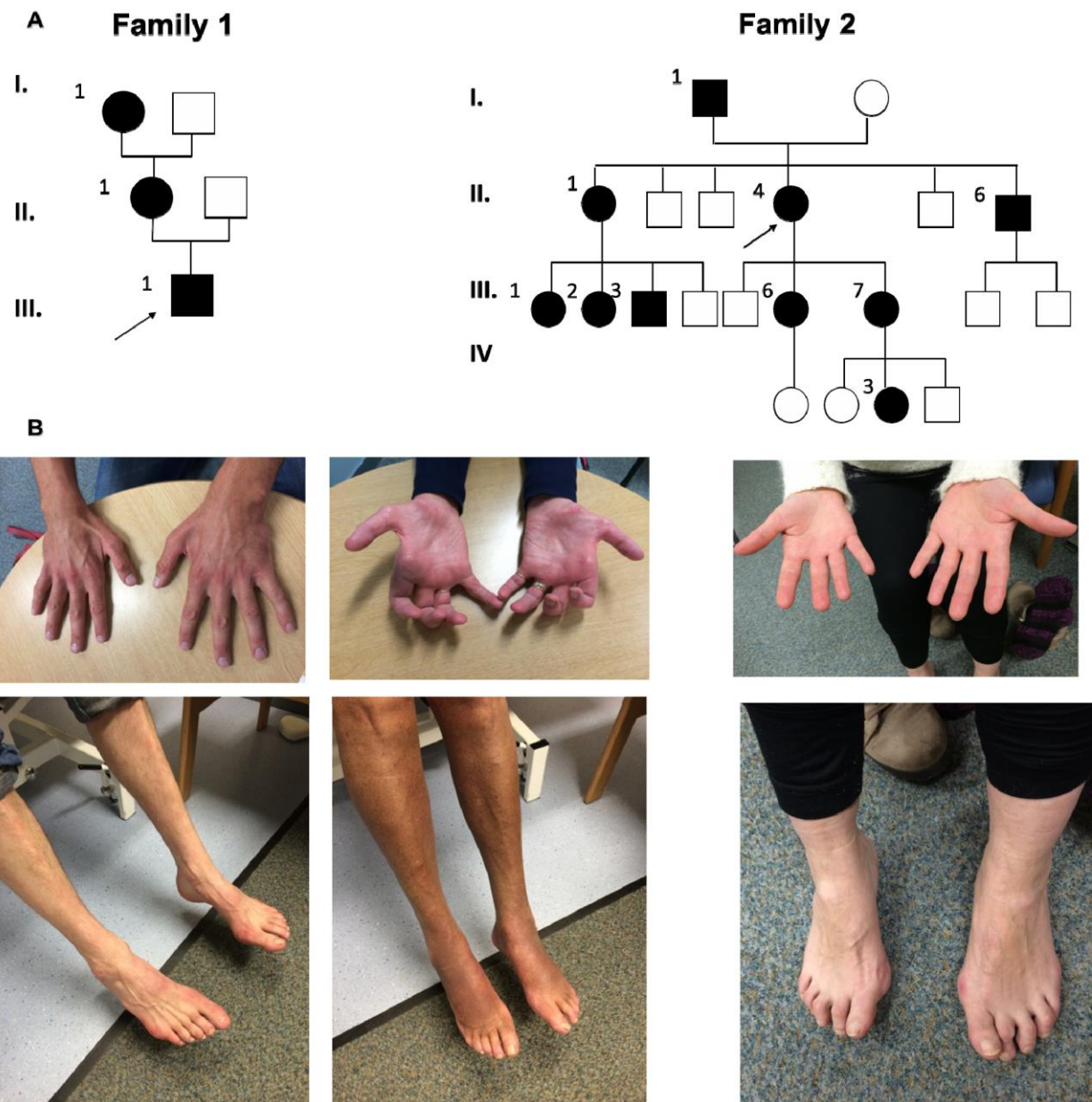


Figure 6.3 Identified *GARS* mutant families

A) Pedigrees of *GARS*-related neuropathy.

B) Images of patients P1/1 and P3/1 from Family 1 and P2/4 from Family 2

His mother (II/1) presented with a similar, early-onset upper limb predominant distal motor neuropathy (**Figure 6.3, A; B**). Her disease course was also slowly progressive, mildly involving her distal lower limb muscles at later ages. She complained of pins and needles in the distal part of her extremities. Her medical history was complicated by Sjogren's syndrome, autoimmune arthritis and vasculitis.

Examination found prominent distal motor atrophy and weakness (MRC grade 1/5), primarily affecting the first dorsal interosseous muscles. Hand grip was lost and she developed curled fingers. The muscle power was preserved in the proximal upper limb muscles. The ankle dorsiflexion was weaker (MRC grade 3+/5) compared to the plantarflexion (MRC grade 4/5). Sensory deficit for pinprick was noted below elbow and knee levels, while vibration was reduced at the ankles. She had a livid skin discolouration on both her legs. The CMTNSv2 score was 15/36 (**Table 6.5**).

The maternal grandmother (I/1) (**Figure 6.3, A**) was reported to suffer from the same condition.

Family 3

The proband (II/4) (**Figure 6.3, A; B**) dated her first symptoms back to the early childhood years, when she had tiptoe walk abnormalities. The lower limb weakness accompanied by ankles contracture progressed slowly. Her foot deformities and hamstring stiffness required surgical correction. Later in adult years her upper limbs became gradually involved with distal muscle weakness and sensory impairment. She experienced pins and needles in her legs and numbness in her hands. Her gait deteriorated and by the age of 40 she required a walking stick. She complained of excessive fatigability. She reported deterioration in hearing and memory functions.

The neurology examination found more prominent lower limb symptoms. There was a distal motor weakness (MRC grade 3/5) and atrophy with clawing toes and pes cavus deformities. There was only a mild muscle weakness in the finger muscles (MRC grade 4/5), while proximal strength was preserved in all extremities. Deep tendon reflexes were rather brisk apart from that the ankle jerks were absent. She had a poorly balanced gait and she was unable to heel or toe walk. The CMTNSv2 score was 11/36 (**Table 6.5**).

Her daughter (III/7) (**Figure 6.3, A**) had a more severe symptom presentation with a relative rapid deterioration. She was a clumsy child with tiptoe walk difficulties. She required surgical tendon lengthening. Later her feet became flat, turned inward and she struggled with recurrent ankle sprains. Her walking ability was impaired by fatigability and pain manifesting in the hips, lower back and knees.

<i>Family Patient Age Sex</i>	<i>Nucleotide Amino acid change</i>	<i>Age onset</i>	<i>Clinical course</i>	<i>First sign</i>	<i>NCS</i>	<i>CMT score</i>	<i>Clinical signs</i>					
							<i>Distal Lower limb</i>			<i>Distal Upper limb</i>		
							<i>Motor</i>	<i>Sensory</i>	<i>Deformity</i>	<i>Motor</i>	<i>Sensory</i>	<i>Deformity</i>
F1/PIII.1 34y m	c.647A>G p.His216Arg	14y	slow asymm	UL	M	11 / 36	+	+	foot drop	+++	++	split hand
F1/PII.1 71y f	c.647A>G p.His216Arg	<10y	slow symm	UL	M	15 / 36	++	++	foot drop	+++	++	split hand
F2/PII.4 50y f	c.1528A>C p.Lys510Gln	5y	slow asymm	LL	M	11 / 36	++	none	tight Achilles	+	none	none
F2/PIV.3 8y f	c.1528A>C p.Lys510Gln	5y	slow symm	LL	M	2 / 36	+	none	tight Achilles	none	none	none

Abbreviations: F, family; P, patient; y, year; m, male; f, female; symm, symmetric; asymm, asymmetric; UL, upper limb; LL, lower limb; NCS, nerve conduction studies; M, motor; +, mild; ++, moderate; +++, severe

Table 6.5 Clinical characteristics of *GARS* neuropathy patients

Later in the disease course she developed had weakness and she was unable to carry bags, accidentally dropping them due to decreased grip strength. Additionally, she experienced pain and intermittent pins and needles in both hands. The CMTNSv2 score was 13/28.

The granddaughter of the proband (IV/3) (**Figure 6.3, A**) had tiptoe walk abnormalities since she started to walk. She developed progressive tendon stiffness. She had frequent falls and fatigability. Aged 9 she was unable to take part in physical education classes but she was good at arts and crafts having no difficulties with her dexterity. Her neurology examination revealed only lower limb symptoms. There was stiffness in her ankles and she was unable to place her heels on the ground. She was continuously tiptoeing while walking or running and she was unable to perform heel walk. She had genu valgus and inward turned flat foot deformities. CMTNSv2 was 2/28 (**Table 6.5**).

Several further family members (I/1, II/1, II/6, III/1, III/2, III/3, III/6) (**Figure 6.3, A**) presented with childhood-onset slowly progressive distal motor neuropathy in the lower limbs supporting the dominant inheritance in the family.

6.1.4.3 Detailed nerve conduction findings in the *GARS* pedigrees

Family 2

In the proband (III/1) upper limb nerve conduction studies showed significantly reduced amplitude left median CMAP response. The left ulnar CMAP recorded from the abductor digitus minimus was entirely normal. This discrepancy between the median and ulnar responses is typical of dHMN-V. In the lower limbs CMAP responses were of significantly reduced amplitude or unrecordable. Sensory nerve responses were within acceptable limits. Concentric needle EMG revealed inactive neurogenic changes. There was no convincing evidence to suggest a significant defect of neuromuscular transmission, given the normal repetitive nerve stimulation of distal muscles and normal SFEMG findings.

In his mother (II/1) nerve conduction studies similarly showed reduced amplitude median CMAP responses, while ulnar CMAP responses recorded from the abductor digitus minimus were normal on both sides. In the lower limbs motor responses were unrecordable. Sensory nerve responses were of reduced amplitude in the upper and lower limbs with mild slowing in the conduction velocity. It was hard to determine, whether this was secondary to her Sjögren's. Concentric needle EMG revealed moderate inactive neurogenic changes. Repetitive nerve stimulation in the right trapezius showed significant decrement following 10

seconds of maximum voluntary contraction (-11%), but this was not reproduced in any of the other muscles studied and there was no concomitant significant jitter in SFEMG of the right trapezius muscle. SFEMG of the extensor digitorum communis showed increased jitter (12%). However, these provided no convincing evidence to suggest a significant defect of neuromuscular transmission.

Family 3

The proband (II/4) had reduced amplitude lower limb CMAP responses with normal conduction velocity. Sensory responses were normal throughout. Electromyography was inactive neurogenic.

There was an evidence of NMJ instability on SFEMG, which recorded increased jitter in the extensor digitorum communis (40% with 5% block) and in the tibialis anterior (19% with no block). Interestingly, the degree of the neuromuscular instability appeared greater in the upper limb, despite the lower limbs being more affected in terms of the neuropathy. This raised the intriguing possibility that in the early stages there might be a reversible defect of neuromuscular transmission, which then becomes fixed as the neuropathy progresses.

In her granddaughter (IV/3) baseline nerve conduction studies were normal. Repetitive nerve stimulation recorded 30% increment in the right tibialis anterior. This provided some evidence of neuromuscular junction instability, even though it could not be confirmed with SFEMG due to her young age. Nevertheless, the possibility of a presynaptic NMJ defect was raised.

6.1.4.4 The identified novel *GARS* variants in the pedigrees

The novel heterozygous c.647A>G, p.His216Arg missense *GARS* variant was detected in the two generation ***Family 2***. The prediction tools suggested that the substitution has a detrimental effect. The amino acid change involves a highly conserved residue in the insertion I domain-like entity, which is likely to be involved in the acceptor stem recognition of the tRNA (Xie *et al.*, 2007).

Another novel heterozygous c.1528A>C, p.Lys510Gln missense *GARS* mutation co-segregated with the disease in the dominant three generation ***Family 3***. This variant is located in the insertion III domain, upstream to the highly conserved motif 3 within the *GARS* catalytic domain. This sequence change might impact on the tRNA recognition, similarly to the closely located p.Asp500Asn *GARS* variant (Nangle *et al.*, 2007; Xie *et al.*, 2007; Griffin *et al.*, 2014).

6.1.4.5 Genotype-phenotype correlations in the identified *GARS* pedigrees

We identified two novel *GARS* mutations accompanied by different dHMN phenotypes in the studied pedigrees.

The novel heterozygous c.647A>G, p.His216Arg *GARS* variant presented with upper limb predominant motor neuropathy in **Family 2**, compatible with the diagnosis of dHMN-V. The striking motor weakness in the first dorsal interossei muscles led to the development of the characteristic split hand deformity. Referring to the literature, the equivalent numbering of the identified *GARS* variant would be the c.485A>G, p.His216Arg in a different 685 codon length transcript, which is lacking the N-terminal 162 bp mitochondrial targeting sequence. The affected residue is located in the insertion I domain-like entity, which is virtually separated from the catalytic domain by its secondary protein structure and is likely to be involved in the acceptor stem recognition. The previously reported pathogenic c.385C>T, p.Leu129Pro *GARS* variant is located in the helix-strand (motif 1), close to the insertion I of the catalytic domain (Xie *et al.*, 2007). This variant also presents with dHMN-V and was extensively investigated. Reduced aminoacylation activity observed *in vitro* and in yeast complement assays and altered axonal localisation have been implicated in the pathomechanism (Antonellis *et al.*, 2003, 2006; Griffin *et al.*, 2014).

The other novel heterozygous c.1528A>C, p.Lys510Gln missense *GARS* variant carried in the large dominant **Family 3** presented with predominant lower limb motor neuropathy accompanied by a less severe hand involvement in later ages. There was a striking intrafamilial phenotype variability. The proband (II/4) and her granddaughter (IV/3) had motor dominant symptoms with normal sensory responses suggesting dHMN-V, while the proband's daughter (III/7) had an axonal motor and sensory neuropathy, CMT2D. The similar coexistence of the two allelic forms of *GARS*-related neuropathy has been reported in an Italian pedigree carrying the nearby p.Asp500Asn *GARS* mutation (Del Bo *et al.*, 2006). Both *GARS* variants are located in the insertion III domain, upstream to the highly conserved motif 3 region of the catalytic domain. The insertion III domain might be involved in tRNA recognition by tRNA-binding across the dimer interface. This hypothesis was supported in the p.Asp500Asn *GARS* mutant, where functional tests indicated stronger dimer formation capacity beside intact aminoacylation activity and axonal localisation (Nangle *et al.*, 2007; Xie *et al.*, 2007; Griffin *et al.*, 2014). Interestingly, severe and early childhood-onset lower limb predominant phenotypes have been previously linked to mutations within the *GARS* anticodon-binding domain in the C-terminal (James *et al.*, 2006; Xie *et al.*, 2007; Eskuri *et al.*, 2012).

6.1.4.6 Conclusion

The novel *GARS* mutations identified in our studied pedigrees provide an illustrative example for the related heterogeneous phenotype variability and highlight the uncertainty in the pathomechanism of *GARS*. The mechanism of selective nerve pathology leading to CMT2D or dHMN-V has still not been fully clarified. Functional studies provided evidence that neither loss in the aminoacylation activity or impaired axonal protein synthesis, due to subcellular *GARS* mislocalisation *per se* is required in the disease pathology. Recent ‘humanized’ yeast assay studies supported that loss-of-function effect on the enzyme activity might be the necessary first step in the pathomechanism. The dimerization between the mutant and residual wild-type *GARS* protein exerts dominant negative effect by reducing the enzyme activity (Antonellis *et al.*, 2003, 2006; Motley *et al.*, 2011; Stum *et al.*, 2011; Griffin *et al.*, 2014; Niehues *et al.*, 2015; Malissovas *et al.*, 2016). Recent *Drosophila* studies suggested that impaired translation, not attributable to loss-of-function aminoacylation defect, but rather to toxic gain-of-function might be a common noncanonical function of mutant tRNA synthetases (Niehues *et al.*, 2015). Very recently, the role of the mutation induced neomorphic conformational changes has been investigated in the mechanism of some *GARS* mutations. The gain-of-function interaction with the neuropilin 1 receptor (Nrp1), via aberrant blocking of the binding of vascular endothelial growth factor (VEGF), resulted in peripheral neurodegeneration in mice (He *et al.*, 2015). Other *ARS* mutants were also found to exert aberrant Nrp1-binding suggesting a common pathomechanism and providing a target for biomarker identification. Furthermore, our research team is investigating whether abnormal mitochondrial translation in neurons could also contribute to the pathology of *GARS*-related neuropathies.

6.2 IGHMBP2-related neuropathy

6.2.1 Literature review

Abnormal DNA/RNA metabolism has been implicated in the pathology of spinal muscular atrophy (SMA) and hereditary motor neuropathies. Homozygous and compound heterozygous *IGHMBP2* mutations have been found to induce progressive loss and dysfunction in the distal groups of spinal motor neurons, leading to the distinctive phenotype of distal spinal muscular atrophy (dSMA).

The classic autosomal-recessive distal spinal muscle atrophy type 1 (DSMA1; OMIM#604320), also known as spinal muscular atrophy with respiratory distress (SMARD1) and distal hereditary motor neuropathy type VI (HMN6), is caused by recessive missense mutations in the *IGHMBP2* helicase domain or homozygous loss of function mutations usually in the 5' promoter region. In contrast to the manifestation of SMA due to *SMN1* mutations, this infantile-onset recessive distal neuropathy presents with symmetric distal muscle weakness and early diaphragmatic palsy with respiratory insufficiency leading to early death (Grohmann *et al.*, 2001, 2003). Decreased foetal movements and intrauterine growth retardation are commonly seen prenatal features, while congenital limb deformities with contractures, distal motor weakness, weak cry with inspiratory stridor and autonomic dysfunctions are the hallmarks of the disease at birth. The prognosis of the condition is poor due to early respiratory impairment and death generally occurs between 6 months and 1 year of age.

Compound heterozygous missense and stop mutations, resulting in residual *IGHMBP2* protein levels, were observed to cause a juvenile-onset DSMA1 phenotype (Guenther *et al.*, 2009). Gross motor development is delayed in these children, who develop distal limb motor weakness, finger contractures and neuromuscular scoliosis until respiratory distress causes their death between 4 and 10 years of age.

IGHMBP2 is a ubiquitously expressed protein possessing specific structural features. Its DNA-binding domain functionally resembles the *SMN1* protein, while its putative helicase motifs show strong homology with the ALS4-causing senataxin RNA helicase, which is involved in ribosomal RNA processing (de Planell-Saguer *et al.*, 2009). The intracellular co-localisation of *IGHMBP2* with ribosomes suggested that dysregulation of RNA metabolism and dysfunctional localisation of protein synthesis may contribute to motor neuron degeneration (Grohmann, 2004; Guenther *et al.*, 2009). The majority of the mutations impair

the helicase function either by loss of the ATPase or by loss of the 5'→3' unwinding capacity (Grohmann *et al.*, 2003; Guenther *et al.*, 2009; Jędrzejowska *et al.*, 2014). The mutant IGHMBP2 seems to be protected from nonsense mediated mRNA decay, as mRNA levels have remained unchanged regardless of the decreased level of protein, which suggests posttranslational degradation processes (Cottenie *et al.*, 2014; Porro *et al.*, 2014). The mutation evoked residual IGHMBP2 protein level was found to correlate with the clinical severity and may provide an explanation for atypical presentations and for broad phenotypic heterogeneity (Guenther *et al.*, 2009; Cottenie *et al.*, 2014; Porro *et al.*, 2014; Vanoli *et al.*, 2015).

6.2.2 Aims and hypothesis

I planned to investigate genotype-phenotype correlation in families, where we identified IGHMBP2 mutations. In collaboration with another research group, we aimed to expand the so far reported IGHMBP2-related phenotypes with the description of the distinct clinical entity of progressive motor and sensory neuropathy without respiratory distress. I intended to investigate the detected single heterozygous IGHMBP2 variants, identified in some studied families, in order to decide on their pathogenicity in an otherwise recessive condition.

6.2.3 Methods

6.2.3.1 Patient inclusion

Patients were selected from the hereditary motor neuropathy cohort for detailed neurology and electrophysiology analysis, where IGHMBP2 mutations were confirmed or identified as the possible cause (*Chapter 5.4.2*). All participants signed an informed consent for natural history and genetic studies.

6.2.3.2 Genetic diagnostic methods

Patient DNA was obtained and IGHMBP2 mutations were detected either by IPN gene panel test (*Family 14, Family 15*) or by analysing WES data (*Family 8, Family 9*) (*Chapter 3.2.1*). Sanger sequencing was performed to investigate the segregation of the disease within the family (*Chapter 3.2.2*). In families, where single heterozygous variants were found, multiplex ligation-dependent probe amplification (MLPA) was carried out at Munich Genetic Laboratory, Germany in order to exclude large IGHMBP2 deletions or duplications.

In *Family 9* I extracted RNA from blood and I synthesised cDNA following the manufacturer's protocol. I used the manufactured cDNA to perform a standard PCR reaction and sequencing analysis (*Chapter 3.2.2.2*).

Additionally, I sequenced the 5'UTR regions using primers provided by the collaborating research team at UCL, London (Prof Dr Henry Houlden and Dr Ellen Cottenie).

Primers used for *IGHMBP2* sequencing are listed in (**Figure 6.4**).



Figure 6.4 Primers designed for *IGHMBP2* cDNA sequencing

6.2.4 Results

6.2.4.1 Clinical phenotypes of patients diagnosed with *IGHMBP2* mutations

Infantile spinal muscular atrophy with respiratory distress type 1 (SMARD1)

The classical SMARD1 phenotype led to the death of 2 male siblings of consanguineous Pakistani origin (*Family 8*). Both of them were born preterm with intrauterine growth retardation. One of them died soon after birth due to respiratory insufficiency, while the other survived until the age of 3 (**Figure 6.5, A**). Motor atrophy and weakness in his distal limb muscles, absent deep tendon reflexes and congenital foot deformities were observed aged 6 months with subsequent delay in his motor development. He was unable to sit and crawl when he was 3 years old and he developed severe neuromuscular scoliosis. His CK level was only mildly increased and muscle biopsy showed neurogenic atrophy in agreement with electromyography findings of acute neurogenic changes. The severe polyneuropathy affected both motor and sensory fibres and secondary demyelination was present in addition to the significant axon loss. Both siblings carried the homozygous c.292_303delinsATGCT, p.Gly98fs frameshift mutation, which disrupted the helicase motifs of the *IGHMBP2* protein.

Juvenile-onset distal spinal muscular atrophy

A 3.5-year-old boy of British origin (*Family 15*) (**Figure 6.5, B**) was found to carry a single heterozygous c.767C>G, p.Ala256Gly missense *IGHMBP2* variant. He was floppy at birth with congenital foot deformities. Motor milestones were delayed and he started walking late, around his third birthday. His muscle tone remained low jointly with lower limb motor weakness and wasting. His deep tendon reflexes were globally reduced with absent ankle jerks. Gower's manoeuvre was markedly positive indicating proximal leg weakness. A hint of bilateral scapular winging was noted but no upper limb and respiratory involvement has developed so far. Nerve conduction studies were within normal limits but EMG showed increased amplitude motor units suggesting a slowly progressive axonal motor neuropathy. His phenotype characteristics prompted us to exclude *BICD2* and *TRPV4* mutations. The single *IGHMBP2* variant detected on WES has not yet been reported. The sequence change affects a highly conserved residue within the helicase domain of the protein, where the majority of pathogenic *IGHMBP2* mutations reside. However, no second mutation could yet be identified and the pathogenicity of this variant has remained ambiguous.

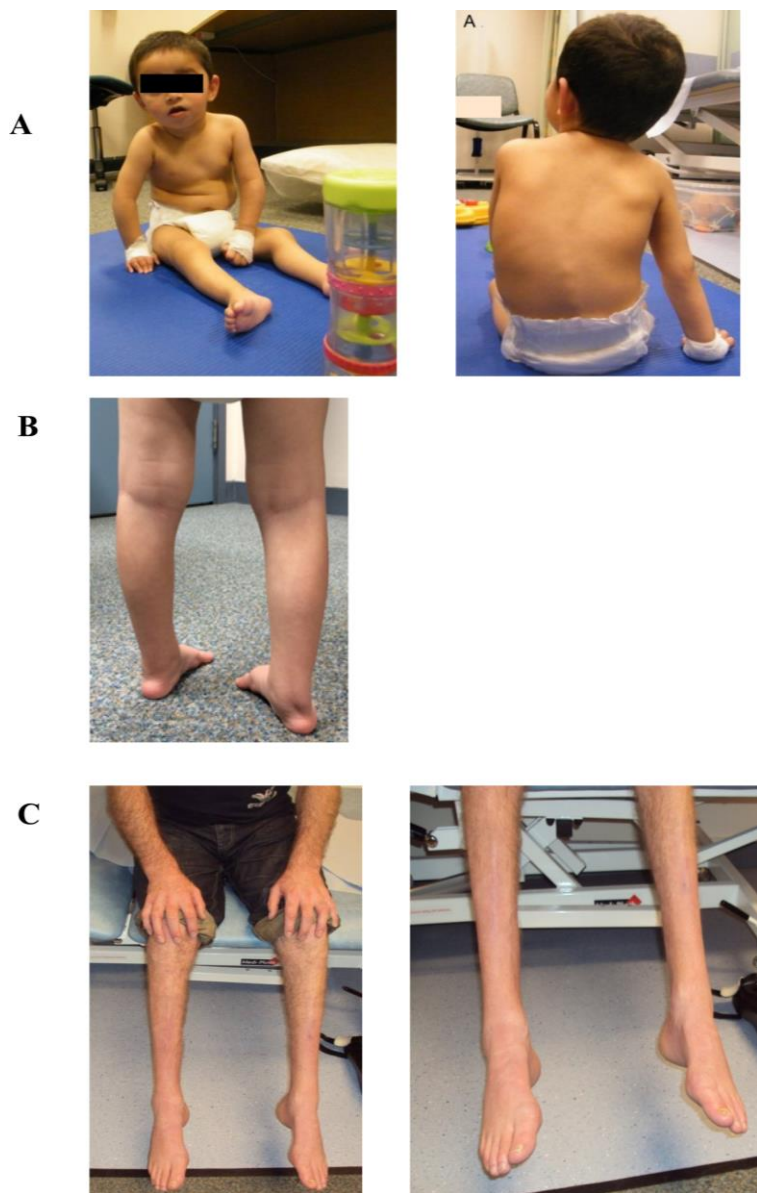


Figure 6.5 Photograph illustration of *IGHMPBP2*-related phenotypes

- A) SMARD1 (Family 8)
- B) juvenile-onset dSMA (Family 15)
- C) dHMN (Family 9)

Charcot-Marie-Tooth disease type 2S / dHMN

A pair of siblings (*Family 9*) presented with childhood-onset, slowly progressive distal spinal muscle atrophy and lack of respiratory involvement related to the heterozygous c.1813C>T, p.Arg605*X nonsense *IGHMBP2* mutation. The same sequence variant has been reported to form compound heterozygous *IGHMBP2* mutations causing CMT2S phenotype. Both siblings had abnormal foot posture and pes cavus deformities in infancy, clumsiness and gait instability in early childhood, but the distal motor symptoms affected more severely the male sibling (**Figure 6.5, C**). He progressed with distal predominant, symmetric muscle atrophy and paralysis in his lower extremities, preserving some muscle strength only in his hip muscles. He remained ambulant until his early 20's but he required two crutches and intermittent wheelchair support. He started noticing mild wrist weakness and wasting of intrinsic hand muscles in his 20's. In comparison, the female sibling developed a slowly progressive, mild to moderate distal motor weakness in her lower limbs. She preserved ambulatory skills with ankle foot orthotic support. Later in the disease course she developed moderate wasting and weakness in her intrinsic hand muscles. Neither of the siblings had cranial nerve involvement or sensory loss. Respiratory insufficiency, recurrent respiratory infections or sleep apnoea never became apparent. Electromyography showed mixed active and chronic neurogenic changes and electric nerve studies indicated reduced CMAPs but preserved motor conduction velocities and sensory responses, compatible with the diagnosis of distal hereditary motor neuropathy.

Another heterozygous c.2752 C>T, p.Arg918Cys missense *IGHMBP2* variant was found in a large Pakistani consanguineous pedigree (*Family 14*) segregating with dSMA and CMT2S allelic forms with no signs of respiratory dysfunction. All 4 investigated family members developed predominant lower limb symptoms of variable severity. They had distal muscle atrophy with foot deformities and motor weakness causing bilateral foot drop and walking difficulties. All of them required orthotic support. The disease-onset was in the first decade followed by a slowly progressive course. There was no associated cranial nerve or diaphragm involvement. Electrophysiology indicated dSMA phenotype in two brothers of the index patient, underlined by exclusive motor response loss and chronic neurogenic changes. The female index patient and her paternal uncle both had distal hand weakness and various degrees of pinprick and vibration sensory loss in their distal extremities. Nerve conduction studies revealed severe axonal motor and sensory neuropathy, compatible with the CMT2S phenotype.

The p.Arg918Cys *IGHMBP2* missense change has not yet been reported. It is predicted to cause the substitution of the moderately conserved arginine for a cysteine within the zinc finger AN1-type domain of the *IGHMBP2* protein. The physicochemical difference between these two amino acids is large and *in silico* analysis suggests, that this change is likely to have a detrimental effect on the protein function. However, the minor allele frequency would be high for a dominant mutation and we have yet been unable to identify a second mutation. The strong evidence of intrafamilial segregation makes the pathogenicity of this novel *IGHMBP2* variant very likely.

6.2.4.2 Experimental genetic studies

The single heterozygous c.1813C>T, p.Arg605*X nonsense *IGHMBP2* mutation was found by WES in *Family 9*. Sanger sequencing of the genomic DNA confirmed that the mutation co-segregated in both siblings and their healthy father (**Figure 6.6**). Larger *IGHMBP2* deletions/ duplications were excluded by MLPA in the patients and no second mutation could be identified with additional Sanger sequencing of the 5' promoter region. Sequencing of the cDNA revealed that the c.1813C>T stop mutation was hemizygous in the affected siblings, indicating that only one allele carried the nonsense mutation while the second allele was completely lost (**Figure 6.7**). Presumably, the complete loss of the second allele can be explained by allele degradation caused by a not yet identified, but possibly intronic mutation.

6.2.5 Discussion

Recently a total of 11 pedigrees, including *Family 9* has been reported with autosomal-recessive inherited CMT2 caused by *IGHMBP2* mutations (CMT2S; OMIM#616155) (Cottenie *et al.*, 2014). The common presentation of all families was a childhood-onset, slowly progressive axonal motor and sensory neuropathy with early foot deformities. Symmetric distal motor atrophy and weakness was described with proximal limb weakness and scoliosis in some cases. Sensory involvement was mild or absent and none of the patients developed respiratory impairment. Neurophysiology and nervus suralis histopathology showed milder features compared to the findings in SMARD1. The identified *IGHMBP2* mutations were mainly compound heterozygous, a loss-of-function nonsense in the 5' region in combination with a truncating frameshift or missense mutation. Investigating further the single c.1813C>T, p.Arg605*X *IGHMBP2* mutation, which led to a recessive phenotype in *Family 9*, we could identify that the stop mutation was hemizygous on cDNA sequencing (**Figure 6.7**). We could not detect the presence of a second mutation by additional sequencing of 5' promoter region of the gene.

IGHMBP2 c.1813C>T, p.Arg605*

DNA

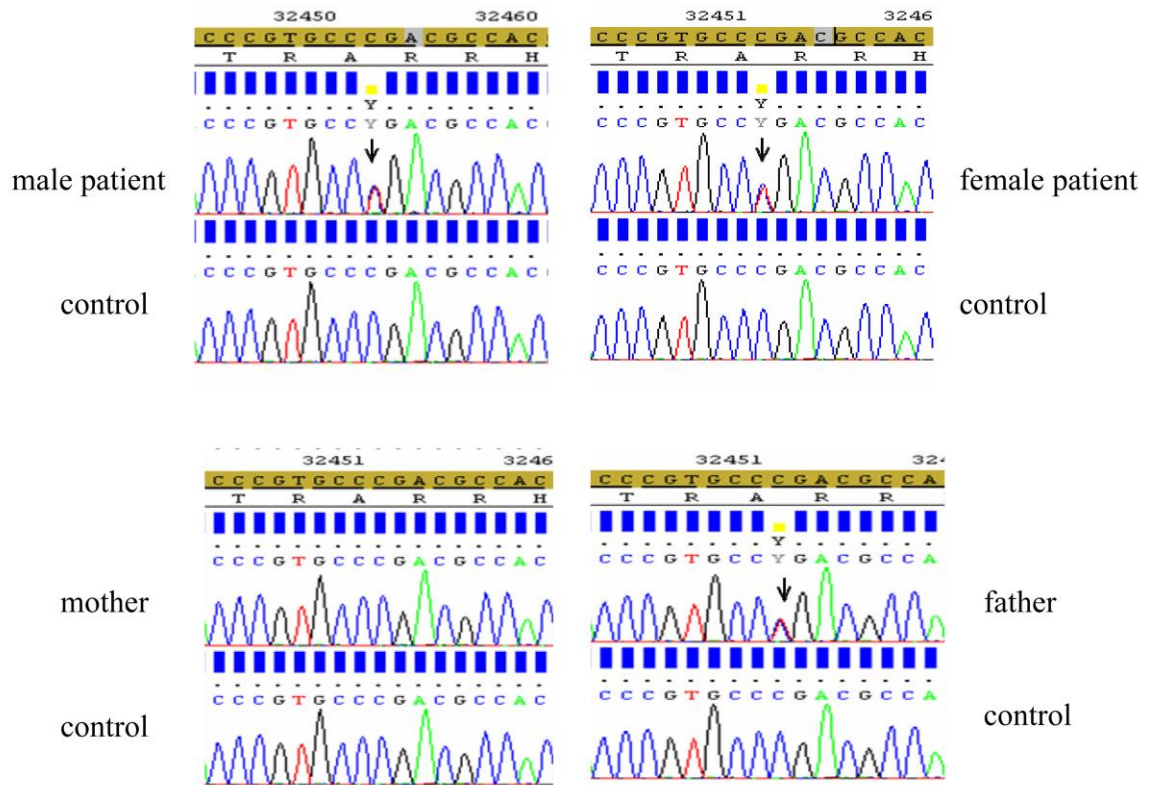


Figure 6.6 Segregation of the identified heterozygous *IGHMBP2* mutation

IGHMBP2 c.1813C>T, p.Arg 605*

cDNA

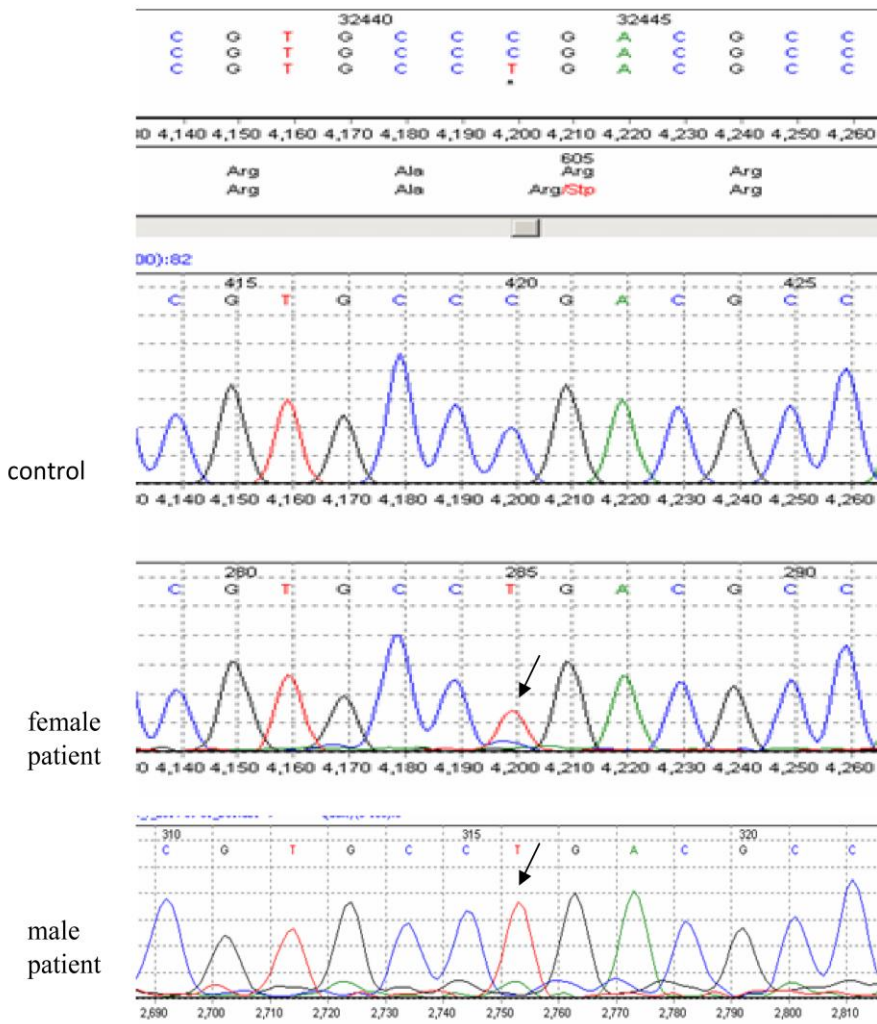


Figure 6.7 Hemizygous *IGHMBP2* mutation on cDNA sequencing

We suggested that a not yet identified, most likely intronic mutation could have led to the complete deletion of the other allele (Cottenie *et al.*, 2014).

Many different missense, nonsense, splice donor site, frameshift and inframe mutations have been reported in the *IGHMBP2* gene, but the localisation and type of mutations do not seem to correlate with the disease severity and genotype-phenotype relations have remained unidentified. However, patients with homozygous mutations tend to develop a more severe phenotype, compared to those carrying compound heterozygous mutations. Several single heterozygous variants have been linked to recessive *IGHMBP2*-related phenotypes, indicating that the second mutation either could not be identified due to limits of the current gene sequencing approach or they remained undetectable due to complex genomic rearrangements (Guenther *et al.*, 2004; Cottenie *et al.*, 2014; Porro *et al.*, 2014; Vanoli *et al.*, 2015). It has been proposed that different mutations result in variably decreased level of IGHMBP2 protein in the motor neurones and this might provide an explanation for the phenotype heterogeneity (Grohmann, 2004; Guenther *et al.*, 2009). The residual protein level in fibroblasts with CMT2 mutations was indeed measured to be significantly higher compared to that in SMARD1 patients, but lower to that in controls (Cottenie *et al.*, 2014). The additional influence of modifier genes as well as epigenetic and environmental factors may further complicate the genotype-phenotype relations.

6.2.6 Conclusion

The *IGHMBP2*-related large phenotype heterogeneity was well illustrated in our families, where the spectrum of classical SMARD1, juvenile-onset distal spinal muscular atrophy with or without respiratory weakness and axonal motor neuropathy CMT2S/dHMN was present. Mutations in the *IGHMBP2* gene cause helicase dysfunction, which might serve as a common pathology behind the development of various neuropathies. A truncated or reduced amount of IGHMBP2 protein may impair the production of error-free mature mRNA in the neurons with subsequent degeneration. The phenotype is suggested to correlate with the mutation specific impairment of the residual level of active IGHMBP2 protein. The detection of single heterozygous *IGHMBP2* variants segregating with a compatible but recessive disease phenotype should be meticulously analysed further for their pathogenicity. It is warranted that *IGHMBP2* mutations should be considered in atypical SMARD1 and hereditary motor and sensory neuropathies regardless the absence of associated respiratory symptoms.

6.3 *TRPV4*-related neuropathy

6.3.1 Literature review

TRPV4 (transient receptor potential vanilloid 4 channel; OMIM#605427) is a calcium permeable non-selective cation channel, which is expressed in several tissues and wide ranges of cell types (Everaerts *et al.*, 2010). *TRPV4* has been acknowledged as the key regulator of cartilage and bone development (Hurd *et al.*, 2015), while it has a pleiotropic role in the nervous system related to its expression in the central nervous glia cells, sensory neurons and to a lesser extent in spinal cord motor neurons.

Many mutations in the *TRPV4* gene have been linked to diverse phenotypes and variably severe manifestations (Aharoni *et al.*, 2011). Related conditions were classified into each of the two major phenotype groups of skeletal dysplasia and peripheral nervous system impairment. Gain-of-function mechanisms have been implicated in several hypothetical pathogenic pathways, including disturbed Ca²⁺ homeostasis, impaired Ca²⁺ channel trafficking, altered axonogenesis, dysfunctional gene expression and protein-protein interactions (Nilius and Voets, 2013; Echaniz-Laguna *et al.*, 2014).

TRPV4-related peripheral neuropathies are rare, autosomal-dominant inherited conditions with incomplete penetrance, which are frequently accompanied by vocal cord palsy, respiratory insufficiency and sensorineural hearing loss. Associated phenotypes encompass hereditary motor and sensory neuropathy type 2C or Charcot-Marie-Tooth disease type 2C (HMSN2C or CMT2C; OMIM#606071), congenital distal spinal muscular atrophy with or without arthrogyriposis or distal hereditary motor neuropathy type VIII (CSMA or dHMN8; OMIM#600175) and scapuloperoneal spinal muscular atrophy (SPSMA; OMIM#181405). (Nilius and Voets, 2013; Echaniz-Laguna *et al.*, 2014)

TRPV4 mutations have been implicated in various skeletal dysplasias, including brachyolmia type 3 (BCYM3; OMIM#113500), familial digital arthropathy-brachydactyly (FDAB; OMIM# 606835), spondylometaphyseal dysplasia, Kozlowski type (SMDK; OMIM#184252), metatropic dysplasia (OMIM#156530), parastremmatic dwarfism (OMIM#168400) and spondyloepimetaphyseal dysplasia, Maroteaux type (SEDM; OMIM#184095).

6.3.2 Aims and hypothesis

I aimed to investigate the clinical variability in patients diagnosed with *TRPV4* mutations, in order to expand the spectrum of related phenotypes. We analysed the hypothesis, whether abnormal protein misfolding might play a role in the pathology of *TRPV4*-related neuropathy.

6.3.3 Methods

6.3.3.1 Patient recruitment

Families identified with *TRPV4* mutations (*Family 10-11*) were selected from the extended hereditary motor neuropathy cohort (*Chapter 5.4.2.1*).

Patients and their family members underwent detailed clinical assessments and provided written consent for the application of genetic and histopathology diagnostic methods.

6.3.3.2 Muscle histopathology

Open muscle biopsy was performed according to standard techniques in both affected patients. Biopsy was taken from the left quadriceps in the patient from *Family 10* and from the left tibialis anterior muscle in the patient from *Family 11*. The biopsies were processed according to standard methods and were analysed at Newcastle-upon-Tyne Hospitals NHS Trust by Dr Tuomo and Dr Evangelista.

6.3.3.3 Neurophysiology

Nerve conduction studies and concentric needle electromyography was performed in the patients according to standard methods. The young patient from *Family 10* was examined at the Neurophysiology Department, Newcastle-upon-Tyne Hospitals NHS Trust by Dr Whittaker, while members of *Family 11* had their test performed in Dundee Teaching Hospital by Dr Spillane.

6.3.3.4 Genetic diagnostic methods

Targeted candidate gene screening was followed by performing either or both of IPN gene panel test and WES. After bioinformatics analysis, putative disease-causing variants were investigated for segregation in available family members. PCR (IMMOLASE™ DNA Polymerase, Bioline UK) and Sanger sequencing (BigDye® Terminator v3.1) was carried out in variants, which were predicted to be deleterious by three online prediction tools (MutationTaster, SIFT and Polyphen2) (**Table 5.8**).

6.3.4 Results

6.3.4.1 Clinical phenotypes of patients diagnosed with *TRPV4* mutations

Family 10

The 8-year-old boy (**Figure 6.8, a**) was born from non-consanguineous parents and had no family history of a neuromuscular condition. He was a generally weak and floppy neonate and he developed torticollis at the age of 10 weeks. His gross motor development was overall delayed and he started to walk only aged 22 months. His unsteady gait, frequent falls and inability to jump or run prompted medical review at the age of 30 months. He developed intermittent hoarse voice changes and minor swallowing difficulties both with solids and liquids.

Physical examination revealed skeletal dysplasia, short stature with disproportionately short lower extremities, genu valgus, brachydactyly, and lumbar lordosis. He had no respiratory or cardiac impairment. There was mild scapular winging and muscle atrophy in the distal part of his legs. A prominent bilateral motor weakness was present, affecting both proximal and distal muscle groups in the lower limbs and proximal muscles in his upper limbs. Gower's manoeuvre was partially positive and he walked with marked waddling gait. His feet were flat and bilaterally dropped. Lower limb reflexes were absent but there were no long tract signs. There was no evidence of ataxia, cranial nerve involvement and sensory changes. His CK level and spinal MRI scan were unremarkable.

Family 11

The 48-year-old female (**Figure 6.9, a**) patient had normal early motor milestones followed by adult-onset motor dysfunction. She had no positive family history other than that her brother was born with bilateral talipes. Recurrent sprains in her right ankle were the earliest symptoms, when she was 40 years old. Later she developed progressive lower limb weakness leading to gait difficulties. She had no cardiac or respiratory manifestations.

Her examination showed prominent motor weakness affecting exclusively her lower limbs with milder distal muscle wasting. The proximal muscle strength was better preserved (MRC grade 4/5) than distal (MRC grade 2/5) in her legs. The patella reflexes were brisk, while the ankle jerks were reduced but present. The plantar reflex was flexor. She had bilaterally dropped foot and she was walking with a poorly balanced steppage gait aided by two walking crutches. She had a remarkable reddish skin discoloration below her knees with extremely cold feet and minor pinprick and vibration sensory loss below her ankle levels.



Figure 6.8 *TRPV4* mutant patient from Family 10

- (a) Photo illustration of patient phenotype
- (b) Muscle biopsy (H&E) showing increased variation in fibre size with atrophic fibres.
- (c) Muscle biopsy (ATPase 4.3) showing type 1 fibre predominance and type-grouping (Evangelista *et al.*, 2015)

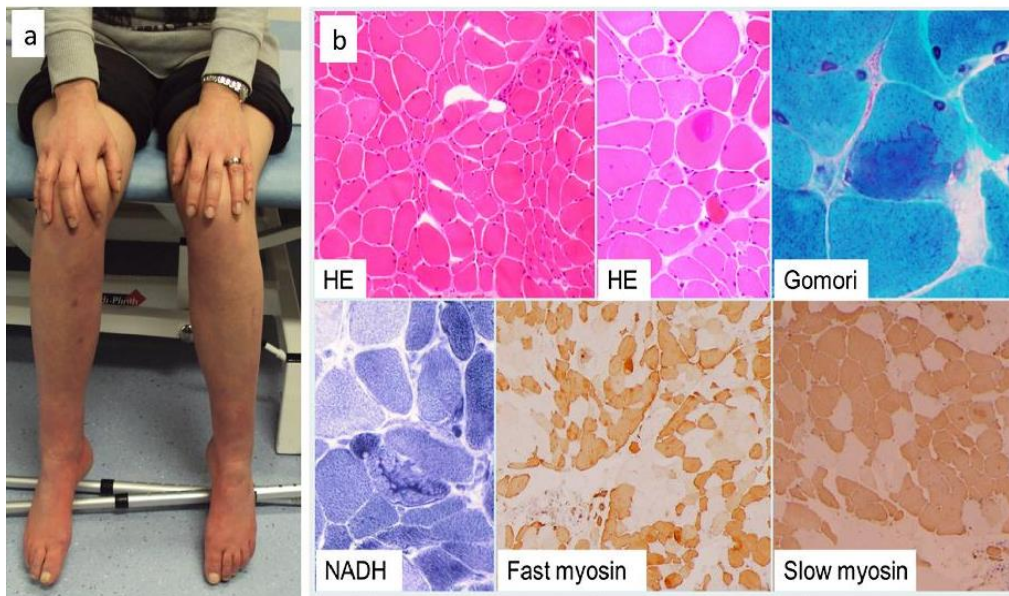


Figure 6.9 *TRPV4* mutant patient from Family 11

- (a) Photo illustration of patient phenotype
- (b) Muscle biopsy showing neurogenic atrophy and accumulations of basophilic material (Evangelista *et al.*, 2015)

Symmetrical atrophy and fat infiltration of her gluteus, hamstrings and calf muscles were seen on muscle MRI imaging. Brain and spinal MRI scans were unremarkable such as her serum CK level.

6.3.4.2 Muscle histopathology result in the patients diagnosed with *TRPV4* neuropathy

Family 10

An increased variation in fibre size and fibre type grouping was observed in the muscle biopsy of the patient. Atrophic fibres were seen scattered and in small groups. ATPase stain indicated type I fibre predominance, with many of the fascicules being entirely type I (**Figure 6.8, b; c**).

Family 11

The patient had an evidence of neurogenic atrophy with increased muscle fibre size variation. Hypertrophic fibres alternated with atrophic fibre clusters and there was an increase in the number of internal nuclei. Intrasarcolemmal basophilic material accumulation was seen in some fibres (**Figure 6.9, b**).

6.3.4.3 Neurophysiology findings in pedigrees with *TRPV4*-related neuropathy

Family 10

Motor and sensory nerve conduction findings were within normal parameters, but needle electromyography revealed a chronic neurogenic pattern suggestive of dSMA. Repetitive nerve stimulation could yet not been carried out due to the young age of the patient.

Family 11

Initial electric nerve tests showed normal parameters when the patient was 42 years old. However, electromyography recorded plentiful fasciculations at rest and marked neurogenic changes, supporting the diagnosis of dSMA. Sensory and motor amplitudes and conduction velocities remained well preserved on repeated studies over a period of 7 years. Electromyography revealed a remarkable progression of neurogenic changes, but this was neither florid nor completely widespread and spared to affect the tongue muscles. Repetitive stimulation of a proximal upper limb nerve muscle group showed evidence of a neuromuscular junction disorder with a significant decrement of 23-24% being seen both prior to and immediately following exercise. In the patient's brother electrophysiology studies were unremarkable.

6.3.4.4 Diagnostic genetic methods and identified *TRPV4* mutations in the pedigrees

Family 10

Phenotype-led targeted candidate gene screening excluded mutations in the *SMN1*, *MFN2* and *IGHMBP2* genes and he was also tested negative for facioscapulohumeral muscular dystrophy-1 (FSHD1). WES detected the heterozygous missense c.805C>T, p.Arg269Cys *TRPV4* mutation, which was reported in previous studies (Auer-Grumbach *et al.*, 2010). Sanger sequencing confirmed that the mutation presented *de novo* in the patient as his healthy parents did not carry the same variant.

Family 11

Diagnostic genetic testing in the female patient did not identify mutations in the *SMN1*, *HSPB1* and *HSPB8* genes. The novel heterozygous c.184G>A, p.Asp62Asn *TRPV4* mutation was detected by IPN gene panel assay and on simultaneously performed WES. Segregation analysis in the family confirmed that the variant was absent in her healthy mother, but was present in the brother. The amino acid change affects a moderately conserved aspartic acid residue in the N-terminal ankyrin repeats motif of the TRPV4 protein. The variant was not reported in dbSNP or in the ESP database and was predicted to have deleterious effects by three online prediction tools.

6.3.5 Discussion

Mutations in the *TRPV4* gene cause a broad spectrum of phenotype manifestations with a marked variability in disease severity. Therefore the proposed classification in the subclasses of skeletal dysplasia and neuropathy needs to be revised. The ‘TRPV4-pathy’ term would better describe related conditions presenting a variable combination of skeletal, motor and neuronal symptoms (Nilius and Voets, 2013).

TRPV4 functions primarily as a homotetrameric channel expressed at the plasma membrane. A single TRPV4 subunit consists of cytoplasm facing N and C termini and six transmembrane alpha-helix domains (S1-S6), with a cation-permeating pore between S5 and S6. The N-terminus is composed by six ankyrin repeats (ARD), a motif mediating protein–protein/protein–ligand interactions and a proline-rich domain (PRD), proximal to the first ARD repeat, which is involved in mechano-sensitivity. The C-terminus consists of several calmodulin-binding sites (Nilius and Owsianik, 2010; Nilius and Voets, 2013). Neuropathy-causing *TRPV4* mutations have been identified restricted to the N-terminal cytosolic tail,

affecting arginine residues at the ankyrin repeats (Auer-Grumbach *et al.*, 2010; Deng *et al.*, 2010; Landouré *et al.*, 2010; Berciano *et al.*, 2011; Nilius and Voets, 2013). The tetramer model of the human TRPV4 channel has been recently generated and by mapping the arginine residues on the convex surface of ARD, the pathogenesis of neuropathy was suggested to rely on impaired binding interactions (Sullivan *et al.*, 2015).

We identified the c.805C>T, p.Arg269Cys *TRPV4* mutation in *Family 10*, which was recurrently reported in patients with CMT2C, SPSMA and with congenital dSMA, indicating wide phenotype heterogeneity (Auer-Grumbach *et al.*, 2010; Deng *et al.*, 2010; Landouré *et al.*, 2010; Zimon *et al.*, 2010; Berciano *et al.*, 2011). The involved Arg269 residue is located between the third and fourth ARD, which is thought to interact with regulatory proteins and might be involved in protein trafficking and multimerization (Nilius and Owsianik, 2010). The detected *de novo* p.Arg269Cys *TRPV4* mutation in the young male patient was associated with the clear neurology and electrophysiology phenotype of scapuloperoneal spinal muscular atrophy (SPSMA) combined with metatropic dysplasia. Previous reports suggested hints that mutations in the *TRPV4* gene can cause simultaneous skeletal and neuropathic changes (Auer-Grumbach *et al.*, 2010; Zimon *et al.*, 2010; Echaniz-Laguna *et al.*, 2014). Three patients were reported to show overlapping syndromes of CMTC2 and either spondylometaphyseal dysplasia (SMDK) or spondyloepimetaphyseal dysplasia (SEDM) (Cho *et al.*, 2012; McEntagart, 2012). The p.Arg269Cys *TRPV4*-related neuropathy has not yet been described with overlapping skeletal dysplasia, even though milder skeletal abnormalities were noted.

We found a not yet described, heterozygous missense c.184G>A, p.Asp62Asn *TRPV4* mutation in the patient from *Family 11*, leading to a phenotype compatible with dSMA/dHMN8. The mutation co-segregated in her brother, who was born with bilateral talipes but did not develop neuropathy symptoms until he was 29 years of age. The affected Asp62 residue is located in the N-terminal region of the TRPV4 protein. *In silico* prediction suggested that the amino acid change is probably deleterious by changing the conformation of the protein. The previously reported N-terminal located c.58G>A, p.Gly20Arg *TRPV4* mutation caused a dHMN phenotype in a female patient, who showed strikingly similar clinical and electrophysiology characteristics, when compared to our patient. The p.Gly20Arg *TRPV4* mutation resulted in variable expression of the disease in the described family, such as it was observed with the p.Asp62Asn *TRPV4* mutation in *Family 11* (Fawcett *et al.*, 2012). It has still remained unclear, how *TRPV4* mutations in the N-terminal localise relative to neuropathy-causing ARD variants, but it was suggested that they might influence ARD mediated ligand interactions (Sullivan *et al.*, 2015).

There was a marked NMJ defect detected with significant decrement on repetitive nerve stimulation in the patient from *Family 11*. Recent studies on transgenic *Drosophila* lines expressing TRPV4^{R269C} revealed disrupted axonal mitochondrial transport and aberrant synapses in axons that project to distal muscles. The hypothesized mechanism of increased calcium-influx due to gain-of-function *TRPV4* mutations might cause axonal and synaptic degeneration (in persona communication Lloyd T et al, 2016). Further investigations are needed to examine whether influencing the NMJ defect has a potential therapeutic benefit in *TRPV4*-related neuropathies.

Only a few reports described abnormal muscle histology in *TRPV4*-related neuropathies, which were demonstrating increased variation in fibre size and fibre type grouping, indicative of chronic denervation (Landouré *et al.*, 2010; Echaniz-Laguna *et al.*, 2014). The same histopathology findings were seen in the patient from *Family 10*. We detected distinguishable histology features in the muscle biopsy of the patient from *Family 11*, where intra-cytoplasmic basophilic inclusions were seen in addition to the neurogenic changes. *In vitro* studies in HeLa cells showed that mutant TRPV4 proteins formed cytoplasmic aggregates, while wild-type TRPV4 proteins were predominantly detected at the plasma membrane (Auer-Grumbach *et al.*, 2010). Preliminary studies investigate whether ubiquitin ligases can regulate the TRPV4 channel surface expression and activity (Wegierski *et al.*, 2006). Abnormal protein degradation with subsequent retention of misfolded proteins has been implicated in the pathogenesis of some inherited neuropathies (*HSPB1*, *HSPB8*). Misfolded proteins tend to aggregate in the cells triggering different cytotoxic pathways. We speculate that *TRPV4* mutations might also induce misfolded protein production, which causes cytoplasmic aggregates, similarly to that in heat-shock protein-related neuropathies. However, we emphasise that we were unable to define the exact nature of the intracellular aggregates, which were detected in the muscle biopsy of the patient from *Family 11*. (Evangelista *et al.*, 2015)

6.3.6 Conclusion

Phenotype variability was examined in two pedigrees diagnosed with neuropathy-causing *TRPV4* mutations. The patient carrying the *de novo* p.Arg269Cys *TRPV4* mutation presented with overlapping syndromes of scapuloperoneal spinal muscular atrophy and skeletal dysplasia. We supported that *TRPV4* mutations need to be considered in case of a combined presentation of skeletal dysplasia and axonal neuropathy. Symptoms of skeletal deformities, in particular short stature, brachydactyly and disproportion between the lower and the upper halves of the body can provide a hint towards the diagnosis. Large phenotype variability and incomplete disease penetrance should be taken into account in *TRPV4* mutations. This was highlighted in *Family 11*, where intrafamilial disease variability associated with the p.Asp62Asn *TRPV4* mutation. We suggested that the presence of cytoplasmic basophilic inclusions in the muscle biopsy, due to possible misfolded protein aggregates, might also indicate *TRPV4*-related pathology (Evangelista *et al.*, 2015).

6.4 *BICD2*-related neuropathy

6.4.1 Literature review of pedigrees with the common *BICD2* mutation

Motor neurons are highly sensitive for intact intracellular trafficking. The cytoplasmic dynein motor complex is responsible for the axonal retrograde transport of numerous subcellular vesicles in the neuron. The dynein motor is essential in neuron maintenance, neuron migration and development by transmitting signals and re-circulating materials from the cell periphery. The cargo-binding is coupled to the microtubular motor by its heavy chain component, DYNC1H1 using ATP hydrolysis. The dynein functionally interact with accessory proteins, such as dynactin and *BICD2*, which regulate the dynein motor and the cargo-binding (Roberts *et al.*, 2013; Fiorillo *et al.*, 2014; Garrett *et al.*, 2014; Peeters *et al.*, 2015).

The *BICD2* adaptor protein acts as a stimulator of dynein and by recognising different cellular cargos participates in the cargo-binding and trafficking via the complex molecular dynein-dynactin motor. *BICD2*-related phenotypes encompass the spectrum of autosomal-dominant lower extremity-predominant spinal muscular atrophy-2 (SMALED2, OMIM#615290), combined lower and upper motor neuron pathology and hereditary spastic paraplegia (HSP).

A large worldwide cohort of 9 families carrying *BICD2* mutations has been reported highlighting associated phenotype-genotype correlations (Rossor, Oates, *et al.*, 2015a). The c.320C>T, p.Ser107Leu was the most commonly identified mutation in *BICD2*. The affected residue is in a methylated CpG dinucleotide, which is prone to methylation-mediated deamination providing a “hot spot” for recurrent mutations. The p.Ser107Leu *BICD2* mutation identified in two large pedigrees originating from Australia and Austria shared a 0.1Mb span 8 single nucleotide polymorphism (SNP) haplotype with a CEU European background frequency of 2%, indicating a common founder in the two families. Another USA family with European ancestors showed the same haplotype background (Oates *et al.*, 2013). In a large Bulgarian pedigree of Turkish ethnic origin the p.Ser107Leu mutation arose *de novo* in the proband and a genome wide linkage analysis could delineate the mutation to a 1.86 Mb region (Peeters *et al.*, 2013). A further three-generation Dutch family carried the same p.Ser107Leu mutation within a 10Mb region of linkage (Neveling *et al.*, 2013).

6.4.2 Aims and hypothesis

I aimed to expand the cohort of p.Ser107Leu *BICD2* with two additional families of North-East England origin, where we achieved the genetic diagnosis by next generation sequencing. I planned to analyse phenotype correlations in comparison to the previously reported families. I wanted to investigate whether the p.Ser107Leu mutation could be a common founder or it arose on a different haplotype background in a *BICD2* region considered as a mutation ‘hot spot’.

6.4.3 Methods

6.4.3.1 Patient recruitment and investigations

In our hereditary motor neuropathy cohort of 105 patients two families (*Families 5-6*) (*Chapter 5.4.2.1*) were diagnosed with the common c.320C>T, p.Ser107Leu *BICD2* mutation, presenting with distal congenital non-progressive SMA. Detailed clinical and neurophysiology investigations were applied to examine the related phenotype characteristics. Participants were consented to genetic and natural history studies.

6.4.3.2 Haplotype analysis and experimental genetic studies

The molecular cause was revealed in both families by WES and the diagnosis was confirmed by Sanger sequencing and segregation analysis (*Chapter 3.2.1.2*; *Chapter 3.2.2*).

The haplotype background in the families was investigated with the assistance of our bioinformaticist, Dr Helen Griffin. Haploview input from the patient exomes and from a further 60 exomes was generated for the region surrounding the *BICD2* mutation. From the exome Haploview-Haplotypes, a maximum region of 0.4Mb (397,470bp) between chr 9:95,476,958-95,874,428 (hg19) could be identified to be shared by the two families. HapMap (data release 28) SNP genotype data from the CEU population, in a region in closer proximity to the *BICD2* mutation was used to generate Haplotypes in Haploview (www.broadinstitute.org). The closest HapMap markers either side of the *BICD2* mutation were only 800bp apart. Combined exome and hapmap data was investigated to show whether our families have a different haplotype surrounding the mutation. I performed Sanger sequencing of the following 7 SNPs (rs10992471, rs10992463, rs2181585, rs4141966, rs10117449 and rs10491804) in order to show whether the mutation is on a different haplotype in the two families, and also of 2 SNPs (rs2296080 and rs10821010) to determine which haplotype background the mutation is on (**Table 6.6**).

Gene	SNP	Forward primer	Reverse primer	Ta (°C)	Size (base pair)	
					Forward	Reverse
<i>BICD2</i>	rs10992471	TCAGCAGGGTAATGGACGTT	ATGGTCAGTTGGCCAGAG	62	20	19
<i>BICD2</i>	rs10992463	GTGAGTGTCACTAACCAACTGA	TGCACCTATATAGTCCCAGG	62	23	20
<i>BICD2</i>	rs2181585	TGTCTAAGTTGAAAGCTTGCCT	TCCAGAAGTCAAGGGAGTA	62	22	20
<i>BICD2</i>	rs4141966	GGAGGTGCCTAATGAGAACTC	TTTTCTCACACAGCAGGCA	62	21	20
<i>BICD2</i>	rs10117449	ACCGAGTCCAAAGTAGAACTCA	CCAATCTGGTTTCCTCAGAGTC	62	22	22
<i>BICD2</i>	rs10491804	TGTGCCACTTGATTCAACGC	CTCTGTGTTCTGGGTTTGGC	62	20	20
<i>BICD2</i>	rs2296080	ACCCTACCTCGAGTCTCCAT	GCTGAAGGAGGTGAGGGG	62	20	18
<i>BICD2</i>	rs10821010	GAGGTGCATCTGTGGCGT	CTGTGCTGGCCTCTGTCTAG	62	18	20

Table 6.6 Designed primers for the sequencing of SNPs in the *BICD2* gene

6.4.4 Results

6.4.4.1 Detailed phenotype characteristics of the investigated *BICD2* families

Family 6

A 41-year-old mother and her 3 children were diagnosed carrying the p.Ser107Leu *BICD2* mutation in the two generation family.

The mother (II/1) (**Figure 6.10, A; B**) had congenital foot deformities with crowding of her toes and she was delayed with walking. She was poor at physical activities and she was always weak to raise herself to stand. Her neuromuscular symptoms were present from birth and remained largely stable later in her life, indicating a non-progressive disease course. Neurology examination found equally decreased strength in both proximal and distal lower limb muscles. The muscle strength in her upper limbs was entirely preserved albeit that she was noted with mild left scapular winging. Deep tendon reflexes were brisk with mild asymmetry but there were no pyramidal signs. She was unable to perform heel walk and her Gower's test indicated proximal limb weakness. There was no indication for sensory disturbance. All laboratory parameters were within physiological limits apart from a very mildly elevated serum creatine kinase level. Electric nerve studies recorded conduction velocities and action potentials within the normal ranges. Electromyography findings of severe chronic neurogenic changes in the L3 (m. vastus lateralis) and in the C5 (m. infraspinatus) myotome were suggestive of a segmental type of anterior horn cell disorder. Muscle MRI indicated marked symmetrical fatty replacement in her lower limb muscles (m. gluteus medius, m. vastus lateralis, m. rectus femoris, m. semi-membranosus, m. lateral and medial gastrocnemius).

Her first child (III/1) was born with mild foot deformities and had a late walk aged 20 months. She was walking on the inner border of her feet. Aged 6 she had more prominent physical difficulties compared to her family members and she developed a broad based waddling gait. Her 5-year-old twin brothers (III/2 and III/3) also had motor delay and similar but milder clinical symptoms (**Figure 6.10, A; B**). All children had disproportionate atrophy and weakness in their lower extremities. Proximal leg weakness was present leading to difficulties in rising from the floor, climbing stairs and running. Scapular winging was observed in addition to good upper limb power and fine motor manipulation. Deep tendon reflexes were brisk with no evidence of long tract signs. They were unable to perform heel walk. Physiotherapy input and orthotic support were required in all children. No other family members were reported with a similar condition.

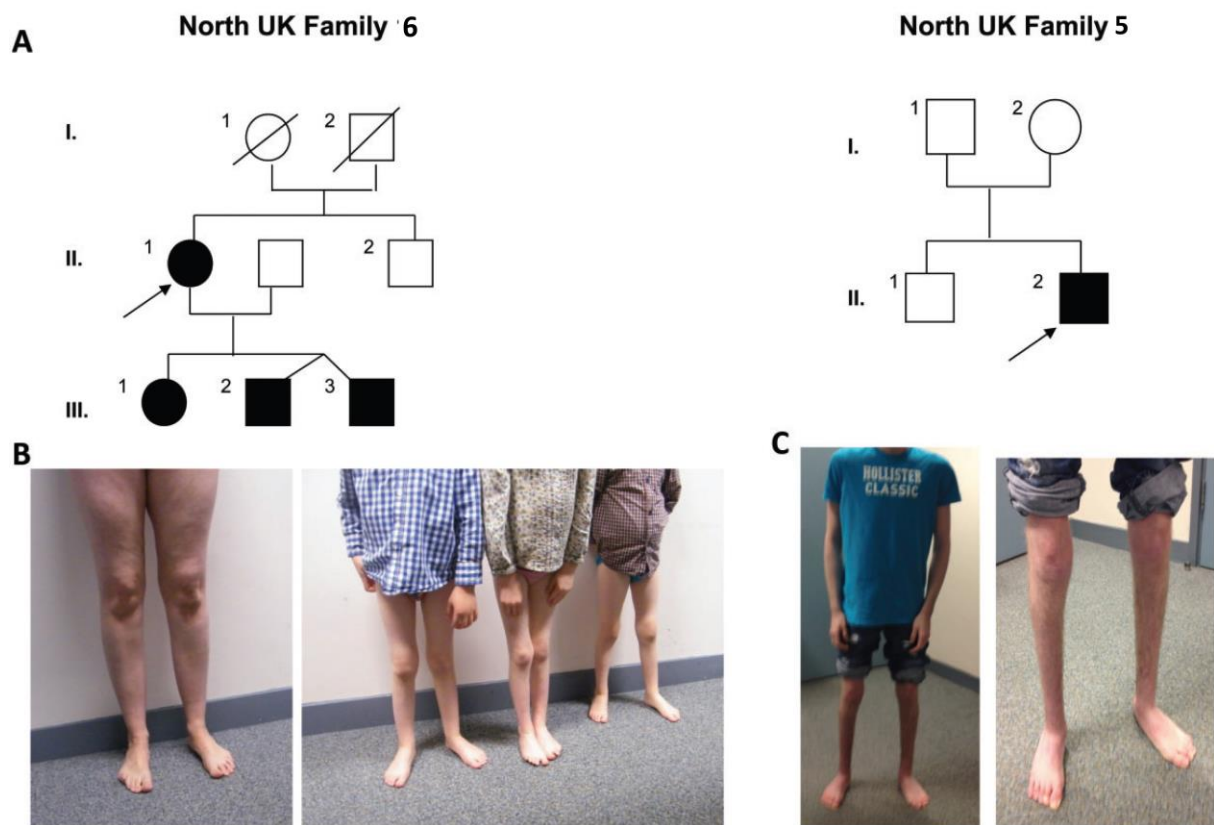


Figure 6.10 Pedigrees and clinical phenotype of *BICD2* mutant families

(A) Pedigrees of Families 5-6, probands are indicated by an arrow

(B) Photo illustration of the phenotype of Family 6

(C) Photo illustration of the phenotype of the patient from Family 5

(Bansagi, Griffin, *et al.*, 2015)

Family 5

In another North-East UK family the disease manifested *de novo* in a 19-year-old man (II/2) (**Figure 6.10, A; C**) with no family history of the condition. He was born with bilateral talipes, which required serial castings and physiotherapy. Ultimately aged 1 it was corrected by surgical interventions. Gross motor development was subsequently delayed with late walking around the age of 3. He had prominent motor difficulties in his early childhood, while later the disease presented with a non-progressive neuromuscular deficit. He developed waddling gait but remained ambulant requiring wheelchair support only for longer distances. His neurology examination found prominent distal lower limb motor atrophy, leading to thin calves and muscle loss in the anterior compartments. There was a marked atrophy in his hip muscles with proximal leg weakness. He had a full power in the shoulders and upper limbs albeit that he presented with bilateral scapular winging. Reflexes were reduced in his lower limbs. There was no sensory impairment. He was walking with steppage and waddling gait and he was unable to perform heel walk. Nerve conduction studies were within normal parameters. Concentric needle electromyography showed markedly increased amplitude motor units, which were polyphasic and unstable. Chronic neurogenic process was indicated with spinal motor neuron involvement, consistent with distal spinal muscular atrophy (dSMA). Muscle biopsy revealed no other changes than neurogenic fibre atrophy.

6.4.4.2 Haplotype analysis in the families carrying the p.Ser107Leu *BICD2* mutation

We performed haplotype analysis in our families in order to determine whether the c.320C>T, p.Ser107Leu *BICD2* mutation is a common founder or it is a mutational “hot spot”. The genomic positions of the closest microsatellite markers (D9S1815, D9S197) to the *BICD2* mutation in the previously reported Bulgarian family (Peeters *et al.*, 2013) span a 1.86Mb region, which was outside the boundaries of the 0.4Mb in our patient exomes. The Dutch pedigree (Neveling *et al.*, 2013) also shared a much larger region (10Mb), which was not surprising given these were larger families. If patient exomes from our two families had a founder mutation in common with either of the published families, then recombination would have led to the shared haplotype region being smaller but we were unable to anchor our exome haplotype to the larger haplotypes from these families. In the CEU European population there were 10 different haplotypes present in a single 0.1Mb block. For the first 5 SNPs of the haplotypes genotype data was available from whole exome sequence, while we genotyped further 7 haplotype tagging SNPs by Sanger sequencing (**Figure 6.11**).



Figure 6.11 Haplotype analysis in the *BICD2* mutant families

Ten European haplotype blocks in a 0.1Mb region surrounding *BICD2* from Haplotype SNP IDs 01 (rs556) to 89 (rs10117449).

The *BICD2* c.320C>T mutation is located between SNPs 19 and 20. Haplotype SNPs 01, 04, 05, 07 and 08 were genotyped from whole exome sequence; SNPs 15, 19, 52, 63, 73, 88 and 89 were genotyped from Sanger sequence (blue arrows).

Affected members of **Family 6** shared haplotype block 3 (yellow box), present in the HapMap CEU population at a frequency of 0.098.

The affected proband in **Family 5** had haplotype blocks 2 and 4 (red and blue boxes) in the region surrounding the mutation; recombination not observed in the CEU population occurred between SNPs 63 and 73, so that this proband also had part of either blocks 7, 8 or 10

(Bansagi, Griffin, *et al.*, 2015)

We could confirm that there were different haplotypes in our two families and the mutation was carried on different haplotype background. Additionally, the p.Ser107Leu mutation presented *de novo* in the patient from *Family 5* as neither of his parents was tested positive. Our findings could further support that the c.320C>T position in the *BICD2* may present as a mutation ‘hot spot’ (Bansagi, Griffin, *et al.*, 2015).

6.4.5 Discussion

Patients with dynein motor abnormalities due to *BICD2* mutations manifest as a distinct clinical entity of SMA-LED. This condition is a birth- or first decade-onset non-length-dependent motor atrophy and weakness affecting predominantly the lower limbs with congenital joint deformities. Deep tendon reflexes are reduced or absent and occasional pyramidal tract involvement indicate concomitant upper motor neuron pathology. Adult disease-onset and mild upper limb features occur only in a minority of patients. The static disease course, presenting initially with delayed motor development and later with variable gait problems, is characteristic and loss of ambulation occurs only in individual severe cases. Nerve conduction studies remain within normal parameters. Electromyography is indicative of chronic but not active denervation changes consistent with the non-progressive phenotype. The uniform thigh MRI pattern with relative sparing and hypertrophy of the adductors and semi tendinosus muscles provides a useful diagnostic tool (Peeters *et al.*, 2014, 2015; Rossor, Oates, *et al.*, 2015a; Scoto *et al.*, 2015; Strickland *et al.*, 2015).

In *BICD2* mutated patients the degree of wasting in the lower limb muscles was found to exceed the severity of the muscle weakness. Congenital deformities, Achilles tightness and scapular winging were commonly associated. Recent reports broadened the *BICD2*-related phenotype with cerebellar hypoplasia (Fiorillo *et al.*, 2016), arthrogryposis multiplex congenital and cortical malformations similarly as in *DYNC1H1* mutations (Ravenscroft *et al.*, 2016) and chronic myopathy with *BICD2* aggregation in different subcellular locations (Unger *et al.*, 2016). Mutations have been reported affecting all three coiled-coil domains of the *BICD2* protein and trafficking impairment serve as a common pathomechanism (Peeters *et al.*, 2014; Rossor, Oates, *et al.*, 2015a; Rossor, Oates, *et al.*, 2015b).

We expanded the worldwide cohort of *BICD2* by additionally diagnosing dominant p.Ser107Leu *BICD2* mutation in North-East England in a two generation family and in an unrelated patient, where the mutation arose *de novo*. The phenotype characteristics of SMA-LED in our families, including congenital foot deformities, early-onset non-progressive lower

limb predominant motor symptoms, specific electromyography and muscle MRI findings, were in agreement with the previously reported cases. Scapular winging was a consistent symptom in our patients, which we suggested to consider a valuable clinical clue toward *BICD2* testing (Bansagi, Griffin, *et al.*, 2015).

We confirmed that the p.Ser107Leu *BICD2* mutation was carried on a different haplotype background in our two families by genotyping the haplotype tagging SNPs. By detecting an incongruence in the haplotype frequency (0.098%) between our and previously reported pedigrees (2%), we could determine that the p.Ser107Leu could not be a common founder in the investigated families. We provided further evidence that the p.Ser107Leu in *BICD2* is a ‘hot spot’, located in a methylated CpG dinucleotide, where recurrent mutations may arise due to methylation-mediated deamination. This suggests that the occurrence of *de novo BICD2* mutations can be relatively high. Therefore, *BICD2* mutations should be considered in sporadic SMA-LED cases, where distinct clinical clues such as Achilles contracture, scapular winging and a specific muscle MRI pattern can be directive for targeted genetic testing (Rossor, Oates, *et al.*, 2015b; Bansagi, Griffin, *et al.*, 2015).

6.4.6 Conclusion

We described two North-East UK families carrying the p.Ser107Leu *BICD2* mutation with the SMA-LED phenotype. Haplotype analysis of the *BICD2* families excluded the presence of a common founder and supported the theory that the c.320C>T position in the *BICD2* gene is a mutation ‘hot spot’. The diagnosis of dominant *BICD2* mutations should be considered even without a positive family history, and particularly when ankle contracture and scapular winging accompany the early-onset distal lower limb motor neuropathy.

6.5 *ATP7A*-related neuropathy

6.5.1 Literature review

Mutations affecting the *ATP7A* heavy metal transporter have been acknowledged to cause Menkes disease and an allelic form, occipital horn syndrome (OHS) due to impaired intestinal copper absorption. Despite increasing knowledge on molecular pathways affected in these X-linked copper metabolism disorders, the precise mechanisms, which lead to the neurological defects and clear phenotype-genotype correlations have remained not yet clarified.

More than 400 diverse *ATP7A* gene mutations have been linked with heterogeneous phenotype manifestations. Loss of function *ATP7A* mutations with subsequent total protein loss result in Menkes disease phenotype, while OHS is evoked by leaky splice site mutations preserving a reduced protein amount. Clinically the disease spectrum differs in age of onset and neurological severity.

The classical Menkes disease is characterised by global neurodegeneration, hypotonia, kinky hair, seizures and early death. The milder allelic OHS is named after the distinguishing feature of symmetric occipital exostosis. Menkes-like hair and connective tissue abnormalities with characteristic plasma/CSF biochemical changes can be found, but no major neurology impairment is related other than autonomic dysfunction caused by a norepinephrinergic defect. An intermediate form referred as mild, moderate or atypical Menkes disease has been described in 5-10% of the patients with longer survival, where moderate developmental delay and cerebellar ataxia predominate (Kaler *et al.*, 1994; Tchan *et al.*, 2013; Tümer, 2013; Kaler, 2014; Møller, 2015).

Recently, a novel phenotype with length-dependent metabolic axonopathy, the X-linked dHMN (SMAX3) has been linked to two unique mutations, inducing aberrant intracellular *ATP7A* trafficking (Kennerson *et al.*, 2010; Kaler, 2011; Yi and Kaler, 2014). Mutated C-terminal di-leucine motif in the *ATP7A*^{P1386S} caused decreased capacity to interact with adaptor protein complexes, which led to preferential plasma membrane accumulation of *ATP7A* and resulted in defected intracellular trafficking (Yi and Kaler, 2015). Abnormal interactions with p97/VCP were described related to *ATP7A*^{T994I} providing a link between the pathomechanism of dHMN and ALS (Yi *et al.*, 2012). Furthermore, a recent WES study identified the combination of a missense mutation in the *ABCB7* gene in close proximity to a deleted *ATP7A* mutation causing a distinctive phenotype of X-linked congenital cerebellar ataxia (Protasova *et al.*, 2016).

Abnormal copper metabolism serves as a common pathway in these neurogenetic conditions. The disturbed homeostasis of copper, an essential trace element, impairs numerous critical intracellular pathways, including mitochondrial oxidative phosphorylation, oxidative stress protection and neurotransmitter production. Altered copper homeostasis has been largely investigated in other neurodegenerative diseases such as ALS, Alzheimer and idiopathic Parkinson disease. Several pathological pathways have been implicated, including deficient cerebral cuproenzyme function, oxidative stress, mitochondrial dysfunction, glutamate excitotoxicity, impaired axonal trafficking and synaptogenesis (Merner *et al.*, 2011; Fu *et al.*, 2014; Ahuja *et al.*, 2015).

The intracellular copper transport is sensitively regulated by two partly homologous P-type ATPase copper transporter proteins, ATP7A and ATP7B. ATP7A is a ubiquitously expressed protein residing in the *trans*-Golgi network of the cells. ATP7A guides copper to intracellular compartments, while in copper excess it relocates to the plasma membrane to pump out copper from the cells. Tissue specificity and trafficking differences of the ATP7B protein lead to Wilson's disease, a phenotypically different copper retention condition (Kaler, 2011; Telianidis *et al.*, 2013; Tümer, 2013; Fu *et al.*, 2014; Ahuja *et al.*, 2015). ATP7B mutations cause dystonia, ataxia, tremor and abnormal copper accumulation in the brain, liver and other organs (Coffey *et al.*, 2013).

6.5.2 Aims and hypothesis

We identified a novel ATP7A mutation in a patient presenting with unusual complex neurology symptoms, which showed an overlap between Menkes and Wilson's disease. I aimed to investigate the pathogenicity of this ATP7A variant by applying functional studies. I wanted to find a common mechanism in the pathology of the two different ATPase copper transporters, which could provide an explanation for the intermediate phenotype manifestation in the patient. The aim was to further extend the wide phenotypic spectrum related to the heterogeneous ATP7A mutations.

6.5.3 Methods

6.5.3.1 Patient inclusion

The 29-year-old male patient was selected from the hereditary motor neuropathy cohort (Family 29) (Chapter 5.4.4.1) for further investigations. His combined upper and lower motor neuron pathology and cerebellar symptoms segregated with a novel ATP7A mutation.

6.5.3.2 Next generation sequencing and segregation analysis

Whole-exome sequencing was applied on the patient's genomic DNA and potentially deleterious variants were identified using QIAGEN Ingenuity Variant Analysis. Protein prediction algorithms were used to analyse the *in silico* effects of amino-acid substitutions (*Chapter 3.2.1.2*).

I performed Sanger sequencing to validate putative variants in the patient and I carried out segregation studies in the larger family (*Chapter 3.2.2*). The coding regions were amplified by PCR using designed primers for the identified candidate *SACS*, *EXOSC3* and *ATP7A* genes.

6.5.3.3 Western blot

Patient fibroblasts were obtained by punch skin biopsy and stored in culture medium according to standard methods. I followed the cell culture protocol to grow fibroblasts from the patient and from healthy controls (*Chapter 3.2.3.1*). I extracted the protein from the fibroblast cells for immunoblot studies. I used anti-rabbit immunoglobulin G (IgG) primary antibodies against *EXOSC3* (Proteintech Group Inc., 15062-1-AP, 1:200) and *ATP7A* (Sigma, SAB2104637, 1:500) for overnight incubation at 4°C followed by secondary anti-rabbit Ig-HRP antibody incubation (*Chapter 3.2.3.2*).

6.5.4 Results

6.5.4.1 Detailed clinical phenotype and investigation findings

The 29-year-old male (**Figure 6.12, A**) patient was the second child in a non-consanguineous family. The X-linked Kennedy's disease, which ran in his father's side family, was discarded regarding the impossibility of a male to male transmission. He achieved age-appropriate developmental milestones and apart from having problems with his handwriting, he had no learning difficulties. Around the age of 9 he developed distal leg muscle atrophy and weakness with tiptoe walk abnormalities. He deteriorated slowly evolving progressive four limb spasticity, cerebellar symptoms and dystonia. He had a spastic and ataxic gait supported by two crutches until he became largely wheelchair bound around the age of 20. He had no history of mental problems and his cognition remained intact.

He had a normal, rather tall stature with no skeletal or joint deformities. There were no signs of skin and connective tissue changes and cardiovascular or hepatic abnormalities. His vision was normal, although horizontal nystagmus, visual field loss and mild optic atrophy were present. There was no evidence of Kaiser-Fleischer ring on slit lamp examination. He had a lower limb predominant spasticity accompanied by marked distal muscle weakness.

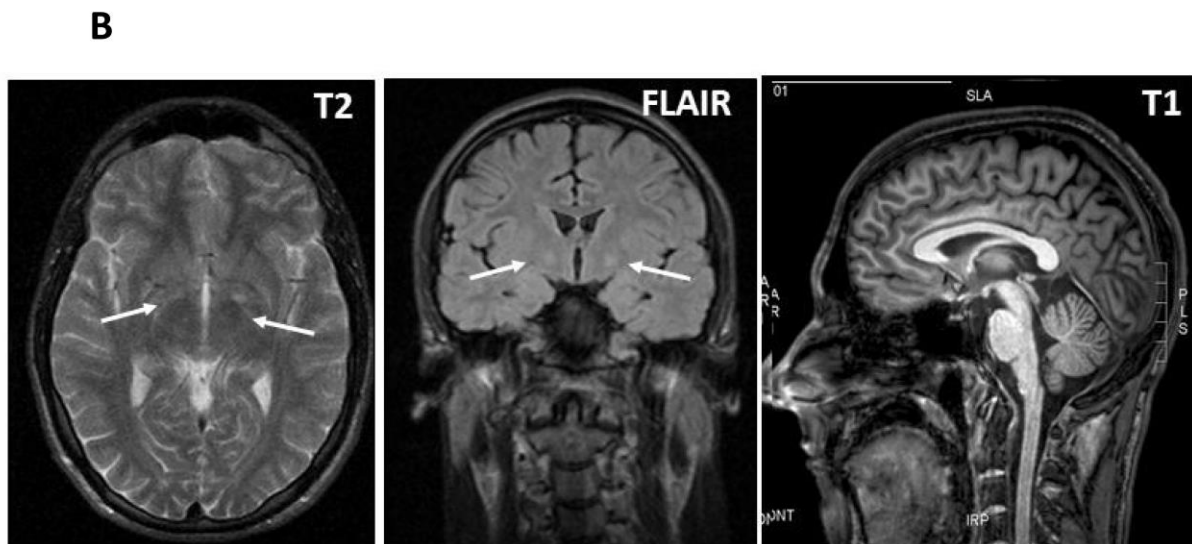


Figure 6.12 Clinical presentation and neuroimaging of the *ATP7A* mutant patient

A) Photo illustrations of the phenotype in the patient

B) Neuroimages indicate bilateral abnormal signal intensity in the globus pallidus (T2, FLAIR) and mild cerebellar atrophy (T1)

(Bansagi *et al.*, 2016)

The muscle power was decreased in hip flexion (MRC grade 4/5), thigh ab- and adduction (MRC grade 3/5) and ankle plantar- and dorsiflexion (MRC grade 2/5). He had bilateral ankle contractures but no other foot deformities. The muscle strength in his upper limbs was preserved despite the stiffness. Deep tendon reflexes were overall increased (4+) with clonus and pyramidal signs, even though the ankle jerks were absent. He had limb ataxia, dysmetria, intention tremor and cerebellar dysarthria. His Romberg's was positive impairing his spastic ataxic gait.

A wide range of investigations was performed over the disease course with inconclusive results. Routine laboratory examinations, including full blood count, blood smear, kidney, liver and thyroid function, serum glucose and electrolytes, iron, folic acid and vitamin metabolism were all tested in the normal range. There was no CK elevation and the autoimmune screen was negative. Metabolic studies (lactate, ammonia, AFP, amino acids, acyl-carnitine, free carnitin, organic acids and very long chain fatty acids) and leukocyte enzymes were normal. The serum caeruloplasmin level (0.19 g/l) and the level of copper in the serum and in the urine were repeatedly normal. The CSF protein was elevated (0.74g/l) with no accompanying oligoclonal bands or metabolic changes, albeit that neurotransmitter measurements were unavailable.

Electromyography showed an increased insertional activity with fibrillations and larger amplitude motor units. Nerve electric studies revealed reduced motor amplitudes in the peroneal and medial nerves beside intact motor conduction velocities, suggesting an axonal motor neuropathy. The muscle biopsy confirmed neurogenic changes.

An initial brain MRI scan at the age of 9 indicated high signal intensity symmetrically in the globi pallidi on T2-weighted images. Follow-up scans showed mild cerebellar atrophy and improved myelination. MRI spectroscopy detected no intracranial metabolic changes. A repeated scan aged 29 showed only mild residual signal changes in the globus pallidus on FLAIR sequences (**Figure 6.12, B**).

6.5.4.2 Identified genetic variants by next generation sequencing

Genetic tests performed before WES excluded spinocerebellar ataxia SCA1, 2, 3, 6, 7, Friedreich ataxia, Kennedy's disease and mitochondrial DNA mutations. Rare, potentially disease-causing variants were identified by filtering the WES data led by the main phenotype characteristics (**Table 6.7**). The compound heterozygous missense c.696T>A, p.Asn232Lys and c.T4076C>A, p.Met1359Thr *SACS* variants did not segregate appropriately in the family, as both variants were also carried by the healthy mother (**Figure 6.13**).

Gene	Position	Variant	SIFT	LRT	Polyphen2	Mutation taster
ATP7A	ChrX:77268482 G	c. 2279A>G, p.Tyr760Cys	D	D	D	D
SACS	Chr13:23913939 G	c. 4076T>C, p.Met1359Thr	B	B	D	N
SACS	Chr13:23930055 T	c. 696T>A, p.Asn232Lys	D	P	D	-
EXOSC3	Chr9:37784795 C	c. 247T>G, p.Cys83Gly	P	B	D	D

Table 6.7 Predicted deleterious variants filtered from WES data

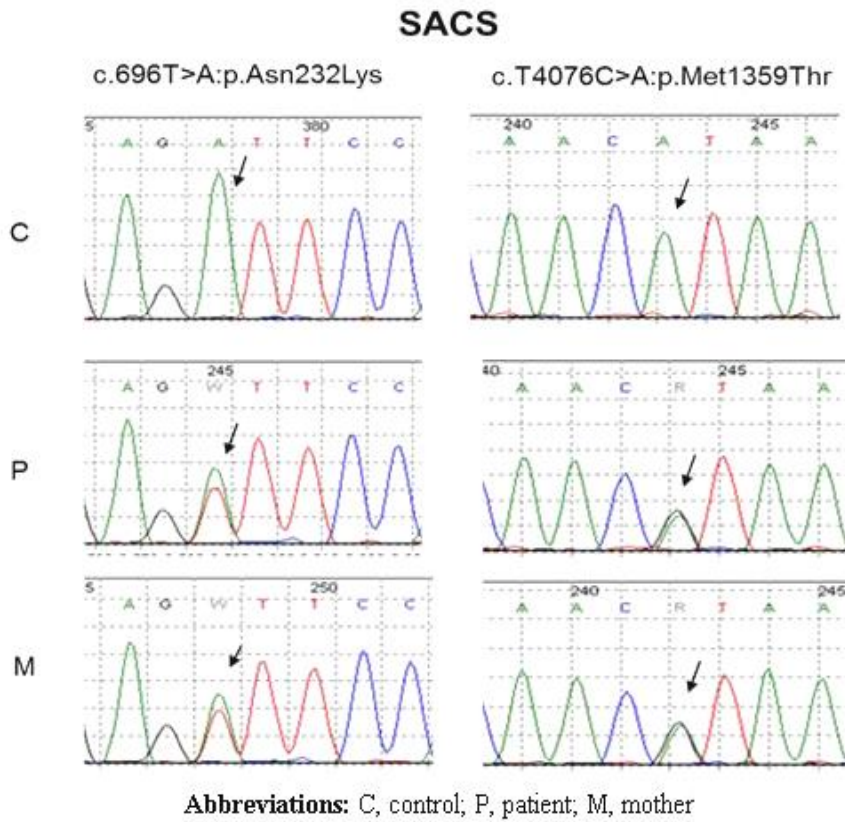


Figure 6.13 Segregation of SACS variants in the patient's family

The heterozygous c.247T>G, p.Cys83Gly *EXOSC3* variant was validated by Sanger sequencing, although *in silico* prediction tools suggested equivocal pathogenicity.

The novel hemizygous c.2279A>G, p.Tyr760Cys missense *ATP7A* mutation was confirmed by Sanger sequencing in the patient and by segregation analysis in the family (**Figure 6.14, A**). The sequence change was heterozygous in the patient's healthy mother and it was absent in the unaffected maternal male relatives. The amino acid change involves the highly conserved Tyr760 residue, which is located in the third trans-membrane domain of the carboxyl half of the *ATP7A* protein. The variant was rare (absent from in-house unrelated, ethnically matched controls, ExAC: 4 in 87766 heterozygous females, no hemizygous male) and was predicted highly deleterious by 5 different protein prediction tools (**Table 5.7. Table 5.8**)

There were no further peripheral neuropathy, motor neuron disease or ataxia-related known disease-causing genes detected by WES. Targeted filtering of the WES data could not find additional deleterious variants in the *ATP7B* and *ABC7B* genes.

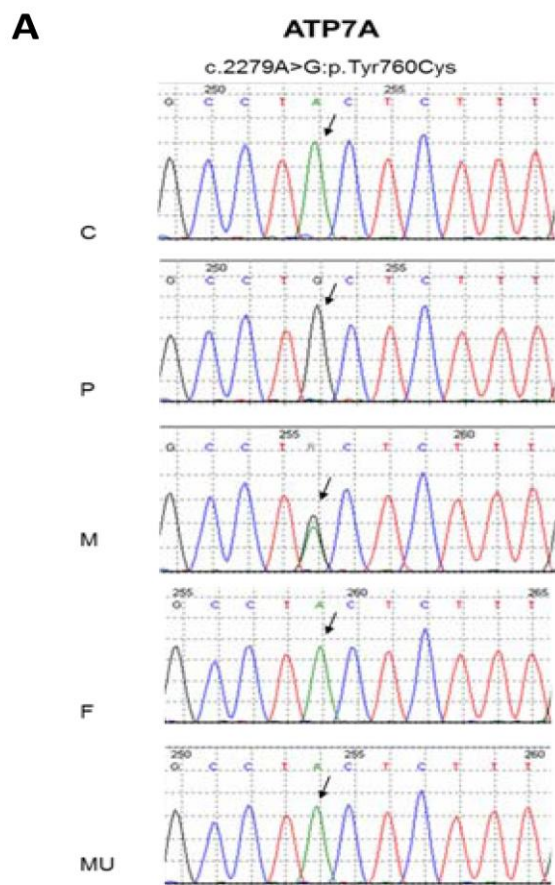
6.5.4.3 Immunoblot analysis in the patient fibroblasts

I performed Western blot analysis to examine whether there is a difference in the level of the *ATP7A* and *EXOSC3* protein in the patient fibroblasts. The immunoblotting detected normal amount of *EXOSC3*^{C83G} protein. The novel p.Tyr760Cys *ATP7A* mutation led to a severely reduced quantity of *ATP7A* protein in the patient fibroblasts when compared to normal control, supporting the pathogenicity (**Figure 6.14, B**).

6.5.5 Discussion

We investigated a male patient with a complex neuropathology, distinct from the previously described *ATP7A*-related phenotypes. We identified the novel hemizygous c.2279A>G, p.Tyr760Cys *ATP7A* mutation, which segregated appropriately with the disease in the family. Predicted deleterious consequences of the missense mutation were confirmed by immunoblotting, which detected a decreased level of the *ATP7A* protein in the patient fibroblasts (**Figure 6.14**).

A small amount of residual normal *ATP7A* protein has been described to cause atypical Menkes phenotypes (Møller, 2015). Furthermore, the neighbouring p.Ser761Pro *ATP7A* change has been linked with moderate Menkes disease (Tümer, 2013). However, the association of spastic tetraparesis, ataxia, dystonia and axonal motor neuropathy in our patient was remarkably different from the few atypical Menkes cases reported so far.



Abbreviations: C, control; P, patient; M, mother; F, father; MU, maternal uncle

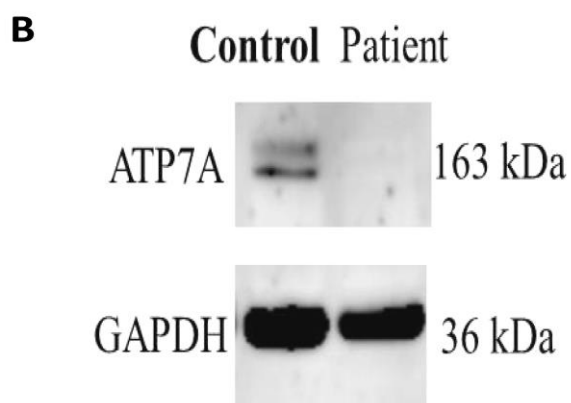


Figure 6.14 The identified novel *ATP7A* mutation in the patient

A) Segregation of the p.Tyr760Cys *ATP7A* variant confirmed by Sanger sequencing

B) Immunoblot analysis detected severely reduced *ATP7A* protein in the patient fibroblasts.

(Bansagi *et al.*, 2016)

White matter lesions and cerebellar atrophy are described neuroimaging findings in mild Menkes forms. However, the T2-weighted high signal intensity, indicating abnormal copper deposition in the globus pallidus is rather characteristic for the Wilson's disease. The latter is a copper retention disorder caused by autosomal-recessive *ATP7B* mutations. The disease presents with a low ceruloplasmin level and with hepatic and/or neurological defects, including variable combinations of dystonia, cerebellar and extrapyramidal symptoms. Previous studies reported patients with biochemical or clinical features of Wilson's disease, where *ATP7B* mutations could not be found (Coffey *et al.*, 2013). Furthermore, a distinct entity was suggested in patients with abnormal copper metabolism, involuntary movements and dysarthria, where *ATP7B* mutations were absent but *ATP7A* changes were not investigated (Tagawa *et al.*, 2001). *ATP7A* variants as modifiers have been investigated, but the so far examined polymorphisms had no impact on the Wilson's phenotype. A recent canine model carrying missense mutations in each *ATP7B* and *ATP7A* genes induced attenuation in the copper accumulation (Fieten *et al.*, 2016).

The two copper transporter ATPase proteins share common morphology features possessing class-specific heavy-metal-binding domains and type-specific transmembrane helices. They show significant sequence homology for residues involved in catalytic phosphorylation and copper transfer. Both proteins are involved in the translocation of copper through membranes, although they exert directionally different copper induced trafficking. A 38 amino acid segment in the third transmembrane domain of the *ATP7A*, encoded by exon 10, has been attributed to ensure the *trans* Golgi retention of the protein (Francis *et al.*, 1998). This region was mutated in the patient, which suggests that the disease mechanism may involve *ATP7A* dislocation to the endoplasmic reticulum with subsequent protein misfolding. Induced conformational changes may have led to aberrant protein-protein interactions and to a defected *ATP7A* trafficking, which caused the atypical phenotype of the patient (Ahuja *et al.*, 2015).

6.5.6 Conclusion

We presented the puzzling case of a patient with impaired copper metabolism, where the neurological features resembled Wilson's disease, but the molecular defect was found in the Menkes disease-related *ATP7A* gene. This underlines the large phenotypic variability of *ATP7A* mutations and highlights the overlap between copper metabolism disorders. Genetic screening toward *ATP7A* mutations in patients presenting with atypical Wilson's disease is recommended when *ATP7B* mutations could not be identified (Bansagi *et al.*, 2016).

Chapter 7. Investigation of novel genes and pathomechanisms in hereditary motor neuropathies

7.1 Presynaptic neuromuscular transmission defect caused by *SYT2* mutations

7.1.1 Literature review

The secretory pathway enables neurons to fuse organelles with the plasma membrane and release substances into the extracellular fluids. The process of exocytosis occurs in response to a signal, which is in many cases the rise of the cytosolic ionised Ca^{2+} . Influx of calcium into the presynaptic terminal during action potential leads to neurotransmitter release in a fast and synchronous manner. A well coordinated molecular framework is required for sensing Ca^{2+} and fusing transmitter-filled synaptic vesicles in a precise and timely coordinated manner (Gundersen and Umbach, 2013).

A standard model described that interactions among a trio of proteins, referred to as SNAREs (soluble, N-ethylmaleimide-sensitive factor attachment protein receptors), are the final common pathway for triggering membrane fusion during regulated exocytosis. The cycle of SNARE complex assembly and disassembly forces opposing membranes into close proximity but this seemed to be insufficient to mediate fusion. Additional levels of regulation are required to couple the calcium trigger with synaptic vesicle fusion and thereby allow for the temporal regulation of exocytosis. Members of the synaptotagmin family have been implicated as the major calcium sensors for the calcium-dependent exocytosis. However, the mechanism that couples Ca^{2+} -binding by synaptotagmin with vesicle fusion remains controversial (Paddock *et al.*, 2008; Gundersen and Umbach, 2013; Südhof, 2013).

According to the ‘allosteric’ model, the Ca^{2+} -binding to synaptotagmins is the key mechanism of calcium-triggered vesicle fusion, which leads to simultaneous activation of the SNARE complex and promotes presynaptic membrane-binding (Paddock *et al.*, 2008). As an alternative, the “dyad model” proposes that synaptotagmins initiate a rapid, Ca^{2+} -dependent exocytotic membrane fusion without direct involvement of the SNAREs, which only serve an essential docking function preceding the assembly of the fusion machinery (Paddock *et al.*, 2008; Kochubey *et al.*, 2011; Gundersen and Umbach, 2013; Südhof, 2013).

Synaptotagmins are evolutionarily conserved proteins with an N-terminal transmembrane region, a linker sequence and two C-terminal C2 domains. Among 14 synaptotagmins only three, SYT1, SYT2 and SYT9 have been shown to be critical for mediating fast synchronous synaptic vesicle exocytosis. Synaptotagmin-2 (SYT2) is abundantly expressed in caudal brain neurons and in spinal cord motoneurons, while it is restricted in populations of forebrain neurons. SYT2 shares the highest homology with SYT1 and both localise to synaptic vesicles. (Pang *et al.*, 2006; Young and Neher, 2009; Südhof, 2013)

Synaptotagmins possess two C2 domains, which are homologous to the calcium-binding domain of protein kinase C and contain Ca^{2+} - and phospholipid-binding motifs. Structural analyses showed that at the tip of the Ca^{2+} -binding loops of each C2 domain there are highly conserved basic residues. The key difference between the two C2 domains is that the C2B domain mediates Ca^{2+} -dependent interactions with phosphatidylinositol 4,5-bisphosphate and (SNARE) proteins and primes vesicles for immediate fusion after Ca^{2+} influx (Lin and Scheller, 2000; Paddock *et al.*, 2008).

SYT2 is postulated to function as a calcium sensor for fast, evoked neurotransmitter release by coupling action potential induced Ca^{2+} influx with vesicle fusion. Deleting the synaptotagmin gene strongly suppresses synaptic transmission in every species. SYT2 deficient mice are normal at birth but subsequently develop severe motor dysfunction and perish after 21 days. *SYT2* knockout reduces fast synchronous evoked release at neuromuscular junctions (NMJs), although slower asynchronous spontaneous miniature release events still persist. Specifically, Ca^{2+} -binding by the C2B domain is required to trigger fast synchronous vesicle fusion. Mutating two of the key Ca^{2+} -binding aspartate residues of the C2B domain in *Drosophila* decreased the Ca^{2+} evoked neurotransmitter release even more than it was seen in synaptotagmin null-mutant controls. However, high frequency of miniature excitatory junction potentials was recorded leading to an increased rate of spontaneous vesicle fusion events. This led to the idea that synaptotagmins act as a fusion clamp and suppress spontaneous release in addition to their primary role as a Ca^{2+} sensor. These effects were not rescued by wild type synaptotagmin, indicating dominant negative gain of function consequences of the mutation (Mackler *et al.*, 2002; Pang *et al.*, 2006; Kochubey *et al.*, 2011; Paddock *et al.*, 2011).

7.1.2 Aims and hypothesis

The novel combined manifestation of congenital non-progressive distal motor neuropathy and neuromuscular junction defect was aimed to be better characterised by extensive clinical investigations. The hypothesis was examined whether the *SYT2* mutation identified by WES in a large dominant family might be causative for the peripheral neuropathy with distinct mechanism of neurotransmission defect.

7.1.3 Methods

7.1.3.1 Patient inclusion

The patients from a large dominant pedigree were investigated in the inherited peripheral neuropathy clinic and were selected into the HMN cohort (*Family 4*) on the base of their unique motor neuropathy phenotype (*Chapter 5.4.2.1*).

7.1.3.2 Electrophysiology studies

All affected family members underwent detailed electrophysiology investigations, which were carried out by Dr Roger Whittaker at the Newcastle-upon-Tyne Hospitals NHS Trust (*Chapter 3.1.2*).

7.1.3.3 Experimental genetic methods

WES was undertaken in two affected family members. Variant calls were filtered against several databases and rare variants were defined with a minor allele frequency of less than 0.01. Putative disease-causing mutations along with their functional annotation were identified using ANNOVAR (*Chapter 3.2.1.2*). Identified pathogenic variants and the segregation in the family were tested and validated by Sanger sequencing (*Chapter 3.2.2*) with the assistance of Maria Lane, MSc in our research group.

7.1.4 Results

7.1.4.1 Clinical phenotype of patients diagnosed with *SYT2* mutation

Six affected members of the large dominant family (*Family 4*) presented with variably severe motor neuropathy symptoms (**Figure 7.1**) (**Table 7.1**).

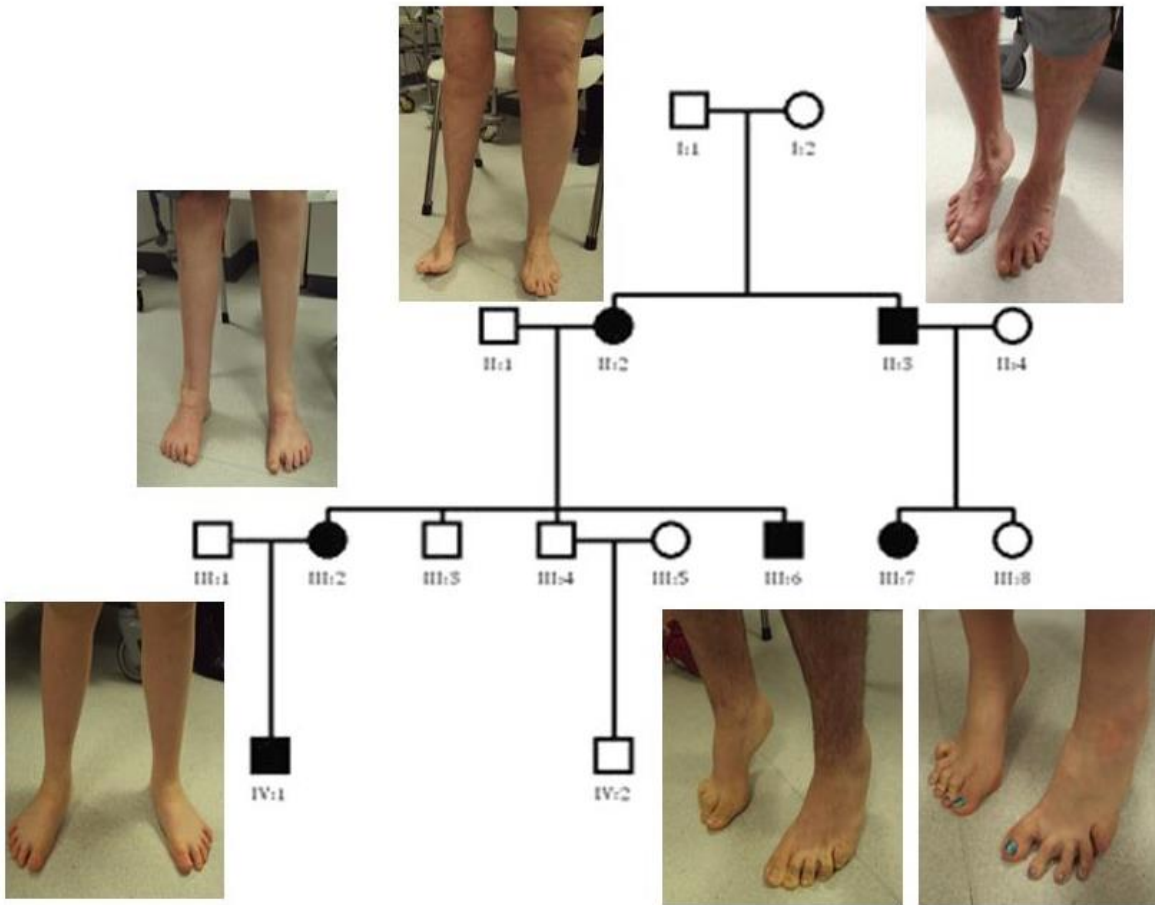


Figure 7.1 Family tree of the *SYT2* mutant family with the foot deformities

Patient	II.2	II.3	III.2	III.6	III.7	IV.1
Age (Yrs)	44	42	27	16	12	7
Gender	F	M	F	M	F	M
Feet/Toes	C,S	H	HA,H	C,H	C,H,S	P
Hip Dysplasia	+	-	+	-	+	-
LL Weakness	R>L R:D,P L:D	D	D	-	R>L D	-
LL Wasting	R:D,P L:D	D	D	-	-	-
LL Tendon Reflexes	A	A,F	A	A	A	A
UL Weakness	D	-	D	-	-	-
UL Tendon Reflexes	A	A	A	A	A	A
Delayed Milestones	-	-	-	-	-	+
Gait abnormalities	W, HW, TW	HW, TW	W, HW, TW	-	HW	W, HW
Orthotics	KO	-	AFO	-	-	FO
Orthopedic surgeries	K,F	A,T	F	-	-	-
Difficulty with Sports	+	-	+	+	-	+
Sensory loss (hands or feet)	+	-	+	-	-	+
CMAP amplitudes	Red.	Red.	Red.	N	Red.	ND
CMAP facilitation	-	+	+++	ND	++	ND
SNAP amplitudes	N	N	N	N	N	N
EMG	R	R	R	R	R	ND

Abbreviations: Female (F), Male (M), pes cavus (C), pes planus (P), high arch (HA), hammer toes (H), splayed toes (S), lower limb (LL), upper limb (UL), proximal (P), distal (D), right (R), left (L), absent (A), facilitation with exercise (F), not present (-), present (+), waddling gait (W), unable/impaired heel walk (HW), impaired toe walk (TW), knee orthotic (KO), ankle foot orthotics (AFO), foot orthotics (FO), knee surgery (K), foot surgery (F), ankle surgery (A), toe surgery (T), reduced (Red.), normal (N), not done (ND), compound muscle action potential (CMAP), 30-49% CMAP amplitude increase post 10 seconds of exercise (+), 50-99% CMAP ampl. increase post ex (++), >100% CMAP ampl. increase post exercise (+++), sensory nerve action potential (SNAP), needle electromyography (EMG), reinnervation (R)

Table 7.1 Clinical and electrophysiological features in the SYT2 patients

(modified from Herrmann *et al.*, 2014)

The index patient, a 27-year-old female (III/2), was investigated due to non-progressive motor difficulties dating back to her early childhood years. She was born with congenital hip dysplasia and foot abnormalities with pes cavus deformity. She struggled with physical activities at school and she underwent early foot surgeries, including tendon reconstruction and ankle arthrodesis. She had bilateral distal wasting in the legs and a pronounced weakness affecting the feet extensors and flexors (MRC grade 3/5) with limited ankle movement range. Her toes were splayed and clawed. She was walking with slapping gait, aided by orthotic support. Her proximal leg muscles and her upper limb muscles had preserved strength. Deep tendon reflexes were globally absent.

Her brother (III/6) had pes cavus deformities and clawed toes but no further motor symptoms at the age of 16, even though his deep tendon reflexes were absent.

Her 7-year-old son (IV/1) had loose hip joint at birth and his motor development was delayed with late walking at the age of 20 months. He had poor balance with frequent falls and he had attention difficulties at school. His muscle tone was generally low with hyperflexible joints. There was only a mild weakness in ankle dorsiflexion (MRC grade 4+/5) and he was unable to walk on his heels. Deep tendon reflexes were absent. He had mild flattening of his foot arches and he walked with a tumbling unsteady gait supported by orthotic shoes.

The 44-year-old mother of the index patient (II/2) presented with a childhood-onset stable distal leg weakness with a remarkable asymmetric wasting on the right side. The accompanying diagnosis of a localised morphea (linear atrophoderma of Moulin) caused lipodystrophy in her right thigh. She had walking difficulties with frequent falls and she complained of fatigability. Her foot deformities required several corrective surgical interventions and she also underwent reconstructive knee surgery. The neurology examination found reduced muscle bulk and power (MRC grade 4/5) in her entire right leg, while there was a mild wasting and weakness (MRC grade 4+/5) present in her distal left leg. She had bilateral pes cavus deformities and splayed toes. Her gait was waddling with bilateral foot drop and she was unable to perform tiptoe and heel walk. Her muscle strength in the upper limbs was normal apart from a very mild finger weakness. Deep tendon reflexes were absent and plantars were flexor.

Her father (I/1) was reported to have pes cavus foot deformities and her paternal uncle had hip problems requiring wheelchair support.

Her 42-year-old brother (II/3) had stable foot deformities since early childhood. His toes were pinned in his 20's and later he required Achilles tendotomy and arthrodesis on both sides. He remained physically active, although he was complaining of muscle pain and fatigable tiredness. He had distal muscle atrophy in his legs and reduced strength in ankle plantar- and dorsiflexion (MRC grade 4/5). He was unable to walk on his tiptoes and heels. Deep tendon reflexes were globally absent. There were no upper limb symptoms and sensory changes accompanied.

His daughter (III/7) was born with developmental hip dysplasia. She presented with bilateral foot deformities from early age. Aged 13 she had difficulties in sports and she complained of painful muscle fatigability. She had pronounced pes cavus deformities with splaying and clawing of her toes. She had only mild distal leg weakness in the right ankle dorsiflexion (MRC grade 4+/5) and she was unable to perform heel walk. Deep tendon reflexes were generally decreased.

7.1.4.2 Detailed electrophysiology findings in the *SYT2* family

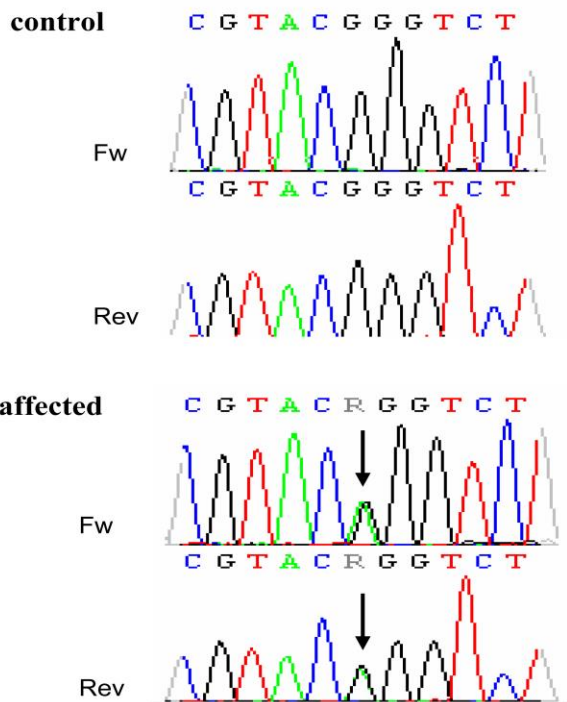
Electric nerve studies showed normal or low amplitude CMAPs in the patients' lower limbs with normal motor conduction velocities. Sensory responses were normal in all patients. On needle electromyography there was slight reinnervation of the distal leg muscles with a reduced number of motor units, resembling the pattern seen in peripheral developmental disorders and congenital multiplex arthrogryposis.

Repetitive nerve stimulation produced decremental responses, while there was a marked and sustained post-tetanic potentiation following brief maximum voluntary contraction, which was especially long lasting in patient III/2. The findings indicated presynaptic neuromuscular junction disorder with a variable degree of post-exercise increment of CMAP amplitude, as it will be discussed in detail in *Chapter 8.4.1.2 (Table 7.1)*.

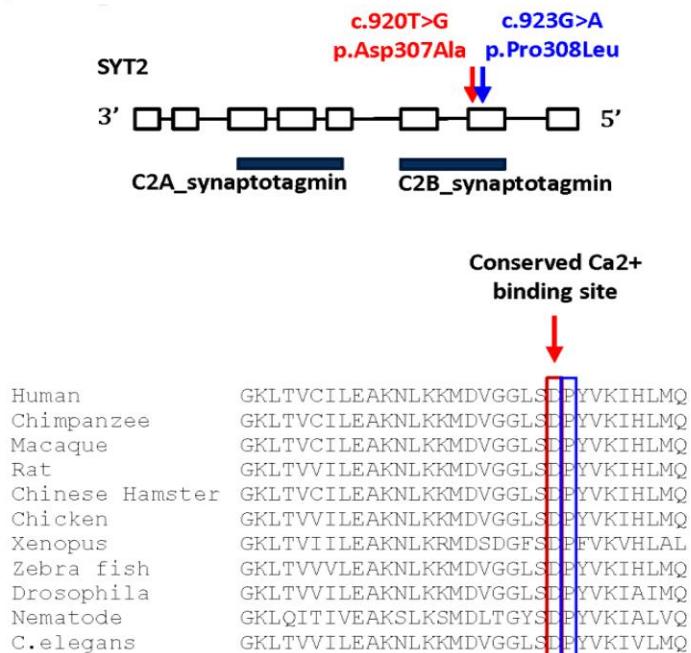
7.1.4.3 Identified *SYT2* mutation in the family

The heterozygous c.923G>A, p.Pro308Leu missense mutation in the *SYT2* gene was identified by WES in the family. The amino acid change involved a highly conserved residue across species in the Ca²⁺-binding aspartate motif of the SYT2 C2B domain. The mutation was predicted to be rare and deleterious and segregated appropriately with the disease in 6 affected members of the family (**Figure 7.2, A**).

A *SYT2*
c. 923G>A, p.Pro308Leu



B



C

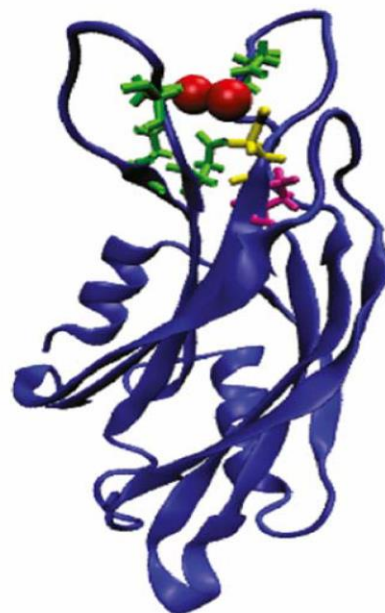


Figure 7.2 Identified *SYT2* mutation in the family

- A) Sanger sequencing of the c.923C>T, p.Pro308Leu *SYT2* mutation in affected family members and control
- B) Position of the described *SYT2* mutations and the conservation of the affected residues across species
- C) Stereoview of the Pro308 residues (magenta) modeled on the rat SYT1 C2B crystal structure. Essential Ca²⁺-binding residues indicated in green and Ca²⁺ ions in red.

7.1.5 Discussion

We identified 6 patients in a three-generation dominant family (*Family 4*) carrying the heterozygous missense c.923C>T, p.Pro308Leu *SYT2* mutation and presenting with congenital lower extremity predominant distal motor neuropathy and fatigable muscle weakness. Beside the common presentation of foot deformities, areflexia and distal leg weakness, some symptoms showed variable penetrance in the family, such as the accompanying congenital hip dysplasia. The asymmetric symptom presentation was also remarkable. All patients remained ambulant over the non-progressive disease course, although some of them required orthotic support. Electrophysiology studies detected a presynaptic neuromuscular transmission defect with dramatic post-stimuli facilitation resembling Lambert-Eaton myasthenic syndrome.

SYT2 is a synaptic vesicle protein that mediates calcium dependent neurotransmitter release functioning as a calcium sensor. The missense c.923C>T, p.Pro308Leu *SYT2* mutation alters a highly conserved residue in the calcium-binding motif of the C2B domain with predicted deleterious consequences. Simultaneously, an independent USA family with a similar clinical presentation was found to carry heterozygous missense *SYT2* mutation involving the Asp307 residue. Both affected residues are highly conserved among species and belong to the Ca²⁺-binding aspartate motif in the *SYT2* C2B domain (**Figure 7.2, B; C**).

Transgenic *Drosophila* containing wild-type and mutant synaptotagmin genes was generated to investigate whether disruption of these residues might lead to altered calcium-binding and dominant-negative impairment of exocytosis (Herrmann *et al.*, 2014). Null-mutant *Drosophila* neuromuscular junction lacked synchronous neurotransmitter release and displayed enhanced asynchronous release with elevated spontaneous fusion rates, which indicated a defected calcium-triggered neurotransmitter exocytosis. Synaptotagmins have been suggested to function as fusion clamps to prevent spontaneous exocytosis, in addition to their role as calcium sensors for evoked release, which likely explains why spontaneous fusion was increased in the *Drosophila* model. In order to mimic the dominant human condition, synaptic transmission was investigated in the presence of endogenous synaptotagmin protein, which resulted in a striking dosage-dependent dominant-negative disruption in the neuromuscular transmission (**Figure 7.3**). High-frequency stimulation revealed increased facilitation of evoked release in the mutant *Drosophila*, similarly to the observed compound muscle action potential (CMAP) amplitude enhancement after exercise in the *SYT2* mutated families (*Chapter 8.4.1.2*).

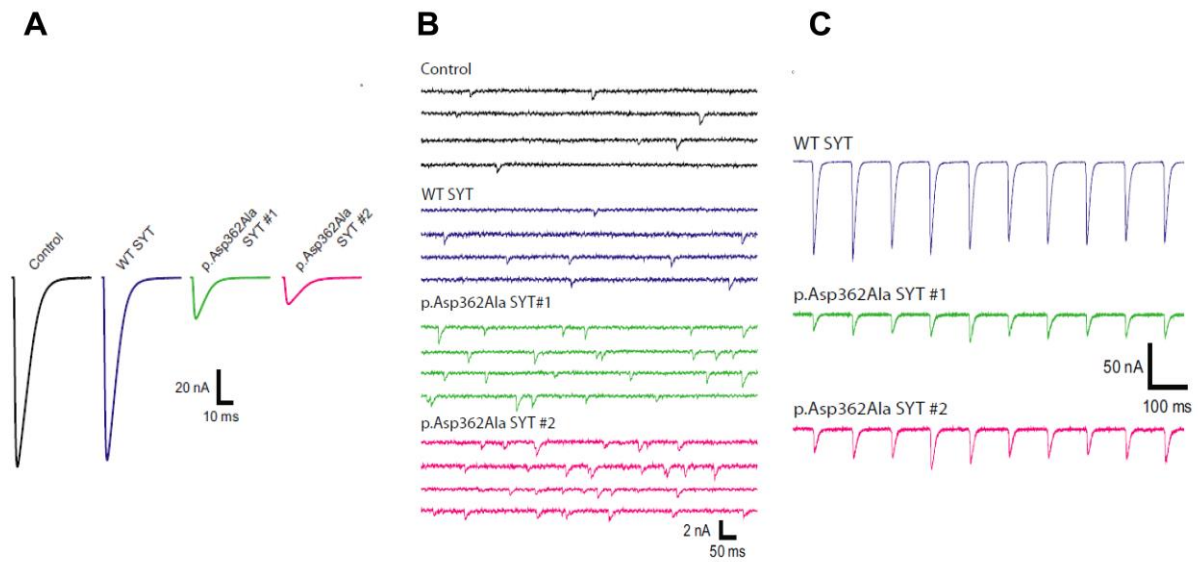


Figure 7.3 *Drosophila* p.Asp362Ala SYT2 disrupts neurotransmitter release

A) Action potential evoked synaptic release decreased in mutant neuromuscular junctions

B) Increased asynchronous neurotransmitter release and enhanced spontaneous fusion rate

C) High frequency stimulation revealed increased facilitation of evoked release.

(taken from Herrmann *et al.*, 2014)

We postulate that the mutant protein likely multimerizes with the endogenous protein pool and disrupts normal SYT2 properties, leading to the synaptic transmission defect. These are the first reported *SYT2* mutations linked to human disorders, where the consequent synaptic dysfunction resulted in the peripheral neuropathology. Analysis of additional families will be necessary to define the spectrum of human phenotypes present with *SYT2* mutations.

(Herrmann *et al.*, 2014)

7.1.6 Conclusion

We described a large dominant family with a novel SMA-LED phenotype characterised by a presynaptic neuromuscular junction defect. The identified novel mutations in the *SYT2* gene have been linked for the first time to a human disease. *SYT2* mutations should be considered in human peripheral motor nerve terminal defects and related phenotypes might range between distal hereditary motor neuropathy and presynaptic NMJ disorders. Furthermore, it raised the possibility that mutant presynaptic protein changes might underlie the mechanism in a subgroup of inherited peripheral neuropathies.

7.2 Altered intracellular signal transduction pathways

In peripheral nerve pathology altered intracellular signal transduction cascades have been recently more frequently described.

We identified pathogenic or likely causative variants in rare known disease genes (*PTEN*, *STAT5B*, *TBX5*), which have not yet been reported in association with peripheral neuropathy. The phenotype related to these gene mutations was a unique motor neuropathy accompanied by unusual features of demyelination with additional involvement of other organs (cardiac, skeletal, endocrinology and immunology defects, hamartoma tumour syndromes). The encoded proteins have been implicated in peripheral neural plasticity, axonal outgrowth and aberrant myelination.

The identification of mutations in non-CMT-related disease genes highlight, that motor neuropathy can be part of other rare genetic disorders. Thorough clinical examination may reveal some clues to identify these gene defects (**Figure 5.2**). More importantly, these overlapping phenotypes highlight basic biological pathways in peripheral nerves.

7.2.1 A novel motor neuropathy phenotype caused by mutation in the *PTEN* gene

7.2.1.1 Literature review

Mutated proteins containing phosphoinositide-binding domains have been implicated in genetically diverse CMT forms with abnormal myelin histopathology and ‘tomacula’ formation (CMT2M, *DNM2*; CMT4J, *FIG4*; CMT4H, *FGD4/frabin*; CMT4B1, *MTMR2*; CMT4B2, *MTMR13/SBF2*) (Goebbels *et al.*, 2012). Changes in phosphoinositide metabolism can have many possible cellular effects interfering with normal myelination, although it is not yet clear where these phosphoinositide pools are found and in what contexts they are functionally relevant to the maintenance of myelin. Abnormal phosphoinositide 3-kinase, (PI3-K) signalling might serve as a common final pathway in the pathology of these CMT forms.

Phosphatase and tensin homolog located on chromosome 10 (*PTEN*) is a tumour suppressor, mutated in sporadic cancers and in inherited tumour susceptibility conditions, *PTEN* hamartoma tumour syndrome (PHTS). Macrocephaly, autism spectrum disorder (ASD), ataxia, tremor and epilepsy have been reported in humans as *PTEN* associated neurology

deficits, while functional implications have been investigated in Parkinson's and Alzheimer's diseases (Kreis *et al.*, 2014; Spinelli *et al.*, 2015).

PTEN directly antagonises class I phosphoinositide 3-kinases (PI3-Ks) by converting phosphatidylinositol 3,4,5-trisphosphate (PIP3) into phosphatidylinositol 4,5-bisphosphate (PIP2). The negatively regulated PI3-K signalling exerts a brake on downstream effector pathways (Akt, m-TOR complexes) interfering with cellular processes such as cell growth, proliferation and survival (Kreis *et al.*, 2014; Leslie and Longy, 2016). Various protein mediated functions have been linked to the dynamic subcellular distribution of PTEN in neurons. Regulation of neuronal cell size, axonal outgrowth, synaptogenesis and neuromuscular assembly are PTEN controlled processes during neuronal development and during regeneration after injury. Dendritic localisation and secretion of PTEN-containing exosomes contribute to synaptic plasticity. There has been some controversy about the role PTEN plays in neuronal survival and apoptosis (Kreis *et al.*, 2014). Furthermore, PTEN mediated regulation of myelination has been modelled in the central and peripheral nerves of the mouse (Goebbels *et al.*, 2012).

7.2.1.2 Aims and hypothesis

I aimed to perform clinical and laboratory examinations to determine the genetic cause of a patient presenting with predominant multifocal motor neuropathy as part of a multisystem disorder. I investigated the hypothesis whether the identified *PTEN* mutation might provide an explanation for the unusual neuropathy phenotype.

7.2.1.3 Methods

7.2.1.3.1 Patient inclusion

A male patient presenting with an unusual combination of progressive motor neuropathy and facial, skeletal and skin deformities was selected for further clinical and genetic investigations from the HMN cohort (*Family 35*) in *Chapter 5.4.4.2*.

7.2.1.3.2 Electrophysiology studies

Electrophysiology investigations were carried out by Dr Roger Whittaker at the Newcastle-upon-Tyne Hospitals NHS Trust according to standard methods, described in *Chapter 3.1.2*.

7.2.1.3.3 Experimental genetic studies

WES was undertaken on the patient's genomic DNA. Identified variants were annotated and filtered against rare minor allele frequency in several databases (ExAC, NHLBI_ESP6500, cg69, InHouse281). Protein prediction and evolutionary sequence conservation algorithms (SIFT, Polyphen2, Mutation Taster, Mutation Assessor, LRT, FATHMM, VEST3, CADD, SiPhy29way) were used to analyse *in silico* effects of amino-acid substitutions (*Chapter 3.2.1.2*).

I performed Sanger sequencing and segregation analysis to validate putative variants. The following primers were used for PCR amplification of *PTEN* chr10:89692785T>C forward TGACCTATGCTACCAGTCCG and reverse AATCTAGGGCCTCTTGCGC (*Chapter 3.2.2*).

7.2.1.3.4 Western blot

Fibroblasts were obtained by skin biopsy from the patient and from healthy controls. I grew fibroblast cell line cultures and extracted protein from the fibroblast cells for immunoblotting according to standard methods described in *Chapter 3.2.3*.

I performed Western blots with two different anti-PTEN antibodies (monoclonal anti-PTEN antibody produced in mouse clone 2G9, WH0005728M1-SIGMA, 1:500 concentration, band runs at about ~ 37 kDa ; rabbit monoclonal anti-PTEN antibody, EPR9941-2 (ab170941), 1:1000 concentration, band runs at ~54 kDa).

7.2.1.3.5 Phosphatase enzyme assay

The enzyme activity assay was carried out by Dr Laura Swan, PhD in the Department of Cellular and Molecular Physiology at the Institute of Translational Medicine in Liverpool. Phosphoinositide phosphatase activity was measured using a chromogenic assay based on the malachite green method (Andrés-Pons *et al.*, 2007).

GST-PTEN fusion (PTEN fused with glutathione S-transferase tag) proteins were purified onto GSA beads (pierce) from BL21 E.coli in a purification buffer (100mM Tris HCl pH 7.4, 250mM NaCl, 10mM DTT plus turbonuclease and EDTA free protease inhibitor (Roche) in a reaction mixture of 25µl). The same buffer was used with 90µM diC8-PIP3 (Echelon) substrate at 37 °C for 1 hour. The reaction was stopped by adding 100µl of malachite green reagent per well and the absorbance was measured at 640nm. Absorbance values were calibrated against phosphate standards.

7.2.1.4 Results

7.2.1.4.1 Patient phenotype

The 29-year-old male (**Figure 7.4**) patient was the youngest of three siblings in a non-consanguineous family with no related medical history. His developmental milestones were globally delayed. He started walking aged 20 months, while his speech was acquired slowly after the age of 24 months. There were concerns about his constant dribbling and evolving squint. Since the age of 3 he presented with left sided facial asymmetry and muscle weakness in the contralateral upper and lower limbs. During early school years he developed discrepancy in his leg lengths jointly with progressive weakness, which led to frequent falls and traumatic injuries. Aged 10 he underwent tendon and limb reconstruction surgery and he was provided with orthotic shoe and regular physiotherapy support. Nerve conduction studies showed demyelination with conduction blocks suggesting an immune aetiology, but trials of steroid and IVIG therapy had no beneficial effects. During his adolescence, his chest and shoulders have become widely spread by multiple papulosus livid lesions, resembling hypertrophic keloids, which required dermatological excisions and systemic steroid treatment. His educational progress was poor and social interaction difficulties manifested, but later in life he managed to obtain part time employment.

Examined aged 29 he had macro- and scaphocephaly with left sided facial hemihypertrophy. The asymmetry involved both bony and soft facial tissues, resulting in oral cavity deformity and unilateral crowding of his teeth. He was tall with skeletal deformities, including scoliosis at upper thoracic level and disproportional shortening of his right leg. Multiple cranial nerve involvement was present. He had right-sided complete ophthalmoparesis with amblyopia. There was a lower motor neuron weakness on the right side of his face and left-sided tongue atrophy. He had pterygomandibular weakness and dysarthria with a nasal tone. Trapezius and periscapular muscles were weak and wasted. There was flaccid paresis, atrophy and areflexia in his left upper limb. He had proximal flexor weakness with preserved grip strength in his right arm. Motor neuron weakness in his lower limbs showed an opposite distribution. His right leg was globally atrophic with distal motor weakness and pes cavus deformities. His left lower limb had preserved muscle bulk and strength. His upper limb reflexes were absent. In his lower limbs deep tendon reflexes were brisk with left ankle clonus, even though ankle jerks were reduced. Sensation to pin prick and vibration was intact throughout. Routine laboratory and metabolic screening tests were repeatedly normal. Imaging studies, including brain and spinal MRI, left upper limb MRI and whole body CT were unremarkable.



Figure 7.4 Photo illustration of the clinical symptoms in the *PTEN* mutant patient

7.4.1.4.2 Electrophysiology findings

Nerve conduction studies showed highly abnormal motor responses with grossly abnormal motor conduction velocities. The motor amplitudes were markedly dispersed along with significant conduction block at multiple sites. Lower limb responses were remarkably asymmetrical being of grossly reduced amplitude in the right leg and normal in the left leg. Sensory responses were within acceptable limits throughout. Concentric needle electromyography showed neurogenic changes in the wasted limbs with no evidence of active denervation. The electrophysiology findings suggested a multifocal motor neuropathy with patchy conduction blocks.

7.2.1.4.3 Identified *PTEN* mutation by WES

Targeted genetic testing for *SMN1* and *C20orf54* was negative, such as the IPN gene panel assay. Analysing the WES data I found a heterozygous c.269T>C, p.Phe90Ser missense mutation in the *PTEN* gene, which has not yet been linked to neuropathy in humans. Sanger sequencing confirmed that the mutation presented *de novo* in the patient, since both his healthy parents were wild type. The sequence change involves a highly conserved residue within the catalytic site of the PTEN phosphatase domain and *in silico* tools predicted deleterious effects (**Figure 7.5, A**) (**Table 5.7, Table 5.8**).

7.2.1.4.4 Normal amount of PTEN protein detected by Western blot

Immunoblot analysis, which I carried out repeatedly by using two different anti-PTEN antibodies, confirmed that the amount of the PTEN protein was normal in the patient's fibroblast when compared to the healthy controls (**Figure 7.5, B**).

7.2.1.4.5 Phosphatase activity of the mutant protein

The phosphatase activity of the p.Phe90Ser *PTEN* mutant protein was investigated. Initially the enzyme function assay revealed impaired activity on phosphatidylinositol 3,4,5-trisphosphate (PIP3) as a substrate ($p < 0.05$) compared to wild type protein. However, this result was contradictory to the published data on the activity of p.Phe90Ser mutant protein on PIP3. Re-evaluation of the assay revealed that the mutant was more vulnerable to oxidation during the earlier test and the more oxidised p.Phe90Ser mutant did not act properly on any substrate. Repeated enzyme assay confirmed, that the p.Phe90Ser *PTEN* mutant protein acts just like the wild type on PIP3, but it was not completely functional against phosphatidylinositol 3,4-bisphosphate PI(3,4)P2. The partial lack of function against PI(3,4)P2 might provide an explanation for the disease mechanism (**Figure 7.5 C**).

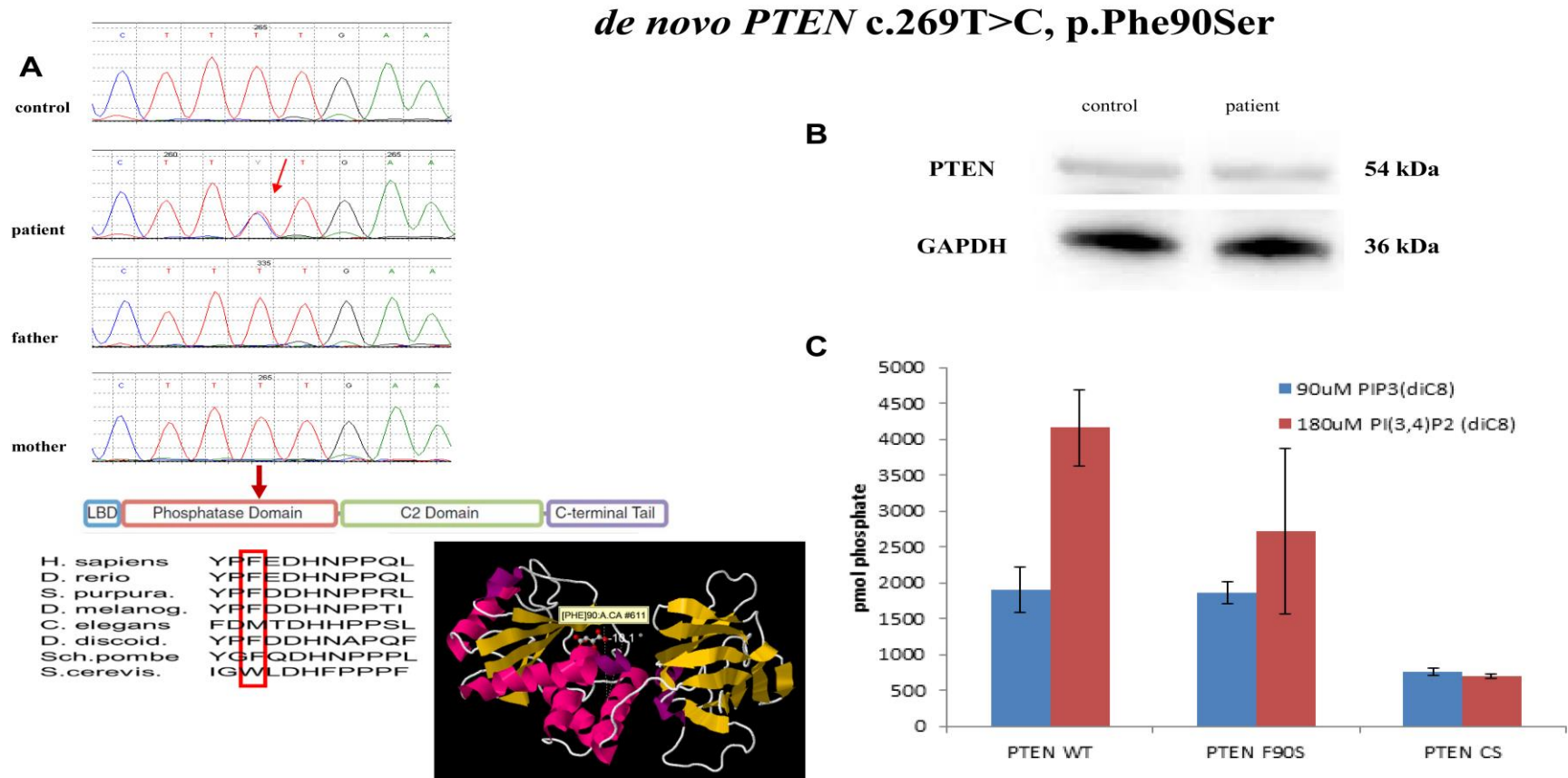


Figure 7.5 The identified *de novo* p.Phe90Ser *PTEN* mutation in the patient

A) Segregation analysis proved that the p.F90S *PTEN* mutation is carried *de novo* in the patient. The *PTEN* structure with its main domains and demonstration that the affected residue is conserved across species. Stereo view of the F90S residue, which locates near to the phosphatase active pocket.

B) Western blot revealed equal amount stable *PTEN* protein in the control and patient fibroblasts

C) The F90S *PTEN* mutation has impaired phosphatase activity on phosphatidylinositol 3,4-bisphosphate (PI(3,4)P2) as a substrate ($p < 0.05$)

7.2.1.5 Discussion

PTEN is the second most frequently mutated tumour suppressor gene, various human cancers have been linked to numerous somatic mutations (Zhou and Parada, 2009). Germline *PTEN* mutations cause various human conditions with poorly understood genotype-phenotype correlations (Spinelli *et al.*, 2015). Loss of function germline mutations have been predominantly described with inherited tumours and severe PHTS, while retained or partially lost *PTEN* activity has been found in neurodevelopmental disorders (Spinelli *et al.*, 2015).

We identified the novel c.269T>C, p.Phe90Ser *PTEN* mutation presenting *de novo* in a male patient with multifocal motor neuropathy and patchy demyelination (**Figure 7.4; Figure 7.5, A**). He showed symptoms overlapping with PHTS, including macrocephaly, hamartomatous skin lesions and autistic spectrum disorder but he did not fully meet the proposed criteria of the condition (Pilarski *et al.*, 2013). Extensive radiology evaluations could not detect evidence of malignant processes. His neurological deficits were dominated by progressive multifocal demyelinating motor neuropathy, a phenotype that has so far not been related to *PTEN* mutations in humans.

The *PTEN* sequence is largely invariable in the human population (1000 Genome Project found 54 SNVs with MAF<0.001) and the encoded protein possesses a strongly conserved amino acid structure among species. The cytosolic *PTEN* consists of 403 amino acids divided into an N-terminal phosphatase domain (7–185), a lipid-binding C2 domain (186–351) responsible for catalytic activity and a C-terminal tail (352–403) containing phosphorylation sites that regulate protein activity and stability. A 173 amino acids extension at the N-terminal contains a secretion signal for exosome mediated *PTEN* secretion (Leslie and Longy, 2016). The p.Phe90Ser missense change identified in our patient is located within the WPD-loop, which is equally near to the phosphatase active pocket and to the membrane-binding regulatory interface of the *PTEN* C2 domain (**Figure 7.5, A**). Most of the mutated WPD residues have been considered not to influence or only partially affect the catalytic activity of *PTEN* (Rodriguez-Escudero *et al.*, 2011). The cancer associated (glioma, endometrium) somatic p.Phe90Ser *PTEN* mutation has been found to have normal phosphatase activity but it was unable to bind membrane phospholipids and recruit *PTEN* for PIP3 signalling (Nguyen *et al.*, 2015). The germline p.Phe90Ser *PTEN* mutation in our patient did not interfere with the protein production and showed wild type phosphatase activity on PIP3. However, the mutant protein had only partial catalytic activity against PI(3,4)P₂, which has a signalling function in many cases similar to PIP3 (**Figure 7.5, B; C**).

Accumulating evidence has demonstrated that PI(3,4)P2 regulates a variety of cellular processes, including neuronal dynamics, clathrin-mediated endocytosis and cell migration (Li and Marshall, 2015). It is an important signalling molecule involved in the coordination of several specific membrane and cytoskeletal responses (Hawkins and Stephens, 2016). A recent report showed interaction between RAB7, and unveiled a novel role of PTEN, as a modulator of late endocytic maturation and trafficking (Shinde and Maddika, 2016).

A similar neuropathology to that of our patient has been described in a mouse model. Targeted mutation of *PTEN* in Schwann cells caused a progressive peripheral neuropathy with focal hypermyelination, myelin outfoldings and ‘tomacula’ formation. The dysfunctional regulation of local PIP3 level in myelin membranes and the autonomous Schwann cells defect due to constitutive Akt/mTOR downstream hyperactivation have been implicated in the *PTEN* mutant pathology (Goebbels *et al.*, 2012). Furthermore, a transheterozygous *PTEN* mutant *Drosophila* developed progressive motor function loss with defects in climbing and flight ability (Mensah *et al.*, 2015).

The expression of PTEN requires sensitive regulations at all levels and mutations inducing even minor structural changes may impair various functions of the protein. Phosphorylation-dependent conformational changes, post-translational modifications and protein interactions have been found necessary in membrane-binding and in forming nuclear and internal organelle (mitochondria, ER) PTEN pools (Kreis *et al.*, 2014). These might explain why functionally selective mutations result in diverse *PTEN*-associated phenotypes (Leslie and Longy, 2016).

7.2.1.6 Conclusion

We detected the *de novo* p.Phe90Ser *PTEN* mutation in a patient presenting with patchy motor neuropathy with focal demyelination, hamartoma-like skin lesions and autism spectrum disorder. PTEN is a lipid phosphatase, which inhibits PI3-K signalling, a pathway that is known to be impaired in several forms of peripheral nerve demyelination (*FIG4*, *FGD4*, *MTMR2*, *MTMR13/SBF2*). PTEN has been implicated in peripheral neural plasticity, axonal outgrowth and hypermyelination. Experimental *PTEN* suppression in mice resulted in progressive peripheral neuropathy with ‘tomacula’ formation and myelin outfoldings. We suggested that the p.Phe90Ser *PTEN* variant, identified in our patient should be considered as a novel motor neuropathy-related gene mutation.

7.2.2 Homozygous *STAT5B* mutations related to a novel neuromuscular phenotype

7.2.2.1 Literature review

The signal transducer and activator of transcription *STAT5B* is an evolutionarily conserved protein that regulates a variety of biological responses, such as cell proliferation, growth, immune surveillance and tumour suppression (Fang *et al.*, 2006).

Homozygous *STAT5B* mutations have been reported only in a few patients worldwide presenting with short stature and facial dysmorphism, resembling Laron syndrome, a growth hormone (GH) insensitivity condition. The implied pathomechanism affects the growth hormone receptor (GHR) signalling cascade (GH-GHR-*STAT5B*-IGFI). In the absence of *STAT5B*, the ability of GH to induce the expression of insulin-like growth factor-1 (IGF-1) is almost completely diminished (Kofoed *et al.*, 2003; Hwa *et al.*, 2005). An immune dysregulation (interleukin-2 signalling defect at the T cell level) result in severe recurrent infections and complex autoimmune disorders in some patients, although it is not an obligatorily associated feature in *STAT5B* defect (Bernasconi *et al.*, 2006; Vidarsdottir *et al.*, 2006; Pugliese-Pires *et al.*, 2010; Casanova *et al.*, 2012; Scaglia *et al.*, 2012).

7.2.2.2 Aims and hypothesis

I aimed to perform genetic studies to identify the molecular cause of the motor neuropathy in combination with short stature and other neuromuscular symptoms in a pair of siblings of consanguineous origin. I examined the hypothesis, whether the impaired intracellular signal transduction due to the identified homozygous *STAT5B* mutations might be the mechanism in the development of peripheral nerve pathology.

7.2.2.3 Methods

7.2.2.3.1 Patient inclusion

A pair of siblings was selected for further clinical and genetic evaluations from the HMN cohort due to their unusual presentation of motor neuropathy as part of a more complex phenotype (*Family 34*) (*Chapter 5.4.4.2*).

7.2.2.3.2 Electrophysiology

Electric nerve studies and electromyography were carried out according to standard methods described in *Chapter 3.1.2*.

7.2.2.3.3 Experimental genetic studies

WES was undertaken in the affected siblings. I filtered the WES data against several databases to define rare homozygous variants with a MAF < 0.01. Putative disease-causing mutations along with their functional annotation were identified using ANNOVAR (*Chapter 3.2.1.2*). I confirmed the putative pathogenic variants by Sanger sequencing. The following primers were used for the PCR amplification of *STAT5B* chr17:40370786T>G (forward AGAGGGGAGTGAGATAACACAGA, reverse CTCCTGTGTACGTCTCTAATTCTGG). (*Chapter 3.2.2*)

7.2.2.4 Results

7.2.2.4.1 Patient phenotype

We examined a 14-year-old male and 16-year-old female sibling pair of Roma origin. Consanguinity in the family could not be excluded. Their parents and their two further siblings were healthy, suggesting an autosomal-recessive inheritance. Both children were apparently short statured in addition to that they shared distinctive neuromuscular features. They had marked muscle weakness in their lower extremities with reduced deep tendon reflexes. Their gait was impaired by frequent falls. Dysmorphic facial features, bilateral ptosis, external ophthalmoplegia and scapular winging were found in association with the condition (**Figure 7.6, A**). The male sibling has been also investigated for cardiac arrhythmia. The serum CK level was normal and acetylcholine receptor antibodies could not be detected. Basal and stimulated growth hormone levels and basal IGF-1 levels were in the normal range.

7.2.2.4.2 Electrophysiology findings

Nerve conduction studies showed motor neuropathy with reduced motor amplitudes and conduction velocities but preserved sensory responses. Electromyography revealed neurogenic changes. Repetitive nerve stimulation did not reveal neuromuscular defect.

7.2.2.4.3 Identified *STAT5B* mutations

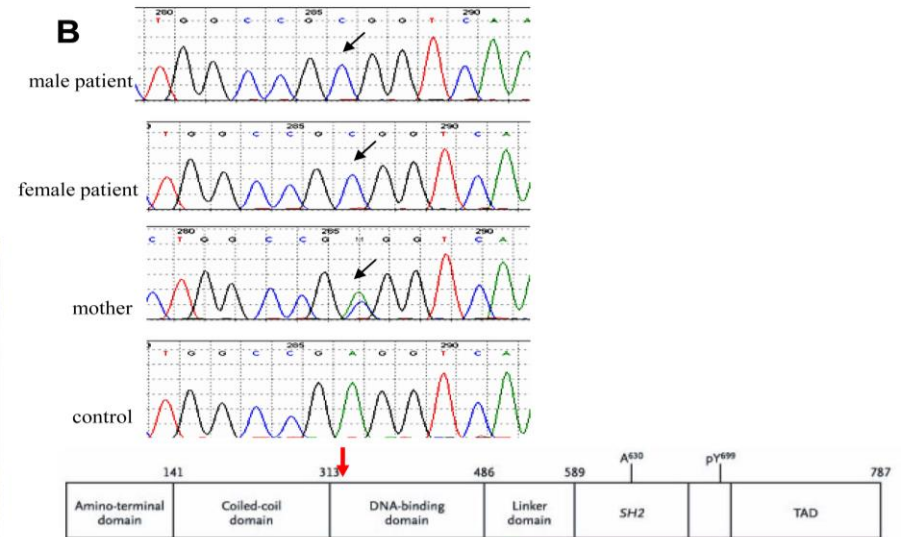
There was no mutation identified by testing for common neuropathy-related disease genes. The homozygous c.944T>G, p.Glu315Ala missense *STAT5B* mutations were identified on WES, which were predicted to be rare (MAF<0.01, ExAC:0.0027) and deleterious by *in silico* prediction tools (**Table 5.7****Table 5.8**). The mutation segregated appropriately with the disease in the family. The mutation was homozygous in the affected siblings, while the healthy mother and one of their siblings were heterozygous carriers (**Figure 7.6, B**).

STAT5B c.944T>G, p.Glu315Ala

A



B



H. Sapiens	QQLPIPGPVEEMLAEY	NATITDI
B. Taurus	QQLPIPGPVEEMLAEY	NATITDI
R. Norvegicus	QQLPIPGPVEEMLAEY	NATITDI
M. Mulatta	QQLPIPGPVEEMLAEY	NATITDI
D. Reiro	QQLPIPGPTEEL	LTE ₃₁₅ NAIVTDI
M. Musculus	QQLPIPGPVEEMLAEY	NATITDI

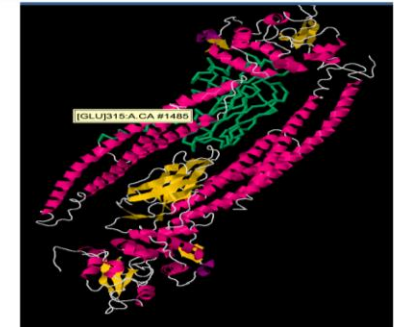


Figure 7.6 The identified p.Glu315Ala *STAT5B* mutation in the family

A) Photo illustration of the phenotype in the patients

B) Sanger sequencing of the c.944T>G, pGlu315Ala *STAT5B* mutation in the family. Position of the identified *STAT5B* mutation and the conservation of the affected residue across species. Stereoview of the Glu315 residue modelled on human *STAT5A* crystal structure, which shows 95% homology with *STAT5B*

7.2.2.5 Discussion

In response to various cytokine stimuli STAT5B translocates to the nucleus and acts as a transcriptional regulator of targeted genes. Ligand-binding of cytokine receptors activates the Janus kinase (JAK) pathway induced phosphorylation, which recruits and dimerizes STAT5B through its SH2 domain. The phosphorylation of conserved tyrosine residues in the C-terminal is essential for STAT5B dimerization and for cytokine dependent nuclear transport. In contrast, nuclear transport of the non-phosphorylated monomer STAT5B is linked to its N-terminal coiled coil domain. The N-terminal coiled coil and DNA-binding domains play a key role in cytokine independent nuclear translocation of STAT5B and in the constitutive expression of target genes (Nakajima *et al.*, 2001; Zeng *et al.*, 2002; Fang *et al.*, 2006) (**Figure 7.7**). Therefore, an intact protein structure, including the main domains and the phosphorylation residues are essential for normal STAT5B functioning. All of the so far described mutations (nonsense/frameshift mutations in the N-terminal coiled coil domain and a frameshift premature truncating mutation in the DNA-binding domain) led to the complete loss of the essential tyrosine residues and the SH2 domain, making the STAT5B biologically inactive (Kofoed *et al.*, 2003; Hwa *et al.*, 2005; Bernasconi *et al.*, 2006; Vidarsdottir *et al.*, 2006).

We found that the previously not yet described missense c.944T>G, p.Glu315Ala *STAT5B* mutation was homozygous in the siblings and caused combined presentation of postnatal growth retardation and neuromuscular impairment. The identified amino acid change affects a conserved residue in the N-terminal coiled coil domain of the STAT5B, which is a key region in transcriptional regulation (**Figure 7.6**). Mutations within this region may contribute to transcriptional enhancement through protein-protein interactions (Nakajima *et al.*, 2001).

IGF-1 is suggested to be a potent survival factor for neuronal cells by inducing cyclin D1 expression. IGF-1 stimulated upregulation of cyclin D1 production is likely to be mediated by STAT5B (**Figure 7.7**). Cyclin D1 expression correlates with Schwann cell function in a rat model of demyelinating neuropathy. Mutations in the early growth response gene, *EGR2* have been associated with autosomal-dominant peripheral neuropathy. *EGR2* induces nuclear expression of cyclin D1 leading to aberrant Schwann cell functions (Nakajima *et al.*, 2001; Atanasoski *et al.*, 2002; Kalita *et al.*, 2013).

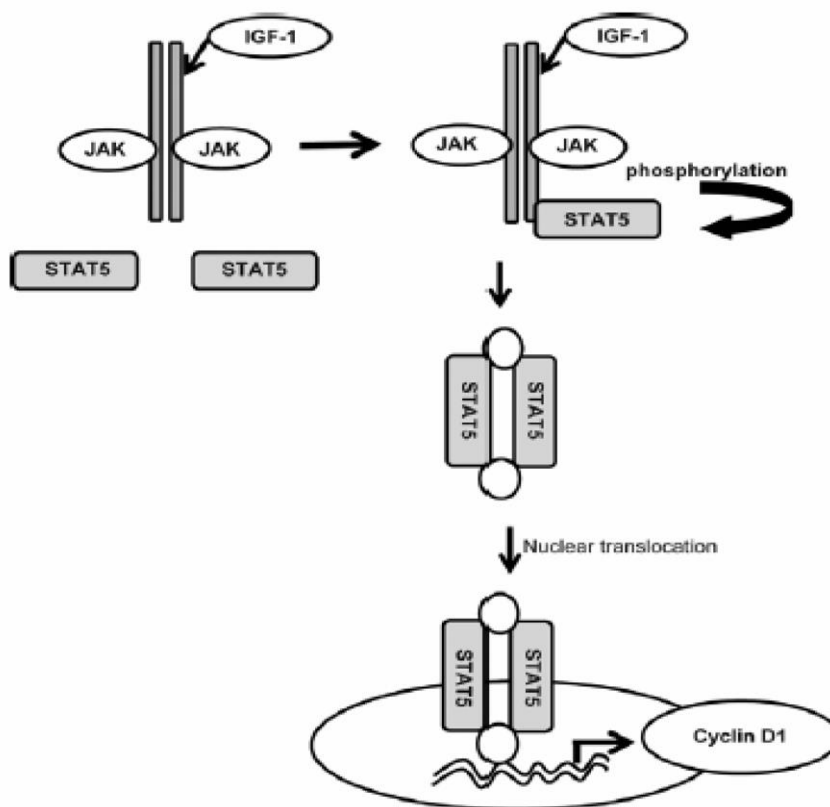
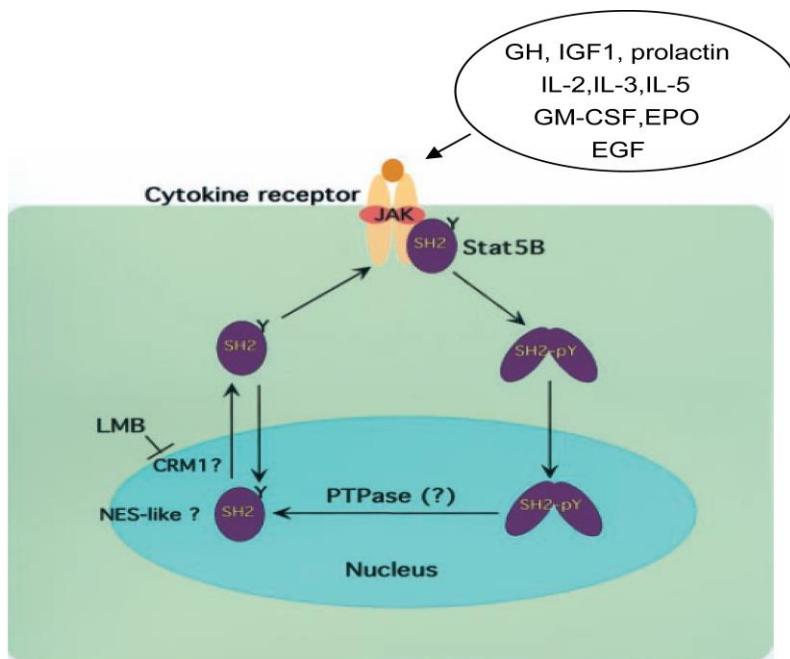


Figure 7.7 Pathomechanisms of STAT5B

Ligand association with cytokine receptors activates JAK induced phosphorylation which recruits and dimerises STAT5B through the SH2 domain. Phosphorylation of conserved tyrosine residue in the C-terminal is essential for STAT5B dimerisation and for cytokine-dependent nuclear transport. Cytokine-independent, nonphosphorylated monomeric STAT5B shuttle is related to the N-terminal coiled coil domain. IGF1 stimulated upregulation of cyclin D1 mediated by STAT5B signalling (taken from Zeng *et al.*, 2002; Kalita *et al.*, 2013)

Furthermore, the insulin/IGF signalling cascade (IIS) acts through the PI3-kinase (PI3-K) /AKT kinase pathway, involving the downstream effector mTORC1 (mechanistic Target of Rapamycin Complex 1) and plays evolutionarily conserved regulatory roles in homeostasis, cell growth regulation, autophagy and longevity. Disruption of the IIS/mTORC1 pathway has been implicated in neurodegenerative disorders and mutations in the IIS antagonist PTEN have been found in a mouse model of neuropathy and in a flightless *Drosophila* model (Chapter 7.2.1.5) (Goebbels *et al.*, 2012; Mensah *et al.*, 2015; Essers *et al.*, 2016).

7.2.2.6 Conclusion

We extended the spectrum of the *STAT5B*-related phenotypes by presenting the combined manifestation of recessively inherited growth hormone insensitivity and impaired peripheral nerve function in the investigated family. The novel c.944T>G, p.Glu315Ala *STAT5B* mutation affects an evolutionary conserved residue in the N-terminal coiled coil domain of *STAT5B*, which has a key transcriptional function both through protein-protein interactions and by ensuring *STAT5B* monomer shuttling between the nucleus and cytoplasm. Impaired *STAT5B* signalling may lead to an aberrant peripheral myelination process through cyclin D1 overexpression and may have an impact on the neuronal growth and differentiation through IIS/mTORC1 signalling cascade. Further studies will be required to confirm the precise mechanism of the *STAT5B*-related neuromuscular pathology.

7.2.3 Motor neuropathy in Holt-Oram syndrome caused by *TBX5* mutation

7.2.3.1 Literature review

T-box 5 gene (*TBX5*) belongs to the evolutionarily conserved T-box family of transcription factor genes (McDermott *et al.*, 2005). It encodes a transcription factor and alternative splicing regulator, which is an essential element in transcriptional regulatory cascades (Heinritz *et al.*, 2005; Granados-Riveron *et al.*, 2012). T-box proteins are essential in cell type specification and morphogenesis. They play an important role during the embryonic development of cardiomyocytes and morphogenesis of the upper limb.

TBX5 is located in the 12q24.1 chromosomal region and consists of 9 exons encoding a 518 amino acid length protein (Heinritz *et al.*, 2005; Mace *et al.*, 2014; Dreßen *et al.*, 2016). Members of the T-box family possess a highly conserved DNA-binding motif, which is involved in protein–protein interactions. A transactivation domain at the C-terminal of the protein mediates the dynamic shuttling of *TBX5* between the nucleus and the cytoplasm. The nuclear availability of *TBX5* determines its transcriptional activity (Al-Qattan and Abou Al-Shaar, 2015).

Mutations in many of the T-box genes are associated with human developmental disorders. Germline *TBX5* mutations cause Holt-Oram syndrome (HOS), while somatic mutations have been described in congenital heart defects (Heinritz *et al.*, 2005; Dreßen *et al.*, 2016). The clinical criteria of HOS are the presentation of radial longitudinal upper limb deficiency and/or congenital heart disease, either as a structural heart malformation or as a cardiac conduction disease. It is a rare, autosomal-dominant syndrome with full penetrance and variable expressivity. The skeletal abnormalities range from subtle to severe defects of the upper limb, while chest wall, vertebral and craniofacial anomalies may accompany the condition (McDermott *et al.*, 2005; Dias *et al.*, 2007; Goldfarb and Wall, 2014; Al-Qattan and Abou Al-Shaar, 2015).

7.2.3.2 Aims and hypothesis

I aimed to investigate the molecular cause of the progressive motor neuropathy in a patient, who presented with unusual neurological and electrophysiological findings. I examined the hypothesis whether the identified mutation in the *TBX5* gene might provide an explanation for the phenotype.

7.2.3.3 Methods

7.2.3.3.1 Patient inclusion

The index patient of (*Family 33*) presented with unusual skeletal anomalies in addition to the distal motor neuropathy and was selected from the HMN cohort for further research-based genetic studies (*Chapter 5.4.4.2*).

7.2.3.3.2 Electrophysiology

Nerve conduction studies completed with repetitive nerve stimulation and electromyography, including single fibre testing, was performed by Dr Roger Whittaker at the Newcastle-upon-Tyne Hospitals NHS Trust (*Chapter 3.1.2*).

7.2.3.3.3 Experimental genetic studies

WES was carried out on the patient's genomic DNA. I analysed the exome data, led by the clinical features of the patient (*Chapter 3.2.1.2*). I performed Sanger sequencing and segregation studies in the family (*Chapter 3.2.2*).

The following primers were designed to PCR amplify *TBX5* chr12:114837349C>A (forward: CTGGAAAACCGGAGCTAATTGT and reverse: TCCCTTAAAATGGATGGAGGCT).

7.2.3.4 Results

7.2.3.4.1 Patient phenotype

The 19-year-old patient (*Family 33*) (**Figure 7.8, A**) showed an unusual condition of distal lower limb weakness with upper motor neuron signs and abnormal shoulder anatomy with periscapular muscle weakness. His development was delayed with late walking at 2 years of age and he had frequent falls. He had flat feet and knocked knees and he developed sloping, forward turning shoulders with upper thoracic kyphosis. His distal motor wasting and weakness was slowly progressive in his legs and his toes were clawing. He complained of muscle aches and increasing fatigability. Later he noted that his hands became weak with mild sensory impairment. He was also diagnosed with attention deficit problems and gynecomastia in his teens, while rapid weight gain with stria formation appeared later.

His physical examination revealed bilateral sloping and forward positioned shoulder girdles with limited movement range. He had bilateral suprascapular muscle atrophy with prominent scapular winging. The muscle strength was preserved in his arms but there was a mild hand and finger weakness (MRC grade 4/5). The weakness in the distal lower limb muscles was more prominent (MRC grade 3/5).

A



B



Figure 7.8 Photo illustration of the phenotype with the identified *TBX5* mutation

- A) The proband showing skeletal deformities and motor neuropathy
- B) His mother and sister demonstrate similar shoulder girdle abnormality

He had wasted legs with unusual foot shapes and clawed toes. His lower limb reflexes were increased along with pyramidal signs. Sensory modalities were not prominently diminished.

Some of his family members presented with the same shoulder girdle anomaly and with a somewhat similar neuromuscular manifestation. His mother suffered from lower limb and back pain, supposedly caused by degenerative vertebral changes, impairing her ambulatory skills. She was fatigable with brisk lower limb reflexes but she had no obvious signs of a concomitant peripheral neuropathy. His sister was in her teens and she had difficulties in physical exercise at school. She complained of constant exhaustion experiencing excessive muscle tiredness, although she was also treated for depression (**Figure 7.8, B**).

7.2.3.4.2 Electrophysiology findings

Nerve conduction studies of the index patient showed a rather unusual pattern. In his upper limbs the sensory amplitudes were markedly reduced, whereas the motor amplitudes were normal. However, in the lower limbs the pattern was reversed with significantly reduced amplitude motor responses and relatively preserved sensory responses. Conduction velocities were moderately reduced with corresponding F-wave prolongation to an extent not readily explainable purely on the basis of the axonal loss. There was no temporal dispersion or conduction block suggesting acquired origin. Concentric needle electromyography revealed pronounced but inactive neurogenic changes. Repetitive nerve stimulation produced no increment or decrement. In contrast, SFEMG recorded increased jitter in 76% of 21 pairs examined, with blocking in 14% of these. There was a clear evidence of a significant defect of neuromuscular transition. However, it has remained uncertain if this was secondary to the immature neuromuscular junctions formed during re-innervation or it was rather a primary defect.

7.2.3.4.3 Identified *TBX5* mutation

Genetic screening for neuropathy disease genes and for facio-scapulo-humeral muscle dystrophy (FSHD) was negative. I found the pathogenic c.331G>T, p.Asp111Tyr *TBX5* mutation in his WES data, which was carried by the patient, as well as his mother and sister in a heterozygous form (**Figure 7.9**).

The same heterozygous missense change has been previously reported causing upper limb and skeletal deformities and developmental heart malformations (Granados-Riveron *et al.*, 2012).

TBX5

c.331G>T, p.Asp111Tyr

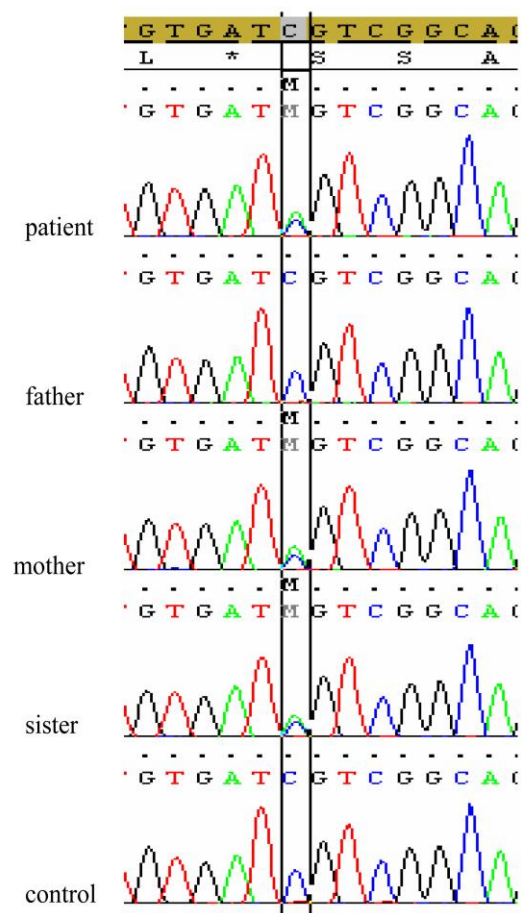


Figure 7.9 Sequencing of the identified *TBX5* mutation and segregation study

7.2.3.5 Discussion

A 19-year-old male patient with an abnormal shoulder girdle function commonly seen in Holt-Oram syndrome, carried the heterozygous c.331G>T, p.Asp111Tyr *TBX5* mutation. Congenital foot deformities, progressive distal motor neuropathy with pyramidal signs and neuromuscular transmission defect with fatigability complicated his phenotype. There was a pronounced intrafamilial variability in the clinical manifestation.

The p.Asp111Tyr missense change affects a universally conserved residue in the T-box element of the protein. The consequences of the variant were analysed on the structural model of *TBX5*. A salt bridge became disrupted when the aspartic acid residue was replaced by an uncharged tyrosine. Therefore, the mutation was supposed to induce conformational change in the *TBX5* protein and impact on the binding to its target promoters. Variably severe structural cardiac anomalies have been reported in association with the p.Asp111Tyr *TBX5* mutation (Granados-Riveron *et al.*, 2012). Extensive heart investigations (ECG, echocardiography, ABPM and Holter-monitor) were carried out in the family, but no structural or functional cardiology change could yet be identified.

Abnormal shoulder girdle function was present in the patient and in affected family members. The characteristic pattern of narrow sloping shoulder was described to be caused by the hypoplasia of the humeral head, clavicle and the surrounding musculature. The number and location of the hypoplastic muscles were reported to be in correlation with the severity of the skeletal involvement. Altered fetal muscle development has been implicated in the bony malformations of the upper limbs (Spranger *et al.*, 1997; Mace *et al.*, 2014). In respect of that the *TBX5* gene is highly regulated through alternative splicing, the translated protein products contain variable C-terminal domains. All *TBX5* isoforms retain their ability to bind DNA, but they display distinctive transcriptional properties that are target gene specific. *TBX5c* is the dominant isoform in skeletal muscle progenitors and its down regulation blocks the myotube formation (Yamak *et al.*, 2015).

No concomitant peripheral nerve involvement has been reported so far, apart from one case report describing carpal tunnel syndrome in combination with Holt-Oram syndrome (Mace *et al.*, 2014). The identification of further patients with motor neuropathy and Holt-Oram syndrome would support the pathogenicity of *TBX5* mutations in neuropathies.

The mechanisms by which *TBX5* mutations evoke certain phenotypes have remained not yet clarified, but neither the type nor the location of the mutation determines the clinical presentation (Dias *et al.*, 2007; Goldfarb and Wall, 2014). Most of the reported pathogenic mutations involve the DNA-binding T-box domain of the gene and the reduced DNA-binding capacity might contribute to the dysregulation of target gene expression. *TBX5* haploinsufficient mutations (nonsense, frameshift, and splice site mutations) induce premature stop and truncated proteins, which are unable to bind to DNA. Missense mutations result in larger phenotype variability with atypical forms, dependent on their location in the DNA-binding domain. It has been suggested that missense mutations at the 5' end lead to more prominent cardiac defects, whereas those at the 3' end are responsible for milder cardiac but more severe skeletal malformations. However, the correlation between the *TBX5* genotype and the severity of the clinical features has remained controversial (Al-Qattan and Abou Al-Shaar, 2015; Dreßen *et al.*, 2016). The transcriptional activity of the *TBX5* protein is controlled by several protein-protein interactions. The alteration of the protein level affects the expression of hundreds of genes and modulates other regulators, such as different transcription factors, as part of an extremely complex regulatory network. MicroRNAs are important in the post-transcriptional regulation of gene expression and they might play a role in the *TBX5* regulatory circuit (D'Aurizio *et al.*, 2016).

7.2.3.6 Conclusion

TBX5 encodes a transcription factor that participates in transcriptional regulatory cascades. Pathogenic *TBX5* mutations impair the DNA-binding of the protein and manifest in the Holt-Oram syndrome. The presentation of motor neuropathy with fatigability and neuromuscular transmission defect, as seen in our patient, might extend the phenotype spectrum of the Holt-Oram syndrome.

7.3 A novel mitochondrial metabolic pathway implicated in motor neuropathies

7.3.1 Literature review

2-ketoadipic aciduria (OMIM#204750) is the biochemical phenotype of defected lysine, hydroxylysine and tryptophan catabolism with questionable clinical significance (Hagen *et al.*, 2015). A wide range of manifestations, including mental retardation, seizures, hypotonia, dysmorphic features, obesity and immunodeficiency have been described, although the majority of the cases remained asymptomatic with isolated 2-oxoadipic and 2-aminoadipic aciduria (Danhauser *et al.*, 2012).

Genetic studies consequently found a molecular linkage between 2-ketoadipic aciduria and mutations identified in the dehydrogenase 1 and transketolase domain containing protein 1, *DHTKD1* gene. The encoded mitochondrial protein is a homolog isoform of the E1 subunit of the 2-oxoglutarat-dehydrogenase complex, which converts 2-oxoadipate into glutaryl-CoA by decarboxylation. The knockdown of *DHTKD1* expression in cell lines resulted in defected metabolic energy regulation, impaired mitochondrial biogenesis and induced early apoptosis (Xu *et al.*, 2013). Despite the clinical uncertainty and the large number of asymptomatic *DHTKD1* genetic abrogation, it can still be presumed that particular mutations may lead to specific disease manifestations (Stiles *et al.*, 2015). Interestingly, the c.1455T>G, p.Tyr485* nonsense *DHTKD1* mutation has been described in association with motor predominant CMT2 in a large multigenerational dominant Chinese family (W. Xu *et al.*, 2012).

Mitochondrial carriers are nuclear encoded proteins with common structural characteristics, which enable them to catalyse the transportation of specific substrates between the cytosol and the mitochondrial compartment. An increasing number of recessively inherited conditions has been linked with defected carriers causing errors in substrate specific metabolic pathways (Palmieri, 2013). *SLC25A21*, a nuclear encoded mitochondrial solute carrier has been described to participate in the 2-oxoadipate metabolism in addition to that it also transporting glutarate, aminoadipate and to a lesser extent citrate. The *SLC25A21* gene encoded mitochondrial 2-oxoadipate carrier imports 2-oxoadipate into the mitochondrial matrix in exchange for 2-oxoglutarate (Fiermonte *et al.*, 2001) (**Figure 7.10**).

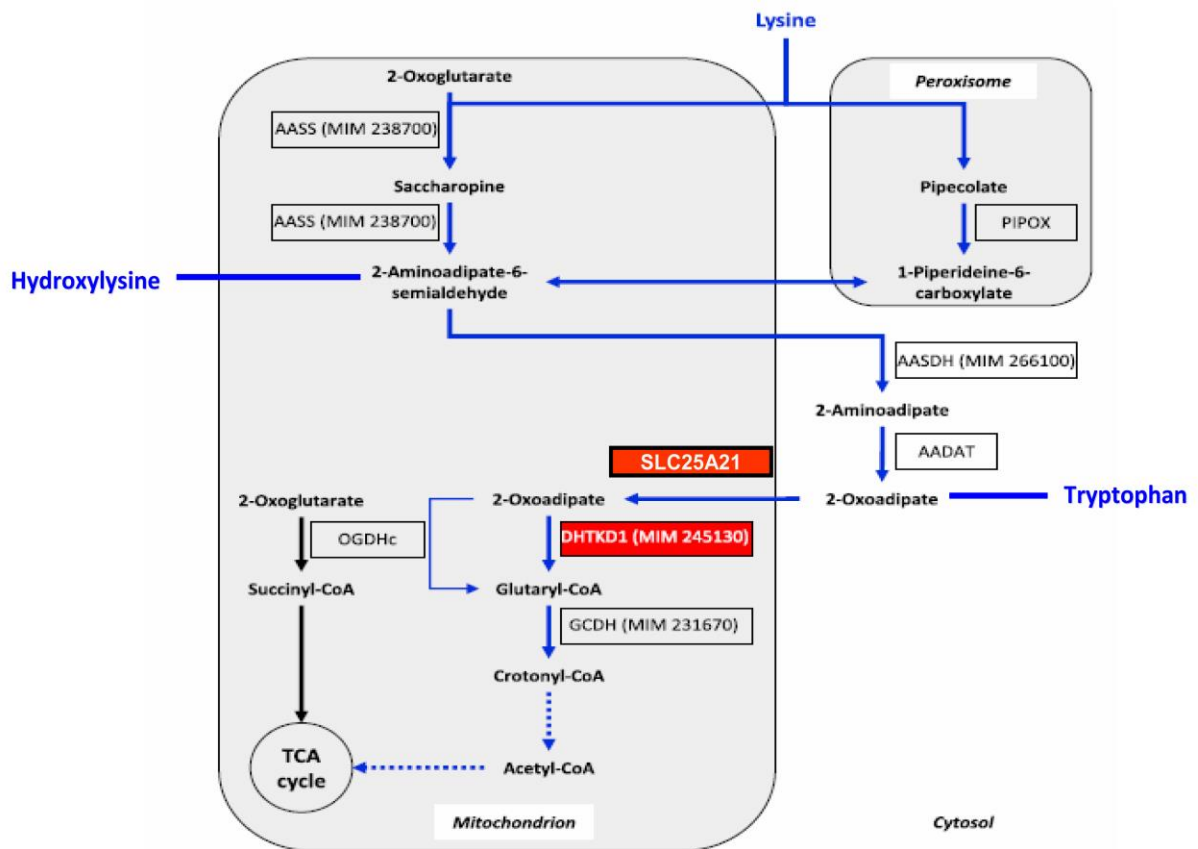


Figure 7.10 Pathway of lysine, hydroxylysine and tryptophan degradation

(modified from Danhauser et al., 2012)

7.3.2 Aims and hypothesis

I aimed to examine the hypothesis, that the 2-oxoadipic metabolic pathway with subsequent mitochondrial dysfunction might be implicated in the pathology of hereditary motor neuropathies by identifying related gene mutations in two families.

7.3.3 Methods

7.3.3.1 Patient inclusion

Patients from two families were selected for further clinical and genetic investigations from the HMN cohort. The Family 1 in this Chapter is equivalent to *Family 16* in the HMN cohort (*Chapter 5.4.2.2*).

7.3.3.2 Electrophysiology

Electric nerve studies and electromyography were performed by Dr Roger Whittaker at the Newcastle-upon-Tyne Hospitals NHS Trust (*Chapter 3.1.2*).

7.3.3.3 Experimental genetic studies

WES was undertaken in both families and the exome data were analysed (*Chapter 3.2.1.2*). I performed Sanger sequencing and segregation studies in Family 1 (*Family 16*), while Maria Lane, MSc from our research group carried out sequencing in Family 2 (*Chapter 3.2.2*). The Western blot in Family 2 was performed by Veronika Boczonadi, PhD Postdoc Fellow from our research group (*Chapter 3.2.3*).

7.3.3.4 Metabolomics studies

Peripheral blood was drawn and collected in Lithium heparin tubes from the patients and healthy controls along with collection of urine samples. All samples were kept immediately on ice and I processed the samples further with the assistance of Veronika Boczonadi, PhD. The blood samples were spun in a refrigerated centrifuge and serum aliquots were transferred into vials on ice. The serum samples were stored on -80°C . The urine samples were also centrifuged, aliquot and frozen to -80°C . The following metabolites were targeted for quantitation; 21 amino acids, 2-oxoadipic acid, quinolinic acid, pipercolic acid and carboxylic acids of the Krebs cycle. Ultrahigh Performance Liquid Chromatography/ Electrospray Ionisation-Multiple-Reaction / Monitoring Mass Spectrometry (UPLC/ESI-MRM/MS) was performed at the collaborative laboratory at University of Victoria Proteomics Centre, Vancouver Island Technology Park in Canada. Quantitation of 2-oxoadipic acid, quinolinic

acid and TCA carboxylic acids was carried out by chemical derivatisation-UPLC-MRM/MS using 3-nitrophenylhydrazine as the derivatising reagent following the protocol (Han *et al.*, 2013). Quantitation of amino acids and pipercolic acid was performed by chemical derivatisation – UPLC-MRM/MS using dansyl chloride as the derivatising reagent.

7.3.4 Results

7.3.4.1 Patient phenotype

Family 1

Three members of Family 1, the mother and her two sons (**Figure 7.11, A**) presented with similar but variably severe distal hereditary motor neuropathy symptoms, suggesting a dominant inheritance pattern in the family.

The mother developed a slowly progressive distal motor weakness in her late adulthood causing walking difficulties, frequent falls and fatigability. She had good power in the proximal part of her lower limbs, while the muscle strength was moderately decreased in her ankle plantar- and dorsiflexion (MRC grade 3/5) and severely in her toe flexion (MRC grade 2+/5). Her feet were flat with bilateral clawing of her toes. Deep tendon reflexes were globally absent. She was walking with a steppage gait and she tended to go over her ankles. Later her fingers became affected and her fine motor co-ordination deteriorated with a hand tremor. There was a mild weakness in her finger extension and atrophy in her intrinsic hand muscles. She indicated pins and needles in her fingertips.

Her sons, especially the younger one, had a more prominent disease course with an onset in their young adulthood. Both sons developed walking and balance problems due to distal leg weakness. Their ankle plantarflexion was weaker (MRC grade 2/5) than the dorsiflexion (MRC grade 3/5). They had pronounced distal motor wasting in their legs. Their feet were highly arched with clawing of their toes. They were walking with a high steppage gait and poor balance control. The younger son had accompanying proximal weakness in the thigh muscles and diminished sensation of vibration below his ankles. Both of them experienced weakness and resting tremor in their hands. There was a unique pattern in the hand muscle weakness, which exclusively affected their bilateral IV and V fingers. Their deep tendon reflexes were overall absent and there were no long tract signs.

A



***DHTKD1* c.628G>T, p.Ala210Ser**

B

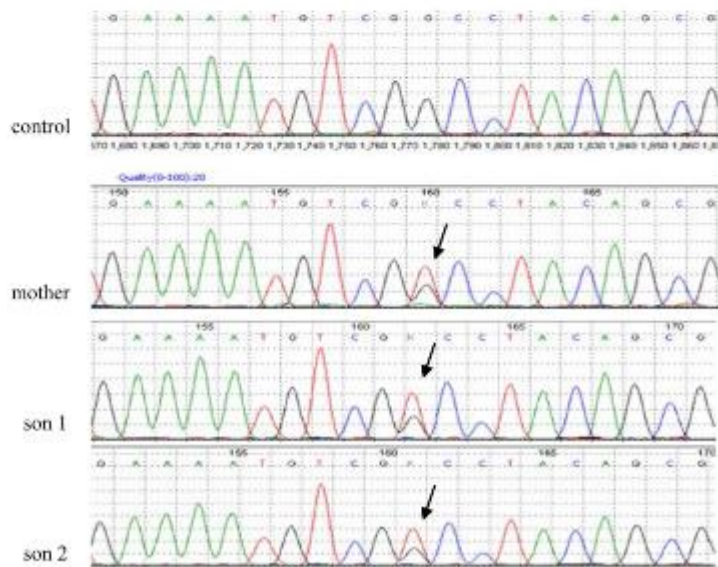


Figure 7.11 The identified *DHTKD1* mutation in the family

- A) Photo illustration of the phenotype in the affected mother and her sons
- B) Sequencing and segregation in the family

Family 2

The 18-year-old female (**Figure 7.12, A**) patient was born from consanguineous parents of Pakistani origin. The patient had no perinatal problems and she made a good early developmental progress and walked by the age of 15 months.

Aged 3 she contracted a gastrointestinal illness, when visiting Pakistan, from which she recovered with malnutrition but no signs of muscle weakness. Over the subsequent 2 years she presented daily bruises from frequent falls, while at the age of 5 she had an acute deterioration in her muscle strength rendering her intermittently non-ambulant. Incomplete burying of her eyelashes and nasal quality of speech indicated mild facial weakness. She had a generalised body tremor, tongue fasciculation and decreased ventilation. She developed wasting of her small hand muscles and her fingers became clawed on both sides. The prominent distal lower limb wasting and weakness caused bilateral foot drop and ankle contractures. Lower motor neuron symptoms were combined with upper motor neuron signs, including brisk deep tendon reflexes and ankle clonus. Her weight decreased dramatically and she required alimentary therapy for her failure to thrive. Gradually she became ambulant again before her teenage years but she was walking with dropped foot and a slapping gait. She underwent tendon surgeries and required ankle-foot orthotic support. She developed a slowly progressive thoracic scoliosis and even though spinal stabilisation surgery was not performed she was provided with a spinal brace. She intermittently received iron supplementation for her sideroblastic anaemia without much benefit. Her symptoms were very slowly progressive, rather stable over the oncoming years. Moderate proximal limb weakness presented in the shoulder girdle and hip muscles. The distal motor symptoms remained predominant, severely impairing the strength of her fingers and the movements of her feet.

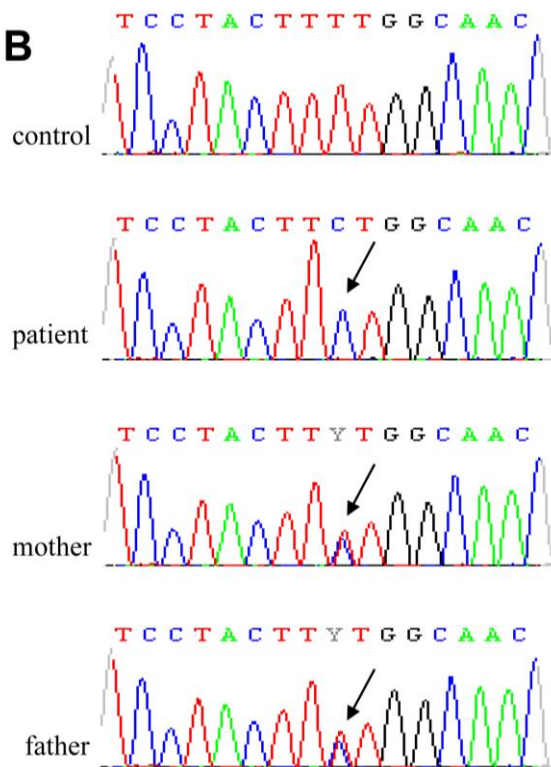
Extensive laboratory, including metabolic tests were performed on her blood and CSF samples and neuroimaging was carried out with unremarkable findings. Her muscle biopsy suggested primarily neurogenic pattern with type I fibres grouping and an increase in adipose tissue. A large proportion of the muscle fibres were cytochrome c oxidase (COX) -deficient. The nerve biopsy findings were compatible with an axonal pathology. The axonal profiles appeared swollen and ballooned with basophilic changes. Electron microscopy showed many fibres with accumulation of membranous and granule debris. Glycogen deposits were present in the cytoplasm of the Schwann cells.

A



***SLC25A21* c.695T>C, p.Lys232Arg**

B



C

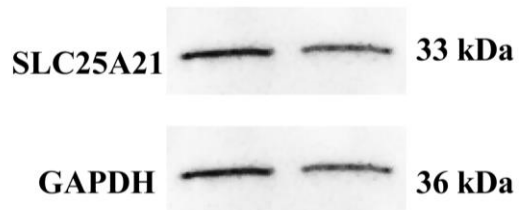


Figure 7.12 The identified *SLC25A21* mutation in the patient

- A) Photo illustration of the phenotype in the patient
- B) Sequencing of the mutation and segregation study in the family
- C) Western blot proved normal level of *SLC25A21* protein

7.3.4.2 Electrophysiology findings

Family 1

The normal nerve conduction studies and the mild chronic neurogenic process recorded in the mother indicated a form of distal SMA. In her sons, the motor responses were essentially normal and there were no convincing features to suggest demyelination. Concentric needle electromyography revealed inactive and longstanding neurogenic changes, more prominently in the distal muscles than in the proximal muscles. These findings were suggestive of a slowly progressive distal SMA. There was a significant defect of neuromuscular transmission, evident on single fibre EMG, but this most probably related to the neurogenic change rather than being a primary defect.

Family 2

Motor responses were of reduced amplitudes in the extremities, while sensory potentials were preserved. Concentric needle electromyography revealed markedly increased amplitude stable motor units with reduced recruitment. The findings indicated a longstanding and slowly progressive motor neuropathy consistent with distal SMA.

There were subtle abnormalities in the neuromuscular transmission. Repetitive nerve stimulation revealed no consistent increment or decrement but there was a 21% increment in the tibialis anterior following 10 seconds maximum voluntary contraction. SFEMG recorded very large amplitude potentials in the right extensor digitorum communis although individual muscle fibre potentials could be seen jittering, it was not possible to quantitate these.

7.3.4.3 Identified gene mutations

Family 1

IPN gene panel assay could not identify the molecular cause in the family. As the WES was undertaken in all of the three affected family members, I could compare their exome data and I could filter for common disease-causing variants. No putative variants were found to support an X-linked inheritance in the family. There were numerous heterozygous calls, including the not yet disease-causing *DHTKD1* and *GPR144* genes, which were overlapping in the WES data sets. Sanger sequencing confirmed that the heterozygous missense c.628G>T, p.Ala210Ser *DHTKD1* mutation segregated with the disease in the family (**Figure 7.11, B**). *In silico* prediction tools suggested an inconclusive pathogenicity but the affected amino acid residue in the thiamine diphosphate-binding domain was highly conserved.

Family 2

Targeted candidate gene testing in the patient excluded *SMN1* and *VCP* mutations. IPN gene panel assay did not detect mutations in neuropathy disease genes. Of note, mitochondrial DNA depletion was found with mitochondrial enzyme complex I and II deficiency. WES identified the homozygous c.695T>C, p.Lys232Arg missense mutation in the *SLC25A21* gene, which segregated appropriately with the disease in the family. The parents were heterozygous for the *SLC25A21* variant, while the healthy sister was wild-type (**Figure 7.12, B**). The mutation affects a conserved residue in the third solute carrier (solcar) repeat protein domain, which is a characteristic structure in mitochondrial anion carrier proteins. Immunoblotting confirmed normal level of the *SLC25A21* protein in the patient fibroblasts compared to healthy controls (**Figure 7.12 C**).

7.3.4.4 Results of the metabolomics studies

Amino acid and carboxylic acid assay panel measurements were performed in serum and urine samples collected from the patients with *DHTKDI* and *SLC25A21* mutations and from healthy controls. The concentration of 2-oxoadipic acid, quinolinic acid and pipercolic acid was significantly increased in the urine samples of all patients when compared to healthy controls. Similar acid concentration changes could not be detected in the serum samples (**Figure 7.13**).

7.3.5 Discussion

We investigated whether the impairment of the 2-oxoadipate metabolism could be the common link between the two novel gene mutations, which we identified by WES in the two independent families presenting with dHMN.

The dominantly inherited dHMN/dSMA phenotype co-segregated with the novel heterozygous missense c.628G>T, p.Ala210Ser *DHTKDI* mutation in one of the families. The prominent crane-leg malformation in the patients was similar to that reported in the large Chinese pedigree (W. Xu *et al.*, 2012). Additionally an unusual pattern of ‘ulnar’ split hand was noted in our family. Even though the affected Ala210 residue was highly conserved in the thiamine diphosphate-binding protein domain, the pathogenicity of the variant has remained uncertain. Metabolomics studies revealed a tendency for increased urinary concentration of the metabolites of lysine, hydroxylysine and tryptophan, suggesting a dysfunctional 2-oxoadipate catabolism. Segregation studies are planned to be carried out in the wider family to further support the pathogenicity of the identified *DHTKDI* mutation.

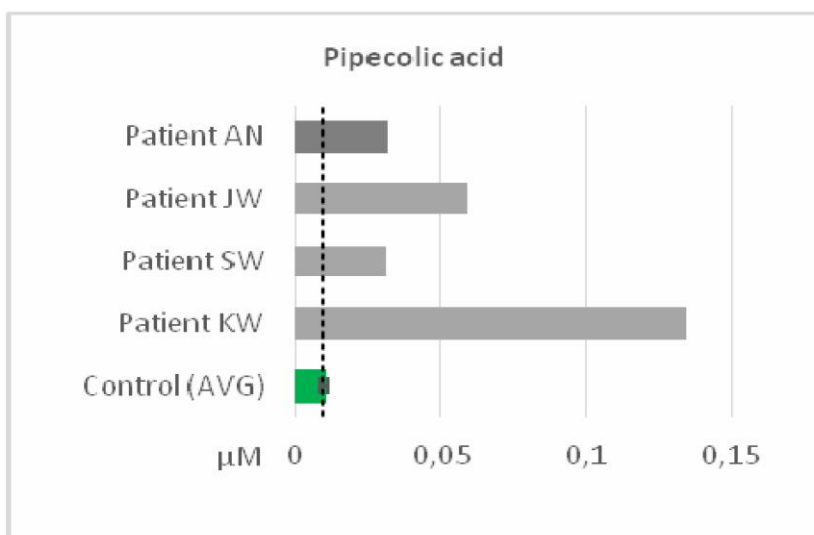
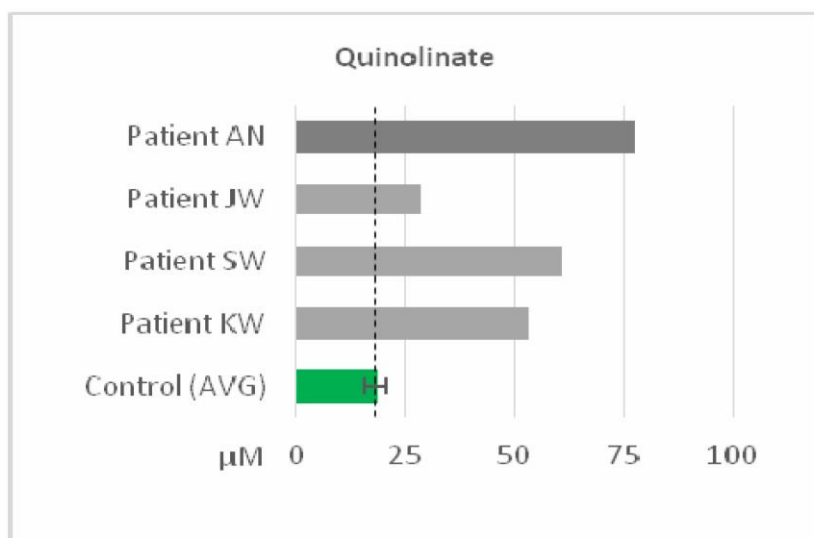
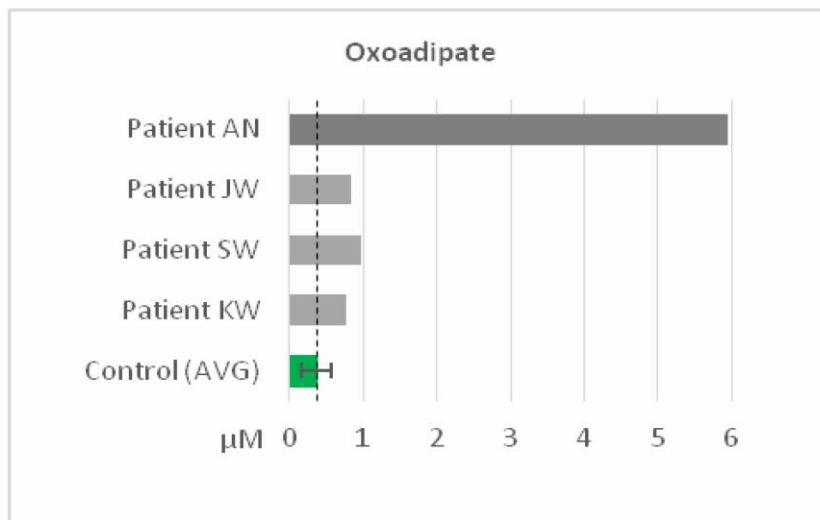


Figure 7.13 Increased concentration of the degrading metabolites in the urine

Family 1: Patients JW, SW and KW

Family 2: Patient AN

The homozygous missense c.695T>C, p.Lys232Arg *SLC25A21* mutation was found in the female offspring of a consanguineous family with severe dSMA. A mouse *SLC25A21* knock-out model was characterised by a decreased red blood cell volume and haemoglobin, by changes in the body fat, abnormal bone mineralisation and decreased levels of aspartate aminotransferase and alanine aminotransferase, decreased NK T cells and an increased monocyte number <https://www.mousephenotype.org/data/genes/MGI:2445059>. A recent report of *SLC25A21* ablation in mice described decreased body weight, a range of dental and craniofacial abnormalities, inflammation and hearing impairment, but did not detect 2-oxoadipate acidemia. The fact that the *SLC25A21* null-mutant mice did not build-up cytoplasmic oxoadipate was explained by unknown compensatory mechanisms or by differences in the substrate specificity of *SLC25A21* (Maguire *et al.*, 2014).

The patient phenotype was evaluated in comparison with the *SLC25A21* ablated mouse model. The female patient had a family history for congenital bone malformations and although she had a normal skull and teeth, she developed progressive scoliosis and rib cage deformities with pectus excavatus. She suffered from frequent bacterial infections and there was a fluctuation in the motor symptoms at the initial stages of her disease. She had issues with insufficient weight gain and she was unresponsive to iron therapy introduced for her microcytaer anaemia.

The p.Lys232Arg *SLC25A21* mutation carried by the patient was rare, affected the highly conserved solcar protein domain and had deleterious consequences on several protein prediction tools. The *SLC25A21* protein level was normal in the patient fibroblasts, and the depletion of amino acids from the culture medium did not induce measurable mitochondrial respiratory enzyme defects. Metabolomics studies confirmed significant oxoadipic and quinolinic aciduria, supporting the impairment of the 2-oxoadipate pathway.

7.3.6 Conclusion

We investigated two independent families with the main clinical manifestation of dHMN/dSMA. In the families novel mutations were identified by WES in the *DHTKD1* and *SLC25A21* genes. These mitochondrial genes participate in the same metabolic pathway of the degradation of lysine, hydroxylysine and tryptophan amino acids. Mutations in the *DHTKD1* gene have already been related to 2-ketoadipic aciduria (OMIM#204750) and one dominant family was described with axonal motor and sensory neuropathy. We suggested that an altered 2-oxoadipate metabolism might serve as a novel common mechanism in these hereditary motor neuropathies. Identification of more patients would further support this hypothesis.

Chapter 8. Investigation of neuromuscular junction as a novel therapeutic target in hereditary motor neuropathies

8.1 Literature review

8.1.1 Neurotransmission at the neuromuscular junction

Neurotransmission is the most important means of fast information transfer in neuron-neuron and neuron-muscle relations. Neuromuscular junction (NMJ) is a highly specialised synapse allowing for controlled signalling between muscle and nerve necessary for skeletal muscle function. Signal transmission at the NMJ is mediated by the release of acetylcholine from the synaptic vesicles. The neurotransmitter release from presynaptic nerve terminals is triggered by Ca^{2+} influx during an action potential, which induces membrane fusion of small synaptic vesicles with the presynaptic plasma membrane. The action potential coupled exocytosis requires synaptic vesicles, which are positioned near the Ca^{2+} channels and possess a calcium sensor, that can rapidly respond to even a small increase in the calcium level (Pang *et al.*, 2006; Young and Neher, 2009; Kochubey *et al.*, 2011; Moloney *et al.*, 2014; Whittaker *et al.*, 2015).

The neurotransmitter release occurs in fast synchronous evoked releases, which are time-locked with the presynaptic action potential and induced by brief transients of high Ca^{2+} concentrations. Following spatial re-distribution of Ca^{2+} , a ‘residual’ calcium signal decays by binding to slow buffers, which is ready to build up repetitive action potentials and can drive a slow asynchronous release. In addition, neurotransmitter release can also occur spontaneously at the NMJ in the absence of stimulation (Katz and Miledi, 1967; Pang *et al.*, 2006; Kochubey *et al.*, 2011).

When two or more action potentials invade a nerve terminal in rapid succession, residual Ca^{2+} in the vicinity of presynaptic calcium channels can build up, which enhances the probability of vesicle release for each subsequent action potential (Katz and Miledi, 1968). Evoked responses at intact NMJs remain completely synchronised throughout stimulus trains with only moderate response facilitation or depression. The lower the initial neurotransmitter release probability, the more facilitation can be achieved (Pang *et al.*, 2006).

The NMJ is an important site of pathology in a number of conditions, such as congenital myasthenic syndromes (CMS) and disorders affecting the motor neurons. According to the “dying-back” hypothesis, motor axons and nerve terminals show pathological changes prior to

the motor neuron degeneration and the onset of clinical symptoms. The neuromuscular synapse degenerates and displays structural alterations, before the axons, and precedes neuron loss. Mutations, which alter presynaptic proteins and impair components of the synaptic basal lamina, endplate development and maintenance, can lead to novel and complex disease phenotypes. Since most CMS are treatable, understanding the downstream mechanisms at the NMJ level may ultimately provide therapeutic options for these conditions (Moloney *et al.*, 2014; Sleight *et al.*, 2014; Whittaker *et al.*, 2015).

8.1.2 Neuromuscular junction defect in motor neuropathy-related gene mutations

8.1.2.1 Neurotransmission defect in SYT2 mutant neuromuscular junctions

Synaptotagmin 2 (SYT2) is a member of the large synaptotagmin protein family and the main isoform expressed at the NMJ. A coordinated network between presynaptic proteins and Ca^{2+} -dependent synaptotagmin dimerisation and phospholipid-binding are required for a timely organised process of exocytosis. SYT2 acts as a calcium sensor for fast synapses by coupling Ca^{2+} -binding with synchronous neurotransmitter release (Südhof, 2013; Whittaker *et al.*, 2015).

SYT2 mutant *Drosophila* and knockout mice display a dominant negative effect on synaptic transmission. A decreased amount of action potential-evoked synchronous synaptic release was observed in mutant NMJs. The evoked release is triggered by intracellular Ca^{2+} , which binds to SYT2 as a calcium sensor for vesicle fusion. SYT2 triggers the high Ca^{2+} dependent release, but inhibits the release at low Ca^{2+} levels, by suppressing the activity of other calcium sensor(s) that operate over a wide range of calcium signals. This 'release-clamping' function of SYT2 has been postulated to explain the increased amount of spontaneous and asynchronous release at mutant NMJs (Lin and Scheller, 2000; Pang *et al.*, 2006; Kochubey *et al.*, 2011).

A decreased neurotransmitter release probability is known to induce an increased facilitation in response to either two closely spaced action potentials (paired-pulse facilitation) or action potential trains. Implicating 10 and 20Hz stimulation frequencies in the SYT2 mutant NMJs exhibited continued facilitation without depression. The increase in the paired-pulse facilitation indicates the reduction in the synaptic release probability caused by the mutant protein.

During high-frequency stimulus trains the release became highly desynchronised in mutant NMJs, as the accumulating Ca^{2+} triggers a more spontaneous and asynchronous release. This

process became manifest by the large increase in the number of miniature release events and the highly variable rise and decay times during the stimulus train (Pang *et al.*, 2006).

8.1.2.2 Neuromuscular junction dysfunction in *GARS* mutations

GARS-mutant models of mice and *Drosophila* demonstrate early morphological defects in the synaptic connectivity at the NMJ in addition to the age and length-dependent axon loss. The compromised development of the NMJ precedes the degenerative synapse changes caused by the progressive loss of lower motor neuron connectivity.

The normal maturation of the NMJs includes an activity-dependent process of synapse elimination, which ensures the selective innervation of each synapse by a single motor axon. In the *GARS*-mutant mice a significantly higher percentage of polyinnervated NMJs were seen, indicating misregulated synapse elimination pathways (Sleigh *et al.*, 2014).

Furthermore, a morphological transition in the synapse ensures a more complex post-synaptic structure for acetylcholine signalling, while a transcriptional switch enables the expression of adult AChR subunit. In *GARS*-mutant mice the complexity of the post-synaptic structures is reduced and there is a delay in the AChR subunit switch at the NMJ. These findings support that the NMJ maturation in mice is impaired both at structural and transcriptional level and provide a substrate for further synaptic degeneration (Sleigh *et al.*, 2014). The length-dependent innervation loss caused an additional degenerative process in the mice motor nerve terminals. An increase in partially innervated or completely denervated NMJs was seen in ageing mice (Seburn *et al.*, 2006; Sleigh *et al.*, 2014). In the *Drosophila* model the *GARS* mutation also interfered with the development of NMJ, while degenerative processes later affected the synapse structure (Ermanoska *et al.*, 2014; Grice *et al.*, 2015).

The morphologically abnormal NMJs caused an unreliable neuromuscular transmission in the *GARS*-mutant mice. High frequency nerve stimulation evoked a decrease in the amplitude of complex motor unit potentials leading to the failure in the muscle force (Seburn *et al.*, 2006; Spaulding *et al.*, 2016). Motor endplate current recordings indicated presynaptic defects in the *GARS*-mutant mice models, which correlated with disease severity and progressed with age. There was a decrease in the potential-evoked release and a reduced amount of neurotransmitter release at the mutant NMJs, which failed to initiate muscle action potentials. Although the structurally impaired nerve terminals contained fewer synaptic vesicles, the vesicle process and trafficking remained intact. The frequency of spontaneous transmitter release was decreased with a maintained postsynaptic current indicating unaffected postsynaptic receptor density. High frequency repetitive nerve stimulation induces an initial release potentiation followed by a moderate depression at normal NMJ. In mutant NMJs the absence of release

potentiation suggested impaired vesicle cycling, while the marked decremental response indicated a reduced probability of neurotransmitter release. Overall, these defects in the synaptic transmission contributed to the muscle weakness and to the impaired neuromuscular performance in mice (Spaulding *et al.*, 2016). The observed phenotype of neuromuscular dysfunction was broadly correlated with the genotype (Sleigh *et al.*, 2014; Spaulding *et al.*, 2016).

8.2 Aims and hypothesis

The aim was to investigate the electrophysiological characteristics and the deficits of neurotransmission, which were previously described in the *SYT2* and *GARS*-mutant NMJs, in patients presenting with dHMN due to *GARS* mutations and SMA-LED due to a heterozygous mutation in the *SYT2* gene. In respect of the overlapping presynaptic pathology with congenital myasthenic syndromes, we examined the hypothesis whether the modulation of acetylcholine release might have a beneficial therapeutic response.

8.3 Methods

8.3.1 Patients inclusion

A large dominant family with *SYT2* mutation (*Family 4*) presented in *Chapter 5.4.2.1*; *Chapter 7.1* and two dominant families carrying novel *GARS* mutations (*Family 2 and 3*) described in *Chapter 5.4.2.1*; *Chapter 6.1.4* were selected for further examinations from the HMN cohort. The project received approval by local ethics committees and patients gave informed consent for all clinical, electrophysiology, and therapeutic studies.

8.3.2 Therapeutic modification of the neuromuscular junction function

8.3.2.1 Treatment with pyridostigmin

Selected patients from the included families were treated with a trial of pyridostigmine 60 mg, three times daily.

Pyridostigmine potentiates the effect of acetylcholine by inhibiting acetylcholinesterase in the synaptic cleft. It is the preferred symptomatic treatment of myasthenia gravis and it has also been used in the treatment of Lambert-Eaton myasthenic syndrome, even though with limited efficacy (Wirtz *et al.*, 2009).

8.3.2.2 Treatment with 3, 4 diamino-pyridin (3,4-DAP)

Patients were subsequently treated with a trial of 3,4-diaminopyridine (3,4-DAP) 20 mg, three times daily.

3,4-DAP is a voltage-dependent potassium channel blocker, which increases calcium entry into the presynaptic terminal. It has been used to improve motor weakness and fatigue in patients with neuromuscular disorders and proved to be a beneficial therapy in Lambert-Eaton myasthenic syndrome (Wirtz *et al.*, 2009; Flet *et al.*, 2010).

8.3.3 Neurology and physiotherapy assessments pre- and post-treatment

Treated patients underwent detailed neurology and physiotherapy examinations with the assistance of Robert Muni Lofra, Physiotherapist at the Newcastle-upon-Tyne Hospitals NHS Trust. The patients were assessed using the CMT Neuropathy Score (CMTNSv2) (**Table 3.1**) and the Congenital Myasthenic Syndromes Scale (CMSS) before, during, and after medication discontinuation (**Table 8.1**).

8.3.4 Electrophysiology studies of the neurotransmission pre- and post- treatment

In addition to the baseline electrophysiology studies, repetitive nerve stimulation (RNS) and single fibre electromyography (SFEMG) were carried out in the patients by Dr Roger Whittaker at the Newcastle-upon-Tyne Hospitals NHS Trust (*Chapter 3.1.2*).

SFEMG measures the variability in the initiation of muscle fibre action potentials (“jitter”) and the failures of neuromuscular transmission (“blocking”). This is the most sensitive test of neuromuscular instability. Normal muscles show jitter and blocking in no more than 10% of the fibres. SFEMG was performed using Natus Neurology disposable 30G concentric needles with a bandpass of 2 to 10 kHz.

RNS was performed on the abductor digiti minimus, abductor pollicis brevis (APB), and tibialis anterior (TA) muscles. Ten supramaximal stimuli were applied, with the percentage increment or decrement calculated between the first and fourth response. An amplitude increase or decrease of greater than 10% was regarded as significantly abnormal, indicating neurotransmission defect.

To assess posttetanic potentiation, single supramaximal stimuli were applied at least 60 seconds apart to establish the baseline amplitude of the compound muscle action potential (CMAP). Participants were then asked to make a 10-second isometric maximum voluntary contraction (MVC) against resistance. Single supramaximal CMAP responses were then recorded every 30 seconds for 5 to 10 minutes, with longer time intervals up to 60 minutes (Whittaker *et al.*, 2015).

<i>Examined Parameters / Scores</i>		<i>Patient II/2 CMTNS: 4/36</i>			<i>Patient III/2 CMTNS: 6/36</i>			<i>Patient IV/1 CMTNS: 2/28</i>
		<i>Initial Visit</i>	<i>1 month Visit</i>	<i>2 month Visit</i>	<i>Initial Visit</i>	<i>1 month Visit</i>	<i>2 month Visit</i>	<i>Initial Visit</i>
Swallowing ability / 0-9 Texture of food (0-3) Meal time (0-3) Swallowing/choking (0-3)		0/9	0/9	0/9	0/9	0/9	0/9	0/9
Respiratory function / Forced Vital Capacity (FVC)	Sitting FVC / Predicted %	3.87 / 112%	3.78 / 113%	3.63 / 109%	3.64 / 99%	not performed	3.60 / 98%	no cooperation
	Supine FVC / Predicted %	not performed	not performed	3.16 / 95%	not performed	not performed	3.07 / 83%	no cooperation
Oculomotor weakness	Double vision / Lateral gaze 1 minute test	1 min /1 min	1 min /1 min	1 min /58sec	28 sec /26 sec	1 min /1 min	12.3 sec /15.8 sec	no cooperation
	Ptosis / Upward gaze 1 minute test	1 min	1 min	1 min	45 sec increased blinking	1 min	1 min	1 min
	Eyelid closure / 0-3	0	0	0	0	0	0	0
Bulbar motor weakness	Oro-facial motor / timed slurp	6:30 sec	5:39 sec	6:10 sec	11:36 sec	7:20 sec	9:87 sec	39:00 sec
	Speech weakness / count up to 50	no change	no change	no change	no change	no change	no change	no change
General and limb muscle weakness	Rise from floor / time	unable	9:09 sec with chair support	7:51 sec with chair support	unable	unable	5:47 sec	3:30 sec
	Sustained arm raise / 4 minute abduction at 90°	4 min	4 min	4 min	4 min	not performed	4 min	55 sec unreliable cooperation
	Sustained head raise / 2 minute supine head flexion at 45°	43 sec	2 min	1:38 min	1:30 min	2 min	1:58 min	no cooperation
	Sustained leg raise / 1:40 minute supine hip- knee flexion at 45°	1:40 min	1:40 min	1:40 min	1:34 min	1:15 min	1:38 min	no cooperation
	Squats / number in 1 minute	unable	unable	unable	unable	unable	not performed	no cooperation
	Repeated sit to stand / number in 1 minute	unable	9	13	unable	unable	16	28
	Repeated rise from floor / time	unable	9:69 sec with chair support	10:62 with chair support	unable	5:00 sec with hand support	5:45 sec	3:09 sec

Table 8.1 Baseline CMSS and CMTNSv2 values and beside 3,4 DAP therapy

8.4 Results

8.4.1 Pre- and post-treatment investigations in the SYT2 mutant patients

8.4.1.1 Neurology and physiotherapy findings pre- and post-treatment

The neurology examination of the patients was consistent with the diagnosis of SMA-LED, a non-progressive lower extremity predominant distal hereditary motor neuropathy. Deep tendon reflexes were absent, but returned following physical exercise, which has been described in Lambert-Eaton myasthenic syndrome. Baseline CMSS values were recorded in the selected patients along with the CMTNSv2 scores.

The introduction of pyridostigmine in the proband (III.2) of *Family 4* and in her mother (II.2) (*Chapter 7.1.4.1*) (**Figure 7.1**) did not show beneficial effect on their muscle strength or daily activities. The CMSS values showed no difference after 1 month of therapy.

Subsequently, the patients were commenced on 3,4-DAP. Both patients reported a mild improvement regarding their exercise tolerance and daily activities. The CMSS evaluation confirmed an improvement in several indices, particularly in eye muscle fatigability (from 26 and 45 seconds to 1 minute), timed head-lifting (from 45 seconds and 1 minute 30 seconds to 2 minutes) and in other complex motor functions (**Table 8.1**).

Following discontinuation of 3,4-DAP for 14 days, these values returned to the original assessment before therapy.

8.4.1.2 Electrophysiology findings pre- and post-treatment

Pre-treatment nerve conduction studies indicated a defected neuromuscular transmission. Low-frequency (0.5 Hz) RNS produced a decrement of -18% in patient III.2, while a decremental response of -20% and -15% were seen in patients III.2 and III.6, respectively. A brief maximum voluntary contraction (MVC) induced a significant amplitude increment in all of the examined muscles. The mean amplitude increase was +87.2% (range +19.0% to +420%) with a larger increment in lower limb versus upper limb muscles (**Table 8.2**).

In order to estimate the time course of this incremental response, the study was repeated in every 30 seconds after MVC for 10 minutes. The initial increment varied between +270% and +19% and in all participants it showed an initial decay over 2 to 3 minutes followed by a persistent +10% potentiation for the entire 10 minutes (**Figure 8.1**). A particularly striking response (+187%) was observed in the patient III.2. However, the potentiated response decayed over the study period, it still remained increased at +53% even after 60 minutes (**Figure 8.1**).

Subject	Nerve	Recording site	Baseline CMAP amplitude (mV)	% change following 0.5Hz RNS	% change following 10s MVC
UK II.2	Ulnar	ADM	11.2		+20.5
	Median	APB	9.4		+23.4
	Peroneal	TA	2.1	-5	+19.0
UK III.2	Ulnar	ADM	4.6		+47.8
	Median	APB	3.8	-18	+52.6
	Peroneal	TA (R)	1.6	-20	+218.8
		TA (L)	0.5		+420.0
UK III.6	Ulnar	ADM	10.6		+30.2
	Median	APB	8.2		+41.5
	Peroneal	TA	2.0	-15	+55.0
UK IV.1	Median	APB	6.8		+30.9

Abbreviations: ADM, abductor digiti minimus; APB, abductor pollicis brevis; TA, tibialis anterior; CMAP, compound muscle action potential; MVC, maximum voluntary contraction; RNS, repetitive nerve stimulation

Table 8.2 Pre-treatment electric studies with low-frequency RNS and brief MVC

(modified from Whittaker *et al.*, 2015)

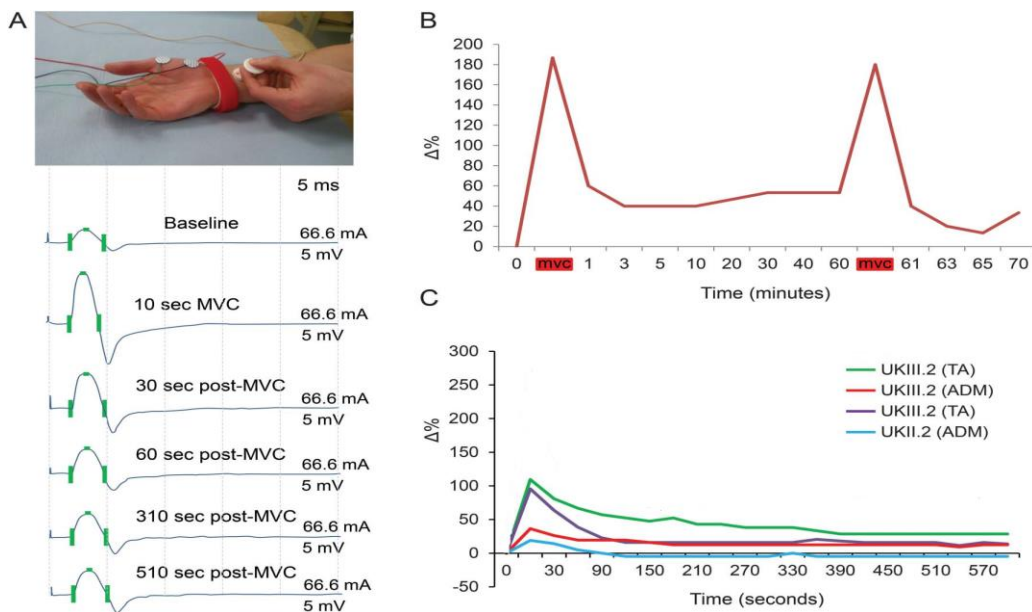


Figure 8.1 Marked and sustained post-tetanic potentiation following brief MVC

A) Electrodes over the APB muscle and supramaximal electrical stimulation was applied to the median nerve. Marked incremental response in CMAP amplitude following brief MVC.

B) Prolonged time course in decay of post-tetanic potentiation in patient III/2 lasting at least for 60 minutes.

C) Posttetanic potentiation lasting at least 10 minutes in all tested muscles and patients

(modified from Whittaker *et al.*, 2015)

SFEMG recorded an increased jitter with intermittent blocking and the mean consecutive jitter difference (MCD) was 193 ms (upper limit 50 ms) indicating a significant transmission failure.

The therapy effects were monitored by repeated electrophysiology studies. Beside the applied pyridostigmine therapy the proportion of fibre pairs showing increased jitter fell to 87%, with blocking in 25% and the mean consecutive jitter difference was 139 ms (upper limit 50 ms). Following the treatment with 3, 4-DAP the increased jitter fell further to 70%, with intermittent blocking in 15% and a mean consecutive difference of 93 ms. Neither medication had a significant effect on the baseline CMAP amplitudes or the degree of the response facilitation (**Figure 8.2**).

8.4.2 Pre- and post-treatment investigations in the GARS mutant patients

8.4.2.1 Neurology and physiotherapy findings pre- and post-treatment

Detailed clinical assessments are still ongoing in the investigated GARS-mutant families. The patients are currently treated with pyridostigmine therapy. They reported a lack of subjective improvement in their muscle weakness or fatigability.

Referring to a recent trial of synaptic modification by drugs tested in GARS-mutant mice; the introduction of physostigmine had a beneficial impact on the muscle performance, while 3,4-DAP proved not to be efficient despite its ability to increase the neurotransmitter release at the mutant synapses (Spaulding et al., 2016).

8.4.2.2 Electrophysiology findings pre- and post-treatment

Pre-treatment electrophysiology studies showed ambivalent evidence of NMJ pathology in *Family 2* carrying the c.647A>G, p.His216Arg missense mutation in the *GARS* gene.

Repetitive nerve stimulation showed a decremental response in the right trapezius muscle of the patient II/1, while SFEMG of the extensor digitorum communis showed an increased jitter (12%). In patient III/1 there was no convincing evidence of a neuromuscular transmission defect.

In *Family 3* carrying the c.1528A>C, p.Lys510Gln missense *GARS* mutation there was an evidence of NMJ instability. SFEMG recorded an increased jitter in the extensor digitorum communis (40% with 5% block) and in the tibialis anterior (19% with no block) in patient II/4, while in her granddaughter IV/3 RNS detected 30% increment in the right tibialis anterior (*Chapter 6.1.4.3*).

We are planning to perform post-treatment electrophysiology studies in both families once the trial of treatment will be completed.

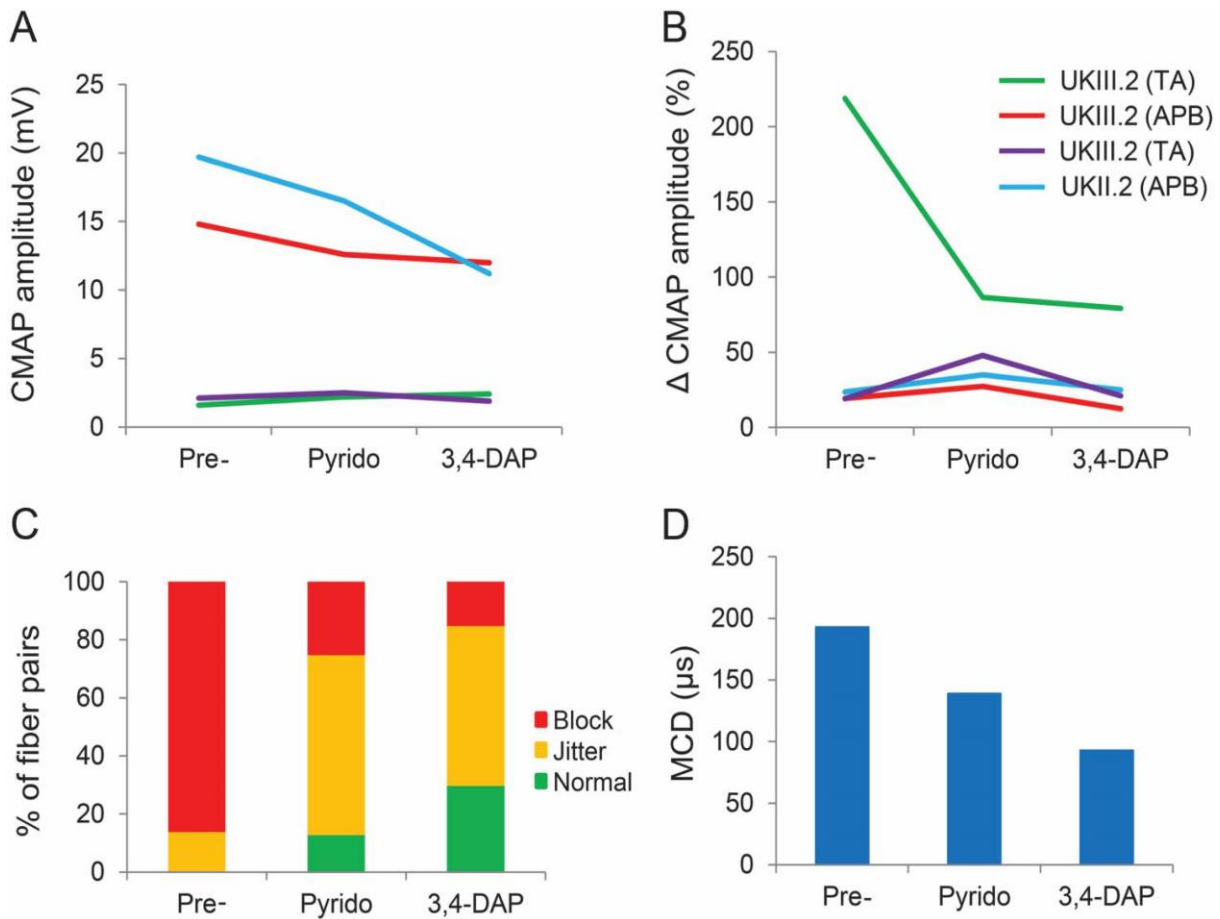


Figure 8.2 Effects of treatment with pyridostigmine and 3,4-DAP

- A) There was no consistent change in initial CMAP amplitude
 - B) There was no change in percentage incremental response following 10-second MVC.
 - C) Reduction in the percentage of muscle fiber pairs showing jitter and blocking, a greater effect with 3,4-DAP treatment
 - D) Reduction in the mean consecutive jitter, a greater reduction with 3,4-DAP treatment.
- (Whittaker *et al.*, 2015)

8.5 Discussion

8.5.1 *The neurotransmission defect and effects of the therapy in SYT2 mutant patients*

We carried out detailed evaluations in order to characterise the neurological and electrophysiological phenotype related to the c.923C>T, p.Pro308Leu *SYT2* mutation in a dominant multigenerational family. The neurology presentation was compatible with a non-progressive distal hereditary motor neuropathy with lower extremity dominance, SMA-LED. The accompanying fatigable muscle weakness and the reflex facilitation following exercise suggested a neuromuscular transmission failure. This prompted us to perform extensive electrophysiology assessments and to investigate the effects of neurotransmission modifying agents in some affected family members.

Electrophysiology studies of the patients indicated a presynaptic deficit of transmitter release, similarly to what was described in *SYT2* mutant animal models. Decreased evoked synaptic release in the mutant NMJs manifested as reduced amplitude CMAP response and as a decrementing response to low-frequency (0.5-Hz) nerve stimulation. Increased facilitation of evoked release produced a marked incremental response either at 50-Hz nerve stimulation or following brief maximal volume contraction. The presumable cause of this is that the raised intracellular calcium overcomes the reduced affinity of the mutant calcium-binding domain. The accumulating calcium during high-frequency stimulus trains triggers an increased asynchronous release and an enhanced spontaneous fusion rate. Posttetanic potentiation was detected in all patients and the incremental response decayed over a markedly prolonged time course. Posttetanic potentiation can also be prolonged in conditions with reduced presynaptic transmitter release, such as Lambert-Eaton myasthenic syndrome and infantile botulism, but the extent of potentiation lasting up to 60 minutes observed in one of the *SYT2* patient was unique. The molecular mechanism of the prolonged posttetanic potentiation still needs to be elucidated. *SYT2* acts not only as a calcium sensor for vesicle release but also plays a role in vesicle priming and tethering. The redistribution of presynaptic vesicles or posttranslational modification of *SYT2* or of another component may influence the fusion machinery and may lead to a long-lasting increase in release probability.

Given the evidence of accompanying significant NMJ dysfunction related to the *SYT2* mutation, we designed a therapy trial with presynaptic modifying medications introduced in selected patients of the family. We performed serial clinical and electrophysiological assessments in the patients before, during and after therapy. The pyridostigmine trial resulted in no valuable changes of CMSS after one month of therapy. Subsequently, the patients were introduced on 3,4-diaminopyridine (3,4-DAP), which caused a reduction in fatigable muscle

weakness and an improvement in several CMSS indices. None of the medications influenced the baseline CMAP amplitudes and the response facilitation on RNS. However, the SFEMG recordings indicated a fall in the increased jittering, more with the 3,4-DAP therapy, and revealed an improvement in the synaptic transmission. These preliminary results suggest the potential treatability of the condition, however long term effects of NMJ treatment will still need to be evaluated.

8.5.2 *The neurotransmission defect and effects of therapy in GARS mutant patients*

We detected variable degree of NMJ transmission defect in the patients from the *GARS*-mutant families. This is in agreement with the observation that different mutant alleles cause a variably severe impairment of the synaptic transmission in mice *GARS* models (Sleigh *et al.*, 2014; Spaulding *et al.*, 2016). Animal studies revealed that an early maturation defect affects the *GARS*-mutant NMJs, which is coupled with degeneration processes and results in a presynaptic transmission defect. Mutant NMJs contributed to muscle weakness in mice, which could be overcome by introducing physostigmine (Spaulding *et al.*, 2016). This suggested that the introduction of drugs, which modify presynaptic transmission at the mutant NMJs, might be beneficial for treating neuromuscular symptoms of *GARS*-mutant patients. Detailed electrophysiological and neurological follow-up of these patients beside pyridostigmine treatment is still ongoing.

8.6 Conclusion

We described the electro-clinical features of the novel human neuromuscular syndrome caused by dominant mutations in the synaptic vesicle calcium sensor *SYT2*. Electrophysiology studies revealed a presynaptic deficit in the neurotransmitter release and a post-tetanic potentiation with a uniquely prolonged decay. Pharmacologic interventions resulted in both a clinical benefit and an improvement in the neuromuscular transmission. We suggested that *SYT2* mutations cause a potentially treatable disease, which is of great clinical relevance since understanding its mechanism might identify a specific treatment strategy in neuropathies. Further detailed electrophysiology studies in more patients, including the *GARS*-mutant families will define, whether an abnormal neuromuscular transmission is characteristic for specific dHMN-related mutations and, whether this could be used as a target in therapy of some neuropathy subgroups to improve the motor function (Whittaker *et al.*, 2015).

Chapter 9. Conclusion and future directions

9.1 Overview

The improving genetic testing technology has led to a rapid increase in the discovery of CMT-causing gene mutations. More and more patients can be genetically diagnosed not only with common, but also with rare CMT forms. The complexity of the disease has been unravelled, phenotype-genotype correlations have become apparent and diverse disease mechanisms have become better understood. The introduction of natural history studies enables to refine the relationship between the patient phenotype and genotype in order to reach a clinical diagnosis and to determine genetic screening strategies. Establishing a genetic diagnosis supports the clinical classification, guides the disease prognosis and provides the patients and their family with an accurate risk assessment for genetic counselling. The detection of common and converging disease pathways might provide future options for specific treatments.

9.2 Summary of the Thesis results

9.2.1 *Clinical and genetic analysis of the hereditary motor neuropathy cohort*

In this Thesis detailed investigations have been carried out in a large cohort of 105 patients of North-East England origin, in order to better understand the clinical and genetic heterogeneity of hereditary motor neuropathies and to explore potential disease mechanisms.

The minimum prevalence of dHMN in the examined cohort was 2.14/100.000 inhabitants (95% CI: 1.62-2.66), which was significantly higher than suggested by previous population surveys. Precise electrophysiology investigations have been performed to differentiate between dHMN and motor CMT2 that were both commonly characterised by motor predominant symptoms. However, the clear distinction between the two clinical categories has remained challenging in some cases by all applied clinical, electrophysiological and molecular methods. ***Therefore we suggested that the dHMN should be considered clinically as a subcategory of CMT.*** Furthermore, distal HMN primarily affects the lower motor neurons but in patients classified into the subgroup of HMN plus, which was introduced in this Thesis, the distal HMN manifestation showed a significant overlap with other motor neuron diseases.

Extensive genetic screening was performed in the studied HMN cohort to assess the genetic spectrum and the mutation detection rate by implicating next generation sequencing methods. ***A significant 47.9% mutation detection rate was achieved considering all clinical HMN subgroups.*** Mutations were confirmed in 35.6% and in an additional 12.3% they were possibly causative. ***The diagnostic success was even more remarkable in the distal HMN group, where the genetic cause was confirmed in 32.5% and further 10% possibly causative gene mutations were identified.*** The significant increase in the detection rate, compared to the previously given 20% positive findings, could be attributed in part to improved genetic technology. ***The results of this Thesis suggested that next generation sequencing should be a routine clinical procedure in this group of disorders. Furthermore, the importance of international genetic data sharing was underscored in this Thesis by the discovery of the SYT2 novel gene.***

9.2.2 Phenotype-genotype correlations in the hereditary motor neuropathy cohort

Thorough clinical characterisation of phenotypes and pragmatic segregation analyses of identified genetic variants helped us to determine phenotype-genotype correlations and to distinguish between overlapping allelic phenotypes.

The natural history of aminoacyl-tRNA synthetases (ARS)-related motor neuropathies has been investigated in detail through a cohort of AARS and GARS mutant families. The phenotype spectrum was widely heterogeneous in both disease groups with a large variability in the age of onset, clinical severity and electrophysiological findings. The presence of severe foot drop was common among the patients and split hand malformation was a frequently seen overlapping feature. Abnormal neuromuscular transmission was detected in some of the GARS patients keeping with the evidence of NMJ defect in GARS animal models. Targeted electrophysiology testing of the AARS patients could not record a concomitant NMJ dysfunction but the demyelination process here was larger beside the axonal degeneration and resulted in a common intermediate neuropathy. ***Genetic screening for ARS-related mutations should always be considered in axonal neuropathology. Among the few dominant loss of function AARS mutations, the p.Arg329His variant is considered a recurrent mutation worldwide, but the haplotype similarity noted in the cohort families raised the potential of a founder effect.*** On the contrary, many mutations have already been described in the GARS gene with many implicated pathological pathways. ***The mutational spectrum was extended with 2 novel GARS variants identified in the studied families.***

Aberrant interactions were found between Nrp1 and mutant proteins in the studied GARS and AARS patients, which suggested a common pathology mechanism among ARS-related neuropathies and might serve as a biomarker for the molecular diagnosis.

Many recessive and compound heterozygous mutations in the *IGHMBP2* gene have been described to cause the SMARD1 phenotype or its juvenile-onset form. ***A novel IGHMBP2- related phenotype has been described in a recent patient cohort, which included a family investigated in this Thesis.*** The common presentation was an early-onset, slowly progressive axonal motor predominant CMT2 without concomitant respiratory involvement and with a better prognosis. ***The hemizygous c.1813C>T, p.Arg605*X stop mutation found on cDNA sequencing in the studied family warrants that single heterozygous IGHMBP2 mutations identified by next generation sequencing should be meticulously investigated toward pathogenicity. The mutation specific impairment of the residual protein level correlates with the clinical severity and provides an explanation for the broad phenotype heterogeneity.***

The large genotype heterogeneity is well known in dominant *TRPV4*-related conditions. ***The diverse phenotype manifestation in TRPV4 neuropathies was further underscored in the families studied in this Thesis.*** It was highlighted that *TRPV4* mutations should be considered even with a highly variable symptom presentation in the same family due to reduced penetrance, and with a combined presentation of axonal motor neuropathy and skeletal dysplasia. ***The accumulation of cytoplasmic basophilic inclusions in the muscle cells of one of the patients suggested the possibility that the retention of misfolded proteins might be implicated in the TRPV4 pathogenesis, similarly to the heat shock protein genes.***

Two families, examined in this Thesis with SMA-LED phenotype, have expanded the worldwide patient cohort of p.Ser107Leu BICD2 mutation caused motor neuropathies. Haplotype investigation in the families further supported that the p.Ser107Leu in the BICD2 gene is a mutation ‘hot spot’ and the occurrence of de novo BICD2 mutations might be frequent. Therefore, sporadic SMA-LED cases should be screened for *BICD2* mutations, in particular when signs of Achilles contracture, scapular winging and specific muscle MRI changes provide a clinical hint.

Numerous diverse mutations in the *ATP7A* gene present with a broad phenotype spectrum, including Menkes disease with severe neurological degeneration, OHS with connective tissue

disorders and the X-linked HMN. However, clear phenotype-genotype correlations have not yet been clarified. ***A novel ATP7A-related phenotype was demonstrated in this Thesis, where an overlap between different copper metabolism disorders resulted in the complex manifestation of severe motor neuro- and neuropathy.***

9.2.3 Novel disease genes and mechanisms in the hereditary motor neuropathy cohort

The detection of novel disease genes and unravelling novel mechanism pathways, previously not implicated in hereditary motor neuropathies, were main goals of this Thesis investigation.

A large dominant family was described in this Thesis with non-progressive SMA-LED phenotype and presynaptic neuromuscular junction defect. The identified novel SYT2 gene mutation was linked for the first time to a human disease. Mutations in the SYT2 gene represent an important cause of disorders of the human peripheral motor nerve terminal with phenotypes ranging between distal hereditary motor neuropathy and presynaptic NMJ dysfunction. ***Mutant presynaptic protein changes might hence be considered in the pathomechanism of neuropathy subgroups.***

Overlapping motor neuropathy phenotypes presenting with demyelinating features were demonstrated in relation to basic biological pathways in the peripheral nerves. Transcription factors and signalling pathways are known to be linked to myelination. These pathogenic or likely pathogenic mutations in rare, known disease genes have not been reported yet in association with peripheral neuropathy. Further studies will be required to examine these transcription factors and signal transduction pathways in the mechanisms of neuromuscular pathology.

A de novo PTEN mutation was identified in a patient with progressive multifocal motor neuropathy with demyelinating features, a phenotype that has not been related yet to PTEN mutations in humans. PTEN is a lipid phosphatase that inhibits PI3-K and the subsequent PIP3 dysregulation and the constitutive hyperactivation of the Akt/mTOR signalling pathway in the Schwann cells might be implicated in the pathology. Experimental PTEN suppression in the mice model led to a similar neuropathology with tomacula formation and myelin outfoldings.

Homozygous mutations affected a key transcriptional regulation region in the STAT5B gene and presented with combined postnatal growth retardation and demyelinating motor neuropathy in a consanguineous family. Cyclin D1 overexpression due to abnormal STAT5B - IGF1 interactions and the disruption of the IGF/mTORC1

signalling cascade might serve a hypothetic pathway that led to an aberrant peripheral myelination process.

A Holt Oram syndrome-causing TBX5 mutation presented with fatigable motor neuropathy with demyelination and NMJ defect in a studied family. The previously described mutation induces conformational change and impairs DNA-binding of the TBX5, which participates in transcriptional regulatory cascades. Abnormal protein interactions in a complex signalling network might be responsible for the pathomechanism.

A novel mitochondrial pathway affecting the 2-oxoadipate metabolism has been suggested to cause dHMN in two independent families. The *DHTKD1* mutation segregated with crane-leg and ‘ulnar’ split hand malformation in a dominant family. The female carrying the homozygous *SLC25A21* mutation presented with severe dSMA and multisystem symptoms resembling the abnormalities seen in *SLC25A21* mutant mice. Metabolomics studies supported the impairment of the 2-oxoadipate pathway in both families. Identification of further patients with the same gene mutations or genes involved in the same pathway would help to determine whether the mitochondrial dysfunction caused by abnormal 2-oxoadipate metabolism might be implicated in the pathology of hereditary motor neuropathies.

9.2.4 Novel therapy approaches in hereditary motor neuropathies

Unravelling the function of neuropathy-causing genes and proteins and better understanding the implicated disease pathways might provide a basis for the development of novel therapy avenues. The objective of this Thesis was to determine common pathomechanisms and targets for therapy approaches in hereditary motor neuropathies.

The Thesis investigations suggested that the abnormal neuromuscular transmission provides a treatable target in some genetic forms of motor neuropathies. Electro-clinical features of presynaptic deficit and post-tetanic potentiation were described in the novel neuromuscular syndrome caused by dominant *SYT2* mutations, where therapeutic modification of the neurotransmission was proven to have beneficial effects. *GARS*-mutant neuromuscular junction pathology was suggested to be a target to develop therapies. ***The neuromuscular junction dysfunction might be considered as a not yet recognised treatable aspect of axonal motor neuropathies with a great clinical relevance.***

9.3 Concluding remarks

The detailed phenotype characterisation and genotype analysis using next generation methods has led to the increased mutation detection rate in hereditary motor neuropathies and highlighted that the clinical expertise is essential in confirming the diagnosis of inherited motor neuropathies. The detection of mutations in rare disease genes, not yet implicated in neuropathy, suggested that the neuropathy can be part of a more complex genetic disease and that related key clinical signs are important to recognise these diseases. (Bansagi et al, 2017). Well-defined phenotype-genotype correlations and detection of molecular pathways facilitated the identification of molecular targets for the development of novel treatment options. No common shared variants were detected in the undiagnosed HMN cases suggesting further genetic heterogeneity in the condition. Most of our undiagnosed patients have undergone whole genome sequencing, which might help to reveal further genetic factors.

Appendix A

Genetic heterogeneity of motor neuropathies

Boglarka Bansagi, Helen Griffin, Roger Whittaker, Thalia Antoniadi, Teresinha Evangelista, James Miller, Mark Greenslade, Natalie Forester, Jennifer Duff, Anna Bradshaw, Stephanie Kleinle, Veronika Boczonadi, Hannah Steele, Venkatateswaran Ramesh, Edit Franko, Angela Pyle, Hanns Lochmüller, Patrick F. Chinnery, Rita Horvath

Neurology, 2017; Ahead of print

Abstract

Objective: We studied the prevalence, the molecular cause and clinical presentation of hereditary motor neuropathies in a large cohort of patients from the North of England.

Methods: Detailed neurological and electrophysiological assessments and next generation panel testing or whole exome sequencing were performed in 105 patients with clinical symptoms of distal hereditary motor neuropathy (dHMN, 64 patients), axonal motor neuropathy (motor CMT2, 16 patients) or complex neurological disease predominantly affecting the motor nerves (HMN plus, 25 patients).

Results: The prevalence of dHMN is 2.14 affected individuals per 100.000 inhabitants (95% confidence interval: 1.62-2.66) in the North of England. Causative mutations were identified in 26 out of 73 index patients (35.6%). The diagnostic rate in the dHMN subgroup was 32.5%, which is higher than previously reported (20%). We detected a defect of neuromuscular transmission in 12 cases and identified potentially causative mutations in 4 patients with demyelinating multifocal motor neuropathy.

Conclusions: Many of the genes were shared between dHMN and motor CMT2, indicating identical disease mechanisms therefore we suggest changing the classification and include dHMN also as a subcategory of CMT. Abnormal neuromuscular transmission in some genetic forms provides a treatable target to develop therapies.

Appendix B

Truncating and missense mutations in *IGHMBP2* cause Charcot-Marie Tooth disease type 2

Ellen Cottenie, Andrzej Kochanski, Albena Jordanova, **Boglarka Bansagi**, Magdalena Zimon, Alejandro Horga, Zane Jaunmuktane, Paola Saveri, Vedrana Milic Rasic, Jonathan Baets, Marina Bartsakoulia, Rafal Ploski, Pawel Teterycz, Milos Nikolic, Ros Quinlivan, Matilde Laura, Mary G. Sweeney, Franco Taroni, Michael P. Lunn, Isabella Moroni, Michael Gonzalez, Michael G. Hanna, Conceicao Bettencourt, Elodie Chabrol, Andre Franke, Katja von Au, Markus Schilhabel, Dagmara Kabzinska, Irena Hausmanowa-Petrusewicz, Sebastian Brandner, Siew Choo Lim, Haiwei Song, Byung-Ok Choi, Rita Horvath, Ki-Wha Chung, Stephan Zuchner, Davide Pareyson, Matthew Harms, Mary M. Reilly, Henry Houlden

Am. J. Hum. Genet. 2014; 95(5): 590-601. doi: 10.1016/j.ajhg.2014.10.002.

Abstract

Using a combination of exome sequencing and linkage analysis, we investigated an English family with two affected siblings in their 40s with recessive Charcot-Marie Tooth disease type 2 (CMT2). Compound heterozygous mutations in the immunoglobulin-helicase- μ -binding protein 2 (*IGHMBP2*) gene were identified. Further sequencing revealed a total of 11 CMT2 families with recessively inherited *IGHMBP2* gene mutations. *IGHMBP2* mutations usually lead to spinal muscular atrophy with respiratory distress type 1 (SMARD1), where most infants die before 1 year of age. The individuals with CMT2 described here, have slowly progressive weakness, wasting and sensory loss, with an axonal neuropathy typical of CMT2, but no major respiratory compromise. Segregating *IGHMBP2* mutations in CMT2 were mainly loss-of-function nonsense in the 5' region of the gene in combination with a truncating frameshift, missense, or homozygous frameshift mutations in the last exon. Mutations in CMT2 were predicted to be less aggressive as compared to those in SMARD1, and fibroblast and lymphoblast studies indicate that the *IGHMBP2* protein levels are significantly higher in CMT2 than SMARD1, but lower than controls, suggesting that the clinical phenotype differences are related to the *IGHMBP2* protein levels.

Appendix C

Genotype/phenotype correlations in AARS-related neuropathy in a cohort of patients from the United Kingdom and Ireland

Boglarka Bansagi, Thalia Antoniadis, Sarah Burton-Jones, Sinead M. Murphy, John McHugh, Michael Alexander, Richard Wells, Joanna Davies, David Hilton-Jones, Hanns Lochmüller, Patrick Chinnery, Rita Horvath

J. Neurol. 2015; 262(8): 1899-908. doi: 10.1007/s00415-015-7778-4.

Abstract

Charcot–Marie–Tooth disease (CMT) is the most common inherited neuropathy with heterogeneous clinical presentation and genetic background. The axonal form (CMT2) is characterised by decreased action potentials indicating primary axonal damage. The underlying pathology involves axonal degeneration which is supposed to be related to axonal protein dysfunction caused by various gene mutations. The overlapping clinical manifestation of CMT2 with distal hereditary motor neuropathy (dHMN) and intermediate CMT causes further diagnostic difficulties. Aminoacyl-tRNA synthetases have been implicated in the pathomechanism of CMT2. They have an essential role in protein translation by attaching amino acids to their cognate tRNAs. To date six families have been reported worldwide with dominant missense alanyl-tRNA synthetase (AARS) mutations leading to clinically heterogeneous axonal neuropathies. The pathomechanism of some variants could be explained by impaired amino acylation activity while other variants implicating an editing defect need to be further investigated. Here, we report a cohort of six additional families originating from the United Kingdom and Ireland with dominant AARS-related neuropathies. The phenotypic manifestation was distal lower limb predominant sensorimotor neuropathy but upper limb impairment with split hand deformity occasionally associated. Nerve conduction studies revealed significant demyelination accompanying the axonal lesion in motor and sensory nerves. Five families have the c.986G>A, p.Arg329His variant, further supporting that this is a recurrent loss of function variant. The sixth family, of Irish origin, had a novel missense variant, c.2063A>G, p.Glu688Gly. We discuss our findings and the associated phenotypic heterogeneity in these families, which expands the clinical spectrum of AARS-related neuropathies.

Appendix D

The p.Ser107Leu in *BICD2* is a mutation ‘hot spot’ causing distal spinal muscular atrophy

Boglarka Bansagi, Helen Griffin, Venkateswaran Ramesh, Jennifer Duff, Angela Pyle, Patrick F. Chinnery, Rita Horvath

Brain 2015; 138(Pt 11):e391. doi: 10.1093/brain/awv159.

Letter to the Editor

Appendix E

Phenotypic variability of TRPV4 related neuropathies

Teresinha Evangelista, **Boglarka Bansagi**, Angela Pyle, Helen Griffin, Konstantinos Douroudis, Tuomo Polvikoski, Thalia Antoniadis, Kate Bushby, Volker Straub, Patrick F. Chinnery, Hanns Lochmüller, Rita Horvath

Neuromuscul. Disord. 2015; 25(6): 516-21. doi: 10.1016/j.nmd.2015.03.007.

Abstract

Mutations in the transient receptor potential vanilloid 4 (*TRPV4*) gene have been associated with autosomal-dominant skeletal dysplasias and peripheral nervous system syndromes (PNSS). PNSS include Charcot–Marie–Tooth disease (CMT) type 2C, congenital spinal muscular atrophy and arthrogyrosis and scapuloperoneal spinal muscular atrophy. We report the clinical, electrophysiological and muscle biopsy findings in two unrelated patients with two novel heterozygous missense mutations in the *TRPV4* gene. Whole exome sequencing was carried out on genomic DNA using IlluminaTruseq™ 62Mb exome capture. Patient 1 harbours a de novo c.805C > T, p.Arg269Cys mutation. Clinically, this patient shows signs of both scapuloperoneal spinal muscular atrophy and skeletal dysplasia. Patient 2 harbours a novel c.184G > A, p.Asp62Asn mutation. While the clinical phenotype is compatible with CMT type 2C with the patient's muscle harbours basophilic inclusions. Mutations in the *TRPV4* gene have a broad phenotypic variability and disease severity and may share a similar pathogenic mechanism with Heat Shock Protein related neuropathies.

Appendix F

Phenotypic convergence of Menkes and Wilson disease

Boglarka Bansagi, David Lewis-Smith, Endre Pal, Jennifer Duff, Helen Griffin, Angela Pyle, Juliane S. Müller, Gabor Rudas, Zsuzsanna Aranyi, Hanns Lochmüller, Patrick F. Chinnery, Rita Horvath

Neurol. Genet. 2016; 2(6): e119.

Abstract

Menkes disease is an X-linked multisystem disorder with epilepsy, kinky hair, and neurodegeneration caused by mutations in the copper transporter *ATP7A*. Other *ATP7A* mutations have been linked to juvenile occipital horn syndrome and adult-onset hereditary motor neuropathy. About 5%-10% of the patients present with "atypical Menkes disease" characterized by longer survival, cerebellar ataxia, and developmental delay. The intracellular copper transport is regulated by 2 P type ATPase copper transporters *ATP7A* and *ATP7B*. These proteins are expressed in the trans-Golgi network that guides copper to intracellular compartments, and in copper excess, it relocates copper to the plasma membrane to pump it out from the cells. *ATP7B* mutations cause Wilson disease with dystonia, ataxia, tremor, and abnormal copper accumulation in the brain, liver, and other organs.

Appendix G

Synaptotagmin 2 mutations cause an autosomal-dominant form of Lambert-Eaton myasthenic syndrome and nonprogressive motor neuropathy

David N. Herrmann, Rita Horvath, Janet E. Sowden, Michael Gonzales, Avencia Sanchez-Mejias, Zhuo Guan, Roger G. Whittaker, Jorge L. Almodovar, Maria Lane, **Boglarka Bansagi**, Angela Pyle, Veronika Boczonadi, Hanns Lochmüller, Helen Griffin, Patrick F. Chinnery, Thomas E. Lloyd, J. Troy Littleton, Stephan Zuchner

Am. J. Hum. Genet. 2014; 95(3): 332-9. doi: 10.1016/j.ajhg.2014.08.007.

Abstract

Synaptotagmin 2 is a synaptic vesicle protein that functions as a calcium sensor for neurotransmission but has not been previously associated with human disease. Via whole-exome sequencing, we identified heterozygous missense mutations in the C2B calcium-binding domain of the gene encoding Synaptotagmin 2 in two multigenerational families presenting with peripheral motor neuron syndromes. An essential calcium-binding aspartate residue, Asp307Ala, was disrupted by a c.920A>C change in one family that presented with an autosomal-dominant presynaptic neuromuscular junction disorder resembling Lambert-Eaton myasthenic syndrome. A c.923C>T variant affecting an adjacent residue p.Pro308Leu produced a presynaptic neuromuscular junction defect and a dominant hereditary motor neuropathy in a second family. Characterization of the mutation homologous to the human c.920A>C variant in *Drosophila* Synaptotagmin revealed a dominant disruption of synaptic vesicle exocytosis using this transgenic model. These findings indicate that Synaptotagmin 2 regulates neurotransmitter release at human peripheral motor nerve terminals. In addition, mutations in the Synaptotagmin 2 C2B domain represent an important cause of presynaptic congenital myasthenic syndromes and link them with hereditary motor axonopathies.

Appendix H

Electrophysiologic features of *SYT2* mutations causing a treatable neuromuscular syndrome

Roger G Whittaker, David N Herrmann, **Boglarka Bansagi**, Bashar Awwad Shiekh Hasan, Robert Muni Lofra, Eric L. Logigian, Janet E. Sowden, Jorge L. Almodovar, J. Troy Littleton, Stephan Zuchner, Rita Horvath, Hanns Lochmüller

Neurology 2015; 85(22): 1964-71. doi: 10.1212/WNL.0000000000002185.

Abstract

Objectives: To describe the clinical and electrophysiologic features of synaptotagmin II (*SYT2*) mutations, a novel neuromuscular syndrome characterized by foot deformities and fatigable ocular and lower limb weakness, and the response to modulators of acetylcholine release.

Methods: We performed detailed clinical and neurophysiologic assessment in 2 multigenerational families with dominant *SYT2* mutations c.920T>G, p.Asp307Ala and c.923G>A, p.Pro308Leu. Serial clinical and electrophysiologic assessments were performed in members of one family treated first with pyridostigmine and then with 3,4-diaminopyridine.

Results: Electrophysiologic testing revealed features indicative of a presynaptic deficit in neurotransmitter release with posttetanic potentiation lasting up to 60 minutes. Treatment with 3,4-diaminopyridine produced both a clinical benefit and an improvement in neuromuscular transmission.

Conclusion: *SYT2* mutations cause a novel and potentially treatable complex presynaptic congenital myasthenic syndrome characterized by motor neuropathy causing lower limb wasting and foot deformities, with reflex potentiation following exercise and a uniquely prolonged period of posttetanic potentiation.

References

- Abrams AJ, Hufnagel RB, Rebelo A, Zanna C, Patel N, Gonzalez MA, et al. Mutations in SLC25A46, encoding a UGO1-like protein, cause an optic atrophy spectrum disorder. *Nat. Genet.* 2015; 47: 926–932.
- Ackerley S, James PA, Kalli A, French S, Davies KE, Talbot K. A mutation in the small heat-shock protein HSPB1 leading to distal hereditary motor neuropathy disrupts neurofilament assembly and the axonal transport of specific cellular cargoes. *Hum. Mol. Genet.* 2006; 15: 347–354.
- Aharoni S, Harlalka G, Offiah A, Shuper A, Crosby AH, McEntagart M. Striking phenotypic variability in familial TRPV4-axonal neuropathy spectrum disorder. *Am. J. Med. Genet. A.* 2011; 155: 3153–3156.
- Ahuja A, Dev K, Tanwar RS, Selwal KK, Tyagi PK. Copper mediated neurological disorder: Visions into amyotrophic lateral sclerosis, Alzheimer and Menkes disease. *J. Trace Elem. Med. Biol.* 2015; 29: 11–23.
- Albulym OM, Kennerson ML, Harms MB, Drew AP, Siddell AH, Auer-Grumbach M, et al. MORC2 mutations cause axonal Charcot-Marie-Tooth disease with pyramidal signs. *Ann. Neurol.* 2016; 79: 419–427.
- Al-Qattan MM, Abou Al-Shaar H. Molecular basis of the clinical features of Holt–Oram syndrome resulting from missense and extended protein mutations of the TBX5 gene as well as TBX5 intragenic duplications. *Gene* 2015; 560: 129–136.
- Andrés-Pons A, Rodríguez-Escudero I, Gil A, Blanco A, Vega A, Molina M, et al. In vivo functional analysis of the counterbalance of hyperactive phosphatidylinositol 3-kinase p110 catalytic oncoproteins by the tumor suppressor PTEN. *Cancer Res.* 2007; 67: 9731–9739.
- Anesi L, de Gemmis P, Pandolfo M, Hladnik U. Two novel homozygous SACS mutations in unrelated patients including the first reported case of paternal UPD as an etiologic cause of ARSACS. *J. Mol. Neurosci.* MN 2011; 43: 346–349.

- Antonellis A, Ellsworth RE, Sambuughin N, Puls I, Abel A, Lee-Lin S-Q, et al. Glycyl tRNA synthetase mutations in Charcot-Marie-Tooth disease type 2D and distal spinal muscular atrophy type V. *Am. J. Hum. Genet.* 2003; 72: 1293–1299.
- Antonellis A, Lee-Lin S-Q, Wasterlain A, Leo P, Quezado M, Goldfarb LG, et al. Functional analyses of glycyl-tRNA synthetase mutations suggest a key role for tRNA-charging enzymes in peripheral axons. *J. Neurosci.* 2006; 26: 10397–10406.
- Antonicka H, Østergaard E, Sasarman F, Weraarpachai W, Wibrand F, Pedersen AMB, et al. Mutations in C12orf65 in patients with encephalomyopathy and a mitochondrial translation defect. *Am. J. Hum. Genet.* 2010; 87: 115–122.
- Araki E, Tsuboi Y, Daechsel J, Milnerwood A, Vilarino-Guell C, Fujii N, et al. A novel DCTN1 mutation with late-onset parkinsonism and frontotemporal atrophy: A novel DCTN1 mutation. *Mov. Disord.* 2014; 29: 1201–1204.
- Armstrong GAB, Drapeau P. Loss and gain of FUS function impair neuromuscular synaptic transmission in a genetic model of ALS. *Hum. Mol. Genet.* 2013; 22: 4282–4292.
- Arnold WD, Isfort M, Roggenbuck J, Hoyle JC. The genetics of Charcot-Marie-Tooth disease: current trends and future implications for diagnosis and management. *Appl. Clin. Genet.* 2015: 235.
- Atanasoski S, Scherer SS, Nave K-A, Suter U. Proliferation of Schwann cells and regulation of cyclin D1 expression in an animal model of Charcot-Marie-Tooth disease type 1A. *J. Neurosci. Res.* 2002; 67: 443–449.
- Attarian S, Vallat J-M, Magy L, Funalot B, Gonnaud P-M, Lacour A, et al. An exploratory randomised double-blind and placebo-controlled phase 2 study of a combination of baclofen, naltrexone and sorbitol (PXT3003) in patients with Charcot-Marie-Tooth disease type 1A. *Orphanet J. Rare Dis.* 2014; 9: 199.
- Auer-Grumbach M, Olschewski A, Papić L, Kremer H, McEntagart ME, Uhrig S, et al. Alterations in the ankyrin domain of TRPV4 cause congenital distal SMA, scapuloperoneal SMA and HMSN2C. *Nat. Genet.* 2010; 42: 160–164.
- Baets J, Timmerman V. Inherited peripheral neuropathies: a myriad of genes and complex phenotypes. *Brain J. Neurol.* 2011; 134: 1587–1590.

- Bainbridge MN, Wang M, Wu Y, Newsham I, Muzny DM, Jefferies JL, et al. Targeted enrichment beyond the consensus coding DNA sequence exome reveals exons with higher variant densities. *Genome Biol.* 2011; 12: R68.
- Bamshad MJ, Ng SB, Bigham AW, Tabor HK, Emond MJ, Nickerson DA, et al. Exome sequencing as a tool for Mendelian disease gene discovery. *Nat. Rev. Genet.* 2011; 12: 745–755.
- Bansagi B, Antoniadi T, Burton-Jones S, Murphy SM, McHugh J, Alexander M, et al. Genotype/phenotype correlations in AARS-related neuropathy in a cohort of patients from the United Kingdom and Ireland. *J. Neurol.* 2015; 262: 1899–1908.
- Bansagi B, Griffin H, Ramesh V, Duff J, Pyle A, Chinnery PF, et al. The p.Ser107Leu in BICD2 is a mutation ‘hot spot’ causing distal spinal muscular atrophy. *Brain* 2015; 138: e391.
- Bansagi B, Griffin H, Whittaker RG, Antoniadi T, Evangelista T, Miller J, et al. Genetic heterogeneity of motor neuropathies. *Neurology* 2017; 88: 1226–1234.
- Bansagi B, Lewis-Smith D, Pal E, Duff J, Griffin H, Pyle A, et al. Phenotypic convergence of Menkes and Wilson disease. *Neurol. Genet.* 2016; 2: e119.
- Bennett MJ. Brown-Vialetto-Van Laere and Fazio Londe syndromes: defects of riboflavin transport with biochemical similarities to multiple acyl-CoA dehydrogenation defects (MADD). *J. Inherit. Metab. Dis.* 2012; 35: 941–942.
- Berciano J, Baets J, Gallardo E, Zimoń M, García A, López-Laso E, et al. Reduced penetrance in hereditary motor neuropathy caused by TRPV4 Arg269Cys mutation. *J. Neurol.* 2011; 258: 1413–1421.
- Berciano J, Sevilla T, Casasnovas C, Sivera R, Vílchez JJ, Infante J, et al. Guidelines for molecular diagnosis of Charcot-Marie-Tooth disease. *Neurologia* 2012; 27: 169–178.
- Berger P, Niemann A, Suter U. Schwann cells and the pathogenesis of inherited motor and sensory neuropathies (Charcot-Marie-Tooth disease). *Glia* 2006; 54: 243–257.
- Bergoffen J, Scherer SS, Wang S, Scott MO, Bone LJ, Paul DL, et al. Connexin mutations in X-linked Charcot-Marie-Tooth disease. *Science* 1993; 262: 2039–2042.

- Bernasconi A, Marino R, Ribas A, Rossi J, Ciaccio M, Oleastro M, et al. Characterization of immunodeficiency in a patient with growth hormone insensitivity secondary to a novel STAT5b gene mutation. *Pediatrics* 2006; 118: e1584–e1592.
- Blumkin L, Bradshaw T, Michelson M, Kopler T, Dahari D, Lerman-Sagie T, et al. Molecular and functional studies of retinal degeneration as a clinical presentation of SACS-related disorder. *Eur. J. Paediatr. Neurol.* 2015; 19: 472–476.
- Bodi K, Perera AG, Adams PS, Bintzler D, Dewar K, Grove DS, et al. Comparison of commercially available target enrichment methods for next-generation sequencing. *J. Biomol. Tech.* 2013; 24: 73–86.
- Bolino A, Piguet F, Alberizzi V, Pellegatta M, Rivellini C, Guerrero-Valero M, et al. Niacin-mediated Tace activation ameliorates CMT neuropathies with focal hypermyelination. *EMBO Mol. Med.* 2016; 8: 1438–1454.
- Bosch AM, Stroek K, Abeling NG, Waterham HR, IJlst L, Wanders RJ. The Brown-Vialetto-Van Laere and Fazio Londe syndrome revisited: natural history, genetics, treatment and future perspectives. *Orphanet J. Rare Dis.* 2012; 7: 1.
- Bouhy D, Timmerman V. Animal models and therapeutic prospects for Charcot-Marie-Tooth disease: Animal Models and CMT. *Ann. Neurol.* 2013; 74: 391–396.
- Braathen GJ. Genetic epidemiology of Charcot-Marie-Tooth disease. *Acta Neurol. Scand. Suppl.* 2012: iv-22.
- Buchert R, Uebe S, Radwan F, Tawamie H, Issa S, Shimazaki H, et al. Mutations in the mitochondrial gene C12ORF65 lead to syndromic autosomal recessive intellectual disability and show genotype phenotype correlation. *Eur. J. Med. Genet.* 2013; 56: 599–602.
- Caroppo P, Le Ber I, Clot F, Rivaud-Péchoux S, Camuzat A, De Septenville A, et al. DCTN1 mutation analysis in families with progressive supranuclear palsy-like phenotypes. *JAMA Neurol.* 2014; 71: 208.
- Carr AS, Polke JM, Wilson J, Pelayo-Negro AL, Laura M, Nanji T, et al. MFN2 deletion of exons 7 and 8: founder mutation in the UK population. *J. Peripher. Nerv. Syst.* 2015; 20: 67–71.

- Carra S, Sivilotti M, Chávez Zobel AT, Lambert H, Landry J. HspB8, a small heat shock protein mutated in human neuromuscular disorders, has in vivo chaperone activity in cultured cells. *Hum. Mol. Genet.* 2005; 14: 1659–1669.
- Casanova JL, Holland SM, Notarangelo LD. Inborn errors of human JAKs and STATs. *Immunity* 2012; 36: 515–528.
- Casasnovas C, Banchs I, Cassereau J, Gueguen N, Chevrollier A, Martínez-Matos JA, et al. Phenotypic spectrum of MFN2 mutations in the Spanish population. *J. Med. Genet.* 2010; 47: 249–256.
- Chaya T, Shibata S, Tokuhara Y, Yamaguchi W, Matsumoto H, Kawahara I, et al. Identification of a negative regulatory region for the exchange activity and characterization of T332I mutant of Rho guanine nucleotide exchange factor 10 (ARHGEF10). *J. Biol. Chem.* 2011; 286: 29511–29520.
- Cho TJ, Matsumoto K, Fano V, Dai J, Kim OH, Chae JH, et al. TRPV4-pathway manifesting both skeletal dysplasia and peripheral neuropathy: A report of three patients. *Am. J. Med. Genet. A.* 2012; 158A: 795–802.
- Choi BO, Nakhro K, Park HJ, Hyun YS, Lee JH, Kanwal S, et al. A cohort study of MFN2 mutations and phenotypic spectrums in Charcot-Marie-Tooth disease 2A patients. *Clin. Genet.* 2015; 87: 594–598.
- Chow CY, Landers JE, Bergren SK, Sapp PC, Grant AE, Jones JM, et al. Deleterious variants of FIG4, a phosphoinositide phosphatase, in patients with ALS. *Am. J. Hum. Genet.* 2009; 84: 85–88.
- Chow CY, Zhang Y, Dowling JJ, Jin N, Adamska M, Shiga K, et al. Mutation of FIG4 causes neurodegeneration in the pale tremor mouse and patients with CMT4J. *Nature* 2007; 448: 68–72.
- Christie KJ, Webber CA, Martinez JA, Singh B, Zochodne DW. PTEN inhibition to facilitate intrinsic regenerative outgrowth of adult peripheral axons. *J. Neurosci.* 2010; 30: 9306–9315.
- Chung KW, Kim SB, Park KD, Choi KG, Lee JH, Eun HW, et al. Early onset severe and late-onset mild Charcot-Marie-Tooth disease with mitofusin 2 (MFN2) mutations. *Brain* 2006; 129: 2103–2118.

- Chung KW, Suh BC, Cho SY, Choi SK, Kang SH, Yoo JH, et al. Early-onset Charcot-Marie-Tooth patients with mitofusin 2 mutations and brain involvement. *J. Neurol. Neurosurg. Psychiatry* 2010; 81: 1203–1206.
- Ciccolella M, Corti S, Catteruccia M, Petrini S, Tozzi G, Rizza T, et al. Riboflavin transporter 3 involvement in infantile Brown-Vialetto-Van Laere disease: two novel mutations. *J. Med. Genet.* 2013; 50: 104–107.
- Claeys KG, Züchner S, Kennerson M, Berciano J, Garcia A, Verhoeven K, et al. Phenotypic spectrum of dynamin 2 mutations in Charcot-Marie-Tooth neuropathy. *Brain* 2009; 132: 1741–1752.
- Coffey AJ, Durkie M, Hague S, McLay K, Emmerson J, Lo C, et al. A genetic study of Wilson's disease in the United Kingdom. *Brain* 2013; 136: 1476–1487.
- Cottenie E, Kochanski A, Jordanova A, Bansagi B, Zimon M, Horga A, et al. Truncating and missense mutations in IGHMBP2 cause Charcot-Marie Tooth disease type 2. *Am. J. Hum. Genet.* 2014; 95: 590–601.
- Danhauser K, Sauer SW, Haack TB, Wieland T, Staufner C, Graf E, et al. DHTKD1 mutations cause 2-aminoadipic and 2-oxoadipic aciduria. *Am. J. Hum. Genet.* 2012; 91: 1082–1087.
- Das I, Krzyzosiak A, Schneider K, Wrabetz L, D'Antonio M, Barry N, et al. Preventing proteostasis diseases by selective inhibition of a phosphatase regulatory subunit. *Science* 2015; 348: 239–242.
- Daud D, Griffin H, Douroudis K, Kleinle S, Eglon G, Pyle A, et al. Whole exome sequencing and the clinician: we need clinical skills and functional validation in variant filtering. *J. Neurol.* 2015; 262: 1673–1677.
- D'Aurizio R, Russo F, Chiavacci E, Baumgart M, Groth M, D'Onofrio M, et al. Discovering miRNA regulatory networks in Holt–Oram syndrome using a zebrafish model. *Front. Bioeng. Biotechnol.* 2016; 4: 60
- Dean FB, Hosono S, Fang L, Wu X, Faruqi AF, Bray-Ward P, et al. Comprehensive human genome amplification using multiple displacement amplification. *Proc. Natl. Acad. Sci. U. S. A.* 2002; 99: 5261–5266.

- Del Bo R, Locatelli F, Corti S, Scarlato M, Ghezzi S, Prella A, et al. Coexistence of CMT-2D and distal SMA-V phenotypes in an Italian family with a GARS gene mutation. *Neurology* 2006; 66: 752–754.
- Deng HX, Klein CJ, Yan J, Shi Y, Wu Y, Fecto F, et al. Scapuloperoneal spinal muscular atrophy and CMT2C are allelic disorders caused by alterations in TRPV4. *Nat. Genet.* 2010; 42: 165–169.
- Devic P, Petiot P, Mauguière F. Spinal Charcot-Marie-Tooth disease: a reappraisal. *Muscle Nerve* 2012; 46: 604–609.
- Dias RR, Albuquerque JM, Pereira AC, Stolf NAG, Krieger JE, Mady C, et al. Holt–Oram syndrome presenting as agenesis of the left pericardium. *Int. J. Cardiol.* 2007; 114: 98–100.
- Dierick I, Baets J, Irobi J, Jacobs A, De Vriendt E, Deconinck T, et al. Relative contribution of mutations in genes for autosomal dominant distal hereditary motor neuropathies: a genotype-phenotype correlation study. *Brain* 2008; 131: 1217–1227.
- DiVincenzo C, Elzinga CD, Medeiros AC, Karbassi I, Jones JR, Evans MC, et al. The allelic spectrum of Charcot-Marie-Tooth disease in over 17,000 individuals with neuropathy. *Mol. Genet. Genomic Med.* 2014; 2: 522–529.
- Dreßen M, Lahm H, Lahm A, Wolf K, Doppler S, Deutsch M, et al. A novel de novo TBX5 mutation in a patient with Holt–Oram syndrome leading to a dramatically reduced biological function. *Mol. Genet. Genomic Med.* 2016; 4: 557–567.
- Drew AP, Zhu D, Kidambi A, Ly C, Tey S, Brewer MH, et al. Improved inherited peripheral neuropathy genetic diagnosis by whole-exome sequencing. *Mol. Genet. Genomic Med.* 2015; 3: 143–154.
- Dyck PJ, Lambert EH. Lower motor and primary sensory neuron diseases with peroneal muscular atrophy. I. Neurologic, genetic, and electrophysiologic findings in hereditary polyneuropathies. *Arch. Neurol.* 1968a; 18: 603–618.
- Dyck PJ, Lambert EH. Lower motor and primary sensory neuron diseases with peroneal muscular atrophy. II. Neurologic, genetic, and electrophysiologic findings in various neuronal degenerations. *Arch. Neurol.* 1968b; 18: 619–625.

- Echaniz-Laguna A, Dubourg O, Carlier P, Carlier RY, Sabouraud P, Pereon Y, et al. Phenotypic spectrum and incidence of TRPV4 mutations in patients with inherited axonal neuropathy. *Neurology* 2014; 82: 1919–1926.
- Echaniz-Laguna A, Nicot AS, Carré S, Franques J, Tranchant C, Dondaine N, et al. Subtle central and peripheral nervous system abnormalities in a family with centronuclear myopathy and a novel dynamin 2 gene mutation. *Neuromuscul. Disord.* 2007; 17: 955–959.
- Ekenstedt KJ, Becker D, Minor KM, Shelton GD, Patterson EE, Bley T, et al. An ARHGEF10 deletion is highly associated with a juvenile-onset inherited polyneuropathy in Leonberger and Saint Bernard dogs. *PLoS Genet.* 2014; 10: e1004635.
- Engelfried K, Vorgerd M, Hagedorn M, Haas G, Gilles J, Epplen JT, et al. Charcot-Marie-Tooth neuropathy type 2A: novel mutations in the mitofusin 2 gene (MFN2). *BMC Med. Genet.* 2006; 7: 53.
- Ermanoska B, Motley WW, Leitão-Gonçalves R, Asselbergh B, Lee LH, De Rijk P, et al. CMT-associated mutations in glycyl- and tyrosyl-tRNA synthetases exhibit similar pattern of toxicity and share common genetic modifiers in *Drosophila*. *Neurobiol. Dis.* 2014; 68: 180–189.
- Eskuri JM, Stanley CM, Moore SA, Mathews KD. Infantile onset CMT2D/dSMA V in monozygotic twins due to a mutation in the anticodon-binding domain of GARS. *J. Peripher. Nerv. Syst.* 2012; 17: 132–134.
- Essers P, Tain LS, Nespital T, Goncalves J, Froehlich J, Partridge L. Reduced insulin/insulin-like growth factor signaling decreases translation in *Drosophila* and mice. *Sci. Rep.* 2016; 6: 30290.
- Evangelista T, Bansagi B, Pyle A, Griffin H, Douroudis K, Polvikoski T, et al. Phenotypic variability of TRPV4 related neuropathies. *Neuromuscul. Disord.* 2015; 25: 516–521.
- Everaerts W, Nilius B, Owsianik G. The vanilloid transient receptor potential channel TRPV4: from structure to disease. *Prog. Biophys. Mol. Biol.* 2010; 103: 2–17.
- Fang P, Kofoed EM, Little BM, Wang X, Ross RJM, Frank SJ, et al. A mutant signal transducer and activator of transcription 5b, associated with growth hormone

- insensitivity and insulin-like growth factor-I deficiency, cannot function as a signal transducer or transcription Factor. *J. Clin. Endocrinol. Metab.* 2006; 91: 1526–1534.
- Fawcett KA, Murphy SM, Polke JM, Wray S, Burchell VS, Manji H, et al. Comprehensive analysis of the TRPV4 gene in a large series of inherited neuropathies and controls. *J. Neurol. Neurosurg. Psychiatry* 2012; 83: 1204–1209.
- Feng J, Gou J, Jia J, Yi T, Cui T, Li Z. Verteporfin, a suppressor of YAP-TEAD complex, presents promising antitumor properties on ovarian cancer. *OncoTargets Ther.* 2016; 9: 5371–5381.
- Fiermonte G, Dolce V, Palmieri L, Ventura M, Runswick MJ, Palmieri F, et al. Identification of the human mitochondrial oxodicarboxylate carrier: Bacterial expression, reconstitution, functional characterization, tissue distribution, and chromosomal location. *J. Biol. Chem.* 2001; 276: 8225–8230.
- Fieten H, Gill Y, Martin AJ, Concilli M, Dirksen K, van Steenbeek FG, et al. The Menkes and Wilson disease genes counteract in copper toxicosis in Labrador retrievers: a new canine model for copper-metabolism disorders. *Dis. Model. Mech.* 2016; 9: 25–38.
- Fiorillo C, Moro F, Brisca G, Accogli A, Trucco F, Trovato R, et al. Beyond spinal muscular atrophy with lower extremity dominance: cerebellar hypoplasia associated with a novel mutation in BICD2. *Eur. J. Neurol.* 2016; 23: e19-21.
- Fiorillo C, Moro F, Brisca G, Astrea G, Nesti C, Bálint Z, et al. TRPV4 mutations in children with congenital distal spinal muscular atrophy. *Neurogenetics* 2012; 13: 195–203.
- Fiorillo C, Moro F, Yi J, Weil S, Brisca G, Astrea G, et al. Novel dynein DYNC1H1 neck and motor domain mutations link distal spinal muscular atrophy and abnormal cortical development. *Hum. Mutat.* 2014; 35: 298–302.
- Flet L, Polard E, Guillard O, Leray E, Allain H, Javaudin L, et al. 3,4-diaminopyridine safety in clinical practice: an observational, retrospective cohort study. *J. Neurol.* 2010; 257: 937–946.
- Foley AR, Menezes MP, Pandraud A, Gonzalez MA, Al-Odaib A, Abrams AJ, et al. Treatable childhood neuronopathy caused by mutations in riboflavin transporter RFVT2. *Brain* 2014; 137: 44–56.

- Foley C, Schofield I, Eglon G, Bailey G, Chinnery PF, Horvath R. Charcot-Marie-Tooth disease in Northern England. *J. Neurol. Neurosurg. Psychiatry* 2012; 83: 572–573.
- Francis MJ, Jones EE, Levy ER, Ponnambalam S, Chelly J, Monaco AP. A Golgi localization signal identified in the Menkes recombinant protein. *Hum. Mol. Genet.* 1998; 7: 1245–1252.
- Fu X, Zhang Y, Jiang W, Monnot AD, Bates CA, Zheng W. Regulation of copper transport crossing brain barrier systems by Cu-ATPases: effect of manganese exposure. *Toxicol. Sci.* 2014; 139: 432–451.
- Furey TS. Comparison of human (and other) genome browsers. *Hum. Genomics* 2006; 2: 266–270.
- Gambarotta G, Pascal D, Ronchi G, Morano M, Jager SB, Moimas S, et al. Local delivery of the Neuregulin1 receptor ecto-domain (ecto-ErbB4) has a positive effect on regenerated nerve fiber maturation. *Gene Ther.* 2015; 22: 901–907.
- Garrett CA, Barri M, Kuta A, Soura V, Deng W, Fisher EMC, et al. DYNC1H1 mutation alters transport kinetics and ERK1/2-cFos signalling in a mouse model of distal spinal muscular atrophy. *Brain* 2014; 137: 1883–1893.
- Gentil BJ, Cooper L. Molecular basis of axonal dysfunction and traffic impairments in CMT. *Brain Res. Bull.* 2012; 88: 444–453.
- Ghaoui R, Palmio J, Brewer J, Lek M, Needham M, Evilä A, et al. Mutations in HSPB8 causing a new phenotype of distal myopathy and motor neuropathy. *Neurology* 2016; 86: 391–398.
- Girard M, Larivière R, Parfitt DA, Deane EC, Gaudet R, Nossova N, et al. Mitochondrial dysfunction and Purkinje cell loss in autosomal recessive spastic ataxia of Charlevoix-Saguenay (ARSACS). *Proc. Natl. Acad. Sci. U. S. A.* 2012; 109: 1661–1666.
- Goebbels S, Oltrogge JH, Wolfer S, Wieser GL, Nientiedt T, Pieper A, et al. Genetic disruption of Pten in a novel mouse model of tomaculous neuropathy: Myelin pathology in conditional Pten mutant mice. *EMBO Mol. Med.* 2012; 4: 486–499.
- Goldfarb CA, Wall LB. Holt–Oram Syndrome. *J. Hand Surg.* 2014; 39: 1646–1648.

- Gonzalez M, Falk MJ, Gai X, Postrel R, Schüle R, Zuchner S. Innovative genomic collaboration using the GENESIS (GEM.app) platform. *Hum. Mutat.* 2015; 36: 950–956.
- Gonzalez M, McLaughlin H, Houlden H, Guo M, Yo-Tsen L, Hadjivassiliou M, et al. Exome sequencing identifies a significant variant in methionyl-tRNA synthetase (MARS) in a family with late-onset CMT2. *J. Neurol. Neurosurg. Psychiatry* 2013; 84: 1247–1249.
- Granados-Riveron JT, Pope M, Bu'Lock FA, Thornborough C, Eason J, Setchfield K, et al. Combined mutation screening of NKX2-5, GATA4, and TBX5 in congenital heart disease: multiple heterozygosity and novel mutations. *Congenit. Heart Dis.* 2012; 7: 151–159.
- Green P, Wiseman M, Crow YJ, Houlden H, Riphagen S, Lin JP, et al. Brown-Vialetto-Van Laere syndrome, a ponto-bulbar palsy with deafness, is caused by mutations in c20orf54. *Am. J. Hum. Genet.* 2010; 86: 485–489.
- Gregianin E, Vazza G, Scaramel E, Boaretto F, Vettori A, Leonardi E, et al. A novel SACS mutation results in non-ataxic spastic paraplegia and peripheral neuropathy. *Eur. J. Neurol.* 2013; 20: 1486–1491.
- Grice SJ, Sleigh JN, Motley WW, Liu JL, Burgess RW, Talbot K, et al. Dominant, toxic gain-of-function mutations in gars lead to non-cell autonomous neuropathology. *Hum. Mol. Genet.* 2015; 24: 4397–4406.
- Griffin LB, Sakaguchi R, McGuigan D, Gonzalez MA, Searby C, Züchner S, et al. Impaired function is a common feature of neuropathy-associated glycyl-tRNA synthetase mutations. *Hum. Mutat.* 2014; 35: 1363-1371.
- Groen EJM, Fumoto K, Blokhuis AM, Engelen-Lee J, Zhou Y, van den Heuvel DMA, et al. ALS-associated mutations in FUS disrupt the axonal distribution and function of SMN. *Hum. Mol. Genet.* 2013; 22: 3690–3704.
- Grohmann K. Characterization of Ighmbp2 in motor neurons and implications for the pathomechanism in a mouse model of human spinal muscular atrophy with respiratory distress type 1 (SMARD1). *Hum. Mol. Genet.* 2004; 13: 2031–2042.

- Grohmann K, Schuelke M, Diers A, Hoffmann K, Lucke B, Adams C, et al. Mutations in the gene encoding immunoglobulin mu-binding protein 2 cause spinal muscular atrophy with respiratory distress type 1. *Nat. Genet.* 2001; 29: 75–77.
- Grohmann K, Varon R, Stolz P, Schuelke M, Janetzki C, Bertini E, et al. Infantile spinal muscular atrophy with respiratory distress type 1 (SMARD1). *Ann. Neurol.* 2003; 54: 719–724.
- Guenther UP, Handoko L, Lagerbauer B, Jablonka S, Chari A, Alzheimer M, et al. IGHMBP2 is a ribosome-associated helicase inactive in the neuromuscular disorder distal SMA type 1 (DSMA1). *Hum. Mol. Genet.* 2009; 18: 1288–1300.
- Guenther UP, Schuelke M, Bertini E, D'Amico A, Goemans N, Grohmann K, et al. Genomic rearrangements at the IGHMBP2 gene locus in two patients with SMARD1. *Hum. Genet.* 2004; 115: 319–326.
- Gundersen CB, Umbach JA. Synaptotagmins 1 and 2 as mediators of rapid exocytosis at nerve terminals: The dyad hypothesis. *J. Theor. Biol.* 2013; 332: 149–160.
- Haberlová J, Mazanec R, Ridzoň P, Baránková L, Nürnberg G, Nürnberg P, et al. Phenotypic variability in a large Czech family with a dynamin 2-associated Charcot-Marie-Tooth neuropathy. *J. Neurogenet.* 2011; 25: 182–188.
- Hagen J, te Brinke H, Wanders RJA, Knecht AC, Oussoren E, Hooijboom AJM, et al. Genetic basis of alpha-aminoacidic and alpha-ketoacidic aciduria. *J. Inher. Metab. Dis.* 2015; 38: 873–879.
- Han J, Gagnon S, Eckle T, Borchers CH. Metabolomic analysis of key central carbon metabolism carboxylic acids as their 3-nitrophenylhydrazones by UPLC/ESI-MS. *Electrophoresis* 2013; 34: 2891–2900.
- Harding AE. Molecular genetics and clinical aspects of inherited disorders of nerve and muscle. *Curr. Opin. Neurol. Neurosurg.* 1992; 5: 600–604.
- Harding AE, Thomas PK. The clinical features of hereditary motor and sensory neuropathy types I and II. *Brain* 1980; 103: 259–280.

- Harms MB, Ori-McKenney KM, Scoto M, Tuck EP, Bell S, Ma D, et al. Mutations in the tail domain of DYNC1H1 cause dominant spinal muscular atrophy. *Neurology* 2012; 78: 1714–1720.
- Hawkins PT, Stephens LR. Emerging evidence of signalling roles for PI(3,4)P2 in Class I and II PI3K-regulated pathways. *Biochem. Soc. Trans.* 2016; 44: 307–314.
- Hayasaka K, Himoro M, Sato W, Takada G, Uyemura K, Shimizu N, et al. Charcot-Marie-Tooth neuropathy type 1B is associated with mutations of the myelin P0 gene. *Nat. Genet.* 1993; 5: 31–34.
- He W, Bai G, Zhou H, Wei N, White NM, Lauer J, et al. CMT2D neuropathy is linked to the neomorphic binding activity of glycyl-tRNA synthetase. *Nature* 2015; 526: 710–714.
- Heidary G, Calderwood L, Cox GF, Robson CD, Teot LA, Mullon J, et al. Optic atrophy and a Leigh-like syndrome due to mutations in the C12orf65 gene: report of a novel mutation and review of the literature. *J. Neuroophthalmol.* 2014; 34: 39–43.
- Heiner CR, Hunkapiller KL, Chen S-M, Glass JI, Chen EY. Sequencing multimegabase-template DNA with BigDye terminator chemistry. *Genome Res.* 1998; 8: 557–561.
- Heinritz W, Shou L, Moschik A, Froster UG. The human TBX5 gene mutation database. *Hum. Mutat.* 2005; 26: 397.
- Herrmann DN, Horvath R, Sowden JE, Gonzales M, Sanchez-Mejias A, Guan Z, et al. Synaptotagmin 2 mutations cause an autosomal-dominant form of Lambert-Eaton myasthenic syndrome and nonprogressive motor neuropathy. *Am. J. Hum. Genet.* 2014; 95: 332–339.
- Høyer H, Braathen GJ, Busk ØL, Holla ØL, Svendsen M, Hilmarsen HT, et al. Genetic diagnosis of Charcot-Marie-Tooth disease in a population by next-generation sequencing. *BioMed Res. Int.* 2014; 2014: 1–13.
- Hung JH, Weng Z. Designing Polymerase Chain Reaction primers using Primer3Plus. *Cold Spring Harb. Protoc.* 2016; pdb.prot093096.
- Hurd L, Kirwin SM, Boggs M, Mackenzie WG, Bober MB, Funanage VL, et al. A mutation in TRPV4 results in altered chondrocyte calcium signaling in severe metatropic dysplasia. *Am. J. Med. Genet. A.* 2015; 167A: 2286–2293.

- Hwa V, Little B, Adiyaman P, Kofoed EM, Pratt KL, Ocal G, et al. Severe growth hormone insensitivity resulting from total absence of signal transducer and activator of transcription 5b. *J. Clin. Endocrinol. Metab.* 2005; 90: 4260–4266.
- Irobi J, Almeida-Souza L, Asselbergh B, De Winter V, Goethals S, Dierick I, et al. Mutant HSPB8 causes motor neuron-specific neurite degeneration. *Hum. Mol. Genet.* 2010; 19: 3254–3265.
- Irobi J, De Jonghe P, Timmerman V. Molecular genetics of distal hereditary motor neuropathies. *Hum. Mol. Genet.* 2004; 13 Spec No 2: R195-202.
- Irobi J, Dierick I, Jordanova A, Claeys KG, De Jonghe P, Timmerman V. Unraveling the genetics of distal hereditary motor neuropathies. *Neuromolecular Med.* 2006; 8: 131–146.
- Irobi J, Van Impe K, Seeman P, Jordanova A, Dierick I, Verpoorten N, et al. Hot-spot residue in small heat-shock protein 22 causes distal motor neuropathy. *Nat. Genet.* 2004; 36: 597–601.
- James PA, Cader MZ, Muntoni F, Childs AM, Crow YJ, Talbot K. Severe childhood SMA and axonal CMT due to anticodon binding domain mutations in the GARS gene. *Neurology* 2006; 67: 1710–1712.
- Jędrzejowska M, Madej-Pilarczyk A, Fidziańska A, Mierzewska H, Pronicka E, Obersztyn E, et al. Severe phenotypes of SMARD1 associated with novel mutations of the IGHMBP2 gene and nuclear degeneration of muscle and Schwann cells. *Eur. J. Paediatr. Neurol.* 2014; 18: 183–192.
- Johnson JO, Gibbs JR, Megarbane A, Urtizberea JA, Hernandez DG, Foley AR, et al. Exome sequencing reveals riboflavin transporter mutations as a cause of motor neuron disease. *Brain* 2012; 135: 2875–2882.
- Jonghe PD, Timmerman V, Broeckhoven CV. 2nd Workshop of the European CMT Consortium: 53rd ENMC International Workshop on Classification and Diagnostic Guidelines for Charcot-Marie-Tooth Type 2 (CMT2–HMSN II) and Distal Hereditary Motor Neuropathy (Distal HMN–Spinal CMT). *Neuromuscul. Disord.* 1998; 8: 426–431.

- Jordanova A, Irobi J, Thomas FP, Van Dijck P, Meerschaert K, Dewil M, et al. Disrupted function and axonal distribution of mutant tyrosyl-tRNA synthetase in dominant intermediate Charcot-Marie-Tooth neuropathy. *Nat. Genet.* 2006; 38: 197–202.
- Juárez P, Palau F. Neural and molecular features on Charcot-Marie-Tooth disease plasticity and therapy. *Neural Plast.* 2012; 2012: 171636.
- Kagiava A, Sargiannidou I, Theophilidis G, Karaiskos C, Richter J, Bashiardes S, et al. Intrathecal gene therapy rescues a model of demyelinating peripheral neuropathy. *Proc. Natl. Acad. Sci. U. S. A.* 2016; 113: e2421-2429.
- Kaler SG. ATP7A-related copper transport diseases - emerging concepts and future trends. *Nat. Rev. Neurol.* 2011; 7: 15–29.
- Kaler SG. Translational research investigations on ATP7A: an important human copper ATPase: Translational research investigations on ATP7A. *Ann. N. Y. Acad. Sci.* 2014; 1314: 64–68.
- Kaler SG, Gallo LK, Proud VK, Percy AK, Mark Y, Segal NA, et al. Occipital horn syndrome and a mild Menkes phenotype associated with splice site mutations at the MNK locus. *Nat. Genet.* 1994; 8: 195–202.
- Kalita A, Gupta S, Singh P, Surolia A, Banerjee K. IGF-1 stimulated upregulation of cyclin D1 is mediated via STAT5 signaling pathway in neuronal cells. *IUBMB Life* 2013; 65: 462–471.
- Katz B, Miledi R. A study of synaptic transmission in the absence of nerve impulses. *J. Physiol.* 1967; 192: 407–436.
- Katz B, Miledi R. The role of calcium in neuromuscular facilitation. *J. Physiol.* 1968; 195: 481–492.
- Kennerson ML, Nicholson GA, Kaler SG, Kowalski B, Mercer JFB, Tang J, et al. Missense mutations in the copper transporter gene ATP7A cause X-linked distal hereditary motor neuropathy. *Am. J. Hum. Genet.* 2010; 86: 343–352.
- Klein CJ, Kimmel GW, Pittock SJ, Engelstad JE, Cunningham JM, Wu Y, et al. Large kindred evaluation of mitofusin 2 novel mutation, extremes of neurologic presentations, and preserved nerve mitochondria. *Arch. Neurol.* 2011; 68: 1295–1302.

- Klein CJ, Middha S, Duan X, Wu Y, Litchy WJ, Gu W, et al. Application of whole exome sequencing in undiagnosed inherited polyneuropathies. *J. Neurol. Neurosurg. Psychiatry* 2014; 85: 1265–1272.
- Kochubey O, Lou X, Schneggenburger R. Regulation of transmitter release by Ca²⁺ and synaptotagmin: insights from a large CNS synapse. *Trends Neurosci.* 2011; 34: 237–246.
- Kofoed EM, Hwa V, Little B, Woods KA, Buckway CK, Tsubaki J, et al. Growth hormone insensitivity associated with a STAT5b mutation. *N. Engl. J. Med.* 2003; 349: 1139–1147.
- Kreis P, Leondaritis G, Lieberam I, Eickholt BJ. Subcellular targeting and dynamic regulation of PTEN: implications for neuronal cells and neurological disorders. *Front. Mol. Neurosci.* 2014; 7: 23
- Kwok AS, Phadwal K, Turner BJ, Oliver PL, Raw A, Simon AK, et al. HspB8 mutation causing hereditary distal motor neuropathy impairs lysosomal delivery of autophagosomes. *J. Neurochem.* 2011; 119: 1155–1161.
- Landouré G, Zdebik AA, Martinez TL, Burnett BG, Stanescu HC, Inada H, et al. Mutations in TRPV4 cause Charcot-Marie-Tooth disease type 2C. *Nat. Genet.* 2010; 42: 170–174.
- Lapin V, Mighion LC, da Silva CP, Cuperus Y, Bean LJH, Hegde MR. Regulating whole exome sequencing as a diagnostic test. *Hum. Genet.* 2016; 135: 655–673.
- Latour P, Thauvin-Robinet C, Baudelet-Méry C, Soichot P, Cusin V, Faivre L, et al. A major determinant for binding and aminoacylation of tRNA^{Ala} in cytoplasmic alanyl-tRNA synthetase is mutated in dominant axonal Charcot-Marie-Tooth Disease. *Am. J. Hum. Genet.* 2010; 86: 77–82.
- Lelieveld SH, Spielmann M, Mundlos S, Veltman JA, Gilissen C. Comparison of exome and genome sequencing technologies for the complete capture of protein-coding regions. *Hum. Mutat.* 2015; 36: 815–822.
- Leslie NR, Longy M. Inherited PTEN mutations and the prediction of phenotype. *Semin. Cell Dev. Biol.* 2016; 52: 30–38.

- Li H, Durbin R. Fast and accurate short read alignment with Burrows-Wheeler transform. *Bioinforma. Oxf. Engl.* 2009; 25: 1754–1760.
- Li H, Marshall AJ. Phosphatidylinositol (3,4) bisphosphate-specific phosphatases and effector proteins: A distinct branch of PI3K signaling. *Cell. Signal.* 2015; 27: 1789–1798.
- Li J. Inherited Neuropathies. *Semin. Neurol.* 2012; 32: 204–214.
- Lin KP, Soong BW, Yang CC, Huang LW, Chang MH, Lee IH, et al. The mutational spectrum in a cohort of Charcot-Marie-Tooth disease type 2 among the Han Chinese in Taiwan. *PLoS ONE* 2011; 6: e29393.
- Lin RC, Scheller RH. Mechanisms of synaptic vesicle exocytosis. *Annu. Rev. Cell Dev. Biol.* 2000; 16: 19–49.
- Lopez-Anido C, Poitelon Y, Gopinath C, Moran JJ, Ma KH, Law WD, et al. Tead1 regulates the expression of Peripheral Myelin Protein 22 during Schwann cell development. *Hum. Mol. Genet.* 2016; 25: 3055–3069.
- Lorenz TC. Polymerase chain reaction: basic protocol plus troubleshooting and optimization strategies. *J. Vis. Exp.* 2012; 63: e3998.
- Lupski JR, de Oca-Luna RM, Slaugenhaupt S, Pentao L, Guzzetta V, Trask BJ, et al. DNA duplication associated with Charcot-Marie-Tooth disease type 1A. *Cell* 1991; 66: 219–232.
- MacArthur DG, Manolio TA, Dimmock DP, Rehm HL, Shendure J, Abecasis GR, et al. Guidelines for investigating causality of sequence variants in human disease. *Nature* 2014; 508: 469–476.
- Mace J, Reddy S, Mohil R. Atypical carpal tunnel syndrome in a holt oram patient: a case report and literature review. *Open Orthop. J.* 2014; 8: 462–465.
- Mackler JM, Drummond JA, Loewen CA, Robinson IM, Reist NE. The C(2)B Ca(2+)-binding motif of synaptotagmin is required for synaptic transmission in vivo. *Nature* 2002; 418: 340–344.
- Maguire S, Estabel J, Ingham N, Pearson S, Ryder E, Carragher DM, et al. Targeting of Slc25a21 is associated with orofacial defects and otitis media due to disrupted expression of a neighbouring gene. *PLoS ONE* 2014; 9: e91807.

- Malissov N, Griffin LB, Antonellis A, Beis D. Dimerization is required for GARS-mediated neurotoxicity in dominant CMT disease. *Hum. Mol. Genet.* 2016; 25: 1528–1542.
- Mardis E, McCombie WR. Preparing Polymerase Chain Reaction (PCR) products for capillary sequencing. *Cold Spring Harb. Protoc.* 2016
- Martikainen MH, Kytövuori L, Majamaa K. Novel mitofusin 2 splice-site mutation causes Charcot-Marie-Tooth disease type 2 with prominent sensory dysfunction. *Neuromuscul. Disord.* 2014; 24: 360–364.
- McDermott DA, Bressan MC, He J, Lee JS, Aftimos S, Brueckner M, et al. TBX5 genetic testing validates strict clinical criteria for Holt-Oram syndrome. *Pediatr. Res.* 2005; 58: 981–986.
- McEntagart M. TRPV4 axonal neuropathy spectrum disorder. *J. Clin. Neurosci.* 2012; 19: 927–933.
- McLaughlin HM, Sakaguchi R, Giblin W, NIH Intramural Sequencing Center, Wilson TE, Biesecker L, et al. A recurrent loss-of-function alanyl-tRNA synthetase (AARS) mutation in patients with Charcot-Marie-Tooth disease type 2N (CMT2N). *Hum. Mutat.* 2012; 33: 244–253.
- McLaughlin HM, Sakaguchi R, Liu C, Igarashi T, Pehlivan D, Chu K, et al. Compound heterozygosity for loss-of-function lysyl-tRNA synthetase mutations in a patient with peripheral neuropathy. *Am. J. Hum. Genet.* 2010; 87: 560–566.
- Mensah LB, Davison C, Fan SJ, Morris JF, Goberdhan DCI, Wilson C. Fine-tuning of PI3K/AKT signalling by the tumour suppressor PTEN is required for maintenance of flight muscle function and mitochondrial integrity in ageing adult *Drosophila melanogaster*. *PLOS ONE* 2015; 10: e0143818.
- Merner N, Dion P, Rouleau G. Recent advances in the genetics of distal hereditary motor neuropathy give insight to a disease mechanism involving copper homeostasis that may extend to other motor neuron disorders. *Clin. Genet.* 2011; 79: 23–34.
- Mohl M, Winkler S, Wieland T, Lutz S. Gef10 - the third member of a Rho-specific guanine nucleotide exchange factor subfamily with unusual protein architecture. *Naunyn. Schmiedeberg Arch. Pharmacol.* 2006; 373: 333–341.

- Møller LB. Small amounts of functional ATP7A protein permit mild phenotype. *J. Trace Elem. Med. Biol.* 2015; 31: 173–177.
- Moloney EB, de Winter F, Verhaagen J. ALS as a distal axonopathy: molecular mechanisms affecting neuromuscular junction stability in the presymptomatic stages of the disease. *Front. Neurosci.* 2014; 8: 252.
- Montenegro G, Powell E, Huang J, Speziani F, Edwards YJK, Beecham G, et al. Exome sequencing allows for rapid gene identification in a Charcot-Marie-Tooth family. *Ann. Neurol.* 2011; 69: 464–470.
- Motley WW, Griffin LB, Mademan I, Baets J, De Vriendt E, De Jonghe P, et al. A novel AARS mutation in a family with dominant myeloneuropathy. *Neurology* 2015; 84: 2040–2047.
- Motley WW, Seburn KL, Nawaz MH, Miers KE, Cheng J, Antonellis A, et al. Charcot-Marie-Tooth–linked mutant GARS is toxic to peripheral neurons independent of wild-type GARS levels. *PLoS Genet.* 2011; 7: e1002399.
- Motley WW, Talbot K, Fischbeck KH. GARS axonopathy: not every neuron’s cup of tRNA. *Trends Neurosci.* 2010; 33: 59–66.
- Murphy SM, Herrmann DN, McDermott MP, Scherer SS, Shy ME, Reilly MM, et al. Reliability of the CMT neuropathy score (second version) in Charcot-Marie-Tooth disease. *J. Peripher. Nerv. Syst.* 2011; 16: 191–198.
- Murphy SM, Laura M, Fawcett K, Pandraud A, Liu YT, Davidson GL, et al. Charcot-Marie-Tooth disease: frequency of genetic subtypes and guidelines for genetic testing. *J. Neurol. Neurosurg. Psychiatry* 2012; 83: 706–710.
- Nakajima H, Brindle PK, Handa M, Ihle JN. Functional interaction of STAT5 and nuclear receptor co-repressor SMRT: implications in negative regulation of STAT5-dependent transcription. *EMBO J.* 2001; 20: 6836–6844.
- Nakhro K, Park JM, Kim YJ, Yoon BR, Yoo JH, Koo H, et al. A novel Lys141Thr mutation in small heat shock protein 22 (HSPB8) gene in Charcot-Marie-Tooth disease type 2L. *Neuromuscul. Disord.* 2013; 23: 656–663.

- Nangle LA, Zhang W, Xie W, Yang XL, Schimmel P. Charcot–Marie–Tooth disease-associated mutant tRNA synthetases linked to altered dimer interface and neurite distribution defect. *Proc. Natl. Acad. Sci.* 2007; 104: 11239–11244.
- Neveling K, Martinez-Carrera LA, Hölker I, Heister A, Verrips A, Hosseini-Barkooie SM, et al. Mutations in BICD2, which encodes a golgin and important motor adaptor, cause congenital autosomal-dominant spinal muscular atrophy. *Am. J. Hum. Genet.* 2013; 92: 946–954.
- Nguyen HN, Yang Jr JM, Rahdar M, Keniry M, Swaney KF, Parsons R, et al. A new class of cancer-associated PTEN mutations defined by membrane translocation defects. *Oncogene* 2015; 34: 3737–3743.
- Nicholson GA, Magdelaine C, Zhu D, Grew S, Ryan MM, Sturtz F, et al. Severe early-onset axonal neuropathy with homozygous and compound heterozygous MFN2 mutations. *Neurology* 2008; 70: 1678–1681.
- Niehues S, Bussmann J, Steffes G, Erdmann I, Köhrer C, Sun L, et al. Impaired protein translation in *Drosophila* models for Charcot–Marie–Tooth neuropathy caused by mutant tRNA synthetases. *Nat. Commun.* 2015; 6: 7520.
- Niemann A, Berger P, Suter U. Pathomechanisms of mutant proteins in Charcot-Marie-Tooth disease. *NeuroMolecular Med.* 2006; 8: 217–241.
- Nilius B, Owsianik G. Channelopathies converge on TRPV4. *Nat. Genet.* 2010; 42: 98–100.
- Nilius B, Voets T. The puzzle of TRPV4 channelopathies. *EMBO Rep.* 2013; 14: 152–163.
- Norwood FLM, Harling C, Chinnery PF, Eagle M, Bushby K, Straub V. Prevalence of genetic muscle disease in Northern England: in-depth analysis of a muscle clinic population. *Brain* 2009; 132: 3175–3186.
- Oates EC, Rossor AM, Hafezparast M, Gonzalez M, Speziani F, MacArthur DG, et al. Mutations in BICD2 cause dominant congenital spinal muscular atrophy and hereditary spastic paraplegia. *Am. J. Hum. Genet.* 2013; 92: 965–973.
- Paddock BE, Striegel AR, Hui E, Chapman ER, Reist NE. Ca²⁺-Dependent, phospholipid-binding residues of synaptotagmin are critical for excitation-secretion coupling in vivo. *J. Neurosci.* 2008; 28: 7458–7466.

- Paddock BE, Wang Z, Biela LM, Chen K, Getzy MD, Striegel A, et al. Membrane penetration by synaptotagmin is required for coupling calcium binding to vesicle fusion in vivo. *J. Neurosci. Off. J. Soc. Neurosci.* 2011; 31: 2248–2257.
- Palmieri F. The mitochondrial transporter family SLC25: Identification, properties and physiopathology. *Mol. Aspects Med.* 2013; 34: 465–484.
- Pang ZP, Melicoff E, Padgett D, Liu Y, Teich AF, Dickey BF, et al. Synaptotagmin-2 is essential for survival and contributes to Ca²⁺ triggering of neurotransmitter release in central and neuromuscular synapses. *J. Neurosci.* 2006; 26: 13493–13504.
- Pareyson D, Saveri P, Sagnelli A, Piscosquito G. Mitochondrial dynamics and inherited peripheral nerve diseases. *Neurosci. Lett.* 2015; 596: 66–77.
- Pareyson D, Scaioli V, Laurà M. Clinical and electrophysiological aspects of Charcot-Marie-Tooth disease. *NeuroMolecular Med.* 2006; 8: 3–22.
- Passage E, Norreel JC, Noack-Fraissignes P, Sanguedolce V, Pizant J, Thirion X, et al. Ascorbic acid treatment corrects the phenotype of a mouse model of Charcot-Marie-Tooth disease. *Nat. Med.* 2004; 10: 396–401.
- Pearn J, Hudgson P. Distal spinal muscular atrophy. A clinical and genetic study of 8 kindreds. *J. Neurol. Sci.* 1979; 43: 183–191.
- Peeters K, Bervoets S, Chamova T, Litvinenko I, De Vriendt E, Bichev S, et al. Novel mutations in the DYNC1H1 tail domain refine the genetic and clinical spectrum of dyneinopathies. *Hum. Mutat.* 2015; 36: 287–291.
- Peeters K, Chamova T, Jordanova A. Clinical and genetic diversity of SMN1-negative proximal spinal muscular atrophies. *Brain* 2014; 137: 2879–2896.
- Peeters K, Litvinenko I, Asselbergh B, Almeida-Souza L, Chamova T, Geuens T, et al. Molecular defects in the motor adaptor BICD2 cause proximal spinal muscular atrophy with autosomal-dominant inheritance. *Am. J. Hum. Genet.* 2013; 92: 955–964.
- Philippakis AA, Azzariti DR, Beltran S, Brookes AJ, Brownstein CA, Brudno M, et al. The Matchmaker Exchange: A platform for rare disease gene discovery. *Hum. Mutat.* 2015; 36: 915–921.

- Pilarski R, Burt R, Kohlman W, Pho L, Shannon KM, Swisher E. Cowden syndrome and the PTEN hamartoma tumor syndrome: systematic review and revised diagnostic criteria. *J. Natl. Cancer Inst.* 2013; 105: 1607–1616.
- Pilliod J, Moutton S, Lavie J, Maurat E, Hubert C, Bellance N, et al. New practical definitions for the diagnosis of autosomal recessive spastic ataxia of Charlevoix-Saguenay. *Ann. Neurol.* 2015; 78: 871–886.
- de Planell-Saguer M, Schroeder DG, Rodicio MC, Cox GA, Mourelatos Z. Biochemical and genetic evidence for a role of IGHMBP2 in the translational machinery. *Hum. Mol. Genet.* 2009; 18: 2115–2126.
- Porro F, Rinchetti P, Magri F, Riboldi G, Nizzardo M, Simone C, et al. The wide spectrum of clinical phenotypes of spinal muscular atrophy with respiratory distress type 1: A systematic review. *J. Neurol. Sci.* 2014; 346: 35–42.
- Protasova MS, Grigorenko AP, Tyazhelova TV, Andreeva TV, Reshetov DA, Gusev FE, et al. Whole-genome sequencing identifies a novel ABCB7 gene mutation for X-linked congenital cerebellar ataxia in a large family of Mongolian ancestry. *Eur. J. Hum. Genet. EJHG* 2016; 24: 550–555.
- Pugliese-Pires PN, Tonelli CA, Dora JM, Silva PCA, Czepielewski M, Simoni G, et al. A novel STAT5B mutation causing GH insensitivity syndrome associated with hyperprolactinemia and immune dysfunction in two male siblings. *Eur. J. Endocrinol.* 2010; 163: 349–355.
- Puls I, Jonnakuty C, LaMonte BH, Holzbaur ELF, Tokito M, Mann E, et al. Mutant dynactin in motor neuron disease. *Nat. Genet.* 2003; 33: 455–456.
- Puls I, Oh SJ, Sumner CJ, Wallace KE, Floeter MK, Mann EA, et al. Distal spinal and bulbar muscular atrophy caused by dynactin mutation. *Ann. Neurol.* 2005; 57: 687–694.
- Pyle A, Griffin H, Yu-Wai-Man P, Duff J, Eglon G, Pickering-Brown S, et al. Prominent sensorimotor neuropathy due to SACS mutations revealed by whole-exome sequencing. *Arch. Neurol.* 2012; 69: 1351–1354.
- Pyle A, Ramesh V, Bartsakoulia M, Boczonadi V, Gomez-Duran A, Herczegfalvi A, et al. Behr's syndrome is typically associated with disturbed mitochondrial translation and mutations in the C12orf65 gene. *J. Neuromuscul. Dis.* 2014; 1: 55–63.

- Pyle A, Smertenko T, Bargiela D, Griffin H, Duff J, Appleton M, et al. Exome sequencing in undiagnosed inherited and sporadic ataxias. *Brain* 2015; 138: 276–283.
- Qiu H, Lee S, Shang Y, Wang WY, Au KF, Kamiya S, et al. ALS-associated mutation FUS-R521C causes DNA damage and RNA splicing defects. *J. Clin. Invest.* 2014; 124: 981–999.
- Raeymaekers P, Timmerman V, Nelis E, De Jonghe P, Hoogendijk JE, Baas F, et al. Duplication in chromosome 17p11.2 in Charcot-Marie-Tooth neuropathy type 1a (CMT 1a). The HMSN Collaborative Research Group. *Neuromuscul. Disord.* 1991; 1: 93–97.
- Ravenscroft G, Di Donato N, Hahn G, Davis MR, Craven PD, Poke G, et al. Recurrent de novo BICD2 mutation associated with arthrogryposis multiplex congenita and bilateral perisylvian polymicrogyria. *Neuromuscul. Disord.* 2016; 26: 744–748.
- Rehm HL, Bale SJ, Bayrak-Toydemir P, Berg JS, Brown KK, Deignan JL, et al. ACMG clinical laboratory standards for next-generation sequencing. *Genet. Med.* 2013; 15: 733–747.
- Reilly MM, Murphy SM, Laurá M. Charcot-Marie-Tooth disease. *J. Peripher. Nerv. Syst.* 2011; 16: 1–14.
- Reilly MM, Shy ME. Diagnosis and new treatments in genetic neuropathies. *J. Neurol. Neurosurg. Psychiatry* 2009; 80: 1304–1314.
- Roberts AJ, Kon T, Knight PJ, Sutoh K, Burgess SA. Functions and mechanics of dynein motor proteins. *Nat. Rev. Mol. Cell Biol.* 2013; 14: 713–726.
- Roberts RC. The Charcot-Marie-Tooth diseases: how can we identify and develop novel therapeutic targets? *Brain* 2012; 135: 3527–3528.
- Rodriguez-Escudero I, Oliver MD, Andres-Pons A, Molina M, Cid VJ, Pulido R. A comprehensive functional analysis of PTEN mutations: implications in tumor- and autism-related syndromes. *Hum. Mol. Genet.* 2011; 20: 4132–4142.
- Rosenblum BB, Lee LG, Spurgeon SL, Khan SH, Menchen SM, Heiner CR, et al. New dye-labeled terminators for improved DNA sequencing patterns. *Nucleic Acids Res.* 1997; 25: 4500–4504.

- Rossor AM, Evans MRB, Reilly MM. A practical approach to the genetic neuropathies. *Pract. Neurol.* 2015; 15: 187–198.
- Rossor AM, Kalmar B, Greensmith L, Reilly MM. The distal hereditary motor neuropathies. *J. Neurol. Neurosurg. Psychiatry* 2012; 83: 6–14.
- Rossor AM, Oates EC, Salter HK, Liu Y, Murphy SM, Schule R, et al. Phenotypic and molecular insights into spinal muscular atrophy due to mutations in BICD2. *Brain* 2015a; 138: 293–310.
- Rossor AM, Oates EC, Salter HK, Liu Y, Murphy SM, Schule R, et al. Reply: The p.Ser107Leu in BICD2 is a mutation ‘hot spot’ causing distal spinal muscular atrophy. *Brain* 2015b; 138: e392–e392.
- Rossor AM, Polke JM, Houlden H, Reilly MM. Clinical implications of genetic advances in Charcot-Marie-Tooth disease. *Nat. Rev. Neurol.* 2013; 9: 562–571.
- Rossor AM, Tomaselli PJ, Reilly MM. Recent advances in the genetic neuropathies. *Curr. Opin. Neurol.* 2016; 29: 537–548.
- Ruderfer DM, Hamamsy T, Lek M, Karczewski KJ, Kavanagh D, Samocha KE, et al. Patterns of genic intolerance of rare copy number variation in 59,898 human exomes. *Nat. Genet.* 2016; 48: 1107–1111.
- Safka Brozkova D, Deconinck T, Beth Griffin L, Ferbert A, Haberlova J, Mazanec R, et al. Loss of function mutations in HARS cause a spectrum of inherited peripheral neuropathies. *Brain* 2015; 138: 2161–2172.
- Salgado D, Bellgard MI, Desvignes JP, Bérout C. How to identify pathogenic mutations among all those variations: variant annotation and filtration in the genome sequencing era. *Hum. Mutat.* 2016; 37: 1272–1282.
- Sanger F, Nicklen S, Coulson AR. DNA sequencing with chain-terminating inhibitors. *Proc. Natl. Acad. Sci. U. S. A.* 1977; 74: 5463–5467.
- Saporta ASD, Sottile SL, Miller LJ, Feely SME, Siskind CE, Shy ME. Charcot-Marie-Tooth disease subtypes and genetic testing strategies. *Ann. Neurol.* 2011; 69: 22–33.

- Sawyer SL, Cheuk-Him Ng A, Innes AM, Wagner JD, Dymment DA, Tetreault M, et al. Homozygous mutations in MFN2 cause multiple symmetric lipomatosis associated with neuropathy. *Hum. Mol. Genet.* 2015; 24: 5109–5114.
- Scaglia PA, Martínez AS, Feigerlová E, Bezrodnik L, Gaillard MI, Di Giovanni D, et al. A novel missense mutation in the SH2 domain of the STAT5B gene results in a transcriptionally inactive STAT5b associated with severe IGF-I deficiency, immune dysfunction, and lack of pulmonary disease. *J. Clin. Endocrinol. Metab.* 2012; 97: e830-839.
- Scoto M, Rossor AM, Harms MB, Cirak S, Calissano M, Robb S, et al. Novel mutations expand the clinical spectrum of DYNC1H1-associated spinal muscular atrophy. *Neurology* 2015; 84: 668–679.
- Seburn KL, Nangle LA, Cox GA, Schimmel P, Burgess RW. An active dominant mutation of glycyl-tRNA synthetase causes neuropathy in a Charcot-Marie-Tooth 2D mouse model. *Neuron* 2006; 51: 715–726.
- Sevilla T, Lupo V, Martínez-Rubio D, Sancho P, Sivera R, Chumillas MJ, et al. Mutations in the MORC2 gene cause axonal Charcot-Marie-Tooth disease. *Brain* 2016; 139: 62–72.
- Shigemizu D, Momozawa Y, Abe T, Morizono T, Boroevich KA, Takata S, et al. Performance comparison of four commercial human whole-exome capture platforms. *Sci. Rep.* 2015; 5: 12742.
- Shimazaki H, Takiyama Y, Ishiura H, Sakai C, Matsushima Y, Hatakeyama H, et al. A homozygous mutation of C12orf65 causes spastic paraplegia with optic atrophy and neuropathy (SPG55). *J. Med. Genet.* 2012; 49: 777–784.
- Shinde SR, Maddika S. PTEN modulates EGFR late endocytic trafficking and degradation by dephosphorylating Rab7. *Nat. Commun.* 2016; 7: 10689.
- Sidiropoulos PNM, Mieke M, Bock T, Tinelli E, Oertli CI, Kuner R, et al. Dynamin 2 mutations in Charcot-Marie-Tooth neuropathy highlight the importance of clathrin-mediated endocytosis in myelination. *Brain* 2012; 135: 1395–1411.
- Simons C, Griffin LB, Helman G, Golas G, Pizzino A, Bloom M, et al. Loss-of-function alanyl-tRNA synthetase mutations cause an autosomal-recessive early-onset epileptic

- encephalopathy with persistent myelination defect. *Am. J. Hum. Genet.* 2015; 96: 675–681.
- Sleigh JN, Grice SJ, Burgess RW, Talbot K, Cader MZ. Neuromuscular junction maturation defects precede impaired lower motor neuron connectivity in Charcot-Marie-Tooth type 2D mice. *Hum. Mol. Genet.* 2014; 23: 2639–2650.
- Spaulding EL, Sleigh JN, Morelli KH, Pinter MJ, Burgess RW, Seburn KL. Synaptic deficits at neuromuscular junctions in two mouse models of Charcot-Marie-Tooth type 2D. *J. Neurosci.* 2016; 36: 3254–3267.
- Spiegel R, Mandel H, Saada A, Lerer I, Burger A, Shaag A, et al. Delineation of C12orf65-related phenotypes: a genotype-phenotype relationship. *Eur. J. Hum. Genet.* 2014; 22: 1019–1025.
- Spinelli L, Black FM, Berg JN, Eickholt BJ, Leslie NR. Functionally distinct groups of inherited PTEN mutations in autism and tumour syndromes. *J. Med. Genet.* 2015; 52: 128–134.
- Spranger S, Ulmer H, Tröger J, Jansen O, Graf J, Meinck HM, et al. Muscular involvement in the Holt-Oram syndrome. *J. Med. Genet.* 1997; 34: 978–981.
- Srouf M, Putorti ML, Schwartzenruber J, Bolduc V, Shevell MI, Poulin C, et al. Mutations in riboflavin transporter present with severe sensory loss and deafness in childhood. *Muscle Nerve* 2014; 50: 775–779.
- Stiles AR, Venturoni L, Mucci G, Elbalalesy N, Woontner M, Goodman S, et al. New cases of DHTKD1 mutations in patients with 2-ketoadipic aciduria. *JIMD Rep.* 2015; 25: 15–19.
- Strickland AV, Schabhüttl M, Offenbacher H, Synofzik M, Hauser NS, Brunner-Krainz M, et al. Mutation screen reveals novel variants and expands the phenotypes associated with DYNC1H1. *J. Neurol.* 2015; 262: 2124–2134.
- Stum M, McLaughlin HM, Kleinbrink EL, Miers KE, Ackerman SL, Seburn KL, et al. An assessment of mechanisms underlying peripheral axonal degeneration caused by aminoacyl-tRNA synthetase mutations. *Mol. Cell. Neurosci.* 2011; 46: 432–443.

- Südhof TC. A molecular machine for neurotransmitter release: synaptotagmin and beyond. *Nat. Med.* 2013; 19: 1227–1231.
- Sullivan JM, Zimanyi CM, Aisenberg W, Bears B, Chen DH, Day JW, et al. Novel mutations highlight the key role of the ankyrin repeat domain in TRPV4 -mediated neuropathy. *Neurol. Genet.* 2015; 1: e29.
- Synofzik M, Soehn AS, Gburek-Augustat J, Schicks J, Karle KN, Schüle R, et al. Autosomal recessive spastic ataxia of Charlevoix Saguenay (ARSACS): expanding the genetic, clinical and imaging spectrum. *Orphanet J. Rare Dis.* 2013; 8: 41.
- Tagawa A, Ono S, Shibata M, Imai T, Suzuki M, Shimizu N. A new neurological entity manifesting as involuntary movements and dysarthria with possible abnormal copper metabolism. *J. Neurol. Neurosurg. Psychiatry* 2001; 71: 780–783.
- Takiyama Y. Autosomal recessive spastic ataxia of Charlevoix-Saguenay. *Neuropathol.* 2006; 26: 368–375.
- Tang B, Zhao G, Luo W, Xia K, Cai F, Pan Q, et al. Small heat-shock protein 22 mutated in autosomal dominant Charcot-Marie-Tooth disease type 2L. *Hum. Genet.* 2005; 116: 222–224.
- Tchan MC, Wilcken B, Christodoulou J. The mild form of menkes disease: a 34 year progress report on the original case. *JIMD Rep.* 2013; 9: 81–84.
- Telianidis J, Hung YH, Materia S, Fontaine SL. Role of the P-Type ATPases, ATP7A and ATP7B in brain copper homeostasis. *Front. Aging Neurosci.* 2013; 5: 44.
- Thompson R, Johnston L, Taruscio D, Monaco L, Bérout C, Gut IG, et al. RD-Connect: An integrated platform connecting databases, registries, biobanks and clinical bioinformatics for rare disease research. *J. Gen. Intern. Med.* 2014; 29: 780–787.
- Tibshirani M, Tradewell ML, Mattina KR, Minotti S, Yang W, Zhou H, et al. Cytoplasmic sequestration of FUS/TLS associated with ALS alters histone marks through loss of nuclear protein arginine methyltransferase 1. *Hum. Mol. Genet.* 2015; 24: 773–786.
- Timmerman V, De Jonghe P. Promising riboflavin treatment for motor neuron disorder. *Brain* 2014; 137: 2–3.

- Timmerman V, Raeymaekers P, De Jonghe P, De Winter G, Swerts L, Jacobs K, et al. Assignment of the Charcot-Marie-Tooth neuropathy type 1 (CMT 1a) gene to 17p11.2-p12. *Am. J. Hum. Genet.* 1990; 47: 680–685.
- Timmerman V, Strickland AV, Züchner S. Genetics of Charcot-Marie-Tooth (CMT) Disease within the Frame of the Human Genome Project Success. *Genes* 2014; 5: 13–32.
- Tinelli E, Pereira JA, Suter U. Muscle-specific function of the centronuclear myopathy and Charcot-Marie-Tooth neuropathy-associated dynamin 2 is required for proper lipid metabolism, mitochondria, muscle fibers, neuromuscular junctions and peripheral nerves. *Hum. Mol. Genet.* 2013; 22: 4417–4429.
- Tsurusaki Y, Saitoh S, Tomizawa K, Sudo A, Asahina N, Shiraishi H, et al. A DYNC1H1 mutation causes a dominant spinal muscular atrophy with lower extremity predominance. *neurogenetics* 2012; 13: 327–332.
- Tucci A, Liu Y-T, Preza E, Pitceathly RD, Chalasani A, Plagnol V, et al. Novel C12orf65 mutations in patients with axonal neuropathy and optic atrophy. *J. Neurol. Neurosurg. Psychiatry* 2014; 85: 486–492.
- Tümer Z. An overview and update of ATP7A mutations leading to Menkes disease and occipital horn syndrome. *Hum. Mutat.* 2013; 34: 417–429.
- Unger A, Dekomien G, Güttsches A, Dreps T, Kley R, Tegenthoff M, et al. Expanding the phenotype of BICD2 mutations toward skeletal muscle involvement. *Neurology* 2016; 87: 2235-2243.
- Untergasser A, Cutcutache I, Koressaar T, Ye J, Faircloth BC, Remm M, et al. Primer3-new capabilities and interfaces. *Nucleic Acids Res.* 2012; 40: e115.
- Van Den Bosch L, Timmerman V. Genetics of motor neuron disease. *Curr. Neurol. Neurosci. Rep.* 2006; 6: 423–431.
- Vance JM, Nicholson GA, Yamaoka LH, Stajich J, Stewart CS, Speer MC, et al. Linkage of Charcot-Marie-Tooth neuropathy type 1a to chromosome 17. *Exp. Neurol.* 1989; 104: 186–189.

- Vanoli F, Rinchetti P, Porro F, Parente V, Corti S. Clinical and molecular features and therapeutic perspectives of spinal muscular atrophy with respiratory distress type 1. *J. Cell. Mol. Med.* 2015; 19: 2058-2066.
- Verhoeven K, Claeys KG, Züchner S, Schröder JM, Weis J, Ceuterick C, et al. MFN2 mutation distribution and genotype/phenotype correlation in Charcot-Marie-Tooth type 2. *Brain* 2006; 129: 2093–2102.
- Verhoeven K, De Jonghe P, Van de Putte T, Nelis E, Zwijsen A, Verpoorten N, et al. Slowed conduction and thin myelination of peripheral nerves associated with mutant rho Guanine-nucleotide exchange factor 10. *Am. J. Hum. Genet.* 2003; 73: 926–932.
- Vester A, Velez-Ruiz G, McLaughlin HM, NISC Comparative Sequencing Program, Lupski JR, Talbot K, et al. A loss-of-function variant in the human histidyl-tRNA synthetase (HARS) gene is neurotoxic in vivo. *Hum. Mutat.* 2013; 34: 191–199.
- Vidarsdottir S, Walenkamp MJE, Pereira AM, Karperien M, van Doorn J, van Duyvenvoorde HA, et al. Clinical and biochemical characteristics of a male patient with a novel homozygous STAT5b mutation. *J. Clin. Endocrinol. Metab.* 2006; 91: 3482–3485.
- Vosberg HP. The polymerase chain reaction: an improved method for the analysis of nucleic acids. *Hum. Genet.* 1989; 83: 1–15.
- Waibel S, Neumann M, Rabe M, Meyer T, Ludolph AC. Novel missense and truncating mutations in FUS/TLS in familial ALS. *Neurology* 2010; 75: 815–817.
- Waibel S, Neumann M, Rosenbohm A, Birve A, Volk AE, Weishaupt JH, et al. Truncating mutations in FUS/TLS give rise to a more aggressive ALS-phenotype than missense mutations: a clinico-genetic study in Germany. *Eur. J. Neurol.* 2013; 20: 540–546.
- Wang J, Kong L, Gao G, Luo J. A brief introduction to web-based genome browsers. *Brief. Bioinform.* 2013; 14: 131–143.
- Wang J, Van Nostrand JD, Wu L, He Z, Li G, Zhou J. Microarray-based evaluation of whole-community genome DNA amplification methods. *Appl. Environ. Microbiol.* 2011; 77: 4241–4245.

- Weedon MN, Hastings R, Caswell R, Xie W, Paszkiewicz K, Antoniadis T, et al. Exome sequencing identifies a *DYNC1H1* mutation in a large pedigree with dominant axonal Charcot-Marie-Tooth Disease. *Am. J. Hum. Genet.* 2011; 89: 308–312.
- Wegierski T, Hill K, Schaefer M, Walz G. The HECT ubiquitin ligase AIP4 regulates the cell surface expression of select TRP channels. *EMBO J.* 2006; 25: 5659–5669.
- Wendelsdorf K, Shah S. Empowered genome community: leveraging a bioinformatics platform as a citizen-scientist collaboration tool. *Appl. Transl. Genomics* 2015; 6: 7–10.
- Westermann B. Mitochondrial fusion and fission in cell life and death. *Nat. Rev. Mol. Cell Biol.* 2010; 11: 872–884.
- Whittaker RG, Herrmann DN, Bansagi B, Hasan BAS, Lofra RM, Logigian EL, et al. Electrophysiologic features of *SYT2* mutations causing a treatable neuromuscular syndrome. *Neurology* 2015; 85: 1964–1971.
- Wirtz PW, Verschuuren JJ, van Dijk JG, de Kam ML, Schoemaker RC, van Hasselt JGC, et al. Efficacy of 3,4-diaminopyridine and pyridostigmine in the treatment of Lambert-Eaton myasthenic syndrome: a randomized, double-blind, placebo-controlled, crossover study. *Clin. Pharmacol. Ther.* 2009; 86: 44–48.
- Xie W, Nangle LA, Zhang W, Schimmel P, Yang XL. Long-range structural effects of a Charcot-Marie-Tooth disease-causing mutation in human glycyl-tRNA synthetase. *Proc. Natl. Acad. Sci.* 2007; 104: 9976–9981.
- Xu H, Luo X, Qian J, Pang X, Song J, Qian G, et al. FastUniq: a fast de novo duplicates removal tool for paired short reads. *PloS One* 2012; 7: e52249.
- Xu WY, Gu MM, Sun LH, Guo WT, Zhu HB, Ma JF, et al. A nonsense mutation in *DHTKD1* causes Charcot-Marie-Tooth disease type 2 in a large Chinese pedigree. *Am. J. Hum. Genet.* 2012; 91: 1088–1094.
- Xu W, Zhu H, Gu M, Luo Q, Ding J, Yao Y, et al. *DHTKD1* is essential for mitochondrial biogenesis and function maintenance. *FEBS Lett.* 2013; 587: 3587–3592.

- Yamak A, Georges RO, Sheikh-Hassani M, Morin M, Komati H, Nemer M. Novel exons in the Tbx5 gene locus generate protein isoforms with distinct expression domains and function. *J. Biol. Chem.* 2015; 290: 6844–6856.
- Yang Y, Muzny DM, Reid JG, Bainbridge MN, Willis A, Ward PA, et al. Clinical whole-exome sequencing for the diagnosis of mendelian disorders. *N. Engl. J. Med.* 2013; 369: 1502–1511.
- d'Ydewalle C, Krishnan J, Chiheb DM, Van Damme P, Irobi J, Kozikowski AP, et al. HDAC6 inhibitors reverse axonal loss in a mouse model of mutant HSPB1-induced Charcot-Marie-Tooth disease. *Nat. Med.* 2011; 17: 968–974.
- Yi L, Donsante A, Kennerson ML, Mercer JFB, Garbern JY, Kaler SG. Altered intracellular localization and valosin-containing protein (p97 VCP) interaction underlie ATP7A-related distal motor neuropathy. *Hum. Mol. Genet.* 2012; 21: 1794–1807.
- Yi L, Kaler S. ATP7A trafficking and mechanisms underlying the distal motor neuropathy induced by mutations in ATP7A: ATP7A trafficking and distal motor neuropathy. *Ann. N. Y. Acad. Sci.* 2014; 1314: 49–54.
- Yi L, Kaler SG. Direct interactions of adaptor protein complexes 1 and 2 with the copper transporter ATP7A mediate its anterograde and retrograde trafficking. *Hum. Mol. Genet.* 2015; 24: 2411–2425.
- Yonezawa A, Inui K. Novel riboflavin transporter family RFVT/SLC52: Identification, nomenclature, functional characterization and genetic diseases of RFVT/SLC52. *Mol. Aspects Med.* 2013; 34: 693–701.
- Young SM, Neher E. Synaptotagmin has an essential function in synaptic vesicle positioning for synchronous release in addition to its role as a calcium sensor. *Neuron* 2009; 63: 482–496.
- Yu-Wai-Man P, Pyle A, Griffin H, Santibanez-Korev M, Horvath R, Chinnery PF. Abnormal retinal thickening is a common feature among patients with ARSACS-related phenotypes. *Br. J. Ophthalmol.* 2014; 98: 711–713.
- Zeng R, Aoki Y, Yoshida M, Arai K -i., Watanabe S. Stat5B shuttles between cytoplasm and nucleus in a cytokine-dependent and -independent manner. *J. Immunol.* 2002; 168: 4567–4575.

- Zhao Z, Hashiguchi A, Hu J, Sakiyama Y, Okamoto Y, Tokunaga S, et al. Alanyl-tRNA synthetase mutation in a family with dominant distal hereditary motor neuropathy. *Neurology* 2012; 78: 1644–1649.
- Zhou J, Parada LF. A motor driving PTEN. *Nat. Cell Biol.* 2009; 11: 1177–1179.
- Zimon M, Baets J, Auer-Grumbach M, Berciano J, Garcia A, Lopez-Laso E, et al. Dominant mutations in the cation channel gene transient receptor potential vanilloid 4 cause an unusual spectrum of neuropathies. *Brain* 2010; 133: 1798–1809.
- Züchner S, De Jonghe P, Jordanova A, Claeys KG, Guergueltcheva V, Cherninkova S, et al. Axonal neuropathy with optic atrophy is caused by mutations in mitofusin 2. *Ann. Neurol.* 2006; 59: 276–281.
- Züchner S, Mersiyanova IV, Muglia M, Bissar-Tadmouri N, Rochelle J, Dadali EL, et al. Mutations in the mitochondrial GTPase mitofusin 2 cause Charcot-Marie-Tooth neuropathy type 2A. *Nat. Genet.* 2004; 36: 449–451.